In-plane Shear Behaviour of Unreinforced Masonry Panels Strengthened with Fibre Reinforced Polymer Strips

Robert Bruce Petersen
BEng (Hons I)

A thesis submitted in partial fulfilment
of the requirements for the degree of

Doctor of Philosophy
(School of Engineering)

October, 2009

THE UNIVERSITY OF
NEWCASTLE
AUSTRALIA

I hereby certify that the work embodied in this thesis is the result of original research and has not been submitted for a higher degree to any other University or Institution.

I hereby certify that the work embodied in this thesis contains a published paper of which I am a joint author. The research work presented in Chapter 3 of this thesis has been published in the Journal of Composites for Construction:

R B Petersen, M J Masia, and R Seracino. Bond Behavior of NSM FRP strips Bonded to Modern Clay Brick Masonry Prisms: Influence of Strip Orientation and Compression Perpendicular to the Strip. Journal of Composites for Construction, 13(3), 169-178, 2009.

I am solely responsible for the research presented in this joint publication, under the supervision of Mark Masia and Rudi Seracino.

(Signed): ______________________________

Robert Petersen

(Signed): ______________________________

Mark Masia (supervisor)

Acknowledgements

I would like to thank my supervisors Mark Masia and Rudi Seracino for their support and excellent supervision. Thanks Mark for always having the time for me and carefully considering all of my questions. Thanks Rudi for your technical input, kind reviews, and for looking after me during my stay at North Carolina.

I would also like to thank my family and friends. Most of all, I would like to thank Alison for her love and support (and for doing all of the housework while I was writing my thesis). I also need to make a special mention of the guys in room EF120. Adrian, Sagy, Juan, Adam, Ang and Dan, thanks for putting up with my annoying antics.

I gratefully acknowledge the support of the technical staff of the Civil, Surveying and Environmental Engineering Laboratory. I acknowledge the financial support provided by the Australian Research Council under DP0559706.

CONTENTS

ABSTRACT

Inserting fibre reinforced polymer (FRP) strips into pre-cut grooves in the surface of masonry walls is an emerging technique for the retrofit of unreinforced masonry (URM) structures. This method, known as near surface mounting (NSM), provides significant advantages over externally bonded FRP strips in that it has less of an effect on the aesthetics of a structure and can sustain higher loading before debonding. As this technique is relatively new, few studies into the behaviour of masonry walls strengthened using this technique have been conducted.

A combined experimental and numerical program was conducted as part of this research project to study the in-plane shear behaviour of masonry wall panels strengthened with NSM carbon FRP (CFRP) strips. In this project the FRP strips were designed to resist sliding along mortar bed joints and diagonal cracking (through mortar joints and brick units). Both of these failure modes are common to masonry shear walls. Different reinforcement orientations were used, including: vertical; horizontal; and a combination of both.

The first stage of the project involved characterising the bond between the FRP and the masonry using experimental pull tests (18 in total). From these tests the bond strength, the critical bond length and the local bond-slip relationship of the debonding interface was determined.

The second stage of the project involved conducting diagonal tension/shear tests on masonry panels. A total of four URM wall panels and seven strengthened wall panels were tested. These tests were used to determine: the effectiveness of the reinforcement; the failure modes; the reinforcement mechanisms; and the behaviour of the bond between the masonry and the FRP in the case of a panel.

The third stage of the project involved developing a finite element model to help understand the experimental results. The masonry was modelled using the micro-modelling approach, and the FRP was attached to the masonry model using the bond-slip relationships determined from the pull tests.

Reinforcement schemes in which vertical FRP strips were used improved the strength and ductility of the masonry wall panels. When only horizontal strips were used to reinforce a wall panel, failure occurred along an un-strengthened bed joint and the increase in strength and ductility was negligible. The vertical reinforcement prevented URM sliding failure by restraining the opening (dilation) of the sliding cracks that developed through the mortar bed joints.

The finite element model reproduced the key behaviours observed in the experiments for both the unreinforced and FRP strengthened wall panels. This model would potentially be useful for the development of design equations.

1

Introduction

Damages caused by earthquakes have highlighted the potential vulnerability of unreinforced masonry (URM) buildings to earthquake loading. Previous investigations have identified the need to develop efficient techniques to retrofit (or strengthen) existing masonry buildings against earthquake loading (Bruneau, 1994). A strengthening technique with a low impact on function and appearance of the building is of particular importance. During an earthquake, the walls in the lower storeys are likely to fail in shear (in the plane of the wall). In this thesis, a technique to strengthen in-plane loaded shear walls is investigated.

The technique of bonding fibre reinforced polymer (FRP) materials to a URM wall is a relatively new retrofit alternative. The FRP reinforcement is designed to provide tensile strength to a wall and increase the wall strength and ductility. The FRP material is either externally bonded (EB) to the surface of a wall (suitable technique for both fabrics, grids or thin strips) or inserted into grooves cut into the surface of a wall using a technique known as near surface mounting (NSM) (this technique is suitable for both thin rectangular strips and bars). The advantages of using FRPs to strengthen/retrofit an existing masonry structure include the materials high strength/stiffness to weight ratio and corrosion insensitivity.

The NSM technique provides the following significant advantages over the EB technique: it is protected from vandalism; it is protected to some extent from fire; if detailed carefully it may not adversely affect the aesthetics of a structure; and it can develop a higher strain in the FRP before debonding. As this technique is relatively new (especially for masonry structures), few studies into the behaviour of masonry walls strengthened using this technique have been conducted.

The objective of this research was to study the in-plane shear behaviour of NSM FRP strengthened masonry wall panels. In particular, the objective was to determine the effectiveness of the technique and also the fundamental shear reinforcement mechanisms. The specific aims for the current research were to:

1. Characterise experimentally the shear bond-slip behaviour of the interface between the NSM FRP strip and masonry. The bond-slip behaviour represents the fundamental behaviour of the FRP-to-masonry interface. This relationship is required in finite element models to predict the behaviour of an FRP reinforced structure.

2. Study the in-plane shear behaviour of NSM FRP strengthened masonry by

conducting laboratory experiments on strengthened wall panels; and

3. Study the in-plane shear behaviour of NSM FRP strengthened masonry wall panels using a rationally based, representative finite element model. The finite element model uses the bond-slip behaviour determined in Aim 1 and is verified using the experiments from aim 2.

Scope and Limitations

The NSM FRP reinforcing system presented in this thesis may be used for both the strengthening of undamaged walls and the repair/retrofit of damaged walls. In this thesis the NSM reinforcing system is only used to strengthen undamaged masonry panels.

Thesis outline

The next chapter provides a review of the literature related to the topic. At the end of the chapter the proposed research work is detailed. The research work is contained in Chapters 3 to 5. Chapter 3 details the experimental tests used to characterise the shear bond-slip behaviour of the interface between the NSM FRP strip and masonry; Chapter 4 details the experimental tests on strengthened wall panels (Aim 2); and Chapter 5 details the development and verification of the finite element model (Aim 3). Conclusions and recommendations for future work are provided in Chapter 6.

2

Literature Review

2.1 Unreinforced masonry shear walls

Unreinforced masonry (URM) is used in buildings for load bearing walls, for infill panels in framed construction, for veneers attached to backup frames, for piers and columns, and for free standing walls. In load-bearing masonry construction URM walls are required to act as shear walls to transfer lateral forces (from earthquake and wind) to the building supports. Also, infill panels in framed construction may interact with the surrounding frames to resist shear forces from lateral load.

In load bearing masonry construction, masonry shear walls are subjected to both vertical and lateral loads in the plane of the wall. The typical failure modes of load-bearing masonry shear walls include: sliding, diagonal cracking and rocking (Figure 2.1). The mechanisms depend primarily on the geometry of the wall (height/length ratio), on the boundary conditions and on the magnitude of vertical loads, and then on the masonry properties (Magenes and Calvi, 1997; Tomaževič, 1999; ElGawady et al., 2007).

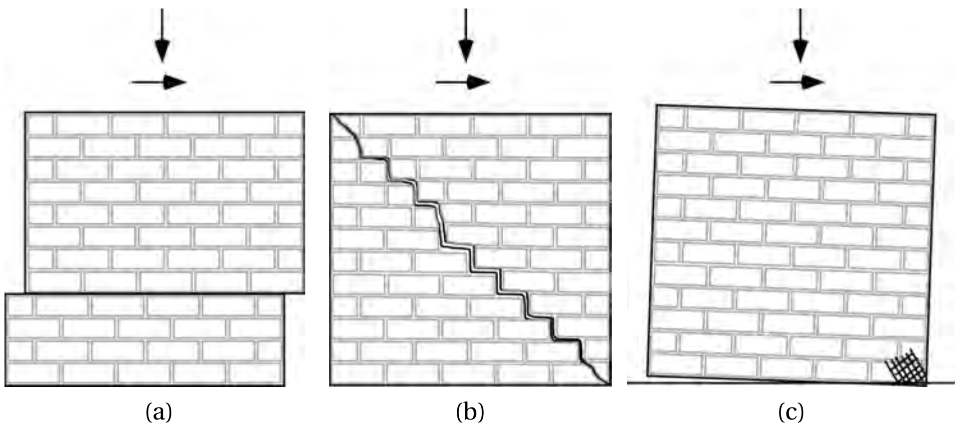

Figure 2.1: Failure modes of URM shear wall: (a) sliding; (b) diagonal cracking (through brick units and mortar joints); (c) rocking (with toe crushing)

1. *Sliding*: In a wall with poor mortar strength or low pre-compression, failure is likely to occur by sliding along the bed joints. Sliding occurs when the fric-

tional resistance along the bed joints is overcome. Sliding planes may also be formed by the connection of flexural tensile cracks that develop during cyclic motions (Magenes and Calvi, 1997).

2. *Diagonal cracking*: In walls with low aspect ratios (height/length) and high axial loads, failure is likely to occur by diagonal cracking. Diagonal cracking may occur through the brick units or in a stepped pattern through the mortar joints, depending on their relative strengths. Under reversing cycles of lateral loading an X-type crack pattern develops (Figure 2.2).

3. *Rocking*: In walls with high moment/shear ratios or improved shear resistance the wall may be set into a rocking motion, with a combination of uplift at the heel and crushing at the toe.

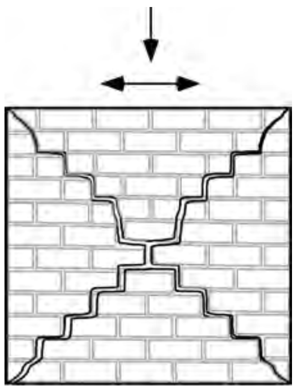

Figure 2.2: Diagonal cracking under cyclic shear loads

The diagonal cracking failure mode is considered the least favourable failure mode of a masonry shear wall. It is generally characterised by brittle behaviour with a rapid decrease in capacity and limited deformations after reaching the peak load (Magenes and Calvi, 1997; Marshall and Sweeney, 2002; Zhao et al., 2003). Rocking and sliding (along a single horizontal bed joint), on the other hand, are considered adequate failure mechanisms when considering deformation capacity, stability and energy dissipation (Marshall and Sweeney, 2002; Corte et al., 2008; Holberg and Hamilton, 2002). Two- to three-storey load-bearing masonry buildings may be able to resist large displacements (and perform adequately during an earthquake event) if the primary failure mode is rocking or bed-joint sliding (Holberg and Hamilton, 2002).

Damage to shear walls, during an earthquake, is normally observed in the lower storeys of a load-bearing masonry building, where the shear loads and compression loads are the greatest (Page, 1996; Bruneau, 1994). In these walls the most common type of damage is the most brittle failure mode: diagonal cracking in an X pattern. Unless major openings or discontinuities are present, damage does not usually result in wall collapse. However, damage can cause a large reduction in capacity of the wall which adversely affects the response of the whole structure (Page, 1996).

In walls with openings (for windows, doors, etc) damage (commonly diagonal X cracking) is concentrated around the openings in the masonry piers and spandrels. The consequences of this damage to the overall structural behaviour of the building is often severe (Wakabayashi, 1986; Key, 1988; Page, 1996; Tomaževič, 1999). Damage in the piers is the most common form of in-plane wall failure in a load bearing masonry structure and can lead to soft storey effects, which are catastrophic during an earthquake (Tomaževič, 1999).

Infill panels in framed construction may interact with the surrounding frames to resist shear forces from lateral loads (Tomaževič, 1999). The masonry acts as a compressive strut and substantially stiffens the frame (Key, 1988). Typical failure of the infill masonry, due to in-plane loads, includes: failure of the diagonal compression strut by diagonal cracking; and horizontal sliding failure of the panel (see Figure 2.3). Once failure occurs the stiffening effect to the frame is reduced. Framed construction with masonry infill walls is generally more effective against earthquakes than load bearing masonry buildings (Wakabayashi, 1986).

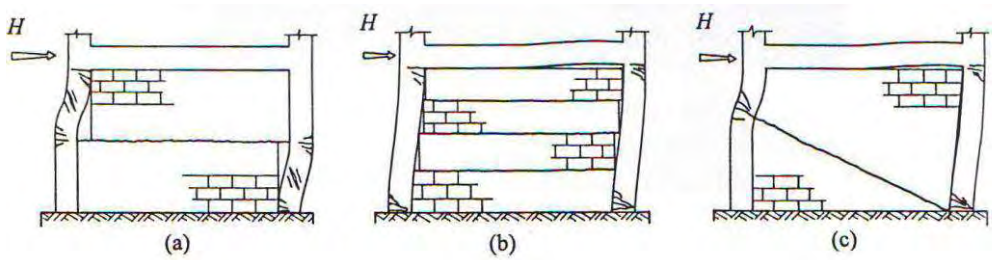

Figure 2.3: Typical failure mechanisms of masonry infilled frames: (a) horizontal sliding failure along a single bed joint; (b) horizontal sliding failures along multiple bed joints; (c) diagonal cracking (Tomaževič, 1999)

2.2 Repair, strengthening and retrofitting of masonry walls

2.2.1 Motivation

Damages caused by earthquakes have highlighted the potential vulnerability of unreinforced masonry buildings to earthquake loading (Bruneau, 1994; Klopp and Griffith, 1998). The reasons for poor performance of masonry structures in earthquakes are as follows (Wakabayashi, 1986):

1. The material itself is brittle, and strength degradation due to load repetition is severe.

2. Heavy weight

3. Large stiffness, which leads to large response to earthquake waves of short natural period.

4. Large variability in strength depending on quality of construction.

5. Poor detailing (connection and support) of walls.

Many load-bearing masonry buildings were constructed before the development of rational design procedures and are under designed for earthquakes as a result (Magenes and Calvi, 1997). For example, in Australia, before the Newcastle earthquake in 1989, there was a perception of low seismicity and buildings were not designed for earthquakes. Particular attention was not given to building layout, detailing, lateral loads on internal walls, or potential soft storey effects; all critical to the structural performance of masonry buildings in earthquakes (Page, 1996). These buildings require strengthening. Masonry buildings may also require strengthening due to deterioration of masonry walls, caused by either environmental factors or past loading events.

2.2.2 Conventional strengthening/retrofitting techniques

Conventional techniques for the repair, strengthening and retrofitting of masonry walls were reviewed by ElGawady et al. (2004) and Chuang and Zhuge (2005). Conventional techniques include (ElGawady et al., 2004):

1. Surface treatment using products such as ferrocement, reinforced plaster, and shotcrete

2. Injecting grout or epoxy into pre-existing cracks or voids

3. Externally reinforcing the masonry with steel plates or tubes

4. Confining the masonry with reinforced concrete tie columns and tie beams

5. Post-tensioning the wall using steel tendons

6. Adding grouted steel reinforcement within cores drilled vertically through the mid-thickness of the wall

7. Inserting steel bars into the edge of the mortar bed joints by a process known as structural repointing.

These techniques have been proven effective, but they also have disadvantages. Many of the techniques are expensive, time and labour intensive, reduce building space (when thick surface treatments are used), adversely affect the aesthetics of a structure, and can add significant mass to a structure. Adding significant mass to a structure can significantly affect its dynamic response. Corrosion of steel reinforcement is also an issue.

2.2.3 FRPs as a strengthening/retrofitting alternative

The technique of bonding fibre reinforced polymer (FRP) materials to an unreinforced masonry wall is a relatively new strengthening/retrofitting alternative. FRPs are a composite material that consist of high strength fibres (in tension) that are embedded in a resin matrix. The fibres are typically carbon, glass, or aramid and the resin is usually epoxy. The fibres are very strong in their longitudinal direction, but weak in their lateral direction. For strengthening/retrofitting purposes, FRPs are produced in fabric sheets, pre-formed pultruded strips, tendons (for pretensioning or post-tensioning) and reinforcing bars or meshes (Shrive, 2006). In strips, tendons and reinforcing bars the fibres are aligned in one direction and this gives the composite anisotropic (or directional) properties. Sheets may be produced with all of the fibres aligned in one direction (uniaxial), aligned orthogonally (bidirectional), or randomly. When the fibres are aligned orthogonally or randomly the composite exhibits orthotropic properties.

Common FRP composites are completely elastic until failure. Attempts have been made recently to introduce some ductility into the composite material by using a combination of different modulus fibres (Wu, 2004). Typical mechanical properties of some of the FRP reinforcement materials used by researchers to strengthen masonry shear walls are shown in Table 2.1.

Table 2.1: Typical mechanical properties of FRP reinforcements used to strengthen masonry shear walls

FRP reinforcement	E (MPa)	Ultimate stress (MPa)	Reference
fabric sheet (glass)	73300	986	Stratford et al. (2004)
pultruded strip (carbon)	147500	2000	Schwegler (1995)
reinforcing bar (glass)	50200	824	Li et al. (2005)

The FRP reinforcement is designed to provide tensile strength to a masonry wall. This increases the strength and ductility of the masonry wall, which in turn improves the behaviour of the wall during an extreme loading event. The FRP reinforcement is either externally bonded (EB) to the surface of a wall or inserted into grooves cut into the surface of a wall (discussed in more detail in Section 2.3). The FRP reinforcement may also be mechanically anchored at the ends of the wall or into adjoining supports. In general, when mechanical anchors are used the FRP reinforcement is also bonded to the wall. In these cases, the mechanical anchorage is used to provide load transfer between the FRP and masonry after the FRP debonds from the wall. In some cases, however, the FRP reinforcement is not bonded to the wall and is only attached to the wall via the mechanical anchorage (El-Gawady et al., 2005).

The advantages of using FRPs to strengthen/retrofit an existing masonry structure include the materials high strength/stiffness to weight ratio and high durability. The light weight of the material improves on-site handling, which reduces labour costs and interruptions to existing services and building occupants. The light weight is also advantageous from a seismic point of view, as an increase in building mass increases the earthquake forces within a building.

The main disadvantage with using FRP for reinforcement is that it has brittle failure modes. FRPs may fail by rupturing or, if no mechanical anchorage is provided, by debonding from the strengthened material. Tensile force in the FRP is transferred through the adhesive (usually epoxy) to the masonry via shear. When the shear strength of the adhesive or the superficial layer of brick is exceeded, debonding occurs. Debonding may also occur along the interface between the brick and adhesive or the interface between the adhesive and FRP. Both rupture and debonding failure modes are brittle in nature, potentially leading to non-ductile behaviour and catastrophic collapse. However, because masonry walls are inherently brittle to begin with, the addition of FRP reinforcement may not only increase the strength but also increase the ductility, even though the FRP may eventually rupture or debond. Other disadvantages of FRP include their limited fire resistance (of the resin matrix and or epoxy adhesive) , sensitivity of some resins to direct sunlight, and their impact on the aesthetics of a structure (e.g. when covering a wall with an externally bonded fabric sheet) (Shrive, 2006).

2.3 FRP application techniques

2.3.1 External bonding

The external bonding (EB) technique is the most common form of application. In this technique, preformed pultruded FRP strips or FRP fabric sheets are bonded to the external surface of a wall typically using a two-part epoxy adhesive.

Before the FRP reinforcement is bonded to the wall the surface must be prepared. Typically the masonry surface first needs to be cleaned using a combination of abrasion and solvent, then a filler layer (typically also epoxy) may need to be applied to produce a flat surface for the FRP to be bonded to (Stratford et al., 2004).

FRP fabric sheets can be externally bonded to the surface of a wall using two methods. The fabric sheets may first be impregnated within a layer of epoxy and allowed to cure before being bonded to the wall. Alternatively, the fabric sheets can be bonded to the wall using the wet lay-up technique. In the wet lay-up technique the fabrics are first pressed into a layer of epoxy painted onto the surface of the wall and are then covered with another layer of epoxy. The wet lay-up technique is described in greater detail in Stratford et al. (2004).

Thin pultruded strips are usually oriented in diagonal patterns (e.g. Figure 2.8a) or in vertical/horizontal grid patterns. Fabric sheets may be applied to the whole surface of a wall (Stratford et al., 2004) or as discrete strips (e.g. Figure 2.8b).

No minimum requirements on the masonry material to be strengthened has been reported in the literature. However, debonding of the FRP from the masonry occurs via cracking through the surface of the masonry and is therefore related to the tensile strength of the masonry. Therefore the stronger the masonry the stronger the FRP-to-masonry bond.

Externally bonded FRP sheets have the following advantages over the other application techniques described in the following sections: wide sheets may provide dowel resistance across sliding joints, and confinement to masonry in compression if applied on both sides of the wall (Section 2.4). The advantage of using FRP sheets bonded to the whole surface of a wall is its simplicity (Stratford et al., 2004). An anchored sheet that has its fibres aligned in the orthogonal directions of the wall can resist sliding, diagonal cracking and rocking failure modes (Marshall and Sweeney, 2002) (see Section 2.4).

Externally bonded FRP sheets and strips have the following disadvantages: they have a large impact on the aesthetics of a wall, they are highly susceptible to debonding failure modes, they may buckle from the surface of the wall in compression, and they are exposed (to vandalism or fire).

2.3.2 Structural repointing

The structural repointing (SR) technique involves inserting an FRP bar or thin pultruded strip into a groove cut into the surface of the mortar joints. Typically the reinforcement is placed horizontally in the mortar bed joints, but can also be placed vertically in the mortar head joints in the case of stack bonded masonry.

A typical cross section through the masonry thickness showing a structurally repointed FRP bar is shown in Figure 2.4. The FRP is usually embedded into the mortar joint space using epoxy, but sometimes other adhesives have been used such as a latex-modified cement paste (e.g. Turco et al. (2006)).

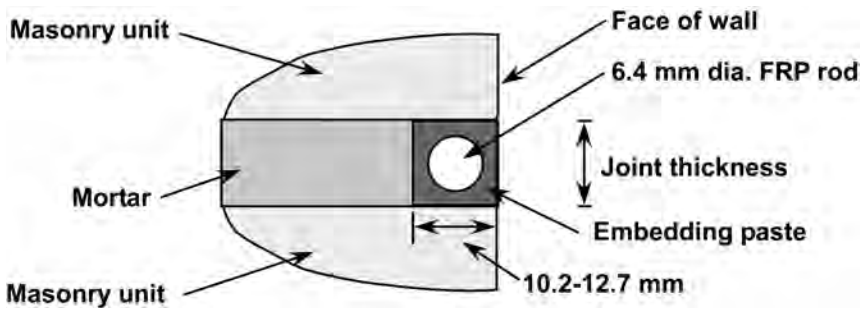

Figure 2.4: FRP bar structural repointing (cross section) from Li et al. (2005)

The grooves in the mortar joint are usually cut using a circular saw equipped with a brick cutting blade. The process of cutting a groove into the wall is easier than the surface treatment procedure that needs to be followed for the externally bonded reinforcement. The other main advantage of structural repointing is that the strengthening intervention is completely hidden once installed.

Structurally repointed FRP reinforcement is suitable for restraining diagonal cracking failure modes, but has limited effectiveness in restraining sliding or in-plane flexural cracking. In cases where the structural repointed reinforcement is not placed in every bed joint, failure will occur along an unstrengthened bed joint. Therefore it is usually necessary to structurally repoint all mortar bed joints. The pull-out bond strength of structurally repointed reinforcement is less than the bond strength of near-surface mounted reinforcement bonded into the brick (Section 2.3.3).

2.3.3 Near-surface mounting

The near-surface mounting (NSM) technique is a relatively new retrofitting technique, and can be used as an alternative to EB FRP sheets or strips. The technique involves bonding thin FRP strips or FRP bars into grooves cut into the surface of a masonry wall (Figure 2.5). The grooves are cut with a circular saw fitted with a brick cutting blade. The FRP reinforcement is then bonded into the groove using a two-part epoxy. Note that the SR technique (discussed previously) is a specific NSM case where the FRP is inserted into grooves cut along the mortar bed joint.

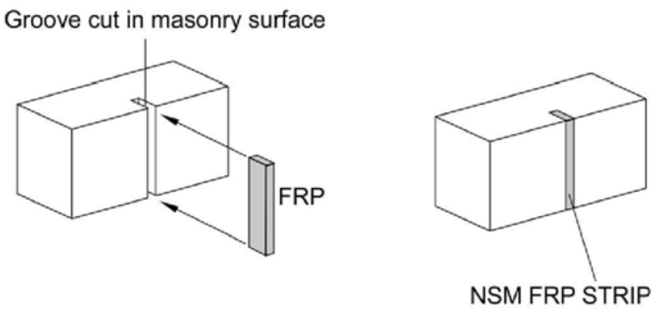

Figure 2.5: Illustration of the near-surface mounted technique (into one brick)

As for externally bonded FRP, the bond strength between the NSM FRP and masonry is related to the tensile strength of the material the FRP is bonded to. Therefore the bond strength of the NSM FRP strip is higher if bonded to the brick rather than mortar or plaster render. The debonding resistance of NSM FRP is larger than the debonding resistance of EB FRP strips due to the increased bond surface area and extra confinement.

The grooves may be oriented in any direction. Some possible applications are shown in a Figure 2.6. The schemes shown in the figure can restrain both diagonal cracking and sliding failure mechanisms. Vertical strips may be inserted into grooves cut into brick units only (for high FRP-to-masonry bond strength, but increased visual impact), or into alternating brick units and mortar head joints (for reduced visual impact, but also a reduced bond strength). Similarly horizontal strips may be bonded into grooves cut into brick units only, or into the mortar bed joints only (structurally repointed reinforcement).

The aesthetic impact of the technique can be reduced by bonding the FRP into the mortar joints. When bonded into the brick units, the aesthetic impact can be reduced by choosing an epoxy colour that is close to the colour of the brick. The NSM reinforcement may also be buried a little deeper than the wall surface and a filler material with a colour similar to that of the brick could be pasted over the embedded reinforcement.

The advantages of the NSM technique compared to the externally bonded technique include: reduced aesthetic impact, less exposure (to vandalism or fire), si-

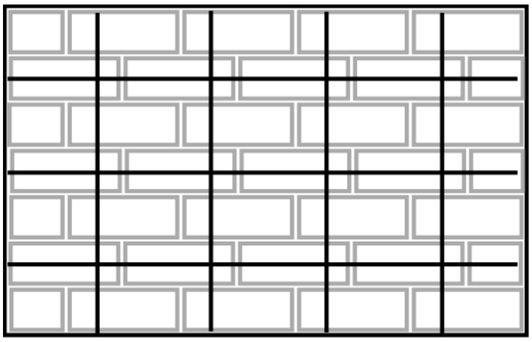

(a) Grooves cut into brick

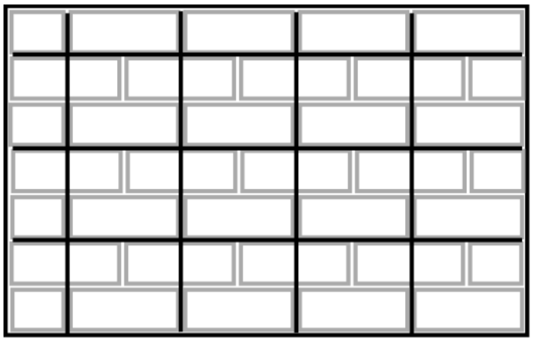

(b) Grooves cut into mortar

Figure 2.6: Possible NSM reinforcement schemes

gnificantly increased debonding resistance, and an increased resistance to buckling. A possible disadvantage of the technique is that it requires deep grooves to be cut into the surface of the masonry which may cause cracking through the thickness of the wall.

The costs associated with the NSM technique are likely similar (or even potentially less than) the costs associated with the EB technique. The NSM technique would require less material (due to increased bond strength), and the installation efforts and costs required for both techniques would be comparable.

2.4 FRP reinforcement mechanisms

FRPs can be used to provide resistance against the three typical URM failure modes: sliding; diagonal cracking; and rocking. The reinforcement mechanisms are now discussed.

2.4.1 Resistance against sliding along a single bed joint

According to Marshall and Sweeney (2002), sliding along a single bed joint is best resisted by placing the FRP reinforcement continuously vertically across the specimen. The FRP is aligned so that no horizontal failure plane can develop without passing through the FRP reinforcement. Vertical reinforcement restrains sliding by providing dowel strength across the joint and also by resisting shear induced dilation.

The dowel strength of externally bonded, bidirectional FRP sheets across a sliding joint has been demonstrated by Ehsani et al. (1997) (Section 2.6.2). In their study 114 mm wide sheets were used. It is likely that the dowel strength of the reinforcement reduces as the width of the sheet reduces. For FRP strips with a small width, the dowel resistance is usually considered negligible (Marshall and Sweeney, 2002). In fact, Triantafillou (1998) has ignored the dowel strength of EB FRP sheets completely in a design model (see Section 2.8).

FRPs crossing a sliding joint can potentially restrict crack separation (normal to the crack face) needed for sliding to occur. Crack opening during sliding is known as dilation. Dilation occurs because the crack surfaces are uneven and one surface needs to move up and over the other to facilitate sliding. Dilatational behaviour upon shearing is common in frictional cementitious materials and has been observed in masonry joints (Van der Pluijm, 1998; Van Zijl, 2004). By resisting dilation with FRP the frictional force along the sliding interface increases, which in turn increases the frictional sliding resistance (Figure 2.7). This mechanism is related to the shear bond behaviour between the FRP and the masonry, where the FRP is loaded in tension (limited by debonding or rupture). It is also related to the frictional and dilatational behaviour of the shear sliding joint. This mechanism is generally not considered or recognised for FRP strengthened masonry structures. It has, however, been shown to be a significant shear resisting mechanism of longitudinal EB and NSM FRP reinforcement bonded to reinforced concrete beams and slabs (Oehlers and Seracino, 2004).

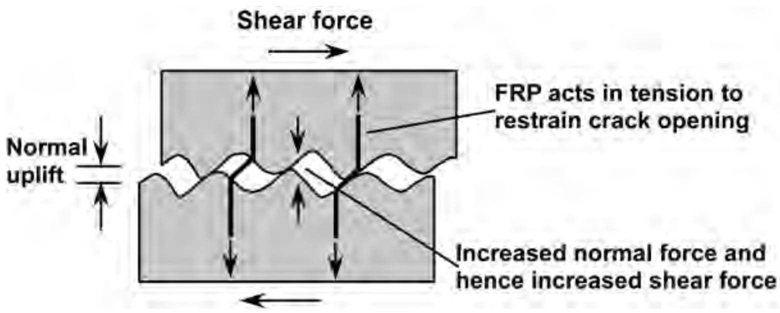

Figure 2.7: Reinforcement mechanism in shear sliding: FRP resists dilation and increases friction

2.4.2 Resistance against diagonal cracking

Reinforcement that spans the crack acts in tension to restrain the crack opening. Either horizontal or diagonal FRP reinforcement is generally used. Note that horizontal reinforcement is effective at restraining diagonal cracks that develop in both directions (X-cracking) as a result of reversing cycles of in-plane lateral loading. Whereas, diagonal reinforcement is effective at restraining diagonal cracks that develop in one direction only. Therefore diagonal reinforcement needs to be applied in an X-type pattern (or similar) to resist X-cracking. As the reinforcement acts in tension, the reinforcement contribution is limited by rupture of the FRP or debonding of the FRP from the masonry.

The presence of the reinforcement, which restrains the opening of the diagonal cracks, allows the average stresses within the wall to increase. This leads to the development of more diagonal cracks (typically parallel to each other) and the formation of diagonal struts within the masonry (Li et al., 2005). In this highly cracked state the wall is said to resist shear by a truss type mechanism (or strut and tie mechanism), with tension carried by the FRP and compression carried by the masonry struts (Zhao et al., 2003; Stratford et al., 2004). Provided that the reinforcement is strong enough, the shear stress within the wall can become high enough to cause crushing of the struts.

2.4.3 Resistance against flexural failure and rocking

Flexural failure within the wall is resisted with vertical reinforcement placed along the vertical edges of the wall. The effectiveness of the reinforcement is again limited by debonding or rupture. To prevent rocking the vertical reinforcement is anchored at the corners of the wall. Crushing capacity at the toe can only be improved through confinement (Marshall and Sweeney, 2002). Confinement can be provided by bonding a bidirectional FRP sheet to both sides of the masonry wall (Hamid et al., 2005).

Hall et al. (2002) recommended that FRP reinforcement not be used to prevent rocking. Using FRP reinforcement to strengthen against rocking would increase the lateral load capacity, but the dynamic energy dissipation provided by impact during rocking would be sacrificed. Also, the FRP may fail by rupture or debonding. According to Hall et al. (2002) failure of the FRP by rupture or debonding would cause a sudden energy release which could cause catastrophic instability in the wall. Hall et al. (2002) recommends that ductile elements (such as steel) could be used to increase the strength and ductility across the connections (see Section 2.5.1).

2.5 Past FRP strengthened wall tests

2.5.1 Externally bonded reinforcement

Discrete strips/sheets

Several researchers have used externally bonded FRP strips to improve the in-plane shear resistance of unreinforced masonry walls (or panels), including: Schwegler (1995); Tinazzi and Nanni (2000); Corradi et al. (2002); Valluzzi et al. (2002); Marshall and Sweeney (2002); Holberg and Hamilton (2002);Chuang et al. (2003); Zhao et al. (2003); Zhao et al. (2004); ElGawady et al. (2005); Maria et al. (2006); Marcari et al. (2007); and Almusallam and Al-Salloum (2007).

Most of these researchers have used EB FRP strips and sheets to strengthen against diagonal cracking. These researchers have aligned the FRP strips/sheets in diagonal patterns, horizontal patterns, vertical patterns, and orthogonal grid patterns. Some examples are shown in Figure 2.8. The results from these tests have shown that EB FRP strips and sheets are effective at restraining the opening of diagonal cracks and increasing the shear strength of the wall. The common failure modes of these tests were: debonding of the FRP from the wall; FRP rupture; or failure of the masonry (provided that the reinforcement was strong enough). Observed failure within the masonry has included: crushing of the masonry (generally at the masonry toe) (Marcari et al., 2007; Corradi et al., 2002); crushing of masonry wall flanges (Schwegler, 1995); and separation of masonry leaves in a double-leaf masonry wall (Corradi et al., 2002). Failure has also been caused by cracking outside of the FRP reinforcement (Zhao et al., 2003).

In tests where debonding was observed, debonding of the FRP from the ma-

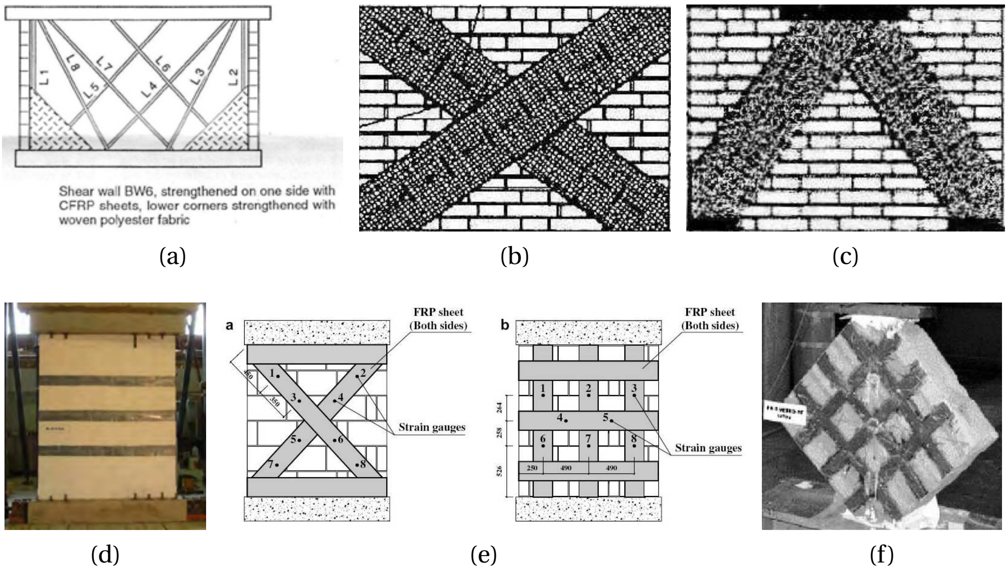

Figure 2.8: Strengthening schemes used by researchers to prevent diagonal cracking: a) Schwegler (1995), b) CFRP sheets Zhao et al. (2003), c) CFRP sheets Zhao et al. (2004), d) CFRP sheets Maria et al. (2006), e) CFRP/GFRP sheets Marcari et al. (2007), f) CFRP/GFRP sheets Valluzzi et al. (2002)

sonry occurred through a thin layer of brick underneath the EB FRP (Schwegler, 1995; Valluzzi et al., 2002; Marcari et al., 2007; Maria et al., 2006). Debonding generally originated at the crack openings and propagated, along the strips, away from the cracks (Marcari et al., 2007). The researchers have found that stiffer materials (such as carbon FRPs) and thicker materials were more susceptible to debonding (Valluzzi et al., 2002; Marshall and Sweeney, 2002; Marcari et al., 2007). When the FRP was not anchored, debonding usually resulted in brittle failure with a sudden decrease in wall load-carrying capacity (Valluzzi et al., 2002; Marshall and Sweeney, 2002; Maria et al., 2006). In some cases, however, debonding was progressive, and resulted in a gradual loss of strength (Maria et al., 2006). In some cases the EB FRP strips/sheets were anchored to the masonry or supporting structures. In these cases debonding of the FRP from the masonry did not cause wall failure because the load was still transferred through the end anchorages (Schwegler, 1995; Zhao et al., 2003, 2004). In these cases significant increases in strength and also ductility were achieved.

By externally bonding CFRP sheets in a diagonal X and Λ pattern to masonry walls (Figure 2.8b and Figure 2.8c respectively), Zhao et al. (2003, 2004) improved the in-plane lateral deformation of the masonry walls by 135-441% (depending on the pattern and width of EB sheet used). They also found that the area within the hysteresis curve (which reflects the energy dissipation capacity of the specimen) was larger for the strengthened wall. The improved deformation and energy dissipation capacity was a result of the FRP strengthening spreading the damage throughout the wall. Schwegler (1995) doubled the ductility of a masonry wall using diagonally aligned FRP strips that were mechanically anchored to concrete slabs above and below the wall. The increase in ductility was a result of the FRP preventing the brittle diagonal cracking failure mode, spreading damage throughout the wall, and forcing failure to occur by crushing in the masonry wall flanges.

A number of researchers have also investigated the effect of single-sided (or non-symmetric) strengthening. Detrimental effects of single-sided strengthening have been observed by Valluzzi et al. (2002), who used the Diagonal Tension/Shear Test (ASTM E519-93) ASTM Standards (1993) to test the specimens. A specimen from Valluzzi et al. (2002) is shown in Figure 2.8f. Valluzzi et al. (2002) observed that when the FRP reinforcement was applied to only one side of the wall, significant out-of-plane deformation occurred. This out-of-plane deformation was characterised by bending about a single diagonal crack towards the reinforced side. They found that in these cases, the FRP reinforcement provided an insignificant increase in strength over the URM specimens. The out-of-plane displacement was likely exaggerated by the little restraint that this test provided (only at the top and bottom corners). In several other tests, however, where the walls had some form of restraint along the top and bottom edges, the effect of the non-symmetric reinforcement was not as severe. In many tests (e.g. Marshall and Sweeney (2002) and Chuang et al. (2003)) where single-sided reinforcement schemes were used, no out-of-plane deformation was reported. Schwegler (1995) compared the behaviour of a wall strengthened on only one side to the behaviour of a wall strengthened on both sides of the wall. Note that both of these walls had the same reinforcement ratio. Schwegler found that on the unreinforced side of the single side reinforced wall, a single diagonal crack formed that stepped through the mortar joints. On the strengthened side (of the single side reinforced wall) fine cracks perpendicular to the reinforcement were observed throughout the wall. The same behaviour was observed for the wall strengthened on both sides. The difference in strength and ductility between the wall strengthened on one side only and the wall strengthened on both sides was found to be negligible.

Externally bonded FRP sheets are also susceptible to buckling, when subjected to compression along their longitudinal axis. If the FRP is only externally bonded to the surface of a masonry wall, lateral restraint against buckling is only provided by the strength of the bond (perpendicular to the surface of wall). Once this bond strength is overcome the FRP can buckle and debond from the wall. Buckling and debonding of the FRP sheets in compression would adversely affect the behaviour of the FRP sheet when it is required to act in tension under a reversing seismic lateral load. For example: diagonal sheets are compressed when subjected to in-plane lateral load in one direction and then they are stretched in tension when the load reverses. Also, vertical sheets may be compressed near the toe of a wall when subjected to an in-plane lateral load in one direction. These sheets are then loaded in tension upon load reversal. Buckling of EB FRP sheets has been observed in tests performed by Marcari et al. (2007). In these tests the FRP sheets were bonded to the surface of the masonry wall in both an X and orthogonal grid arrangement. FRP buckling in one of the tests is shown in Figure 2.9.

Figure 2.9: Buckling of a compressed EB FRP sheet from Marcari et al. (2007)

Holberg and Hamilton (2002) and Hall et al. (2002) designed a hybrid strengthening system to improve the in-plane shear behaviour of masonry walls and piers. In their system FRP composites are designed to strengthen against in-plane shear and flexural failures within the wall, and ductile steel is used to connect the wall pier to the rest of the structure. To improve the in-plane behaviour of the wall the steel connections were designed to yield before the FRP ruptured (or debonded, if the FRP was not anchored into the steel connection). An example of the system is shown in Figure 2.10.

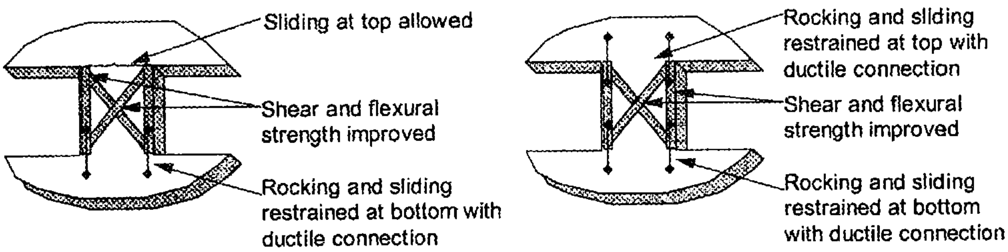

Figure 2.10: Ductile connection from Holberg and Hamilton (2002)

Holberg and Hamilton (2002) tested their system on unreinforced concrete masonry walls designed to fail by a rocking mode. Note that rocking has been shown to be an adequate failure mode of a masonry shear wall, considering ductility, stability and energy dissipation (Section 2.1). Holberg and Hamilton (2002) aimed to improve the behaviour further. They strengthened four unreinforced masonry walls with externally bonded GRFP sheets, used in combination with structural steel and reinforcing steel connections. They used vertical FRP sheets to strengthen against in-plane flexural failure within the wall and diagonally oriented FRP sheets to strengthen against in-plane shear type failures (such as diagonal cracking that developed as a result of the increased flexural strength). In general, the system was effective. The structural steel and reinforcing steel connections yielded and the in-plane rocking behaviour of the wall was improved, in terms of both strength and ductility. They concluded that, although the system was effective, further work was required on the design and detailing of the ductile connections.

FRP sheets covering the whole wall surface

The following researchers have strengthened masonry walls by externally bonding FRP sheets to the entire surface of the wall: Marshall and Sweeney (2002); Al-Chaar and Hasan (2002); Stratford et al. (2004); Hamid et al. (2005); and ElGawady et al. (2006, 2007). The most common fabric material used by these researchers has been GFRP. CFRP sheets have also been used by Marshall and Sweeney (2002) and aramid FRP (AFRP) sheets have been used by ElGawady et al. (2006).

Stratford et al. (2004) increased the sliding resistance of masonry walls using a bidirectional GFRP sheet bonded to the surface of the wall. In the strengthened walls, Stratford et al. (2004) found that as cracks developed in the masonry, the FRP sheet debonded from the surface of the masonry wall. The cracking through the masonry developed primarily along the mortar joints in a diagonal stepping pattern. The debonding progressed until the sheet was fully debonded and the FRP load was then transferred to the masonry via the end anchorages. The strengthened wall then transferred the in-plane shear load via a truss mechanism: diagonal tensile action through the GFRP reacted by vertical compression in the masonry (Figure 2.11). Stratford noted that the vertical load carried through the masonry is increased by truss action in the GFRP sheet. This increased vertical load increases the friction and hence sliding resistance along the mortar joints. The GFRP strengthening increased the shear strength of the walls by approximately 65% (compared to the URM walls). Both the unstrengthened and strengthened walls displayed the same amount of ductility.

ElGawady et al. (2006) recommended full surface cover over X-type configurations for retrofitting pre-damaged walls. They found that the existing cracks in the pre-damaged walls influenced the results of the walls retrofitted with sheets in an X-type pattern. The existing cracks did not, however, affect the results of the wall retrofitted with FRP covering the full surface of the wall. In subsequent testing programmes ElGawady et al. (2007) therefore only used FRP sheets bonded to the entire surface of the wall.

ElGawady et al. (2006, 2007) retrofitted pre-damaged walls that originally failed in either a rocking or shear (diagonal cracking) failure mode. ElGawady et al. found that FRPs externally bonded to the whole surface of a wall improved the specimens' in-plane lateral resistance by a factor of 1.4 - 5.9 compared to URM. In most cases the retrofitted specimens failed by a rocking mode, with rupture/tearing of the FRP at the heel and crushing of the masonry at the toe. Sliding along the flexural cracks that developed at the base of the wall usually accompanied rocking. The energy dissipation of the retrofitted specimens was higher than the unrein-

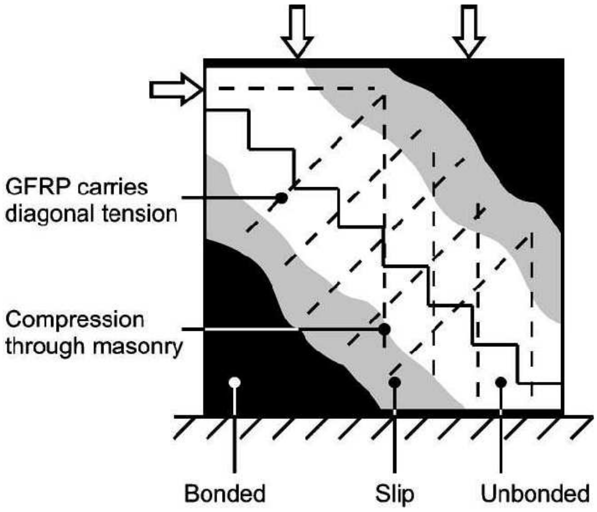

Figure 2.11: Truss mechanism of debonded FRP sheet Stratford et al. (2004)

forced specimens. Most of the energy dissipation was due to rocking and sliding friction at the base of the wall after the FRP ruptured. They found that the most important function of the FRP retrofit was in holding the wall together, even at high drifts. It would seem that the same favourable behaviour would have occurred if the FRP was not anchored into the foundations.

In the majority of tests the FRP strengthening was applied to one side of the wall only (Marshall and Sweeney, 2002; Al-Chaar and Hasan, 2002; Stratford et al., 2004; ElGawady et al., 2006, 2007). No out-of-plane effects were observed, however, demonstrating the efficiency of a single side strengthening scheme for in-plane lateral loads.

2.5.2 Structurally repointed reinforcement

Several researchers have structurally repointed (SR) the horizontal mortar joints with FRP bars to prevent diagonal cracking in masonry shear walls. The results of these tests are provided in: Tinazzi and Nanni (2000); Tumialan et al. (2001); Li et al. (2005); and Turco et al. (2006). Turco et al. (2006) has also structurally repointed the vertical mortar joints in a stack-bonded wall. In the tests reported, GFRP bars with a diameter of 6.4 mm were used. The FRP bars were either inserted into every bed joint or in every second bed joint, on one side or both sides of the wall.

Tinazzi and Nanni (2000) strengthened clay brick masonry walls, whereas the other researchers strengthened CMU walls. The wall specimens measured 0.6 m by 0.6 m (Tinazzi and Nanni, 2000), and approximately 1.6 m by 1.6 m (Tumialan et al., 2001; Li et al., 2005; Turco et al., 2006), respectively. Tinazzi and Nanni (2000) tested their walls using the Diagonal Tension/Shear Test (ASTM E519-93) ASTM Standards (1993). The other researchers used a similar test setup, except that the wall specimens were tested in an upright position with the diagonal load applied using a hydraulic jack in a closed loop system.

The results from the tests have shown that SR GFRP bars are effective at restraining the opening of diagonal cracks in the walls. Failure of these walls was commonly caused by debonding of the SR GFRP bars from the masonry, with debonding occurring at the masonry-paste interface. Significant increases in shear strength and ductility have been reported when the GFRP bars were inserted into every bed joint. The following increases in shear strength were reported (compared to URM): 45% (Tinazzi and Nanni, 2000); 100% (Tumialan et al., 2001); 80% (Li et al., 2005); and 150% (Turco et al., 2006).

When SR GFRP bars were not inserted into every mortar joint, sliding failure usually occurred along an unstrengthened joint. The researchers have therefore recommended that the reinforcement be used in every bed joint. Even though the SR GFRP reinforcement does not cross the mortar joint vertically, it does increase the resistance to sliding along a single bed joint. This is because the bond between the embedding paste (usually epoxy) and the masonry unit is stronger than the bond between the mortar and the masonry unit. Sliding along a strengthened bed joint may still occur, but at a higher load (Tinazzi and Nanni, 2000).

When the SR FRP reinforcement was not equally distributed on both sides of the wall, out-of-plane deformation was observed. This out-of-plane deformation was characterised by crack opening on the unreinforced side of the wall, and bending towards the reinforced side of the wall. Turco et al. (2006) observed significant out-of-plane displacement when the GFRP bars were embedded in the epoxy; but not when the bars were embedded in the modified cement paste. They suggested that the lower bond strength and stiffness of the modified cement joint reduced the out-of-plane effects. Li et al. (2005) reported that out-of-plane deformation did not affect the maximum load-carrying capacity of walls strengthened with SR GFRP in epoxy, but noted that the out-of-plane deformation affected the stability of the walls.

Corte et al. (2008) used structurally repointed (SR) CFRP strips to strengthen masonry in-fill panels in a real two storey reinforced concrete building. Corte et al. performed two lateral-loading inelastic tests on this building. The lateral load was distributed between the first and second floors and was applied in pushing and pulling cycles. The first test was performed on the original building (unstrengthened) and resulted in extensive damage to the in-plane masonry in-fill panels and reinforced concrete columns and staircase. The main failure mode observed in the in-plane masonry panels was diagonal tension cracking. At the end of the test the damage at the first storey was extensive, with out-of-plane collapse of almost all of the in-plane masonry panels. Corte at al. then partially repaired the damaged building. The perimeter columns were repaired and the external in-plane masonry walls were rebuilt and strengthened with structurally repointed CFRP strips. The CFRP strips were 1.5 mm thick and 5 mm wide and were structurally repointed into every bed joint. The FRP strengthening changed the failure mode of the masonry infill panels from diagonal cracking to shear sliding. As the building was only partially repaired the strengthening effect (in terms of an increase in load or displacement) can not be isolated. The maximum lateral strength of the partially repaired building (second test) was 60%/50% (pushing cycle/pulling cycle) lower than the strength of the original building.

Tests on strengthening of masonry panels with structurally repointed FRP strips have also been reported by De Lorenzis et al. (2004). They strengthened calcareous stone masonry panels with SR CFRP strips in every second bed joint (applied to one or both sides of the wall), and tested the panels in diagonal tension. They found that the strengthening technique could be effectively used for the in-plane strengthening of walls when sliding of the mortar bed joints (across several courses) is the controlling mechanism of the URM wall. The strengthening technique provided an increase in strength, but did not provide an increase in the stiffness nor ductility.

2.5.3 Near-surface mounted reinforcement

To the author's knowledge, Marshall and Sweeney (2002) are the only researchers that have used NSM FRP strips to improve the in-plane behaviour of a masonry wall. Note, however, that the tests on the walls strengthened with NSM FRP strips were not the only focus of their investigation. They were only part of a much larger investigation.

Marshall and Sweeney (2002) conducted 53 in-plane, cyclic shear tests on unreinforced double leaf masonry walls and lightly reinforced single leaf concrete masonry unit (CMU) walls. Of the 53 walls tested, only four walls were strengthened with NSM reinforcement. Of these four walls, two (1 clay brick and 1 CMU) were strengthened with NSM carbon strips, that were 2.3 mm thick and 15.2 mm wide. The other two walls (clay brick and CMU) were strengthened with NSM glass bars with a diameter of 6.4 mm. The majority of the walls (38 in total, leaving 11 URM walls) were strengthened with either discrete EB strips (arranged in different patterns) or EB sheets covering the entire surface of the wall.

Marshall and Sweeney expected that the vertically aligned NSM reinforcement (strips and bars) would not be effective at preventing diagonal cracking. They also expected the improvement to bed joint sliding would be insignificant. They did, however, expect that the vertically aligned NSM reinforcement would be effective against rocking. They therefore arranged the NSM FRP reinforcement along the vertical borders of the walls to prevent rocking.

The authors reported strength increases of approximately 20 kN (clay brick) and 40 kN (CMU) when the CFRP strips were used. The authors reported a strength increase of approximately 20 kN (clay brick) and a strength decrease of 10 kN (CMU) when glass bars were used. Note that the authors did not report the strength of the unreinforced specimens, nor did they report a percentage increase in load compared to the unreinforced specimens. As these tests were part of a larger testing program, the individual failure modes of these walls were not reported. Given that the failure mode of the URM specimens was either rocking or diagonal cracking, it is likely that the NSM FRP strengthened walls failed by diagonal cracking.

As well as strengthening walls with SR bars (Section 2.5.2), Tinazzi and Nanni

(2000) also strengthened walls with vertical NSM GFRP bars. They found that this strengthening method prevented bed joint sliding and diagonal cracking, and increased the wall load capacity and ductility (by a similar amount as the horizontal reinforcement). Unlike the horizontally reinforced wall, where damage was spread throughout the wall, damage was localised with the development of one large diagonal crack. Failure of this wall occurred by debonding of the FRP from the masonry at the epoxy-masonry interface (similar to horizontally reinforced walls), which allowed the diagonal crack to open.

2.6 FRP-to-masonry bond characterisation tests

2.6.1 Pull tests

The tensile behaviour of FRP reinforcement (be it EB laminates, NSM bars or strips, or structurally repointed (SR) bars) is usually governed by the debonding behaviour of the joint. To accurately predict the behaviour of an FRP strengthened/retrofitted URM wall subjected to in-plane (or out-of-plane) loads the behaviour of the FRP-to-masonry bond in shear needs to be determined. This is particularly the case where the FRP reinforcement is not mechanically anchored to the wall or supporting structures.

The bond behaviour is generally characterised experimentally using the pull test. The test involves subjecting the FRP reinforcement, which is bonded to a masonry prism, to a direct tensile force (Figure 2.12). This results in the FRP-to-masonry interface being loaded in shear. In Figure 2.12b lateral restraint provided at the top and bottom. The restraint at the top is provided by friction from a plate applying the compressive force. Some other alternatives to the pull test have also been used by researchers to determine bond behaviour. These include double-lap shear tests and modified beam tests (Chen and Teng, 2001; Yao et al., 2005).

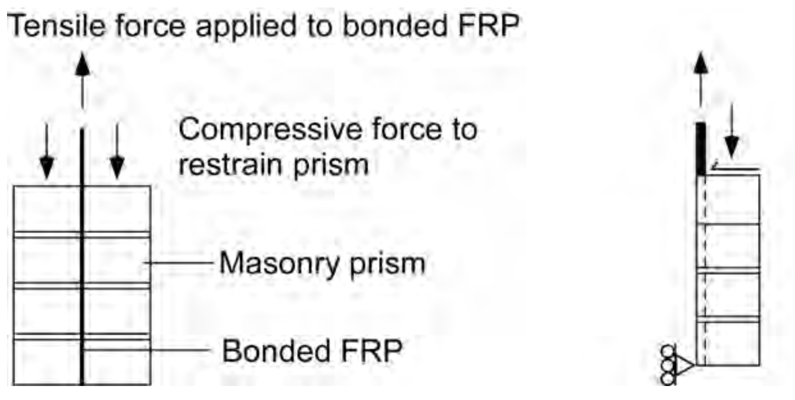

(a) Front view (b) Side view

Figure 2.12: Typical pull test (NSM strip application shown)

The information that can be gathered from the pull test includes the bond strength, the critical bond length and the local bond-slip relationship of the debonding interface. Properties such as the bond strength and critical bond length may be used directly in simple analytical models to predict the strength of structures that are reinforced with FRPs. The local bond-slip behaviour represents the fundamental behaviour of the FRP-to-masonry interface. This relationship may be used in finite element models to predict the behaviour of an FRP reinforced structure.

Examples of pull test investigations on EB FRP-to-masonry connections are provided in: Aiello and Sciolti (2006, 2008); Camli and Binici (2007); Willis et al. (2008). Willis et al. also studied the bond behaviour of NSM FRP-to-masonry connections. In these investigations the FRP has been bonded to different masonry substrates, including: hollow clay bricks (from Australia and from Turkey); and natural stones (Naples Tuff and Leccese Stone) used to construct masonry in Italy. The variables investigated in these studies include: surface preparation; FRP material and geometry; and location of FRP in relation to perpend joints and brick cores.

In general, the majority of pull tests have been performed on FRP-to-concrete joints. Research on the bond behaviour between the FRP and concrete is now at a stage where analytical models have been developed to predict the important bond properties such as bond strength, critical bond length and the local bond-slip relationship (Seracino et al., 2007b). Due to material similarities between concrete and masonry (particularly comparable tensile strength and brittleness), results of pull tests on FRP bonded to concrete are generally transferable to FRP bonded to masonry. In terms of a NSM FRP bond, the variables that affect the bond behaviour include the: concrete strength; bond length; FRP reinforcement cross-section dimensions; material properties of the FRP reinforcement; strength of the adhesive; distance between the FRP reinforcement and concrete edge; and distance between multiple, parallel FRP reinforcement (Seracino et al., 2007a,b; Oehlers et al., 2008; Rashid et al., 2008).

2.6.2 FRP strengthened masonry triplets and assemblages

Apart from the pull test, other tests on FRP strengthened masonry assemblages have been used to characterise the composite behaviour between FRP and masonry. Ehsani et al. (1997) investigated the contribution of externally bonded FRP sheets to the shear strength across a sliding joint. They conducted thirty-seven direct shear tests on triplet specimens strengthened with bidirectional GFRP sheets (Figure 2.13). They varied the strength, bonded length and fibre orientation. The strength of the FRP sheet was varied by using different FRP materials with different glass fibre densities. The fibres were orientated at either 0/90 degrees or 45/135 degrees, with respect to the loading direction. A lubricated piece of plywood was placed between the bricks (instead of bonding the bricks together with mortar) to simulate a frictionless joint. Also, no precompression was applied to the triplet specimens, and therefore the shear resistance of the joint was only provided by the GFRP laminate.

Ehsani et al. (1997) observed two failure modes: shear failure (of the GFRP) along the bed joint; and/or debonding of the GFRP laminate in the middle brick

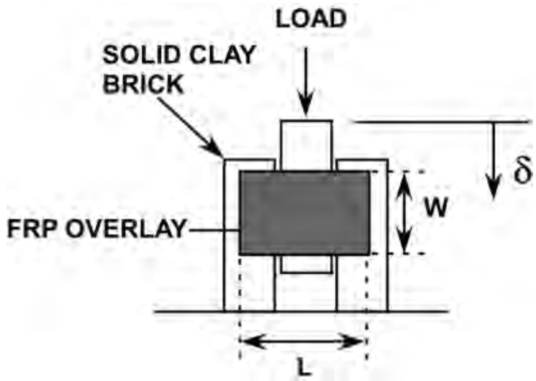

Figure 2.13: Ehsani et al (1997) FRP strengthened triplet test specimen

region of the fabric edges. These failure modes were influenced by the strength and bonded length of the GFRP sheets. For strong GFRP sheets debonding typically occurred, whereas for weak GFRP sheets, shear failure occurred. Weak GFRP sheets with a short bonded length failed in a combination of shear and debonding.

The fibre orientation was shown to have an effect on the strength and stiffness of the specimens. When the fibres were aligned at 45 degrees and 135 degrees a stiffer response was observed with a higher load. When the fibres were aligned at 0 degrees and 90 degrees a more ductile response was observed. The shear capacity of the specimens was approximately 18 kN. This equated to an average shear strength of 0.57 MPa for solid bricks with a contact area of 102 mm x 152 mm, used in the tests (Ehsani and Saadatmanesh, 1996).

Hamid et al. (2005) conducted a variety of tests to study the in-plane behaviour of URM wall assemblages strengthened with FRP laminates. The assemblages were tested under different stress conditions present in masonry shear and infill walls. The tests included prisms loaded in compression, with different bed joint orientations (on/off axis compression), diagonal tension specimens, and specimens loaded under joint shear (Figure 2.14). The masonry wall assemblages were constructed using face shell bedded hollow concrete blocks. The assemblages were strengthened on both sides with externally bonded GFRP sheets, covering the whole surface.

Hamid et al. (2005) found that the behaviour of the masonry assemblages that failed by shear sliding (specimens tested in direct shear, diagonal tension and 30 degrees/ 45 degrees off-axis compression) was significantly improved with FRP strengthening. Instead of brittle shear sliding, the strengthened specimens failed by crushing or web splitting of the masonry units (which was a more ductile failure mode). The greatest increase in strength was that for the direct joint shear assemblages. The average joint shear strength of these strengthened specimens was eight times greater than that of the unreinforced specimens. For the specimens tested in diagonal tension an increase in strength of 4.6 times the unreinforced case was reported. The assemblages that failed in compression (by web splitting) were least improved using the FRP laminates in terms of strength. The FRP laminates did,

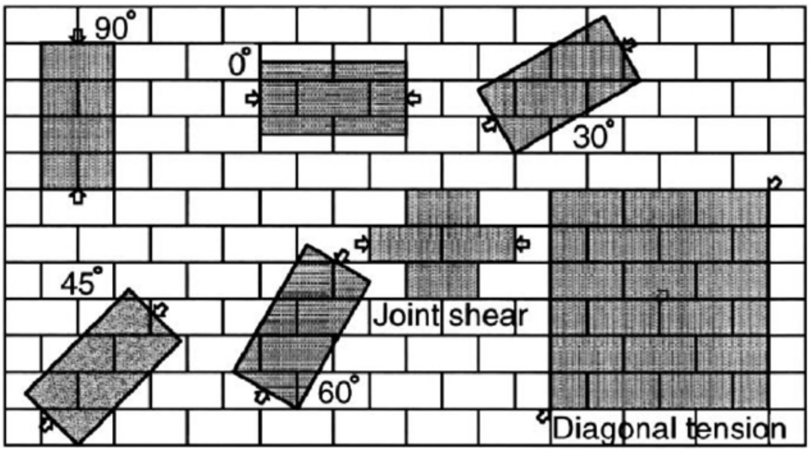

Figure 2.14: Assemblages tested by Hamid et al. (2005) as parts of a wall

however, provide stability to the shells of the masonry units after the webs had split.

Similar investigations have been performed by El-Dakhakhni et al. (2004) (joint shear and compression specimens) and Campanaro et al. (2005) (joint shear specimens).

2.7 Finite element models for FRP reinforced masonry

Advanced structural modelling (using numerical techniques) is necessary for understanding the behaviour and damage of complex masonry constructions, understanding experimental testing programs and to assist in the development of design rules (Lourenço, 2008). This is also the case for masonry structures that are reinforced with FRPs. The displacement finite element method is the most common numerical technique used to model the behaviour of masonry structures (with and without FRP reinforcement). Other numerical approaches such as limit analysis (Grande et al., 2008) and the discrete element method (Zhuge, 2008b) have also been used.

To accurately model the behaviour of an FRP strengthened masonry wall, the structural response and failure modes of the masonry, FRP reinforcement and the interface between them (bond) need to be considered.

2.7.1 Modelling masonry

Masonry is a composite material that is composed of brick units and mortar joints. Masonry displays distinct directional properties due to the presence of mortar joints, which act as planes of weakness. The overall behaviour of masonry is determined by the properties of the masonry components (unit, mortar and unit/mortar interface) and the orientation of the unit/mortar interfaces (Sutcliffe et al., 2001). The behaviour of masonry is therefore complex. Two different approaches are used to model masonry, depending on the level of simplicity and accuracy desired. They are the micro-modelling approach and the macro-modelling approach (Figure 2.15, Lourenço (2008)).

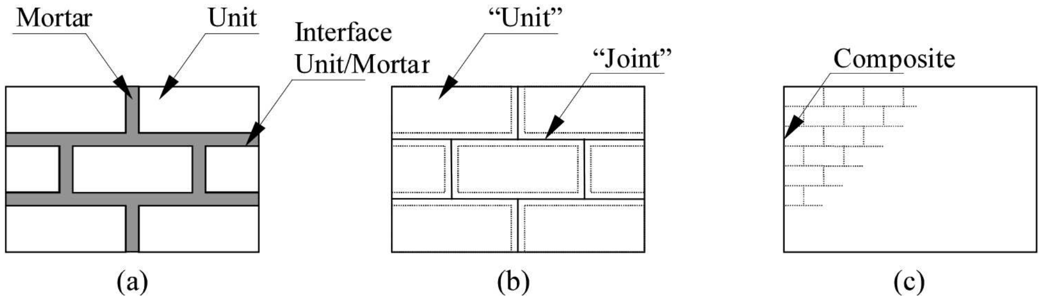

Figure 2.15: Modelling strategies for masonry structures (Lourenço 2008): a) detailed micro-modelling; (b) simplified micro-modelling; (c) macro-modelling

Micro-modelling

In the micro-modelling approach the individual components of the masonry assemblage are modelled separately. Depending on the level of accuracy and simplicity desired the following micro-modelling strategies may be used (Lourenço, 2008):

Detailed micro-modelling: in which the units and the mortar in the joints are represented by continuum elements and the unit/mortar interface are represented by discontinuum elements;

Simplified micro-modelling: in which expanded units are represented by continuum elements and the behaviour of the mortar joints and the unit/mortar interface is lumped into discontinuum elements. In this approach the units are expanded to retain the initial geometry of the masonry assemblage.

Zero-thickness interface elements (a type of discontinuum element) are normally used for the interfaces. Interface elements relate the interface stresses (normal stress and shear stress) to the relative displacements across the interface (normal displacement and shear displacement). Contact elements, which are a special kind of interface element, have also been used to model the interfaces (Han, 2008).

A complete micro-model needs to include all of the failure mechanisms of masonry including: joint cracking in tension; joint sliding; cracking of the units; and crushing of the masonry. Micro-models that incorporate these failure mechanisms (with post peak softening included) are able to reproduce crack patterns and the complete load-displacement path of a masonry structure up to and beyond the peak load (Lourenço, 2008).

The material properties required for the micro-model are determined from experimental tests on masonry joints and assemblages. A detailed description on the types of tests used to determine the material properties is provided in Rots (1997). Some recommendations on the typical material properties to use in a masonry micro model are given in Lourenço (1996a, 2008).

Macro-modelling

In the macro-modelling approach all of the components of the masonry assemblage (the brick units, mortar joints, unit/mortar interface) are smeared into a homogeneous continuum. The continuum is commonly modelled with orthotropic material behaviour to account for the directional properties of masonry. The material stress-strain behaviours are determined from experimental tests on masonry assemblages (for example the biaxial tests of Page (1983)), or using a process known as homogenisation. Homogenisation involves using analytical micro-models of small masonry assemblages to determine the combined response. A review of homogenisation techniques is provided in Lourenço (2008).

The macro-modelling technique is unable to model local failure modes (unlike the micro-modelling technique). The macro-modelling technique is, however, suitable for modelling large sections of masonry, where only a simplified representation of composite behaviour is required, and local failure modes are not so important.

For FRP strengthened structures, local failure modes of the masonry (particularly cracking) are important because debonding starts at the opening of cracks. As such, a macro-model (which can not reproduce detailed local crack patterns) may not be able to simulate local debonding behaviour (Grande et al., 2008). On the other hand, a micro-model (which can capture detailed local crack patterns) would be able to simulate local debonding behaviour.

2.7.2 Modelling FRP and attachment to masonry

FRP reinforcement can be modelled with tension only elements (such as truss elements for thin reinforcements), or other continuum elements (such as typical quadrilateral elements) for fabric sheets. To model debonding of the FRP from the masonry a discontinous element (such as an interface element) is modelled between them. The debonding behaviour of the interface element is characterised by a local bond-slip relationship determined from pull tests (Section 2.6.1).

2.7.3 Examples of FRP strengthened masonry models from the literature

Several authors have used finite element models (or related approaches - limit analysis and the discrete element method) to predict the in-plane behaviour of FRP strengthened masonry walls: Ascione et al. (2005); Van Zijl and de Vries (2005); Verhoef and van Zijl (2002); Zhuge (2008b); Grande et al. (2008); Haroun and Ghoneam (1996, 1997); Gabor et al. (2005, 2006); Farshchi and Marefat (2008); Engebretson et al. (1996); Prakash and Alagusundaramoorthy (2006).

Debonding of the FRP from the masonry was considered in only a few of these models (Ascione et al., 2005; Van Zijl and de Vries, 2005; Zhuge, 2008b; Grande et al., 2008). Both Zhuge (2008b) and Grande et al. (2008) verified their models with experiments where debonding was a failure mode (these investigations are discussed in more detail below). Conversely, Ascione et al. (2005) and Van Zijl and de Vries (2005) did not. Ascione et al. (2005) used their model to perform simulations on hypothetical structures, including a 3-storey FRP strengthened masonry wall with openings. As the model was not verified against experimental data, the results of the analysis were qualitative in nature. The model results did, however, highlight the importance of the bond strength between the FRP and the masonry. On the other hand, Van Zijl and de Vries (2005) did verify their model with experimental results, but in both the experiment and the model debonding was not observed.

Zhuge (2008b) used a micro-modelling approach, based on the distinct element method (DEM) (a special version of the discrete element method), to simulate the behaviour of a masonry shear wall strengthened with EB CFRP strips (Figure 2.16a). To model the debonding interface between the masonry and the FRP, Zhuge used an interface type element, with an elastic-perfectly plastic bond-slip relationship. The bond-slip relationship used in the interface elements was taken from pull tests on CFRP-to-concrete joints conducted by Ueda and Dai (2004). Zhuge used this data as there was not enough pullout test data available for masonry at the time the work was conducted. In general, Zhuge's model was capable of simulating the behaviour of the experimental walls, well into the non-linear range of the test (Figure 2.16b). Zhuge noted, however, that as the bond strength was assumed to behave as an elastic-perfectly plastic material, the descending branch of the load-displacement curve could not be simulated by the model. (It seems that Zhuge omitted the descending data from the experimental plot in Figure 2.16b.)

(a)

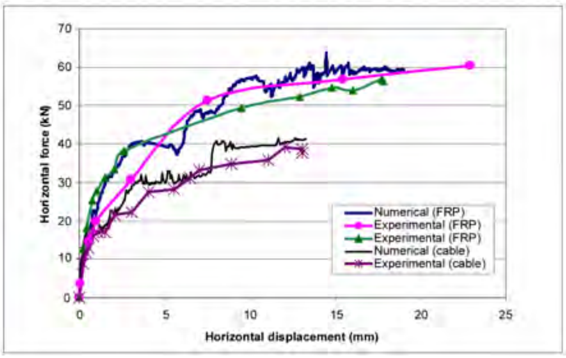

(b)

Figure 2.16: Zhuge (2008b): (a)FRP reinforced wall; (b)Lateral load-deflection diagram comparison

Grande et al. (2008) used both a macro-modelling approach and a homogenised limit analysis to simulate the behaviour of un-strengthened and FRP strengthened masonry panels, supported on beams (Figure 2.17). They noted that the limit analysis approach is based on the use of a perfectly plastic material response of the masonry and the FRP-to-masonry interface. It therefore cannot model softening behaviour and may not be as suitable for the analysis of FRP strengthened masonry structures as displacement FE methods. They did find, however, that the loads and failure mechanisms, predicted by the limit analyses, were similar to the experimental results in some cases (Figure 2.18).

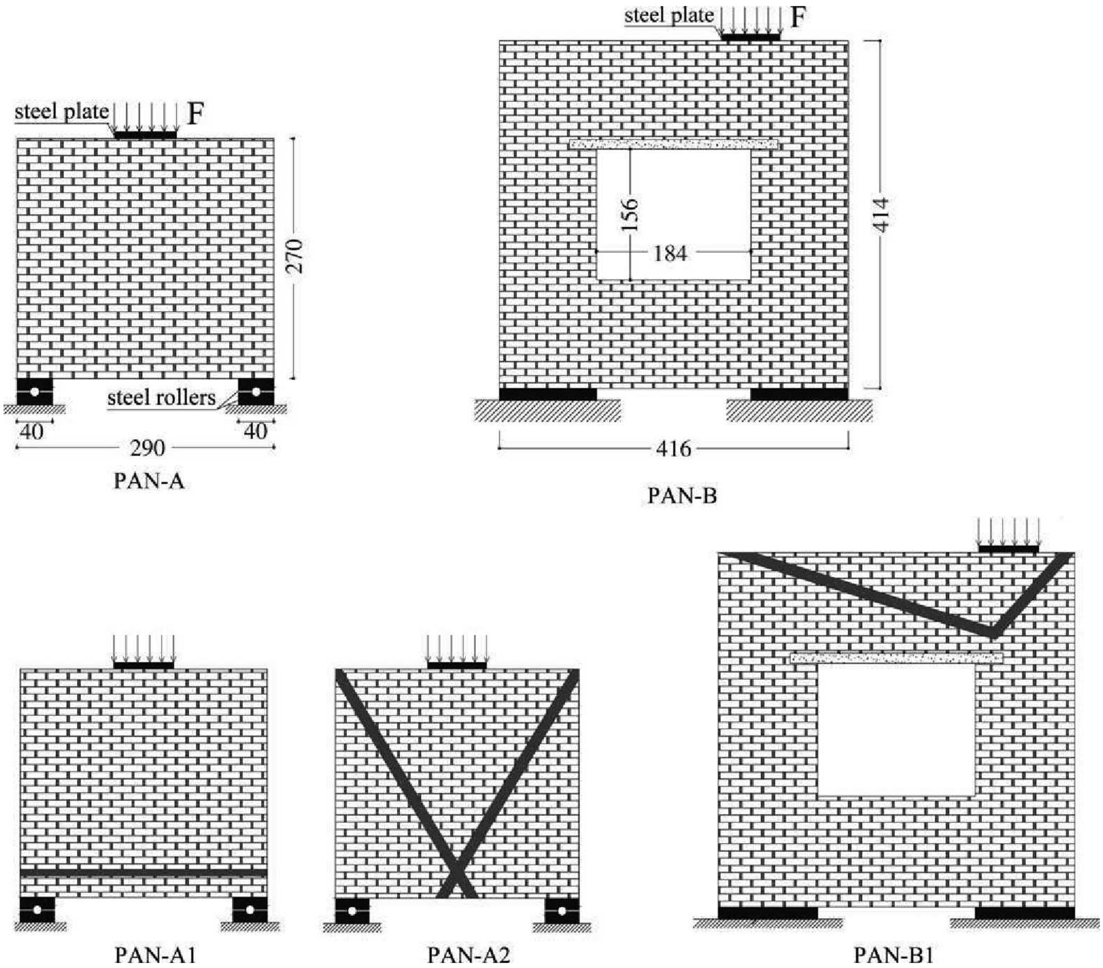

Figure 2.17: Wall panels modelled by Grande et al. (2008)

In the finite element macro-model, Grande et al. (2008) attached the nodes of the FRP elements (modelled using truss elements) perfectly to the corresponding nodes of the masonry elements. To account for debonding of the FRP from the masonry they treated the FRP truss elements as an elastic-brittle material. They limited the tensile strength of the FRP truss elements, based on the maximum FRP debonding strength given in CNR-DT200 (2006). The authors decided not to use interface elements (with a local bond-slip relationship) because there was not enough experimental data on the complex behaviour of the FRP-to-masonry interface. In particular, there was not enough experimental data taking into account the heterogeneity of the masonry. The authors agreed that a more representative model would include the use of interface elements. They did, however, demonstrate that their simplified approach was capable of reproducing the experimental pre- and post-peak behaviour (including debonding) with a good level of accuracy (Model MRB in Figure 2.18). They also performed simulations where debonding was not accounted for. In these cases the model was found to over predict the strength of the FRP strengthened walls (Model MRA in Figure 2.18).

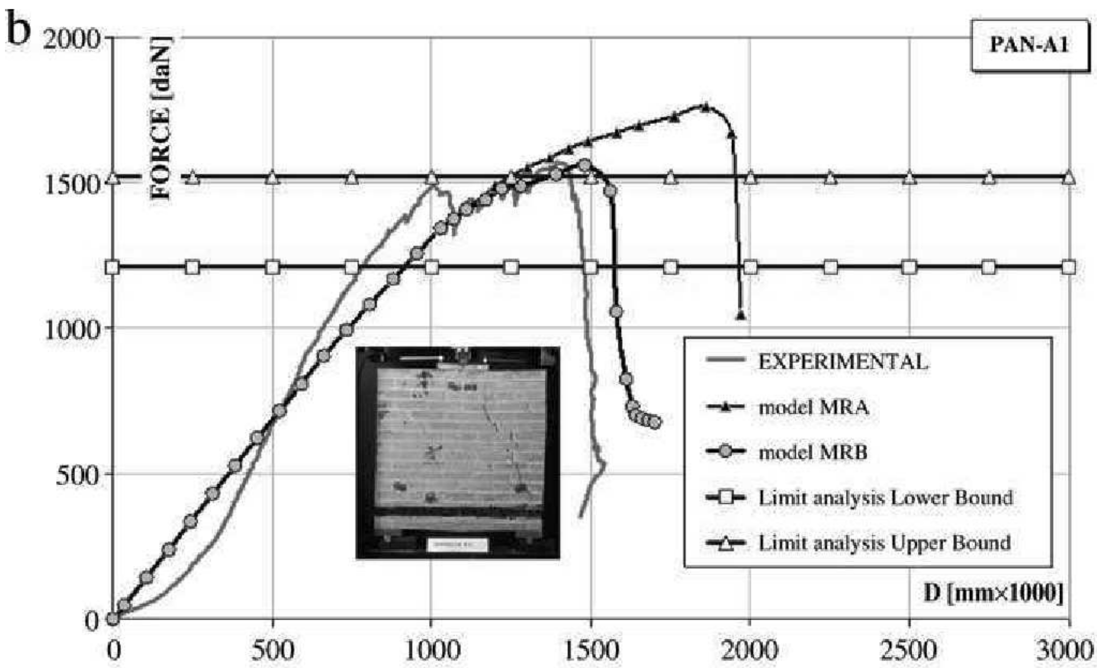

Figure 2.18: Results of PAN-A1: MRA - no debonding; MRB - debonding. Grande et al. (2008)

In the remaining modelling investigations (previously cited) debonding was not accounted for in the model. However, in many cases it was not critical, because debonding was not a critical failure mode. Take for example the investigation by Gabor et al. (2005, 2006). They did not include debonding of the FRP in their models, but this did not affect their results. It did not affect their results because debonding was not observed in the experimental tests that they used to verify their models. In this case the authors fixed elastic FRP elements directly to the elements of the underlying masonry walls (perfect bond).

Gabor et al. (2005, 2006) used their finite element model to simulate the behaviour of FRP strengthened walls that were tested in diagonal tension. To model the masonry they used a micro-modelling approach. They modelled both the brick units and the mortar joints separately, with continuum elements. They modelled the bricks as fully elastic and used an elastic plastic model in the mortar joint to represent the non-linear behaviour of the brick/mortar interface in shear. In general, their model reproduced the key behaviours observed in the experimental tests, including the strengthening effect of the EB FRP reinforcement schemes. In particular, the FRP restrained the opening of a single diagonal crack (unreinforced wall failure mode), and changed the failure mode to crushing in the diagonal corners of the wall. The load displacement response and the ultimate loads produced by their model also compared well with the experiments. In one of the strengthened wall tests, the wall failed once a crack formed outside of the reinforcement, in line with the diagonal load. This failure mode was not reproduced by the model.

2.8 Analytical models

Several design models have been proposed for the design of FRP strengthened masonry shear walls. Models exist for walls strengthened with:

- Discrete EB sheets/strips: Triantafillou (1998); Triantafillou and Antonopoulos (2000); Nanni et al. (2003); Zhao et al. (2003, 2004); CNR-DT200 (2006); AC125 (2007)
- Bars: Li et al. (2005); Tinazzi and Nanni (2000); Tumialan et al. (2001), and
- Sheets covering the whole surface of a wall: Stratford et al. (2004).

The models are based on the truss analogy and assume the total in-plane shear strength of an FRP strengthened wall is equal to the sum of the contributions of the masonry wall (V_m) and the FRP reinforcement (V_f):

$$V = V_m + V_f \tag{2.1}$$

The contribution of the masonry wall (V_m) is assumed equal to the in-plane shear strength of an unreinforced masonry wall. The contribution of FRP reinforcement (V_f) is taken as the horizontal component of the FRP tensile force, which depends on the failure mode (rupture or debonding) and the anchorage length. The contribution of the vertical reinforcement is usually ignored (e.g. Triantafillou (1998)). Stratford et al. (2004) does consider it, however (see Section 2.8.2).

The truss model is based on lower bound plasticity theory, and relies on stress redistribution. If brittle reinforcement is used (such as FRP), with little or no stress redistribution, the lower bound plasticity theory is no longer applicable (Stratford and Burgoyne, 2003). Therefore the truss model may not be suitable for FRP strengthened masonry structures.

A select number of models are discussed in more detail in the following sections. A review of some of the design models has also been given in Zhuge (2008a).

2.8.1 Externally bonded discrete strips/sheets

Triantafillou (1998); Triantafillou and Antonopoulos (2000) model

Triantafillou (1998) proposed a model to determine the in-plane shear resistance of masonry walls strengthened with discrete strips arranged in an orthogonal grid pattern (Figure 2.19).

In Triantafillou's (1998) model the in-plane shear capacity of the FRP strengthened wall is limited by the shear/compressive strength of the masonry (as per Eurocode 6 (1994)):

$$V = V_m + V_f \leq \frac{0.3 f_k t d}{\gamma_m} \tag{2.2}$$

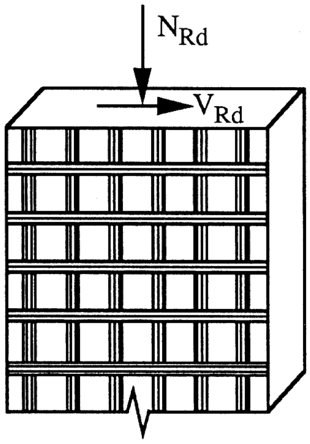

Figure 2.19: FRP strengthened masonry wall subjected to in-plane shear with axial force from Triantafillou (1998). Note V_{RD} in figure is same as V in Equation 2.1

.

where f_k is the characteristic compressive strength of masonry, t is the thickness of the wall, γ_m is a partial safety factor for masonry, and d is the effective depth of the wall = 0.8 x the wall length (l).

The contribution of masonry is determined using the URM shear strength equations given in Eurocode 6:

$$V_m = \frac{f_{vk} t d}{\gamma_m} \tag{2.3}$$

where f_{vk} is the characteristic shear strength of the masonry, given by:

$$f_{vk} = min[f_{vk0} + 0.4\frac{N_{Rd}}{lt}, 0.7 f_{vk,lim}, 0.7 max(0.065 f_b, f_{vk0})] \tag{2.4}$$

where f_{vk0} is the characteristic shear strength of masonry under zero compressive stress (between 0.1 and 0.3 MPa in the absence of experimental results), N_{Rd} is the design vertical axial force acting on the wall, $f_{vk,lim}$ is the limiting value of f_{vk} and depends on the type of masonry units and mortar strength, and f_b is the normalised compressive strength of the masonry units.

In Triantafillou's (1998) model the contribution of vertical reinforcement to the shear strength of the masonry wall is ignored. Triantafillou (1998) comments that the vertical FRP reinforcement provides mainly a dowel action effect. The increase in shear strength provided by the dowel action effect is negligable because of the high flexibility of the FRP strips and local debonding in the vicinity of the shear cracks. The shear resistance mechanism is therefore provided only by the horizontal FRP strips.

The contribution of the horizontal FRP strips to the shear strength of the wall is calculated using:

$$V_f = \rho_h E_{frp}\left(\frac{\varepsilon_{frp,e}}{\gamma_{frp}}\right) t 0.9 d \tag{2.5}$$

where ρ_h is the horizontal reinforcement ratio, defined as the total cross-sectional area of horizontal FRP divided by the cross-sectional area of the wall in plan (tl), E_{frp} is the longitudinal elastic modulus of the FRP, γ_{frp} is a partial safety factor for FRP in uni-axial tension (1.15, 1.2 and 1.25 for CFRP, AFRP and GFRP respectively), and $\varepsilon_{frp,e}$ is the effective FRP strain. The effective FRP strain $\varepsilon_{frp,e}$ accounts for the failure mode of the FRP (debonding or rupture) and depends on the FRP axial rigidity $(\rho_h E_{frp})$. The effective FRP strain $\varepsilon_{frp,e}$ is calculated using:

$$\varepsilon_{frp,e} = 0.0119 - 0.0205(\rho_h E_{frp}) + 0.0104(\rho_h E_{frp})^2 \tag{2.6}$$

Equation 2.6 was developed through regression analysis of experimental data for concrete beams, and may not be suitable for masonry walls (Zhuge, 2008a). The expression for the FRP effective strain was later improved by the same author in Triantafillou and Antonopoulos (2000) to separate different failure modes (rupture or debonding) and types of materials (CFRP or AFRP):
Fully wrapped CFRP (failure by rupture of FRP):

$$\varepsilon_{frp,e} = 0.17\left(\frac{f_c^{2/3}}{E_{frp}\rho_h}\right)^{0.3} \varepsilon_{frp,u} \tag{2.7}$$

Side or U-shaped CFRP jackets (failure by debonding, failure by rupture of FRP):

$$\varepsilon_{frp,e} = min\left[0.65\left(\frac{f_c^{2/3}}{E_{frp}\rho_h}\right)^{0.56} \times 10^{-3}, \quad 0.17\left(\frac{f_c^{2/3}}{E_{frp}\rho_h}\right)^{0.3} \varepsilon_{frp,u}\right] \tag{2.8}$$

Fully wrapped AFRP (failure by rupture of FRP):

$$\varepsilon_{frp,e} = 0.048\left(\frac{f_c^{2/3}}{E_{frp}\rho_h}\right)^{0.47} \varepsilon_{frp,u} \tag{2.9}$$

where f_c is the compressive strength of concrete and $\varepsilon_{frp,u}$ is the ultimate FRP strain in uni-axial tension (failure by rupture). Similar to Equation 2.6, these equations were determined for FRP strengthened concrete beams, and may not be suitable for FRP strengthened masonry walls.

Zhao et al. (2003, 2004) model

Zhao et al. (2003, 2004) proposed a model to determine the shear resistance of masonry walls strengthened with externally bonded FRP sheets aligned in an X- and Λ-type pattern (Figure 2.20).

The contribution of masonry to the shear strength of the wall is assumed equal to the strength of a URM wall failing by diagonal cracking, which is calculated using (Tomaževič, 1999):

$$V_m = 0.9\frac{f'_{tb}}{b} A_n \sqrt{1 + \frac{\sigma_n}{f'_{tb}}} \tag{2.10}$$

where f'_{tb} is the tensile strength of masonry, b is a shear stress distribution factor = 1.2, σ_n is the average compressive stress in the wall due to vertical load, and A_n is the net cross sectional area of the masonry wall.

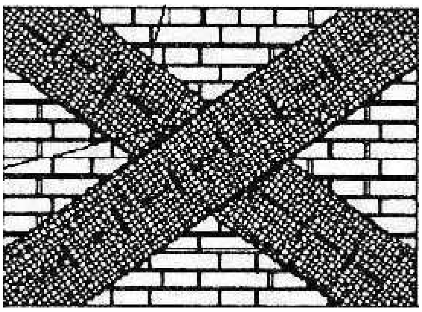

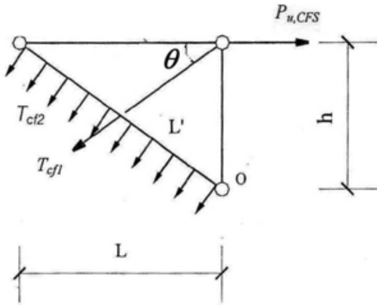

(a) X-pattern strengthening (b) Analytical model

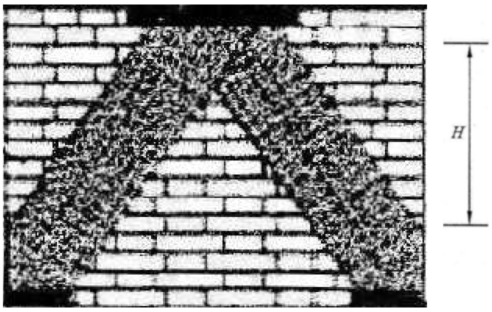

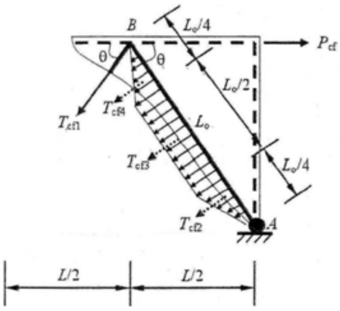

(c) Λ-pattern strengthening (d) Analytical model

Figure 2.20: Strengthening schemes and analytical models from Zhao et al. (2003, 2004)

The FRP sheets act as diagonal braces in a truss model. Only the sheets loaded in tension are considered to contribute to the shear strength of the wall. The tensile strength of biaxial FRP sheets in the transverse direction is also considered (Figure 2.20). The FRP contribution to the shear strength (V_f) is calculated using:

- X-strengthening, Zhao et al. (2003):

$$V_{fx} = n\alpha_{cfs}Et'(\varepsilon_1 bLsin\theta + 0.5\varepsilon_2 L'^2)/h \tag{2.11}$$

- Λ-strengthening, Zhao et al. (2004):

$$V_{f\Lambda} = nEt'(\varepsilon_1 bLsin\theta + 0.375\varepsilon_2 L_o^2)/H \tag{2.12}$$

where n is the number of FRP sheets, E is the elastic modulus of the FRP sheet, t' is the thickness of the FRP sheet, ε_1 and ε_2 are the strains in the longitudinal and transverse directions of the FRP sheets, b is the width of the FRP sheet, L is the length of the wall, $L'(or L_o)$ is the length of the FRP sheet, and $h(or H)$ is the height of the wall. The term α_{cfs} is a coefficient that takes into account the strength of the brick, the quality of the bond between the FRP and the masonry and whether anchors are used. No guidance on this coefficient is given, however. They assume a value of 1.0. This term is only applied in Zhao et al. (2003).

These models were verified with experimental results by Zhao et al. (2003, 2004). Reasonable agreement between the models and experiments were found when the experimentally recorded strains in the FRP sheets were used in the model. Note that these strains were not equal to the maximum tensile strains of the sheets. No guidance was given in order to determine the strains in the FRP strips for design purposes. These drawbacks strongly limit the models usefulness.

2.8.2 Externally bonded sheets covering the whole wall surface

Stratford et al. (2004) proposed a model for the design of masonry shear walls strengthened with an FRP sheet that covers the whole surface of the wall and is also mechanically anchored at the top and bottom. In Stratford et al. (2004)'s model it is assumed that the FRP is fully debonded from the wall and the forces in the FRP are transferred to the masonry via the end anchorages. The debonded FRP sheet acts in tension along a diagonal band (Figure 2.21).

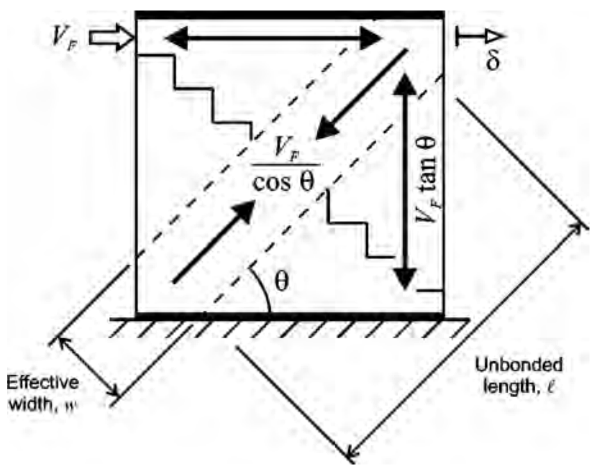

Figure 2.21: Truss mechanism for carrying load through debonded strengthening Stratford et al. (2004)

In Stratford et al. (2004)'s model the strengthened wall is designed to fail in shear/compression (in the masonry) rather than by FRP rupture. This design strategy is used because shear/ compression failure in the masonry is a more ductile failure mode than rupture of FRP. To ensure that FRP rupture does not occur before shear/compression failure in the masonry, the strain capacity in the FRP strip must be greater than ε_1:

$$\varepsilon_1 = \frac{\delta_1}{l cos\theta} \tag{2.13}$$

where δ_1 is the in-plane lateral displacement capacity of the unreinforced masonry, l is the unbonded length of the FRP (which is determined by the anchorage arrangements), and θ is the angle of inclination of the FRP band acting in tension.

The anchorages must also be able to resist the load carried through the FRP at failure of the masonry:

$$\frac{V_F}{cos\theta} = \frac{w t_f E_{f\theta}}{l}\delta_1 \tag{2.14}$$

where w is the effective width of the FRP sheet active in carrying tension, t_f is the thickness of the FRP sheet, and $E_{f\theta}$ is the elastic modulus of the sheet parallel to the tensile diagonal.

The vertical component of the diagonal tensile force, through the FRP sheet, increases the vertical compression through the masonry wall. This additional vertical compression is:

$$N_F = V_F tan\theta \tag{2.15}$$

The additional compression acts to confine the masonry and increase the unreinforced masonry strength that contributes to the overall shear strength of the wall (V'_M). The total shear strength of the wall is then:

$$V = V'_M + V_F \tag{2.16}$$

2.8.3 Structurally repointed reinforcement

Li et al. (2005) proposed a model to determine the shear resistance of masonry walls strengthened with horizontal structurally repointed (SR) FRP bars.

The contribution of masonry to the shear strength of the wall is based on the URM failure envelope developed by Mann and Müller (1982), with revisions by Crisafulli et al. (1995) (Figure 2.22a). The failure envelope incorporates the possible failure modes of URM walls subjected to a combination of shear and compression stresses. These include sliding along a single bed joint, stepped shear sliding failure, diagonal tensile cracking through the brick units and compression failure of the brick units.

The shear capacity due to sliding along a single bed joint ($V_{m,1}$) is determined by Equation 2.17:

$$V_{m,1} = (\tau_0 + \mu\sigma_n)A_n \tag{2.17}$$

where τ_0 is the cohesive strength of the mortar joints, μ is the coefficient of internal friction, σ_n is the normal compressive stress on the wall, and A_n is the cross-sectional net area of the masonry wall.

The shear capacity due to stepped shear sliding failure ($V_{m,2}$) is determined by Equation 2.18:

$$V_{m,2} = (\tau_0^* + \mu^*\sigma_n)A_n \tag{2.18}$$

where the cohesion and coefficient of internal friction are modified to account for the distribution of normal and shear stresses acting on a brick unit:

$$\tau_0^* = \frac{\tau_0}{1 + 1.5\mu b/d} \tag{2.19}$$

$$\mu^* = \frac{\mu}{1 + 1.5\mu b/d} \tag{2.20}$$

In these equations b and d are the length and height of the masonry unit, respectively.

The shear capacity due to diagonal tension cracking through the brick units ($V_{m,3}$) is determined by Equation 2.21:

$$V_{m,3} = \frac{f'_{tb}}{2.3}\sqrt{1+\frac{\sigma_n}{f'_{tb}}}A_n \tag{2.21}$$

where f'_{tb} is equal to the tensile strength of the masonry.

The shear capacity due to compression failure of the brick units ($V_{m,4}$) is determined using Equation 2.22:

$$V_{m,4} = (f'_m - \sigma_n)\frac{2d}{3b}A_n \tag{2.22}$$

where f'_m is equal to the compressive strength of the masonry. Note that this represents a limit on the shear strength of the masonry wall as the SR FRP bars cannot prevent this type of failure.

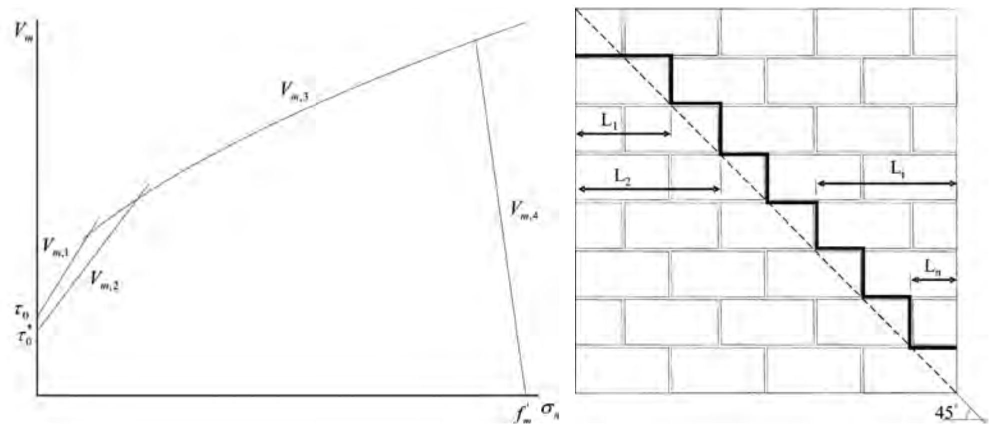

(a) (b)

Figure 2.22: (a)Failure envelope of URM wall Li et al. (2005); (b)Effective bond length of horizontal SR FRP bars Li et al. (2005)

The horizontal FRP reinforcement crossing a diagonal shear crack contributes to the shear resistance of the wall. In Li et al. (2005)'s model the reinforcement contribution of a horizontal bar depends on the bond strength between the paste (used to embed the bar into the bed joint) and the brick unit. This is because in experimental tests failure usually occurs by debonding along this interface (see Section 2.5.2). It is assumed that the bond stress between the paste and the brick unit is uniform along the length of the bar at ultimate bar stress. The force in the FRP bar resisting diagonal crack opening is then the average bond strength multiplied by the surface area between the paste and the masonry:

$$V_{f,1bar} = \tau_b(2D + t_m)L \tag{2.23}$$

where τ_b is the bond strength between the paste and the masonry, D is the depth of the groove, t_m is the thickness of the mortar joint and L is the shortest bonded length of the bar intersected by the crack (Figure 2.4). In the model a 45° degree diagonal shear crack is assumed in order to determine L (Figure 2.22b).

The tensile force in the bar is limited by using the principle of an effective length L_e, where $L \leq L_e$. The effective length is calculated using Equation 2.24:

$$L_e = \frac{f_u A_f}{(2D + t_m)\tau_b} \tag{2.24}$$

where f_u is equal to the maximum tensile stress in the FRP bar and A_f is the cross-sectional area of the FRP bars. In Li et al. (2005)'s model the maximum tensile stress in the FRP bar is based on the results of pull tests. In the pull tests the ultimate tensile stress in the FRP was related to cracking in the masonry unit (debonding through the brick). The ultimate tensile stress in the FRP may also be due to rupture.

It is assumed that the ultimate bond stress is reached in all of the bars at the ultimate load. The total contribution of the horizontal reinforcement is then equal to the sum of all the forces calculated in the bars crossing the shear crack:

$$V_f = \tau_b(2D + t_m)\sum_{i=1}^{n} L_i, \qquad L_i \leq L_e \tag{2.25}$$

where n is the total number of bars intersected by the diagonal crack, and L_i is the effective bond length of the i-th bar intersecting the diagonal crack (Figure 2.22b).

Li et al. (2005) verified this model with the test results of walls tested in diagonal tension (see Section 2.5.2). In these tests the reinforcement was inserted into every bed joint (on one side of the wall, or alternately on both sides of the wall) or in every second bed joint (on one side of the wall). Li et al. (2005) found that the model provided a reasonable fit to the experimental results, except that the model tended to overpredict the experimental ultimate load when the reinforcement was applied to one side only. For the walls strengthened with reinforcement in only every second joint, where failure occurred by sliding along an unstrengthened bed joint, the capacity of the wall was approximately equal to $V_{m,1}$ (Equation 2.17).

The model in Li et al. (2005) was also proposed in previous reports by some of the common authors in Tinazzi and Nanni (2000) and Tumialan et al. (2001), with some differences. In Tinazzi and Nanni (2000) rod pull-through failure was also considered as a potential failure mode (in addition to bond failure between the paste and epoxy). In Tumialan et al. (2001) rod pull-through failure was the only bar debonding failure mode considered. Tinazzi and Nanni (2000) also considered the effect of compressive stresses on the bond strength of the paste/unit sliding interface.

2.9 Research gaps and Proposed Work

2.9.1 Research gaps

The need to develop efficient techniques to retrofit (or strengthen) in-plane masonry shear walls was identified. In particular, retrofit techniques are required to increase the ductility and strength of walls failing by diagonal cracking (most critical) and mortar joint sliding within the wall. Also, retrofit techniques should have a low impact on function and appearance. Of the FRP application techniques reviewed the NSM technique is the most suitable.

As the NSM technique is a relatively new retrofitting technique, very few investigations on masonry strengthened using the technique have been conducted. Therefore, there is a need to do substantial experimental and numerical work to investigate the effectiveness of this new technique and to investigate the behaviour of walls strengthened using this technique.

The specific research gaps are identified as follows:

Characterisation tests

Information on NSM FRP-to-*concrete* interfaces is well developed, with many experimental pull test results and also design models. Such information and pull test results are not available for NSM FRP bonded to masonry. Tests need to be conducted to determine the effect of variables specific to masonry, such as the orientation of the FRP strip, and the effect of mortar joints. Also, when NSM FRP strips are used to horizontally reinforce walls the debonding properties may change depending on the amount of compression acting vertically through the wall (see Chapter 3). One set of pull tests have been conducted on NSM FRP bonded to masonry Willis et al. (2008) but more tests are required to expand the database.

Experimental tests on strengthened wall panels

Only a very few studies have been conducted into the behaviour of masonry shear walls retrofitted with NSM FRP reinforcement, and in particular where the NSM FRP reinforcement is aligned vertically. Marshall and Sweeney (2002) have used CFRP NSM strips to prevent heel uplift, occurring during rocking of masonry shear walls, but they did not, however, use the strengthening technique to prevent sliding or diagonal cracking failure. Tinazzi and Nanni (2000) strengthened URM shear panels using NSM circular glass FRP bars, but still, only the results of a few tests were reported and not enough information on the reinforcement mechanisms of the technique could be gained from such a limited amount of tests.

Experimental tests are required to determine: the effectiveness of the reinforcement scheme (in terms of strength and ductility increase); the failure modes; the reinforcement mechanisms; and the behaviour of the bond between the masonry and the FRP within the strengthened panel/wall. In particular not much is known about the effectiveness and the reinforcement mechanisms of vertical reinforcement used to prevent sliding.

Finite element models

No numerical models have been developed to study the behaviour of NSM strengthened masonry. The modelling strategies presented in Section 2.7 can potentially be used to model the behaviour of NSM FRP strengthened masonry walls subjected to in-plane loading.

Analytical design models

The current design models presented in Section 2.8 are specific to particular strengthening schemes and therefore cannot be applied generally to other strengthening schemes (such as NSM). Also, the models have been verified with only a limited number of experimental results, strongly limiting their usefulness. None of the current models can be used to design vertical FRP reinforcement.

2.9.2 Proposed Work

In this project the in-plane shear behaviour of URM panels strengthened with near-surface mounted CFRP strips was investigated. In this investigation thin rectangular FRP strips were used. Using a thin rectangular strip maximises the confinement around the strip, and increases the resistance to debonding. The FRP strips were designed to prevent sliding along mortar bed joints (within the wall panel) and diagonal cracking (through mortar joints and brick units). Different reinforcement orientations were studied, including: vertical; horizontal; and a combination of both.

The project was divided into three stages (which form the basis of the following three chapters). The first stage of the project involved characterising the bond between the NSM CFRP and the masonry using experimental pull tests (18 in total). From these tests the bond strength, the critical bond length and the local bond-slip relationship of the debonding interface was characterised. The second stage of the project involved conducting diagonal tension/shear tests on masonry panels. A total of four URM wall panels and seven strengthened wall panels were tested. The third stage of the project involved developing a finite element model to help understand the experimental results. The masonry was modelled using the micro-modelling approach, and the FRP was attached to the masonry model using the bond-slip relationships determined from the pull tests. The FE model was not fitted to the results of the panel tests. Rather it was based on the pull tests and other material characterisation tests (for the masonry) then used to predict the panel behaviour.

It was considered outside the scope of this thesis to attempt to develop an analytical design model for the NSM strengthening scheme. However, the proposed work aims to provide the understanding of the strengthening scheme required to develop such a model.

3

Pull tests

3.1 Introduction

As mentioned previously in the literature review (Chapter 2, Section 2.6.1) a large database of pull test results exists for FRP-to-concrete joints. Variables that affect the bond behaviour of an FRP-to-concrete joint include: concrete strength; bond length; FRP reinforcement cross-section dimensions; material properties of the FRP reinforcement; strength of the adhesive; distance between the FRP reinforcement and concrete edge; and distance between multiple, parallel FRP reinforcement (Seracino et al. (2007a,b); Oehlers et al. (2008); Rashid et al. (2008)).

Including those previously mentioned, other variables need to be considered when investigating the bond behaviour between FRP and masonry. Additional variables that affect the behaviour include the alignment of FRP (vertical, horizontal, +/- 45 degrees etc.), the distance between FRP reinforcement and parallel mortar joints, and the presence of cores in some types of bricks. Also, when NSM FRP strips are used to horizontally reinforce walls the debonding properties may change depending on the amount of compression acting vertically through the wall. Compression forces may arise (after the installation of NSM reinforcement) due to: live loads; in-plane shear loads in load bearing and infill walls; and by confinement with vertical FRP reinforcement. The effects of these variables need to be quantified.

For a NSM FRP-to-masonry connection the effects of reinforcement position relative to mortar head joints (also referred to as perpend joints) and brick cores on the bond properties were investigated previously by Willis et al. (2008). In all specimens the FRP was aligned in the vertical direction (i.e. perpendicular to the mortar bed joints) and all of the clay brick units had cores. The current work expands upon the tests by Willis et al. (2008) using NSM FRP reinforcement. Firstly, the tests on vertically aligned FRP strips are repeated with solid clay brick units to remove cores as a variable when assessing the influence of mortar head joints on the FRP-to-masonry interface properties. Secondly, a new pull test specimen is developed where the FRP is aligned parallel to the mortar bed joint. This specimen is used to study bond behaviour of horizontally aligned NSM FRP reinforcement. For these new specimens the effect of compression on the joint is considered. Testing to investigate the effect of compression on FRP-to-masonry (or concrete) joints is unique and it is shown to have a significant effect on the joint behaviour.

In this chapter the results of 18 pull tests, which include the bond strength, critical bond length and local bond-slip relationships are presented. The local bond-slip relationships are used in the finite element model in Chapter 5. In this chapter discussions on the failure modes, and the effects of the tested variables on the results are also provided.

3.2 Experimental Program

3.2.1 Pull test specimens

Pull test specimens used for this investigation are shown in Figure 3.1. All specimens were constructed using solid clay brick units with nominal dimensions 230 mm long, 110 mm wide and 76 mm high. The brick unit flexural tensile strength was determined from lateral modulus of rupture tests (AS/NZS 4456.15) Standards Australia (2003). See Section 5.3.4 in Chapter 5 for more information on this test. The mortar used to construct the specimens was mixed in three batches, all with a mix ratio of 1:1:6 (cement:lime:sand by volume) (type 'N' in the USA). Bond wrench tests to AS3700-2001 Standards Australia (2001c) were used as a quality control measure between the batches. The mortar joints were 10 mm thick.

Pultruded CFRP strips were used in this study. The CFRP reinforcement was provided in strips 50 mm wide and 1.4 mm thick. The strips were cut to a width of 15 mm. The width of the CFRP strip was chosen to ensure full embedment in typical Australian modern masonry walls. Also, the width was chosen to not be too large, because of concerns of cracking through the thickness of the brick. Other variables such as strip thickness and bonded length were selected to ensure that the specimen failed by debonding, and the full bond-slip data could be derived.

Two 1.4 mm thick by 15 mm wide carbon FRP strips were glued together with 'Super Strength' Araldite to make 2.8 mm thick by 15 mm wide carbon FRP strips. Two strips were glued together to provide sufficient cross-sectional area of FRP to ensure that failure of the joint occurred by debonding through the brick rather than by FRP strip rupture. FRP rupture occurred in a preliminary test when only one strip of CFRP was bonded to the masonry. The CFRP strip rupture in the trial test also shows that a lower strength FRP (such as glass FRP) would not be suitable in the current application. Debonding of the FRP from the masonry could also be achieved by reducing the bonded length, however by doing this the full non-linear bond-slip response could not be determined, nor could the actual maximum bond strength of the interface.

The elastic modulus of the FRP strip was determined during the pull tests from two strain gauges, placed on either side of the un-bonded portion of the strip, located 21 mm above the top of the brick prism (strain gauges 9 and 10 in Figure 3.2). The FRP strip was glued into a groove, previously cut with a brick-cutting saw, with a two-part epoxy adhesive. The grooves were approximately 20 mm deep and 6 mm wide. The specimens were painted white to aid in the identification of cracks. Material properties are shown in Table 3.1.

The specimens are separated into two series. In the first series of pull tests the

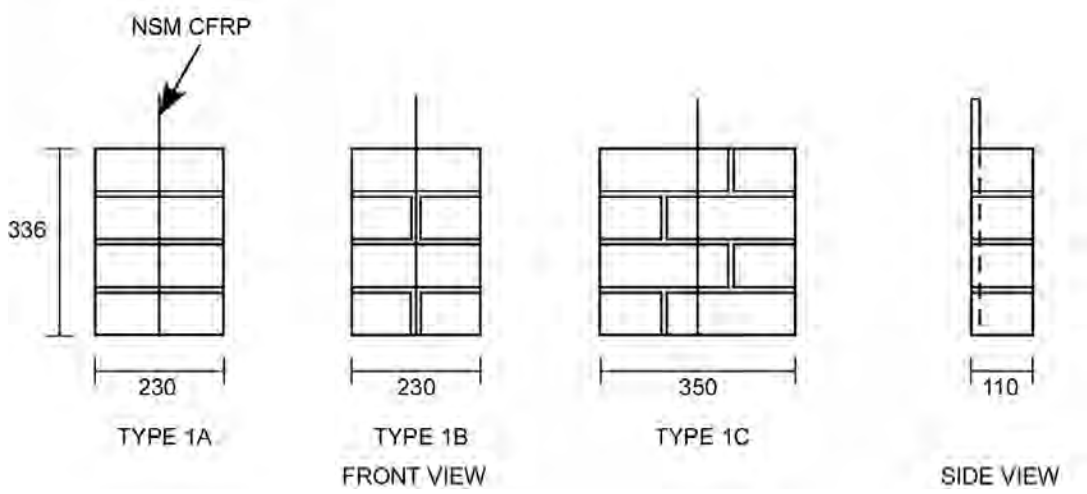

(a) Series 1

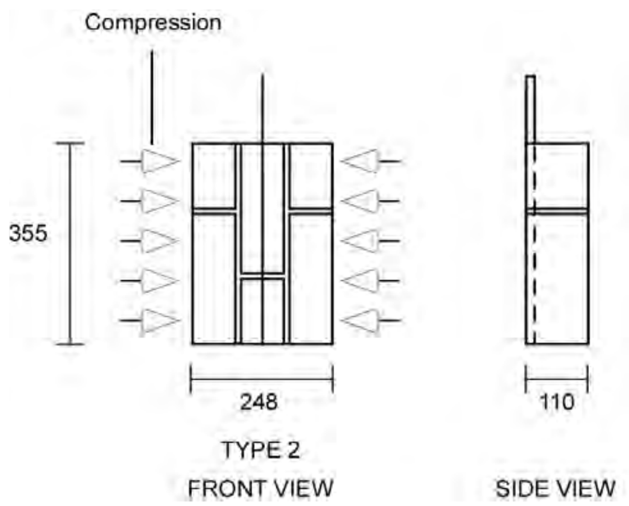

(b) Series 2

Figure 3.1: Pull test specimens

Table 3.1: Material properties

Material	Property	Mean	Std dev	Source
Masonry unit	Lateral mod. of rupt. (MPa)	3.57	0.75	AS/NZS 4456.15
Mortar batch 1	Bond strength (MPa)	1.84	0.43	
Mortar batch 2	Bond strength (MPa)	1.73	0.38	AS3700-2001
Mortar batch 3	Bond strength (MPa)	1.22	0.38	
CFRP	Elastic modulus (MPa)	207021	1951	Current pull tests
CFRP	Rupture strain ($\mu\varepsilon$)	12000	-	Manufacturer's data
Epoxy	Flexural strength (MPa)	>30	-	Manufacturer's data

FRP strip is aligned in the vertical direction (perpendicular to mortar bed joints). As previously discussed, similar tests have already been performed by Willis et al. (2008) on cored specimens. The first specimen, type '1A' (constructed in a stack bond pattern), was constructed to be a control specimen. Specimen types '1B' and '1C' (constructed in a running bond pattern) were used to better represent the masonry bonding pattern typically used in walls. Specimen type '1B' was tested to investigate the effect on the bond in walls when the FRP passes through mortar head joints. Specimen type '1C' was constructed to investigate the bond in walls when the FRP is inserted into brick units only.

In the second series of tests the FRP strip was aligned in the horizontal direction (parallel to bed joints). The horizontal strips were bonded into the brick units (as opposed to the mortar joints) to maximise the bond strength. Tests were performed on this specimen using compression levels of 0 MPa, 0.5 MPa, and 1.0 MPa.

The bonded length (L_b) (and hence the height of the specimen) was selected to be greater than the critical bond length (L_e). The critical bond length is the minimum anchorage length of FRP strip required to develop the maximum axial force in the FRP strip. Also, any extra bond length greater than L_e results in an insignificant increase in load (Oehlers and Seracino, 2004). The critical bond length was initially approximated as 100 times the FRP strip thickness (L_e = 280 mm). The specimens were designed so that the bonded length was larger than 280 mm. The bonded length (L_b) was 336 mm for series 1 specimens and 355 mm for series 2 specimens.

Different bonded lengths for each specimen type were not tested to reduce the number of variables and number of tests. By testing specimens with different bonded lengths the critical bonded length can be determined. The critical bonded length can also be determined from the interface shear stress distribution (if the bonded length is larger than the critical bond length), as demonstrated in Section 3.3.4). It was therefore considered unnecessary to test specimens with different bond lengths.

In diagonal tension tests (ASTM Standards, 1993) (Chapter 4), the average normal stress in the vertical direction was in the order of 1.0 MPa. These tests were performed on both unreinforced and FRP strengthened masonry wall panels. The range of compression values here were therefore suitable.

To account for variability, each test was conducted 3 times. For one repeat of each test strain gauges were sandwiched between the two FRP strips (used to construct the reinforcement) to measure the strain distribution along its bonded length. The strain gauges were spaced at 42 mm as shown in Figure 3.2. The strain gauges were sandwiched between two FRP strips to eliminate the effect they may have on the epoxy-FRP bonded interface.

The specimens in the testing program are identified as follows: the first term denotes which series of tests the specimen is from (S1 or S2); the second term denotes the specimen type (A,B,or C) for series 1 specimens or the amount of compression applied for series 2 specimens (e.g. P0, P0.5 and P1 for zero, 0.5 MPa, and 1 MPa compression respectively); the third term signifies whether strain gauges

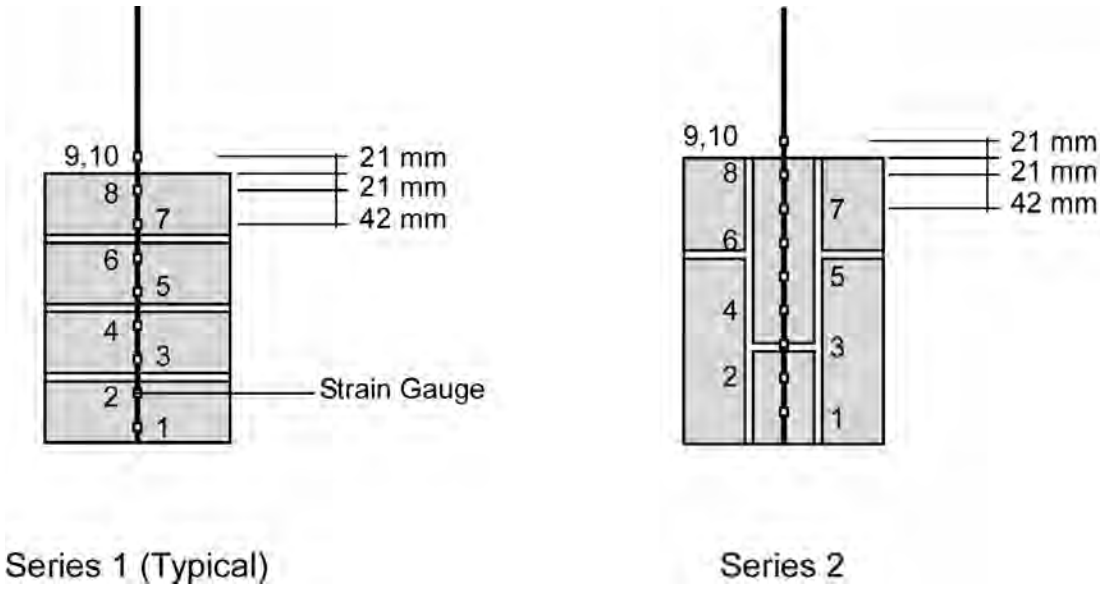

Figure 3.2: Pull test instrumentation

were attached along the bonded length (NG meaning no gauges and SG meaning gauges); and the last term signifies the test number where more than one test was performed with the same parameters (Table 3.2).

3.2.2 Test setup and procedure

The test setup is shown in Figure 3.3a and Figure 3.3b for FRP strips aligned perpendicular to the bed joint (series 1) and Figure 3.4a and Figure 3.4b for FRP strips aligned parallel to the bed joints (series 2). The specimens were restrained and a direct tensile force (P) was applied to the FRP using an Instron Universal Testing Machine under displacement control at a rate of 0.3 mm/min. Finite element analysis was used to size the top and bottom restraining plates to ensure negligible bending in these plates during testing. Before placing the specimens in the testing apparatus a 12 mm thick specimen plate and a 5 mm thick piece of plywood were placed on top of the specimen (see Figure 3.3). Both the specimen plate and plywood had a small gap cut into the edge to allow the FRP strip to pass through. The piece of plywood was used to ensure full contact between the top of the masonry specimen and the 12 mm specimen plate. For Series 2 the compression force was applied at the mid-points of two stiff universal beam sections that bear on both sides of the specimen. Plywood boards (5 mm thick) were placed between the sides of the specimen and universal beam sections to ensure full contact between them. The universal beam sections were designed to distribute the compression force over the height of the specimen and thus produce a normal stress along the FRP joint that was as uniform as possible. The compression force was applied prior to the FRP tension force. The compression force was continually logged with a load cell and was held constant throughout the test.

Table 3.2: Summary of pull test specimens

Specimen	Mortar Batch	Series	Type	Compression (MPa)	Strain gauges along bonded length
S1-A-NG-1	1	1	A	-	no
S1-A-NG-2	1	1	A	-	no
S1-A-SG	3	1	A	-	yes
S1-B-NG-1	1	1	B	-	no
S1-B-NG-2	1	1	B	-	no
S1-B-SG	1	1	B	-	yes
S1-C-NG-1	1	1	C	-	no
S1-C-NG-2	1	1	C	-	no
S1-C-SG	3	1	C	-	yes
S2-P0-NG-1	2	2	-	0	no
S2-P0-NG-2	2	2	-	0	no
S2-P0-SG	3	2	-	0	yes
S2-P0.5-NG-1	3	2	-	0.5	no
S2-P0.5-NG-2	3	2	-	0.5	no
S2-P0.5-SG	3	2	-	0.5	yes
S2-P1-NG-1	2	2	-	1.0	no
S2-P1-NG-2	2	2	-	1.0	no
S2-P1-SG	3	2	-	1.0	yes

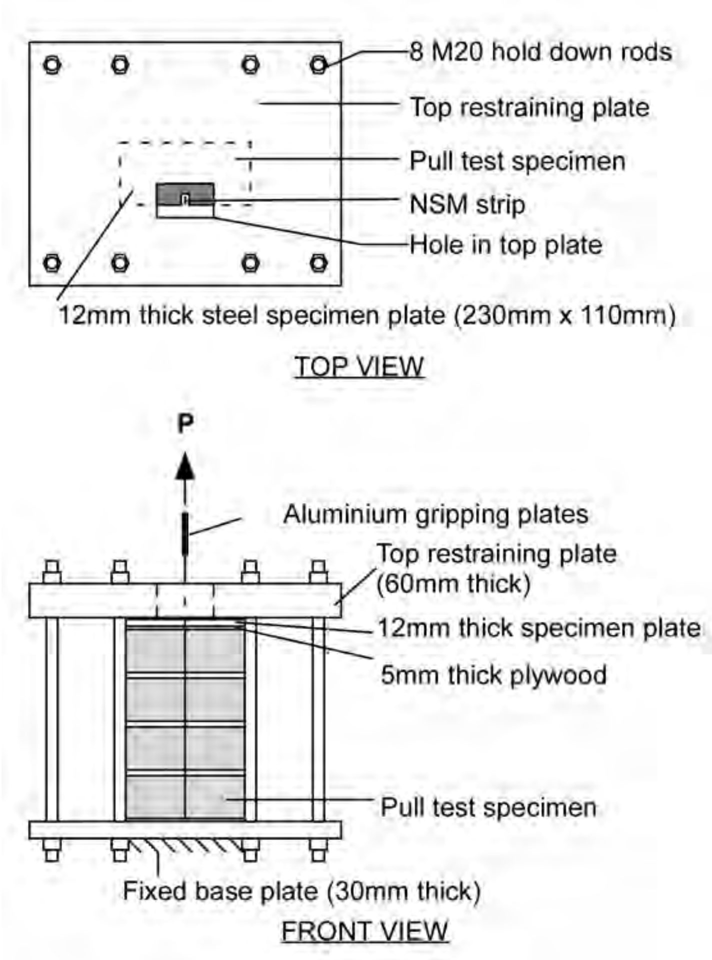

(a) Test schematic

(b) Photograph of test apparatus

Figure 3.3: Series 1 pull test setup

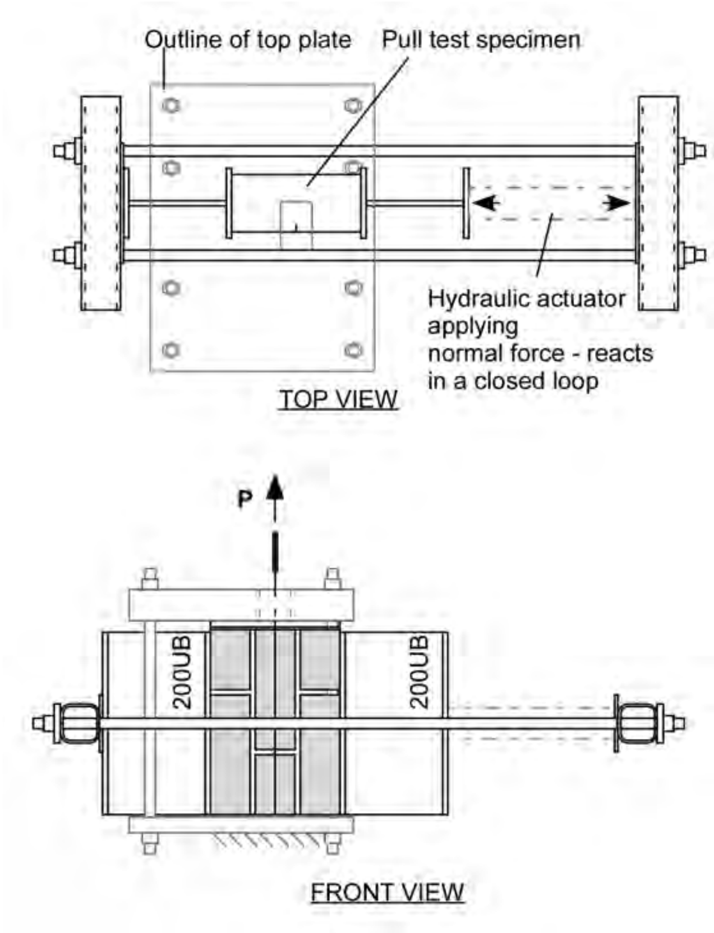

(a) Test schematic

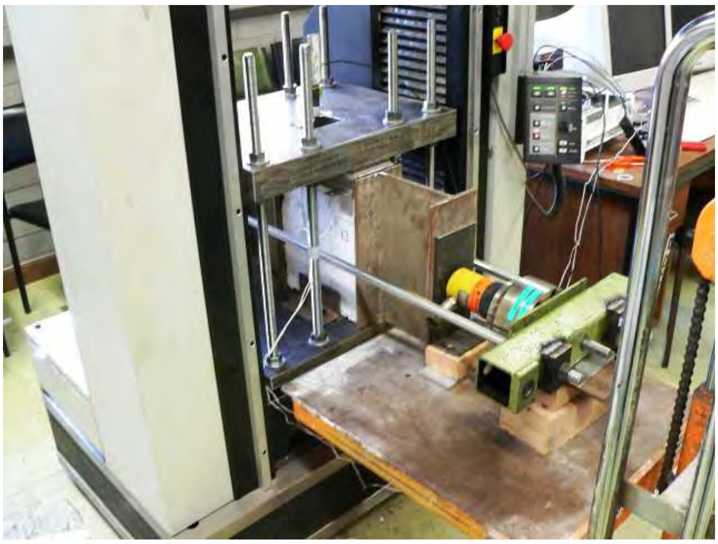

(b) Photograph of test apparatus

Figure 3.4: Series 2 pull test setup

3.3 Experimental Results

3.3.1 Failure modes: Series 1

Most specimens failed by debonding through the brick. This failure mode started with small diagonal cracking in the masonry adjacent to the FRP strip at the loaded end of the specimen (shown in Figure 3.5a for specimen S1-A-NG-1 with black lines added to illustrate the angle of cracking). The cracking propagated down the specimen as the load increased until the FRP strip completely debonded (shown in Figure 3.5b). After debonding failure a layer of masonry, typically between 1 mm and 5 mm thick, remained attached to the surface of the FRP strip. This failure mode is common for adhesively bonded FRP-to-masonry connections (see Willis et al. (2008)). When the FRP strip was bonded through a mortar joint (S1-B-NG-1, S1-B-NG-2 and S1-B-SG) debonding occurred through the mortar joint (shown in Figure 3.5c at the second brick course from the top). Minimal cracking was observed in the brick adjacent to the mortar head joint.

In addition to debonding, specimen S1-B-SG failed by sliding along the epoxy-FRP interface at the top of the specimen where the FRP strip was bonded into the brick as shown in Figure 3.5d. Where the FRP was bonded into the mortar the main failure mode was identified as debonding through the mortar joint. Sliding failure within the top brick was likely caused by a reduction in bond strength at the interface by the presence of strain gauges. Unlike all other specimens where strain gauges were sandwiched between the FRP strips, gauges used for S1-B-SG were attached to the outside of the FRP strips, and hence they were within the bonded area between FRP strip and masonry. As a result, the bond-slip relationships determined from this specimen, at positions where sliding has been identified, will not represent the true debonding behaviour of the connection (i.e. the connection without strain gauges). At the mortar joint, where the failure mode was debonding and was similar to that seen in specimens S1-B-NG-1 & 2, the maximum shear strength was estimated. Results from this specimen were kept for this reason.

After removing Series 1 specimens from the testing apparatus cracking was observed in line with the FRP, extending through the thickness of the specimens. This type of cracking was visible on the top of the specimen (Figure 3.6a). In some instances (e.g. specimen S1-A-NG-1) the cracking was also visible on the back of the specimen, in line with the FRP. In both S1-C-NG-2 and S1-C-SG a vertical crack had formed completely through the thickness of the specimens, following a path through both mortar head joints and the FRP as shown in Figure 3.6b. This kind of cracking in the direction of the reinforcement may have adverse effects in an FRP retrofitted wall with through brick cracking potentially weakening the retrofitted wall system.

3.3.2 Failure modes: Series 2

Before debonding occurred for specimen S2-P0-SG, the middle course of bricks was 'pulled-through' the specimen. Figure 3.7a shows how the diagonal cracks that formed during the debonding process in the middle course of bricks were intercepted by cracking through the mortar bed joints. In the case of this specimen,

(a) Crack pattern

(b) S1-A debonding

(c) S1-B debonding

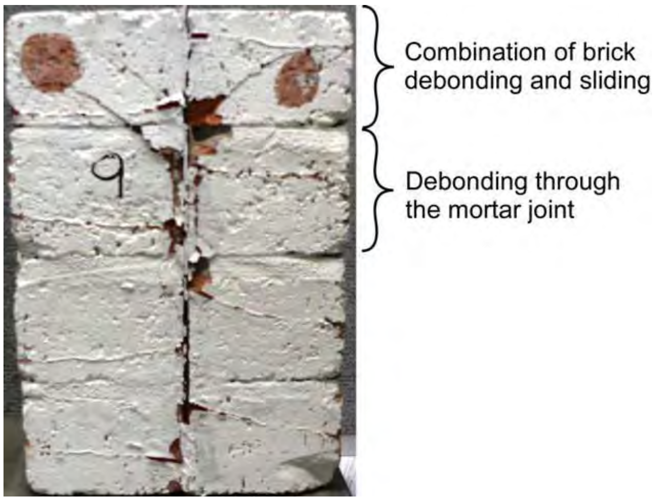

(d) S1-B-SG failure

Figure 3.5: Failure modes

(a) Cracking at top of specimen in line with FRP

(b) Crack through thickness S1-C-SG

Figure 3.6: Cracking through thickness of series 1 specimens

cracking in the mortar bed joints developed fully at a load of 38 kN and the outer brick courses separated from the middle course of the specimen. Surface irregularities that prevented the middle course of bricks from bearing against the restraining plate securely may have also contributed to 'pull-through' of the middle course of bricks. That is the piece of plywood placed between the top of the specimen and the specimen plate may not have been able to adequately take up the irregularities as shown schematically in Figure 3.7b. After the outer brick courses separated, the specimen, now consisting of only the FRP and middle course of bricks, continued to take load until the FRP debonded from the specimen at a load of 54.6 kN (Figure 3.7c).

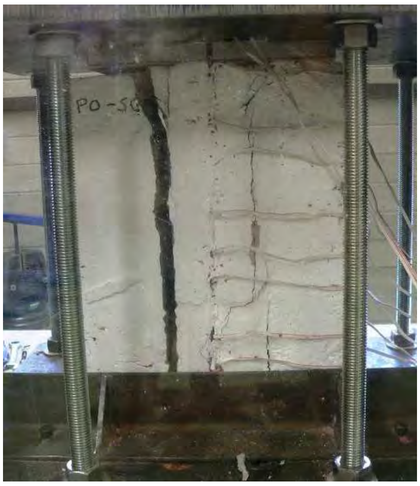

(a) Bed joint cracking (P=38 kN)

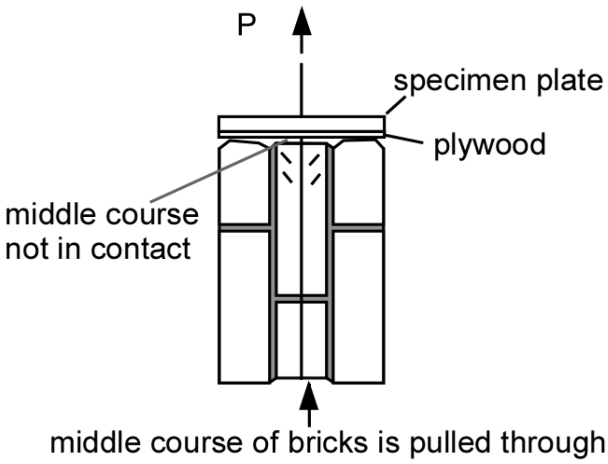

(b) Pull through of middle course

(c) Debonding (P=54.6 kN)

Figure 3.7: 'Pull-through' of middle course S2-P0-SG

Similar behaviour was observed for S2-P0-NG-1 and S2-P0-NG-2. In these two specimens only one outer course of masonry separated from the specimen (instead of both) (Figure 3.8a). Cracking was, however, observed through both mortar bed joints. When testing S2-P0-NG-1 one outer course of masonry separated from the specimen at ultimate load, when the FRP debonded from the masonry. When testing S2-P0-NG-2 one outer course of masonry separated at approximately 50% of the failure load. When specimens were loaded with compression (0.5 MPa or 1.0 MPa) no cracking was visible along the mortar bed joints. Diagonal cracking was still, however, confined to the middle course of bricks indicating that bed joint cracks were likely present (Figure 3.8b).

(a) Failure S2-P0-NG-1 (b) Failure S2-P1-SG

Figure 3.8: Typical failure modes for series 2 specimens

Surface irregularities played a major role in the observed behaviour of these specimens. The combination of inadequate contact of masonry courses with the reaction plate and the restraint effect of the confining steel plates may have changed the results. Therefore the results of the series 2 specimens are merely indicative and could be incorrect. Capping or other methods could have been used to reduce such affects.

Pull through failure is unlikely to be a failure mode in a URM wall retrofitted with horizontal FRP reinforcement. Horizontal reinforcement would likely be used for shear walls where diagonal cracking is the main failure mode. Diagonal cracking usually occurs in walls with strong mortar or precompression, and these two parameters would prevent a pull through type failure.

A summary of results is shown in Table 3.3 and includes: the critical bond length (L_e) (determined in Section 3.3.4); maximum strain in FRP (ϵ_{max}); and the bond strength. The bond strength is the maximum load resisted in the test. The average bond strength and corresponding coefficient of variation (COV, shown in brackets) is also included.

Table 3.3: Summary of test results

Specimen	L_e [a] (mm)	ε_{max} ($\mu\varepsilon$)	Bond Strength (kN)	Avg Bond Strength (kN)
S1-A-NG-1	-	9638	83.45	
S1-A-NG-2	-	8094	71.09	
S1-A-SG	300	8773	81.48	78.67 (COV 8.4%)
S1-B-NG-1	-	7974	70.36	
S1-B-NG-2	-	6865	59.41	
S1-B-SG	NA	6490	56.60[b]	64.89 (COV 11.9%)
S1-C-NG-1	-	7416	63.88	
S1-C-NG-2	-	7890	69.41	
S1-C-SG	300	8963	84.50	72.60 (COV 14.7%)
S2-P0-NG-1	-	6245	54.00	
S2-P0-NG-2	-	6228	53.59	
S2-P0-SG	NA	5793	54.62	54.07 (COV 1.0%)
S2-P0.5-NG-1	-	NA	57.88[c]	
S2-P0.5-NG-2	-	6748	58.55	
S2-P0.5-SG	330	8047	68.45	63.50 (COV 11.0%)
S2-P1-NG-1	-	8496	78.63	
S2-P1-NG-2	-	9272	78.49	
S2-P1-SG	300	7741	68.31	75.14 (COV 7.9%)

[a] Determined visually from shear stress distribution (Section 3.3.4)
[b] Sliding at epoxy-FRP interface (omitted from average bond strength)
[c] Setup failure resulted in rupture (omitted from average bond strength)

3.3.3 Effect of variables on bond strength

Effect of mortar joints parallel to FRP strip

To demonstrate the effect that parallel mortar joints adjacent to the FRP strip had on the behaviour of the FRP to masonry bond, the stack bonded specimens (S1-A-NG-1&2, S1-A-SG) are compared to the running bond specimens (S1-C-NG-1&2, S1-C-SG). In the S1-C specimens diagonal cracking in brick courses was intercepted by cracking through mortar head joints (can be seen in Figure 3.6b). Cracking in the mortar joints reduced the region of masonry effective in the load transfer and reduced the bond strength by 8% when compared to S1-A specimens. When the FRP strip passed through mortar head joints as well as units (S1-B-NG-

1&2) the average bond strength was reduced by 11% when compared to the specimens constructed using a running bond with the FRP bonded into brick unit only (S1-C-NG-1&2, S1-C-SG). Note that the bond strength was reduced by 18% when compared to the stack bonded specimen.

In a study similar to the current one, Willis et al. (2008) also performed pull tests on clay brick masonry prisms strengthened with NSM FRP strips. As previously noted in the introduction, they used cored bricks and bonded the FRP strips to the prisms in the vertical direction (perpendicular to the bed joints). They investigated the effect of reinforcement position relative to the mortar head joints and brick cores. Figure 3.9 shows the location of the brick cores and NSM strips. The similarities between Willis et al.'s study and the current study include: the specimen types (Specimen types '1A', '1B' and '1C'); the CFRP strip width in many tests (15 mm), the epoxy used; and the lateral modulus of rupture of the brick (≈ 3.55 MPa). The main difference between the tests (apart from the brick cores) was that the CFRP strips used by Willis et al. were thinner (1.2 mm thick) and had a lower elastic modulus (162,000 MPa). These differences make it difficult to directly compare the specimens tested in the current investigation to the specimens tested by Willis et al. (2008). For this reason the results of their tests are not included in this thesis. However, comparisons can be made based on the reduction of capacity for different types of test specimens.

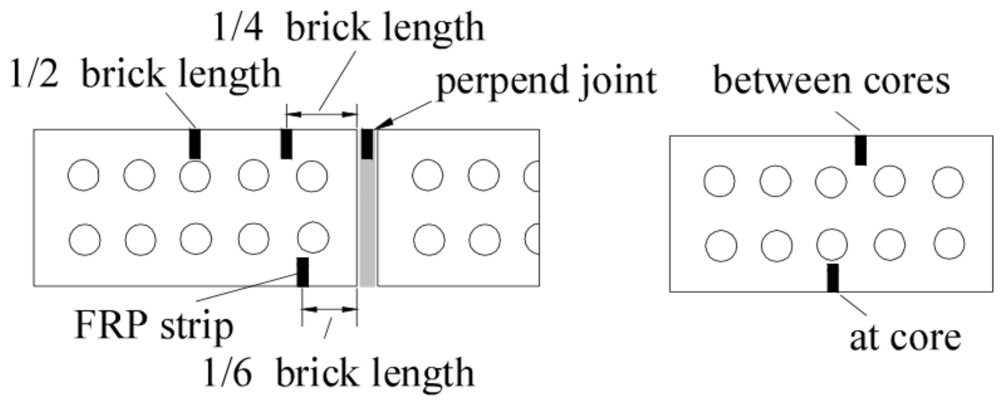

Figure 3.9: Position of cores and NSM strips, Willis et al. (2008) specimens

Willis et al. (2008) found when FRP was bonded to cored bricks there was no difference between the bond strengths of S1-A type specimens and S1-C type specimens (unlike the 8% reduction observed for the solid brick specimens). It is likely that cores in the brick units affected the region of masonry effective in the load transfer more than the mortar joint, and cores in the brick units decreased the bond strength of the joint. Willis et al. (2008) also found that when the FRP strip passed through mortar head joints and cored units the average bond strength was reduced by 8.5%. This reduction in bond strength is similar to that observed from the presented results on solid brick units (reduction of 11%).

When the FRP strips were aligned parallel to the bed joints (S2-P0-NG-1&2, S2-P0-SG), the region of masonry effective in the load transfer was confined to the middle course of bricks. Compared to the stack bonded specimen (S1-A specimens), the reduction in bond strength was 31%. The reduction in bond strength can be attributed to the small edge distance (between the FRP and the edge of the middle course) on both sides of the FRP, which for these specimens was equal to 38 mm. Reduction in bond strength due to reduction in edge distance has been previously investigated by Rashid et al. (2008) on NSM FRP-to-concrete joints. They found that NSM strips interact strongly with the edge when the lateral spacing between the NSM strip and the edge of the concrete was less than 3.5 times the depth of the strip. Using their result, the minimum edge distance for 15 mm NSM CFRP strips (used in the current study) would be 52.5 mm. Figure 3.10a shows the crack pattern, after failure, on the side of the middle course of specimen S2-P0-NG-2, with the outer brick course moved aside. Note that in specimens with adequate edge distance cracking was not observed on the side of the specimen. The failure mode shown in Figure 3.10a was similar to the results observed by Rashid et al. (2008) (typical failure mode shown in Figure 3.10b).

(a) Specimen S2-P0-NG-2

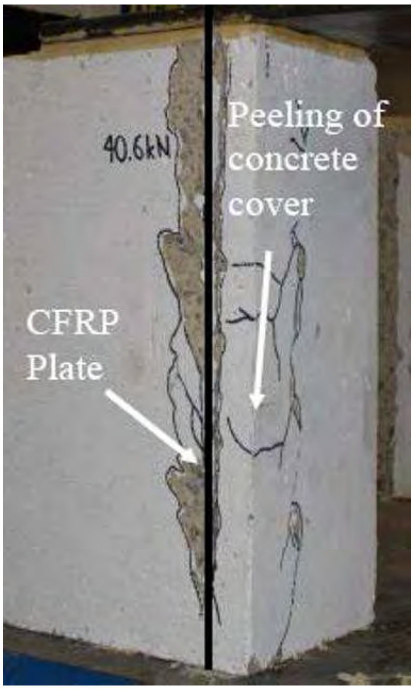

(b) Specimen with 30 mm edge distance (Rashid et al 2008)

Figure 3.10: Interaction between FRP and specimen edge

Effect of compression applied normal to FRP strip longitudinal direction

The bond strength increased linearly with an increase in compression as shown in Figure 3.11 (within the tested range of 0 to 1 MPa). Compression applied perpendicular to the joint prevented tensile cracks, that formed during the debonding process, from opening and lead to an increase in bond strength. Applying a compression stress of 0.5 MPa and 1 MPa to the specimens increased the average failure loads by 17% and 39% respectively, compared to that of the specimens without compression. Compression of 1 MPa increased the strength so that it was similar to S1-A type specimens. Note that these results were likely affected by the inadequate contact of the masonry courses with the reaction plate, and therefore are indicative only.

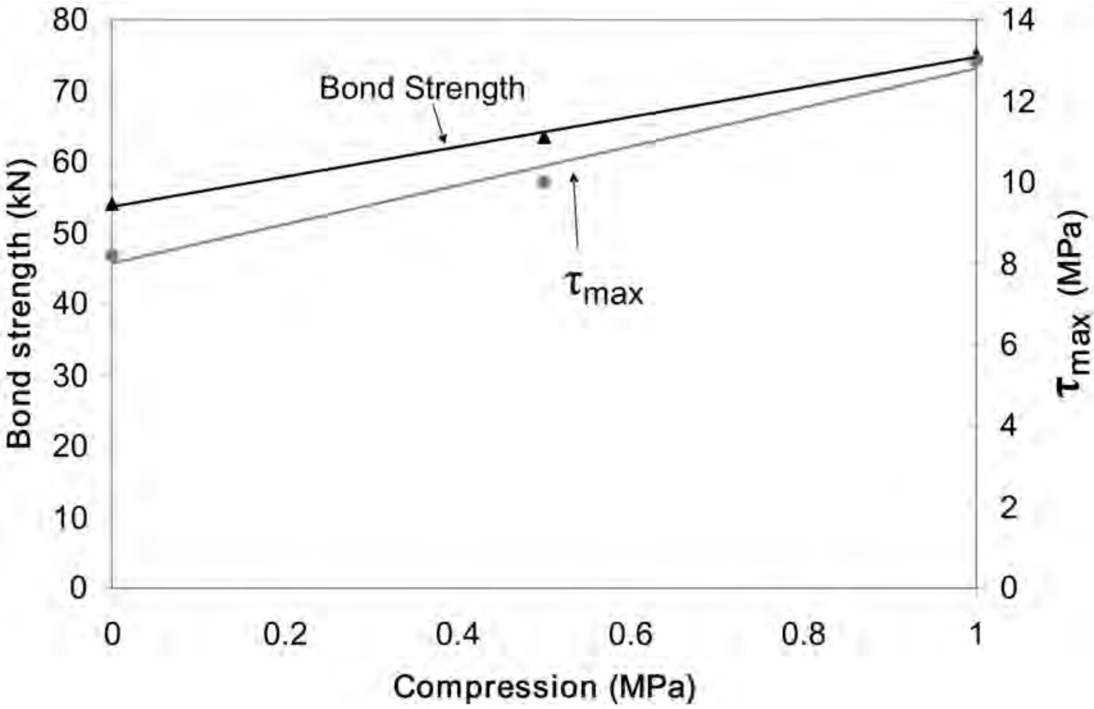

Figure 3.11: Effect of compression on bond strength and maximum shear stress for FRP aligned parallel to the bed joint

3.3.4 FRP to masonry interface behaviour

The distribution, along the bonded length, of axial strain in the FRP for increasing increments of load, is shown in Figure 3.12 for specimen S2-P1-SG. The peak, post-peak and failure loads indicated on Figure 3.12 are shown on a load versus loaded end slip curve in Figure 3.14. Shear stress transferred from the FRP to the masonry through the epoxy was determined from the strain distributions, for all specimens with strain gauges, using Equation 3.1:

$$\tau_{avg} = \frac{(\Delta\varepsilon) E_p b_p t_p}{(\Delta L)(2b_p + t_p)} \tag{3.1}$$

Where τ_{avg} is the average shear stress transferred from the FRP to the masonry through the epoxy over the length ΔL, $\Delta\varepsilon$ is the change in axial strain in the FRP over length ΔL, E_p is the elastic modulus of the FRP strip, b_p is the width of the strip, t_p is the thickness of the strip, and ΔL is the incremental length along the FRP (equal to strain gauge spacing).

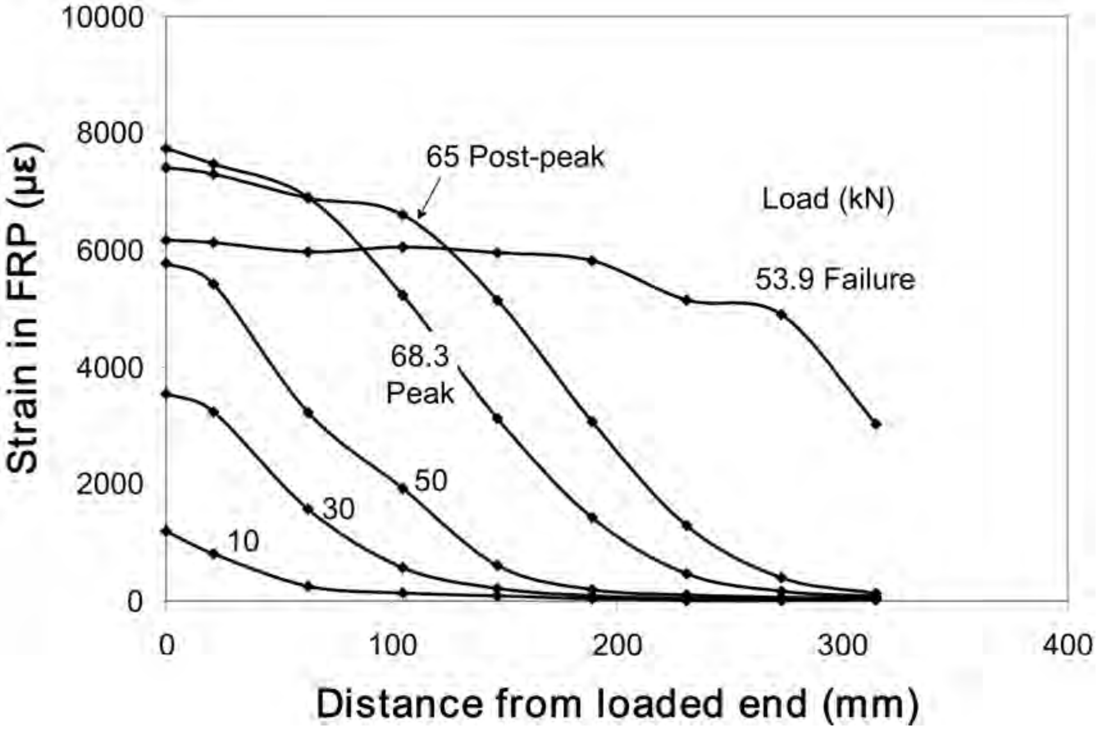

Figure 3.12: Strain distribution S2-P1-SG

The distribution, along the bonded length, of shear stress through the epoxy for increasing increments of load, is shown in Figure 3.13 for specimen S2-P1-SG (typical). The shear stress distribution shows the transfer of the load from the FRP to the masonry and how the region of masonry effective in the load transfer moved away from the loaded end as the load increased and cracks developed. After the peak load was reached, debonding cracks propagated towards the unloaded end, whilst the specimen maintained an almost constant load.

For the brittle FRP-masonry interface the maximum FRP force is attained once the bell-shaped shear-stress distribution shown in Figure 3.13 (at peak load) is developed. The bonded length required to develop such a distribution is the critical bond length (L_e) as indicated on Figure 3.13. For bonded lengths greater than L_e (the case here), the bell-shaped shear-stress distribution propagates away from the loaded end as debonding occurs. Therefore any increase in bonded length (past L_e) does not increase the maximum axial force that can be developed in the FRP.

The critical bond length was estimated from the shear stress distribution (at the maximum load) as the distance between the 2 points: i) where interface cracks are fully developed and the shear stress is approximately equal to zero; and ii) in the uncracked masonry where the shear stress is approximately equal to zero. For specimen S2-P1-SG (Figure 3.13), these points were determined from the curve plotted at 68.3 kN as: 0 mm (i) and 300 mm (ii). The critical bond length was then 300 mm. The critical bond lengths for specimens S1-A-SG, S1-C-SG, and S2-P0.5-SG were also around 300 mm and are included in Table 3.3. The critical bond

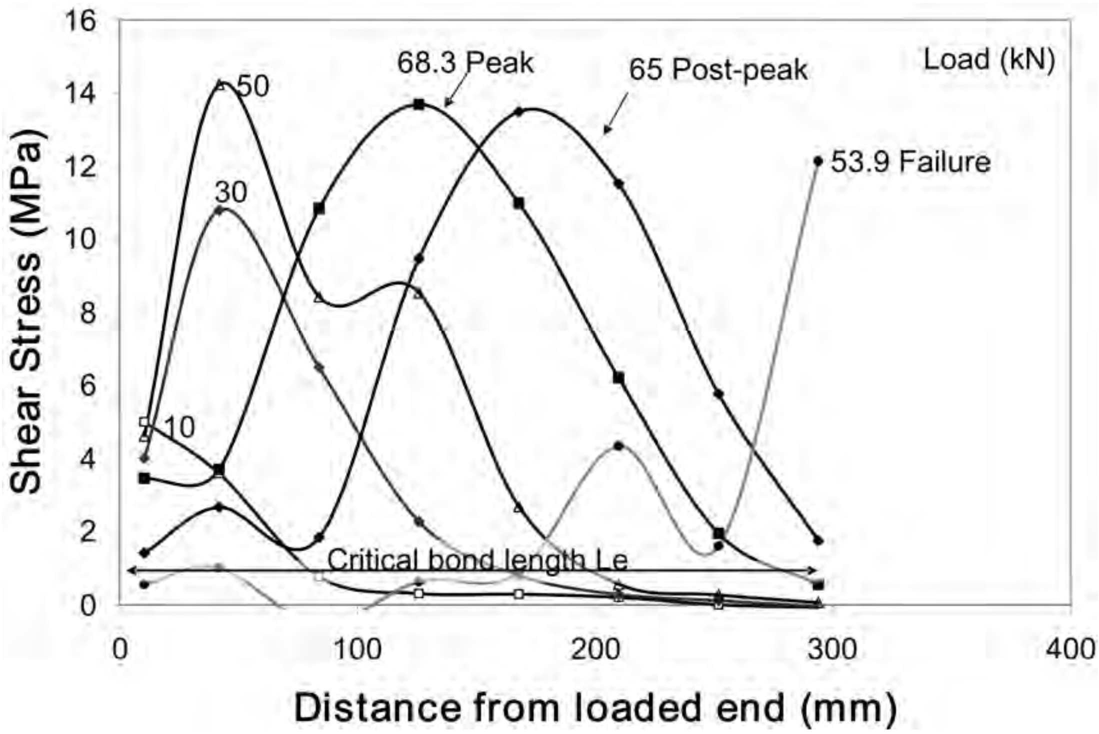

Figure 3.13: Shear stress distribution S2-P1-SG

length was not determined for specimens S1-B-SG because failure was by premature sliding and S2-P0-SG because of the premature sliding of the middle brick course.

Local slip (of FRP relative to the masonry) distributions were calculated at increasing load increments up to the failure load by numerically integrating the strain distributions. It was assumed that the axial strain in the masonry was negligible and the slip at the unloaded end was zero. Using the calculated slip, the load-slip response at the loaded end was determined for all strain gauged specimens (shown in Figure 3.15). The load-slip responses show that: stiffness reduced in all specimens with increasing load (indicating progressive damage) after the point of first cracking (load ≈ 20 kN); the displacement capacities of all specimens were similar; the stiffness of specimens S1-A-SG and S1-C-SG were similar; the overall stiffness reduced when FRP passed through mortar joint and when the width of masonry section was reduced; and the stiffness increased when compression was applied. All of these behaviours were expected. Note that the specimens had some ductility indicating that the bonded length was larger than the critical bond length. The effect of the outer courses separating for specimen S2-P0-SG is also shown.

By combining the shear stress and the slip distributions the local shear stress-slip (or bond-slip) relationship was determined. The bond-slip relationships for all specimens with strain gauges along the bonded length are shown in Figure 3.16 to Figure 3.21.

The average maximum shear strengths determined for specimens S1-A-SG and

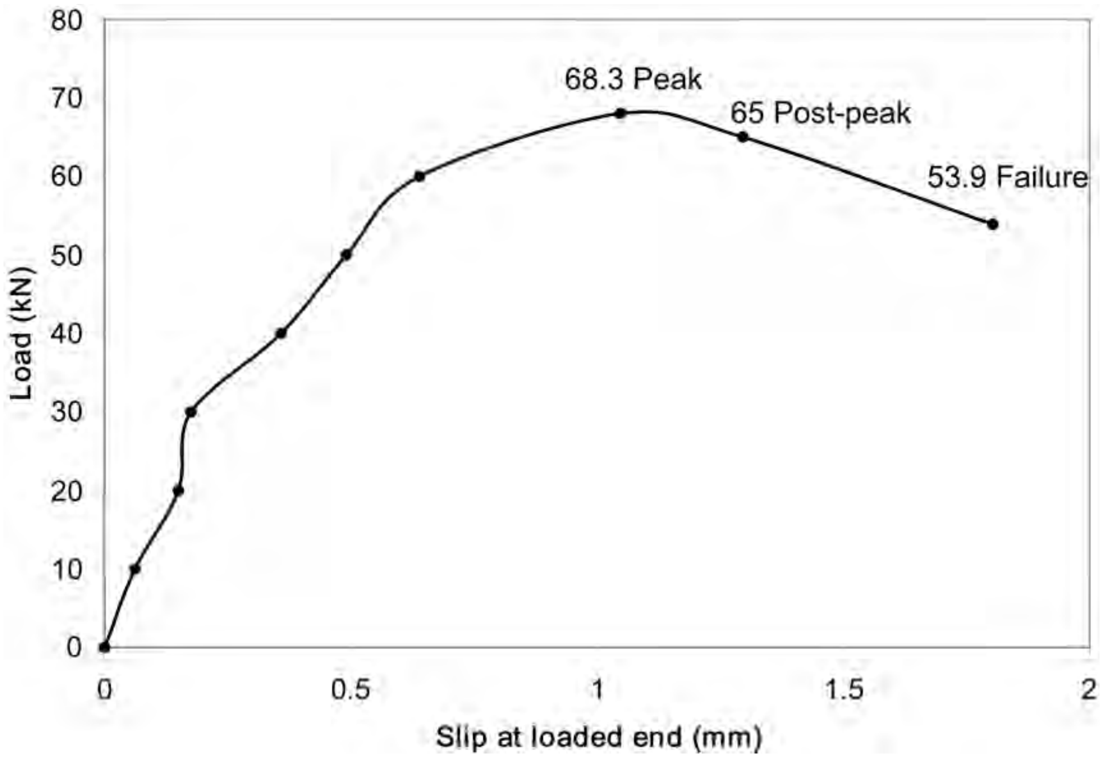

Figure 3.14: Load-slip response at the loaded end for S2-P1-SG

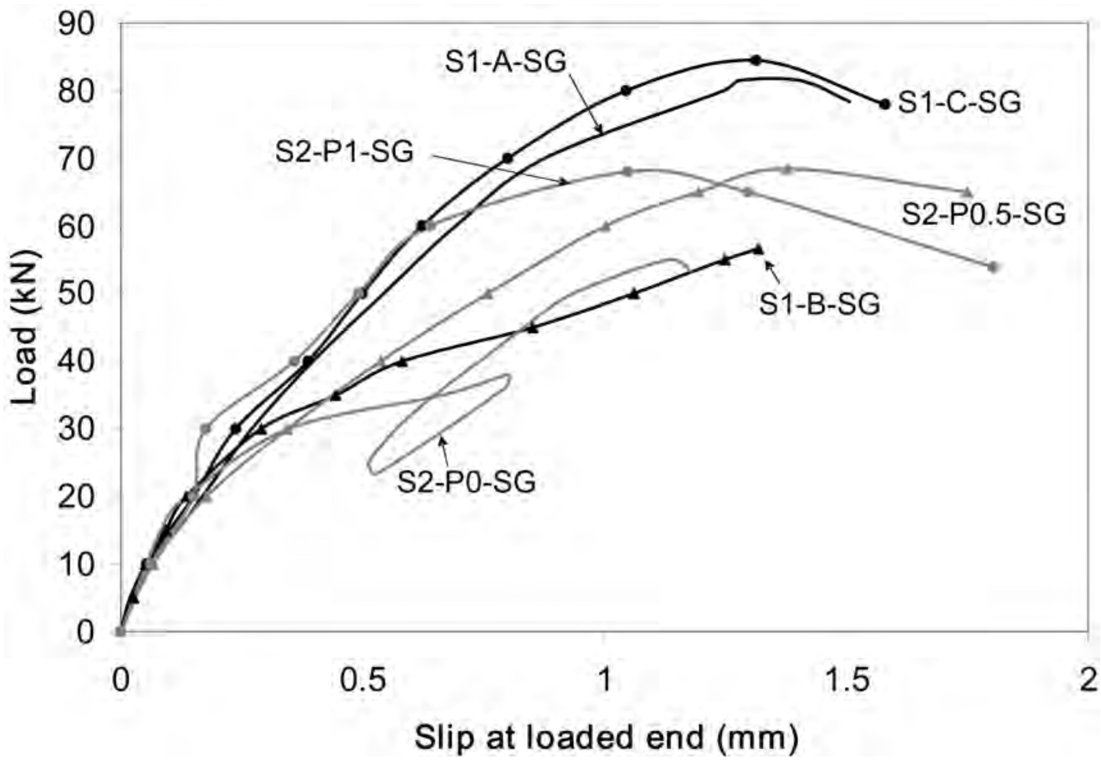

Figure 3.15: Load-slip response at the loaded end

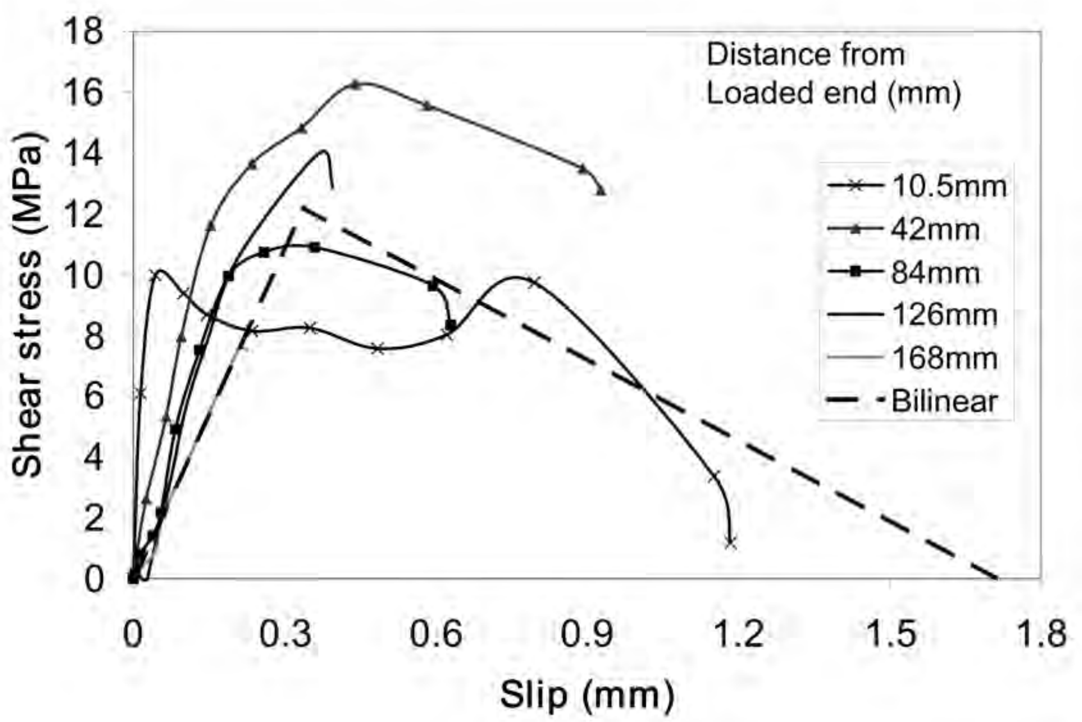

Figure 3.16: Bond-slip curve S1-A-SG

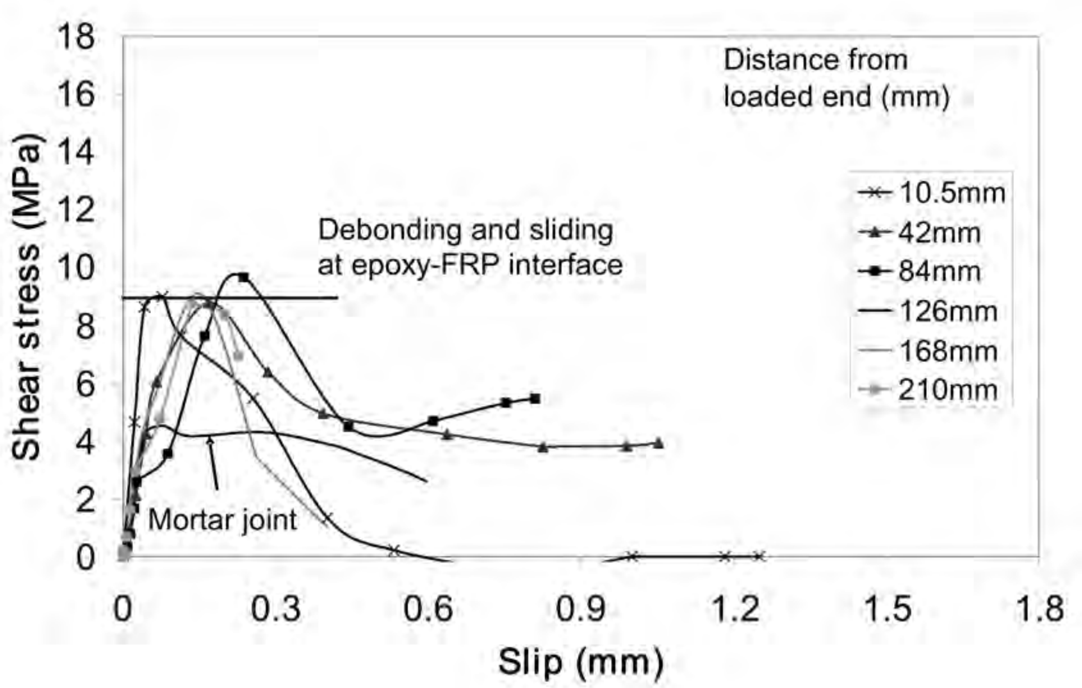

Figure 3.17: Bond-slip curve S1-B-SG

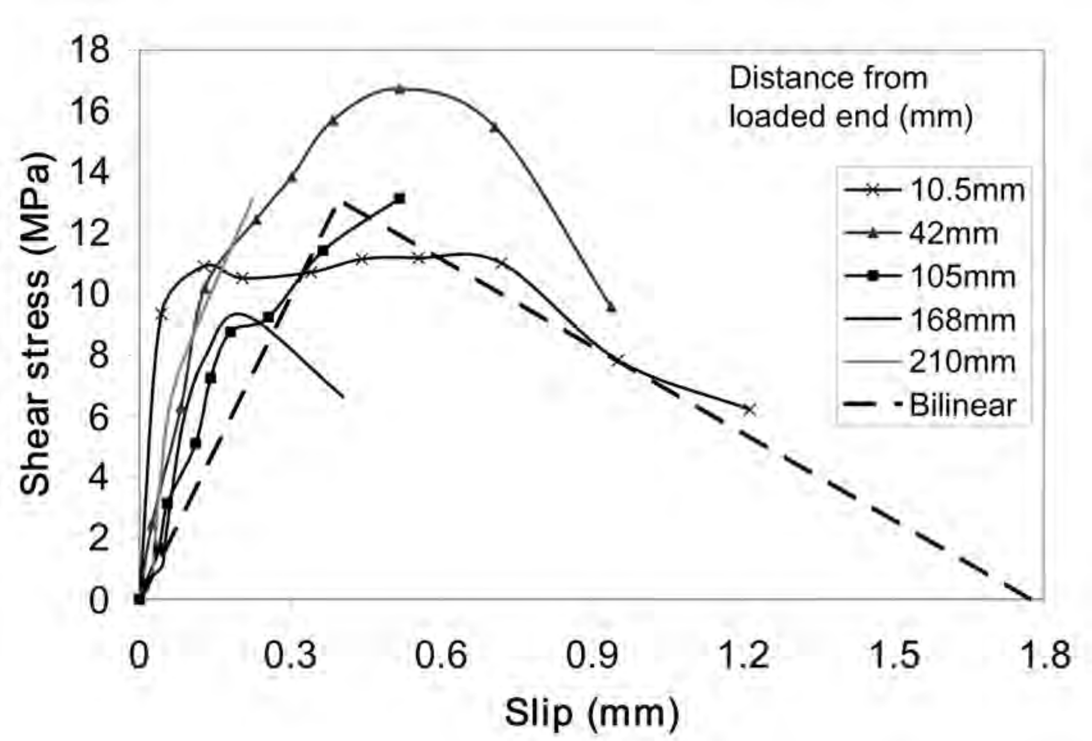

Figure 3.18: Bond-slip curve S1-C-SG

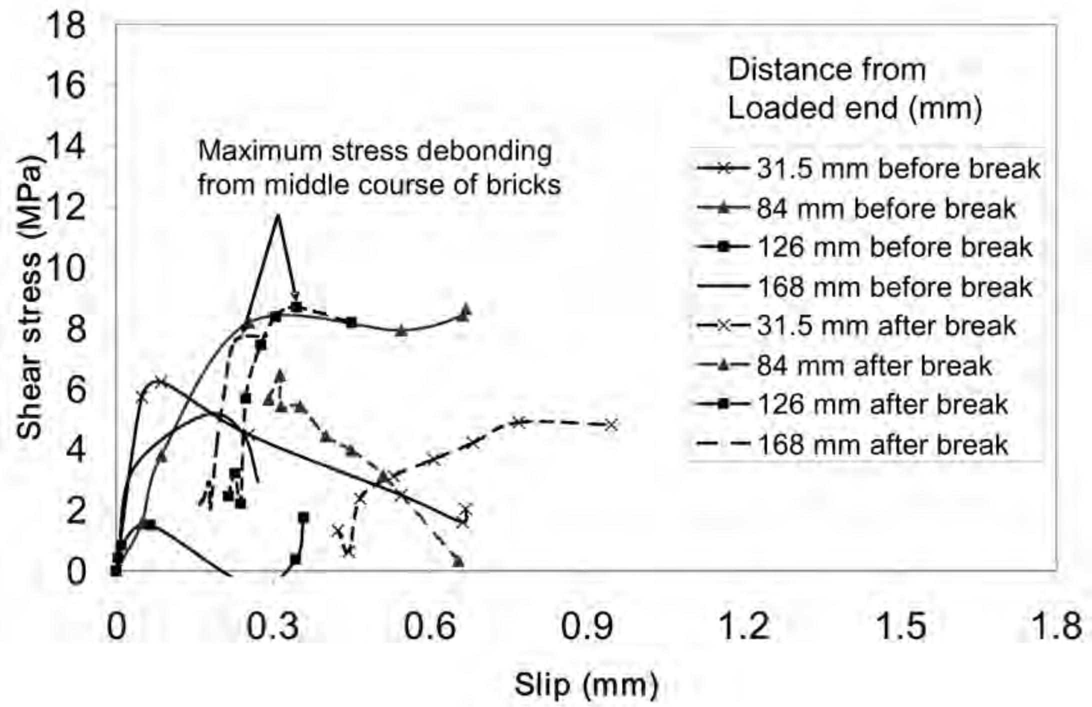

Figure 3.19: Bond-slip curve S2-P0-SG

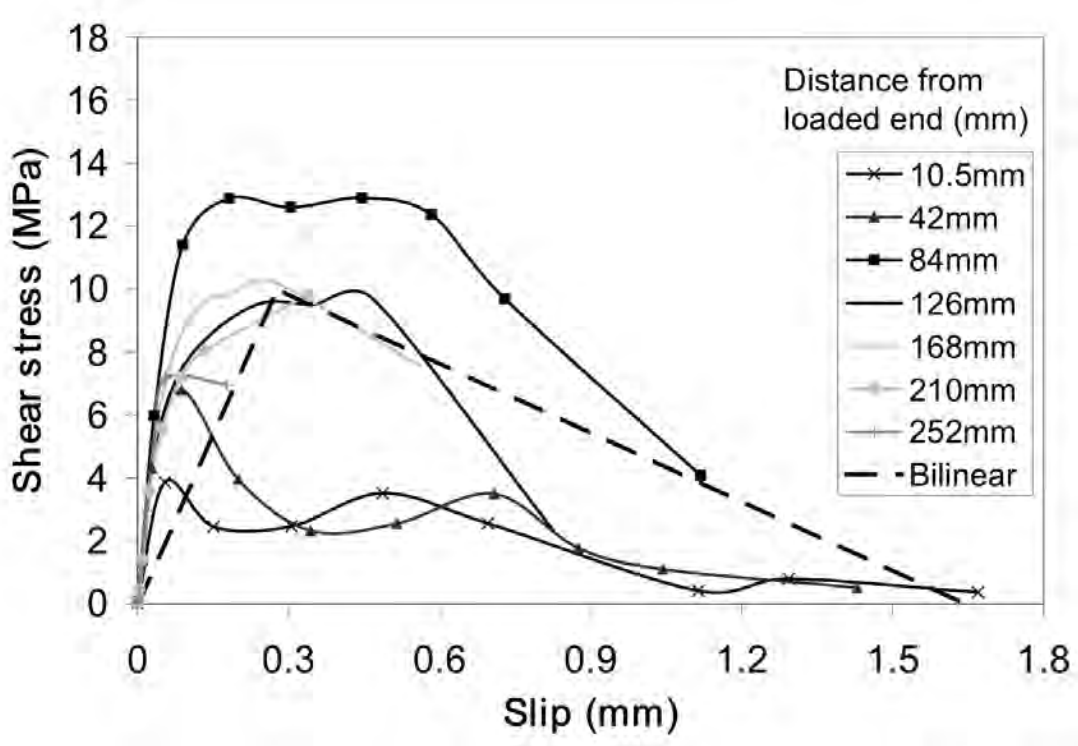

Figure 3.20: Bond-slip curve S2-P0.5-SG

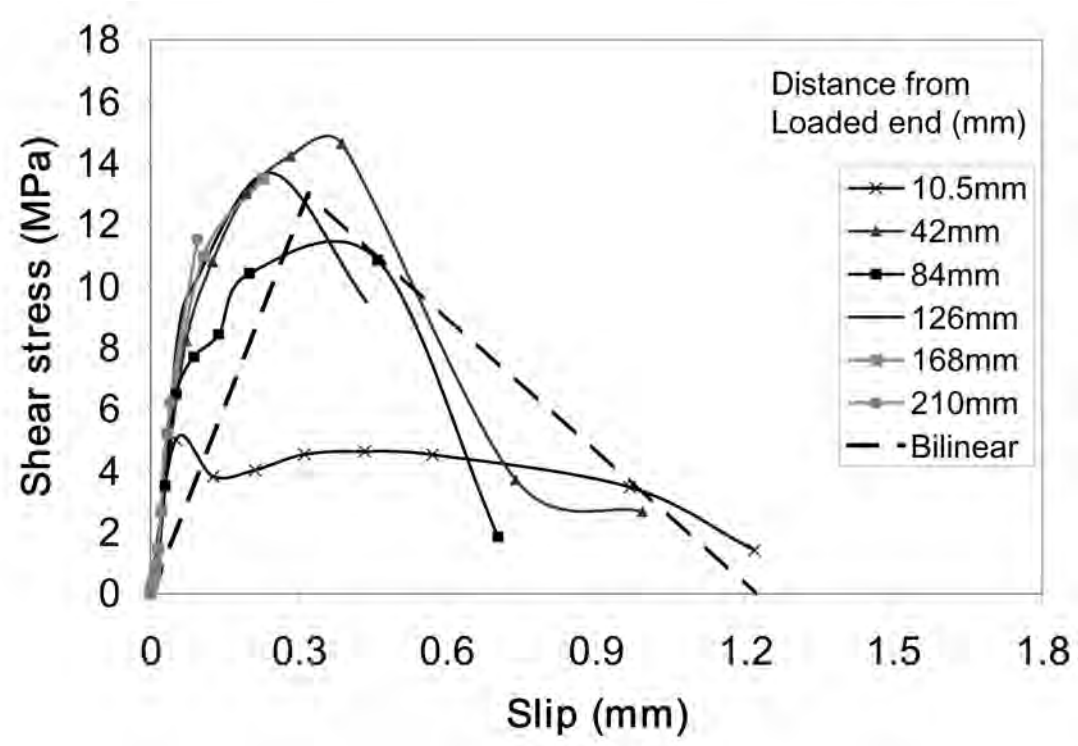

Figure 3.21: Bond-slip curve S2-P1-SG

S1-C-SG were 12.2 MPa and 13.1 MPa, respectively. The bond-slip curves derived for S1-B-SG (Figure 3.17) confirm the mixed failure modes observed during the test (discussed previously). The maximum shear stresses at positions along the bonded length, where the FRP was bonded to brick (10.5 mm, 42 mm, 84 mm, 168 mm, and 210 mm from the loaded end), were constant, and were equal to approximately 9.0 MPa. This was lower than the average maximum shear strength determined for specimens S1-A-SG and S1-C-SG, where debonding occurred through the brick. This reduction in bond strength for specimen S1-B-SG confirms that failure through the adhesive had occurred. Significant residual shear strength plateaus were also evident at these positions for S1-B-SG (unlike all other bond-slip curves) providing further evidence that sliding was a significant failure mode. The curve at 126 mm from the loaded end shows the bond-slip behaviour within the mortar joint. The maximum shear stress within the mortar joint was 4.5 MPa and was significantly lower than the maximum shear stress for debonding through brick or adhesive. The maximum shear stress transferred from FRP to masonry was reduced by approximately 64% when debonding occurred through the mortar joint (as opposed to debonding through the brick).

The bond-slip curves for specimen S2-P0-SG (Figure 3.19) were separated into curves before the break (i.e. when the two outer courses of masonry separated from the middle, reinforced course at 38 kN) using solid lines, and after the break using broken lines. The bond-slip curves derived from strain gauge readings recorded before the break were likely affected by cracking along the bed joint and the 'pull through' of the middle course of bricks. It can be seen from the curves before the break that at the initial stages of loading, load transfer and failure was closest to the loaded end (eg. 31.5 mm and 84 mm from the loaded end). The bond-slip curves derived from strain gauge readings recorded after the break (until ultimate failure) represent progressive damage of the specimen by cracking in the middle course of bricks (brick debonding). After the break, masonry within 100 mm from the loaded end was already damaged significantly and the majority of load transfer was shifted further down the bonded length. As a result bond-slip curves at 126 mm and 168 mm show the brick debonding behaviour of the middle course of masonry (a masonry section that is 76 mm wide). The average maximum shear strength of the middle course of masonry was 8.2 MPa. Compared to the wider masonry specimens (S1-A-SG and S1-C-SG) the maximum shear stress developed was reduced by 35%.

The average maximum shear stresses for specimens S2-P0.5-SG and S2-P1-SG were 10.0 MPa and 13.0 MPa respectively. Similar to bond strength, the average maximum shear stress increased linearly with an increase in compression as shown in Figure 3.11. Note that the bond-slip curve at 10.5 mm away from the loaded end was discounted when calculating the average maximum shear stress. The bond-slip curve at this location was not used because it was affected by the restraint conditions at the loaded end. The same was done when calculating the average maximum shear stresses for specimens S1-A-SG and S1-C-SG.

The bond-slip curves were not equal at all points along the bonded length for each specimen, in large part due to the location of cracking relative to the strain gauges. For future use in finite element and analytical models a single idealized bilinear model was fitted to the experimental data. For each bilinear model the maximum shear stress (τ_{max}) and corresponding slip (δ_1) were averaged from the experimental bond-slip curves. Rather than estimating the final slip (δ_{max}) from the curves, δ_{max} was determined by back calculation in Equation 3.2 using the experimentally determined bond strength for P_{IC}. Equation 3.2 represents the theoretical strength model for a strip bonded to concrete (or masonry). The equation is derived by considering equilibrium and compatibility of a strip-to-concrete joint with a bilinear relationship to model the interface (Seracino et al., 2007b). Using the bilinear model determined this way for the interface behaviour in a finite element or analytical model, the experimental bond strength is reproduced. The bilinear bond-slip model determined in this way produced a reasonable fit (see Figure 3.16 to Figure 3.21).

$$P_{IC} = \sqrt{\tau_{max}\delta_{max}}\sqrt{L_{per}(EA)_p} \tag{3.2}$$

Where P_{IC} is the bond strength of the specimen determined from the specific test with the strain gauges, L_{per} is the bonded perimeter of FRP which was 33 mm, $(EA)_p$ is the axial stiffness of the strip determined using the strain ϵ_{max} in the FRP at maximum load P_{IC} for each specimen.

As mentioned previously a bond-slip relationship for S1-B-SG could not be determined from the test data because of sliding at the interface. For specimen S2-P0-SG an average of the maximum shear stresses after the break was used for τ_{max} so that the bond-slip curve represented debonding through the middle course of bricks. δ_1 was estimated as 0.2 mm by finding the intersection of the elastic part of the bond-slip curve at 126 mm (after the break) with the x-axis ($\delta \approx 0.16$) and subtracting from the slip at maximum stress ($\delta \approx 0.36$). For clarity the bilinear relationship for specimen S2-P0-SG is not shown in Figure 3.19. The parameters describing the bilinear bond-slip models are tabulated in Table 3.4, and defined in Figure 3.22.

Table 3.4: Bilinear bond-slip parameters

Specimen	δ_1 (mm)	τ_{max} (MPa)	δ_{max} (mm)
S1-A-SG	0.34	12.2	1.71
S1-B-SG	NA	NA	NA
S1-C-SG	0.40	13.1	1.77
S2-P0-SG	0.20	8.2	1.30
S2-P0.5-SG	0.28	10.0	1.64
S2-P1-SG	0.32	13.0	1.22

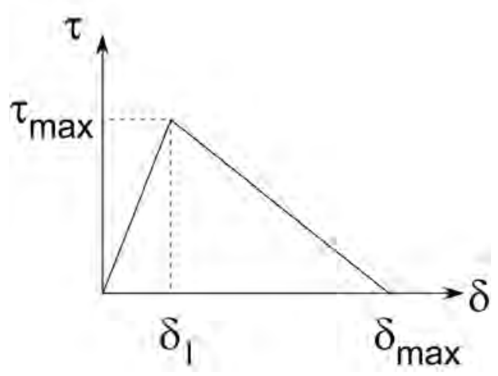

Figure 3.22: Bond slip model parameters

3.4 Summary and conclusions

A series of 18 pull tests was conducted on clay brick masonry prisms strengthened with NSM CFRP strips. The bond strengths, critical bond lengths and the local bond-slip relationships were determined. Both vertically aligned FRP strips (FRP perpendicular to bed joints) and horizontally aligned FRP strips (FRP parallel to bed joints) were tested. For the vertically aligned FRP strips the tests included: bonding FRP to a stack bonded specimen; bonding FRP to brick units in a running bond specimen; and bonding FRP to alternating brick and mortar head joints in a running bond specimen. For horizontally aligned FRP strips the effect of compression was investigated.

The main failure mode of the specimens was by debonding of the FRP from the masonry prism. The behaviour of series 2 specimens was affected by surface irregularities and therefore the results of these specimens were indicative only. It is recommended that capping techniques or similar be used to reduce such affects.

Mortar joints parallel to the FRP reinforcement reduced the region of masonry effective in load transfer, thus reducing the bond strength. The largest reduction in bond strength was 31%, and occured for specimens where the FRP was aligned horizontally and the distance between FRP and parallel mortar joint was the least.

For solid bricks a reduction in strength of 8% was observed between the stack bonded and running bonded specimens (FRP inserted into brick only), and was attributed to the presence of parallel mortar joints. When the FRP strip passed through mortar head joints as well as units, the average bond strength was reduced by 11% when compared to the specimens constructed using a running bond with the FRP bonded into brick unit only. As this reduction in strength is not too significant, it can be recommended that vertical NSM FRP reinforcement is bonded into alternating brick unit and mortar joints to hide the retrofit.

Thin rectangular strips were selected in order to maximize the confinement around the strip and increase the bond between the FRP and the masonry. The use of thin rectangular strips required deep grooves to be cut into the surface of the masonry prisms. For the prisms where the FRP was aligned vertically, the deep grooves caused cracking through the thickness of the prism in line with the FRP.

This type of cracking will potentially create a plane of weakness in a masonry wall and adversely affect the overall behaviour of the wall. Through wall cracking is therefore a potential problem when using NSM FRP strips, particularly for weak, hollow and cored masonry. Extra confinement by the surrounding masonry in a wall (compared to a prism) may help prevent through wall cracking. The results suggest that minimizing the groove depth would be a key factor in enhancing the overall behaviour of the strengthened masonry member.

The failure mode of the specimens involving transverse cracking was dependent upon the out-of-plane thickness of the specimen. Therefore the related bond results are only representative of the behaviour of the strengthening system in walls having the same thickness of the specimen (which was 110 mm).

Although the bond strength was reduced when aligning the FRP horizontally, compression normal to the joint increased the bond strength significantly and at a compression of 1.0 MPa the bond strength increased to a value similar to the vertically aligned FRP. For the range of tested compression values, based on the typical range found in a URM building, the bond strength, and interface shear strength increased linearly with applied compression. Note that these results are indicative only, due to the results of series 2 specimens being affected by surface irregularities.

The results of the pull tests conducted in this chapter illustrate the significant difference between the bond behaviour for NSM FRP strips aligned vertically and horizontally. It is important in design and analysis that the differences are taken into account.

4

Experimental tests on FRP strengthened masonry wall panels

4.1 Introduction

In this chapter the results of the experimental tests on masonry wall panels strengthened with NSM CFRP strips are presented. To investigate the in-plane shear behaviour of masonry strengthened with NSM FRP strips, four unreinforced masonry (URM) wall panels and seven strengthened wall panels were tested using the Diagonal Tension/Shear Test (ASTM E519-93) ASTM Standards (1993). For the strengthened panels, four different reinforcement schemes were used, and included: reinforcing one side of the panel with 2 vertical strips; reinforcing each side of the panel with 2 vertical strips; reinforcing each side of the panel with 2 horizontal strips; and reinforcing one side of the panel with 2 vertical strips and reinforcing the other side with 2 horizontal strips.

The reinforcement strategies were designed to prevent sliding along mortar bed joints (within the wall panel) and diagonal cracking (through mortar joints and brick units). The experimental tests were used to determine: the effectiveness of the reinforcement scheme (in terms of strength and ductility increase); the failure modes; the reinforcement mechanisms; and the behaviour of the bond between the masonry and the FRP.

Of particular interest was the reinforcement mechanism of the vertical NSM FRP strips. The vertical reinforcement can potentially restrain sliding along mortar bed joints and diagonal cracking through the brick units. Marshall and Sweeney (2002) did not expect vertical NSM strips to be effective at increasing sliding resistance or diagonal cracking. As described in the literature review (Section 2.4, page 11), vertical reinforcement can potentially restrain crack sliding by two different mechanisms. These mechanisms are dowel action and restraining dilation. The contribution of dowel strength is likely to be low, but it may contribute some resistance due to confinement of the reinforcement with the brick. It was hypothesized that the other mechanism, where the FRP resists crack separation upon sliding (dilation), would be significant. The restraint of dilation would result in an increased resistance to frictional sliding.

The test results presented in this chapter include: the load-displacement behaviour; crack patterns; failure modes; and FRP strain measurements. This chapter also includes a comparison of the reinforcement schemes, and comparisons of the results with other tests from the literature.

4.2 Experimental program

The Diagonal Tension/Shear Test involves subjecting a square section of masonry, with height and length both equal to 1.2 m, to a compressive load applied along the diagonal. A schematic of the test is shown in Figure 4.1a. A photograph of the test is shown in Figure 4.1b.

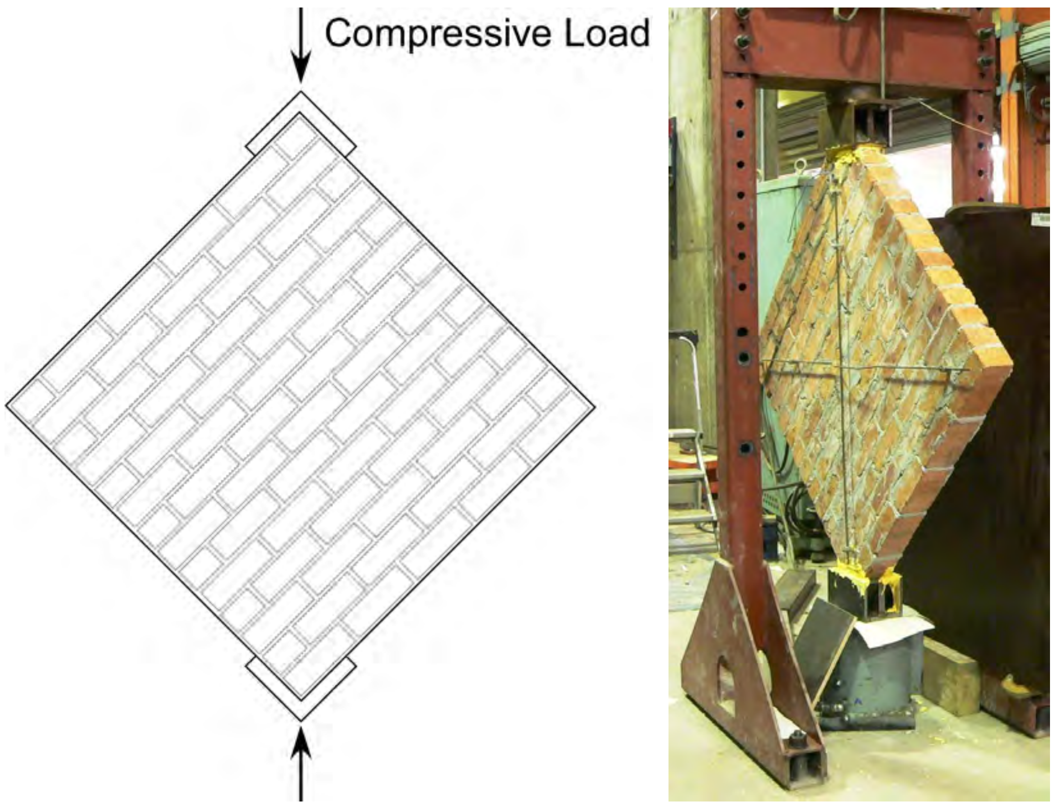

(a) Test schematic (b) Setup URM-1

Figure 4.1: The Diagonal Tension/Shear Test

The panels were constructed from solid clay masonry units with nominal dimensions 230 mm long, 110 mm wide and 76 mm high. Five batches of mortar were used in the construction of the panels, all having a mix ratio of 1:1:6 (cement:lime:sand by volume). The mortar joints were 10 mm thick. These are the same material specifications as used for the pull tests presented in Chapter 3.

The mortar batches used to construct each panel are presented in Table 4.1. The flexural tensile bond strength of each mortar batch was determined using the bond wrench test, AS3700-2001, Standards Australia (2001c). The bond wrench test is described in further detail in Section 5.3.1. The average flexural tensile bond strength (coefficient of variation in brackets) of each mortar batch is also presented in the table.

During the construction of panels V4B, V2H2B and H4B, and also at the start of construction of panels URM-3 and URM-4, the mortar was retempered (water added) to improve its workability. Bond wrench tests were conducted on the retempered mortar batches, with the results identified as 'batch no. +W' in Table 4.1. The height of the panel (during construction) when the water was added to the mortar for panels V4B, V2H2B and H4B was not recorded. URM-4 was constructed over 2 days, with a new mortar batch used on the second day of construction. The height of URM-4 (during construction) where the new mortar batch was started was not recorded. In Table 4.1 the heading 'mortar batch (lower)' refers to the mortar batch used to construct the lower part of the panel (normally before retempering the mortar batch), and the heading 'mortar batch (upper)' refers to the mortar batch used to construct the upper part of the panel (in most cases the retempered mortar). Table 4.1 also shows the age at testing of the bond wrench piers (BW) and panel tests.

Table 4.1: Wall panel data

Panel	Mortar batch (lower)	Bond strength (MPa)	Mortar batch (upper)	Bond strength (MPa)	Age at test (weeks)	
					Panel	BW
URM-1	5	1.26 (COV 32%)	-	-	8	8
URM-2	5	1.26 (COV 32%)	-	-	8	8
URM-3	5+W	0.41 (COV 59%)	-	-	8	8
URM-4	3+W	0.31 (COV 57%)[a]	4	0.57 (COV 48%)	46	14
V2	4	0.57 (COV 48%)	-	-	30	14
V4A	2	0.49 (COV 37%)	-	-	45	14
V4B	2	0.49 (COV 37%)	2+W	0.29 (COV 46%)	45	14
V2H2A	3	0.47 (COV 47%)	-	-	45	14
V2H2B	3	0.47 (COV 47%)	3+W	0.31 (COV 57%)[a]	46	14
H4A	1	1.25 (COV 51%)	-	-	46	14
H4B	1	1.25 (COV 51%)	1+W	0.65 (COV 34%)	46	14

[a] Only 5 joints tested. Pier constructed with other 5 joints broke during transport

The reinforced panels were strengthened with carbon FRP (CFRP) strips 15 mm wide and 2.8 mm thick. The FRP strips had an elastic modulus equal to approximately 210,000 MPa, and a rupture strain equal to 12,000 $\mu\varepsilon$ (manufacturers data). The same reinforcement specification was used for the pull tests. The FRP strips were constructed by gluing two FRP strips 15mm wide and 1.4 mm thick together with a 'super-strength' araldite adhesive. Six strain gauges , spaced 170 mm apart and 170 mm from the ends, were sandwiched between the two strips to measure the FRP strain distribution during the test. The two FRP strips were glued together to provide sufficient cross-sectional area of FRP to ensure that failure of the joint occurred by debonding through the brick rather than by plate rupture. The FRP reinforcement was glued, using a two-part epoxy adhesive, into rectangular grooves cut into the surface of the masonry with a circular saw. The grooves were 20 mm deep and 6 mm wide and had the same dimensions as the grooves cut into the pull test specimens. To cut vertical grooves near the base of the panels, the panels were tilted and an angle grinder was used (shown in Figure 4.2). After insertion, the FRP was flush with the surface of the panel (no brick or mortar pieces were placed over the FRP).

Figure 4.2: Cutting grooves into specimens with angle grinder

The reinforcement schemes used for the strengthened panels are shown in Figure 4.3. Panel V2 was reinforced with 2 vertical NSM CFRP strips (i.e. aligned perpendicular to the bed joints) on one side of the panel (shown in Figure 4.3a). Panel V2 was tested to observe the effect of single sided strengthening. Panels V4A and V4B were reinforced with 2 vertical NSM CFRP strips on each side of the panel (shown in Figure 4.3b). Rather than aligning the FRP strips symmetrically on either side of the panel the strips were staggered as shown to prevent through brick cracking between the 2 strips. The distance between the staggered vertical reinforcement was 120 mm. Panels V2H2A and V2H2B were reinforced with 2 vertical NSM CFRP strips on one side of the panel and 2 horizontal NSM CFRP strips (i.e. aligned parallel to the bed joints) on the other side of the panel (shown in Figure 4.3c). Panels H4A and H4B were reinforced with 2 horizontal NSM CFRP strips on each side of the panel (shown in Figure 4.3d and Figure 4.3e). Separate figures are shown because the strain gauge numbering was different for each test. Similar to panels V4A and V4B the reinforcement in panels H4A and H4B was staggered. The distance between the staggered horizontal reinforcement was 86 mm. The vertical reinforcement was located midway between mortar head joints and the horizontal reinforcement was located midheight between the mortar bed joints as shown in Figure 4.3. The FRP strips were bonded into the brick units to maximise the bond strength and hence effectiveness of the reinforcement (see Section 2.3.3). The vertical reinforcement was used to restrain sliding along the bed joint, and the horizontal reinforcement was used to restrain diagonal cracking.

The load was applied with a hydraulic jack. The flow rate of the hydraulic fluid was kept constant throughout all tests until failure. The hydraulic pressure caused an initial loading rate (before cracking) of around 40 kN/min. The loading scheme was not strict displacement control, but was able to capture the post-peak softening behaviour of the panel if the test did not become unstable.

Potentiometers were used to measure the vertical and horizontal displacement on each side of the panel in accordance with ASTM E519-93 ASTM Standards (1993). The gauge lengths were 1300 mm and 1400 mm for the vertical and horizontal directions respectively. A potentiometer was also used to measure the displacement of the hydraulic jack that was used to apply the load.

The debonding strain (FRP loaded in direct tension) of the vertical reinforcement FRP to masonry connection used here was determined from pull tests (see previous chapter). Of the pull test specimens, specimen type '1C' best represented the vertical connection used in the panel tests. The debonding strain of this specimen ranged from 7416 $\mu\varepsilon$ to 8963 $\mu\varepsilon$. The debonding strain of the horizontal reinforcement was determined for a range of compression values. At zero compression, the debonding strain ranged from 5793 $\mu\varepsilon$ to 6245 $\mu\varepsilon$, and at 1 MPa compression , the debonding strain ranged from 7741 $\mu\varepsilon$ to 8496 $\mu\varepsilon$.

4.3 Experimental results

4.3.1 Unreinforced masonry (URM) panels

The experimental load-displacement responses of the 4 URM panels are shown in Figure 4.4. The vertical displacement measurement was the average of the vertical potentiometer gauge displacements on each side of the panel. In general, all panels behaved approximately linearly until failure.

URM-1 and URM-2, panels constructed with the same strong mortar (high flexural tensile bond strength as measured using bond wrench tests), both failed by diagonal cracks that developed through both brick units and mortar joints (shown for specimen URM-1 in Figure 4.5a). Multiple cracks were observed in both specimens before failure (Figure 4.5a). The ultimate loads of panels URM-1 and URM-2 were measured as 237 kN and 290 kN respectively.

URM-3 and URM-4, panels constructed with weak mortar, both failed by sliding along bed joints (Figure 4.5b–Figure 4.5d). During the testing of URM-4 a crack developed through the mortar bed joints at the top of the panel, at a load of 163 kN. The load then dropped to 143 kN (Figure 4.4). The crack is shown in Figure 4.5c. The panel should have failed along this crack but the top support shoe restrained the section of masonry and allowed the panel to transfer more load. The

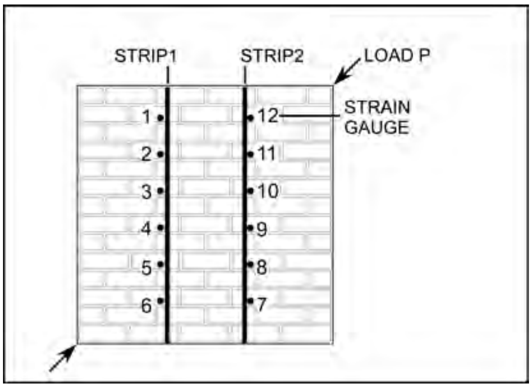

(a) V2

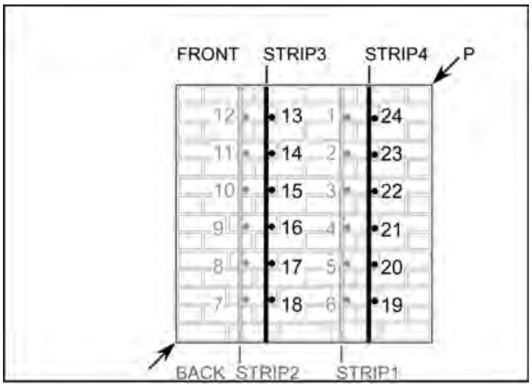

(b) V4A and V4B

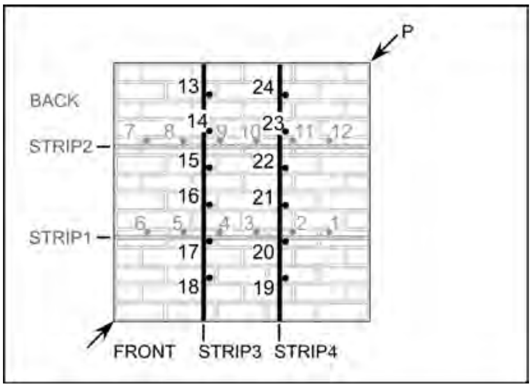

(c) V2H2A and V2H2B

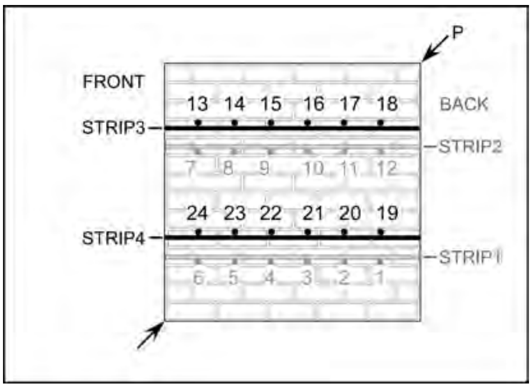

(d) H4A

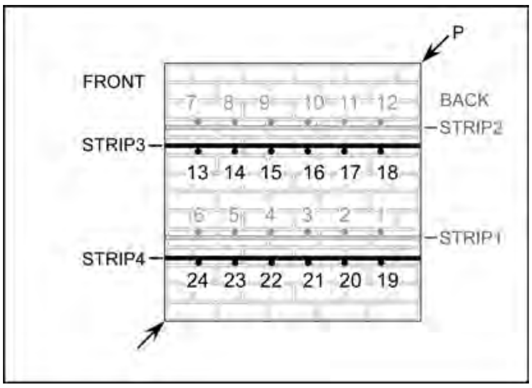

(e) H4B

Figure 4.3: Reinforcement schemes

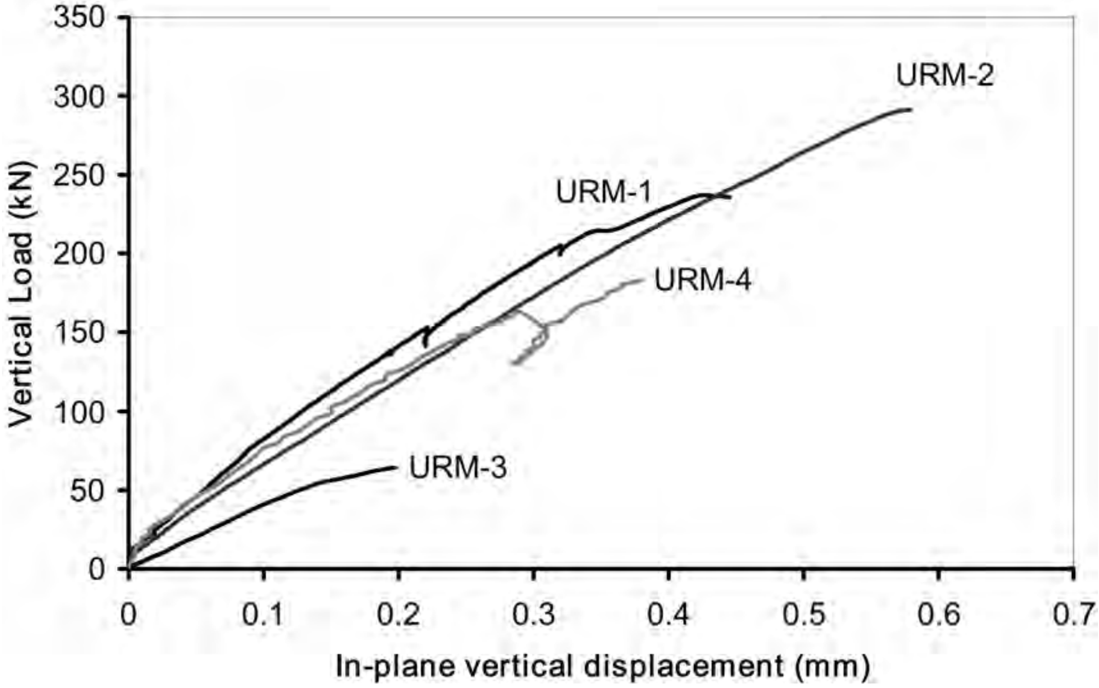

Figure 4.4: Load-displacement response of URM panels

panel eventually failed along another sliding crack at a load of 183 kN (shown in Figure 4.5d).

The ultimate load of panel URM-3 was 65 kN which was considerably less than the ultimate load of URM-4. A higher ultimate load for panel URM-4, compared to URM-3, was reasonable given that failure occurred in the top half of panel URM-4. The flexural bond strength of URM-4 was 0.57 MPa at the top of the panel. This bond strength was larger than the bond strength of URM-3 (0.41 MPa). The difference in ultimate strength was, however, greater than expected. Two out of the ten joints tested to determine the bond strength of the mortar used to construct URM-3 (batch 5+W) broke during test setup. This indicated that the bond strength was essentially zero. It is possible that, in panel URM-3, joints with very little to no bond strength were present, which could have led to the very low ultimate strength observed.

4.3.2 FRP strengthened panels

Panel V2

The load versus the vertical displacement (average of potentiometer gauge displacements on each side of the panel) of panel V2 is shown in Figure 4.6. The vertical potentiometers used to measure the vertical displacement of the panel reached their travel capacities shortly into the test. To show the load displacement behaviour of the whole test the load versus the vertical displacement of the hydraulic jack (that was measured using a larger potentiometer) is plotted in Figure 4.7.

The panel behaved linearly until cracks began to form at a panel vertical dis-

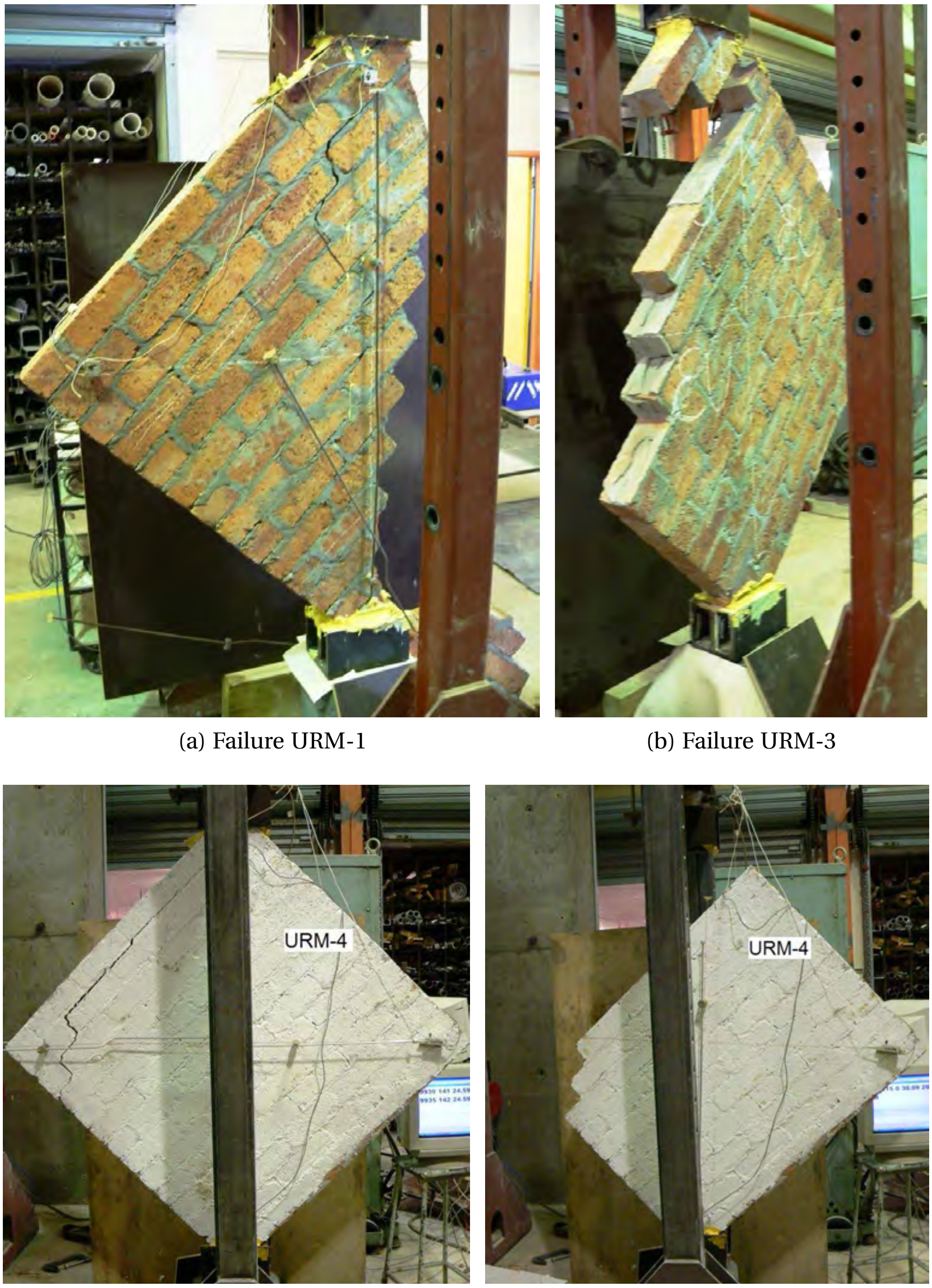

(a) Failure URM-1

(b) Failure URM-3

(c) 1st crack URM-4 (P=163 kN)

(d) Failure URM-4

Figure 4.5: Failure modes of URM specimens

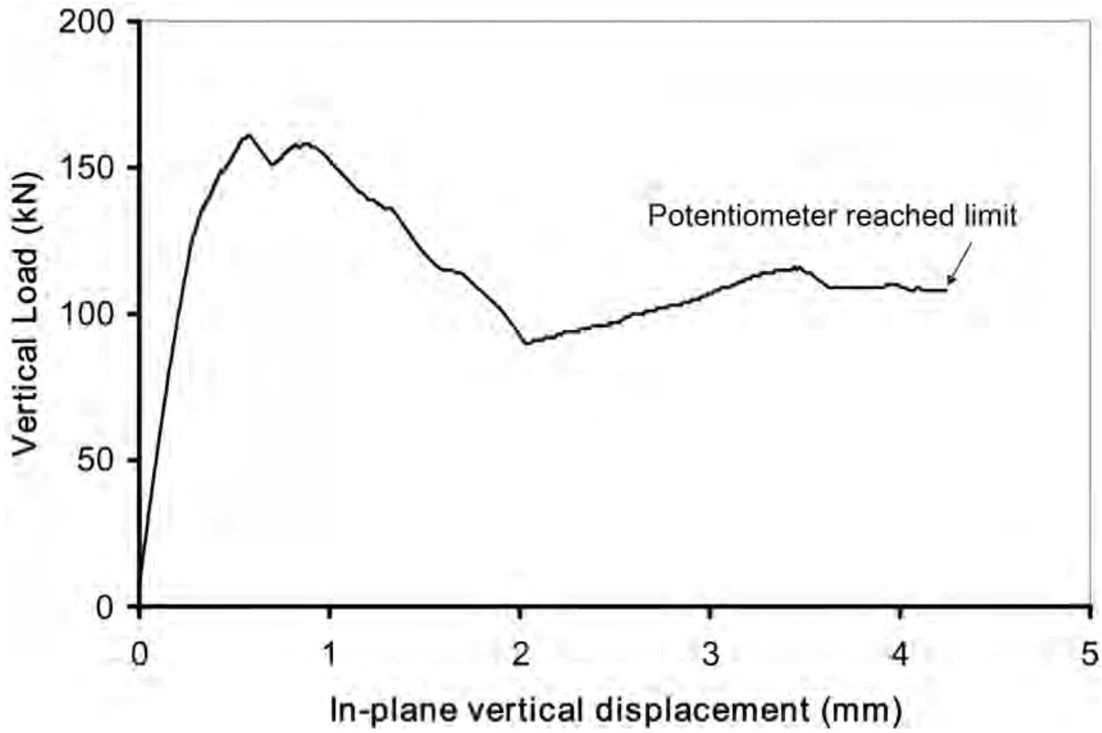

Figure 4.6: Load versus panel displacement V2

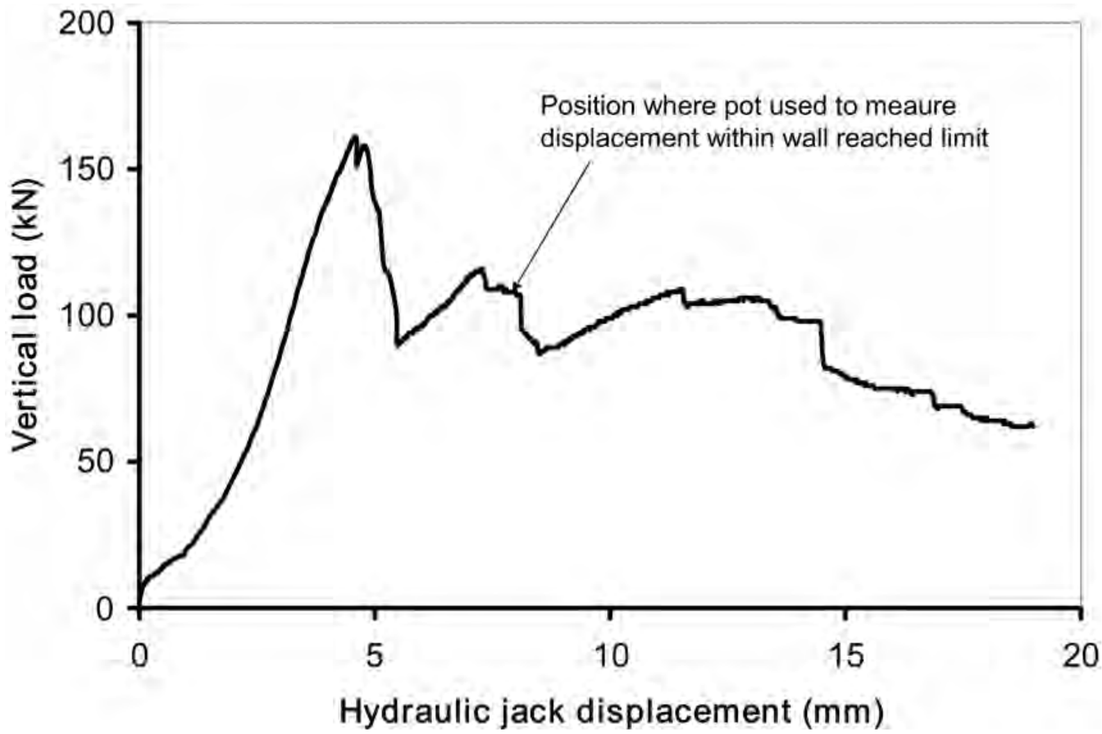

Figure 4.7: Load versus jack displacement V2

placement of 0.3 mm (load equal to 125 kN). Note that the panel would have likely failed at this point if the panel was unreinforced. The reinforced panel did not fail, but instead the load increased as cracking developed and the stiffness of the panel gradually decreased. The panel attained a maximum load of 160 kN (at a panel vertical displacement of 0.59 mm) and at this point a large diagonal shear crack had developed through mortar joints and some brick units. This crack is shown in Figure 4.8a and Figure 4.8b.

After the diagonal crack formed through the panel the load reduced to approximately 100 kN. The capacity of the panel remained at approximately 100 kN (varying between 88 kN and 115 kN) as the top section of the panel slid relative to the bottom section of the panel along the crack. The panel also bent (out of plane) about the crack towards the reinforced side of the panel. The out-of-plane displacement (shown in Figure 4.8c) occurred during the test because the reinforcement was applied to one side only. At the later stages of the test, after a large amount of vertical displacement, the load gradually reduced to 60 kN. The load reduction was likely caused by the large out-of-plane displacement. To avoid a potentially dangerous out-of-plane failure the test was stopped at this stage.

A large amount of bending in the plane of the panel occurred in the FRP across the shear cracks during the test (shown at the end of the test in Figure 4.9). For this panel the shear transferred via dowel action (at this stage of damage) was likely to be very small because the FRP, with small cross sectional area was bent over a large length and about its weak axis. Given that the dowel strength would have been very small the main mechanism of the reinforcement would have been the restraint of dilation. The restraint of dilation increased the resistance to frictional sliding.

Plots of the tensile strain in the FRP at strain gauge locations versus the panel vertical displacement (measured by potentiometers within the panel) for panel V2 are shown in Figure 4.10 (for strain gauge locations refer to Figure 4.8b). In Figure 4.8b gauges which were damaged prior to testing and yielded no data are labelled with a lighter font. When the first diagonal crack formed (at a vertical displacement of 0.3 mm) the tensile strain measured at strain gauges close to the crack (SG3, SG5, SG11 and SG12) increased significantly. The FRP strains were highest in the vicinity of the crack and reduced further away from the crack as the load was transferred to the masonry. The tensile strain in the FRP strips increased as the vertical displacement of the panel increased and cracking developed.

Plots of the tensile strain in the FRP at strain gauge locations versus the vertical displacement of the hydraulic jack are shown in Figure 4.11. The figure shows that strains in the FRP reached a maximum value after a significant amount of displacement. The maximum strain recorded in the FRP strips was 3100 $\mu\varepsilon$ (in strip 1, SG3) and was significantly lower than the FRP strain required to cause debonding (range = 7416 $\mu\varepsilon$ - 8963 $\mu\varepsilon$) or rupture (12,000 $\mu\varepsilon$). Debonding or rupture of either strip was not observed during the test. At the later stages of the test, the FRP strains started to reduce as the load carrying capacity of the panel also reduced.

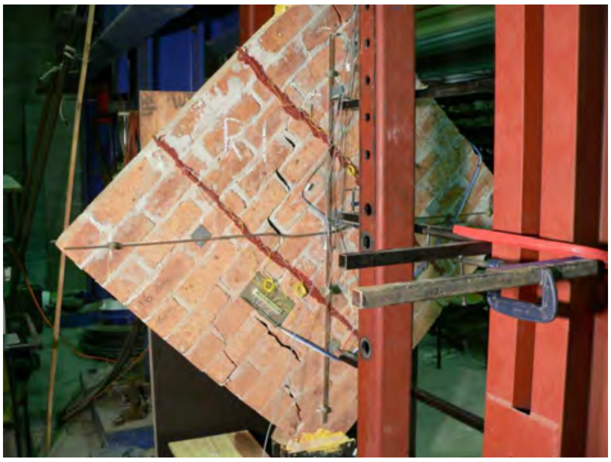

(a) Crack pattern

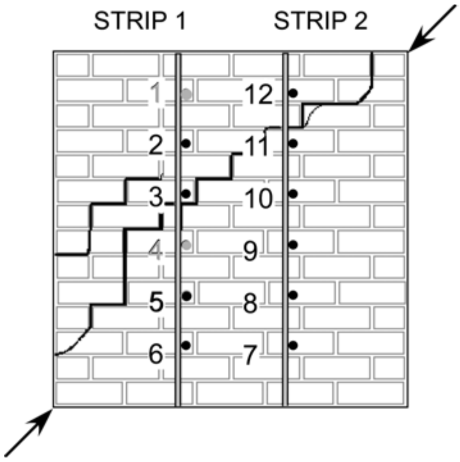

(b) Crack schematic

(c) Out-of-plane bending

Figure 4.8: Test observations for panel V2

(a) Strip 1

(b) Strip 2

Figure 4.9: FRP bending across shear crack in panel V2

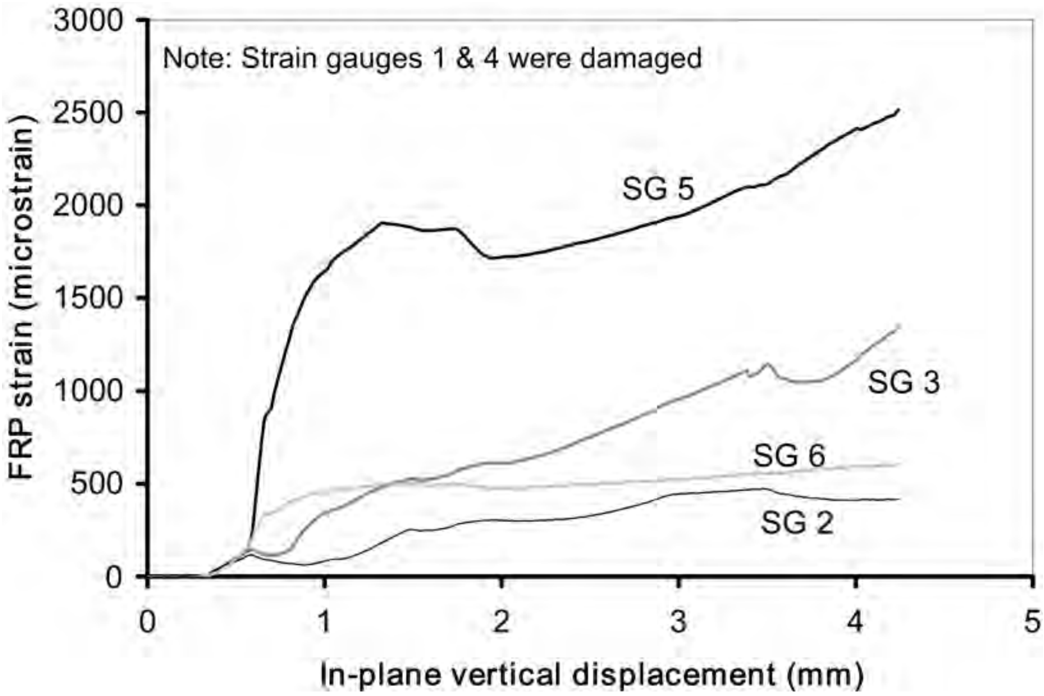

(a) Strip 1

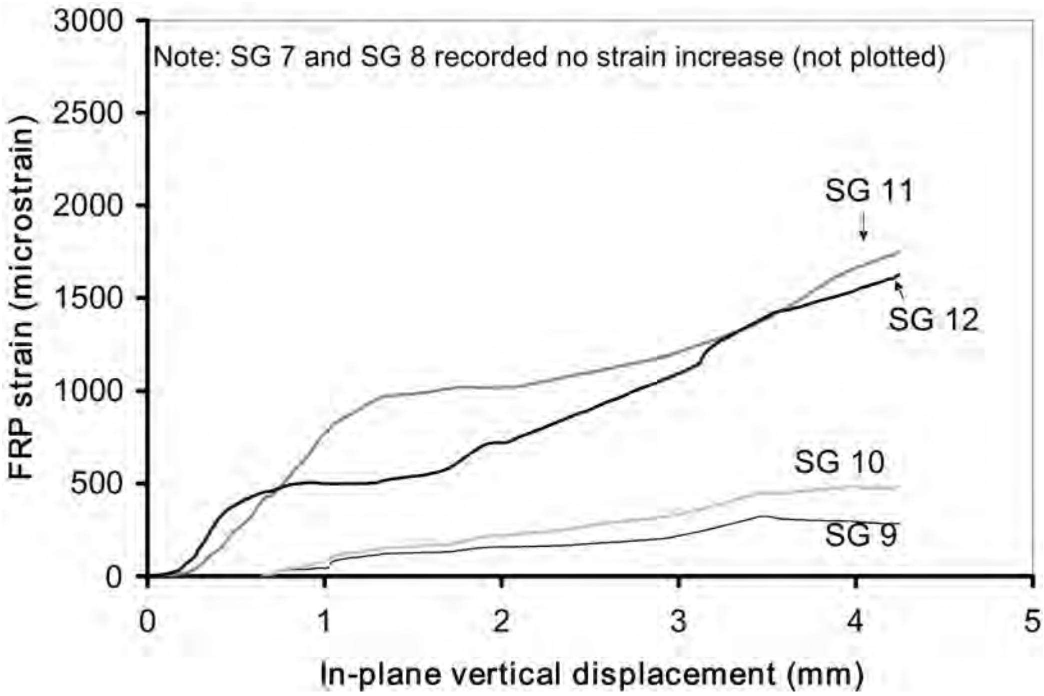

(b) Strip 2

Figure 4.10: Strain in FRP strips vs panel vertical displacement V2

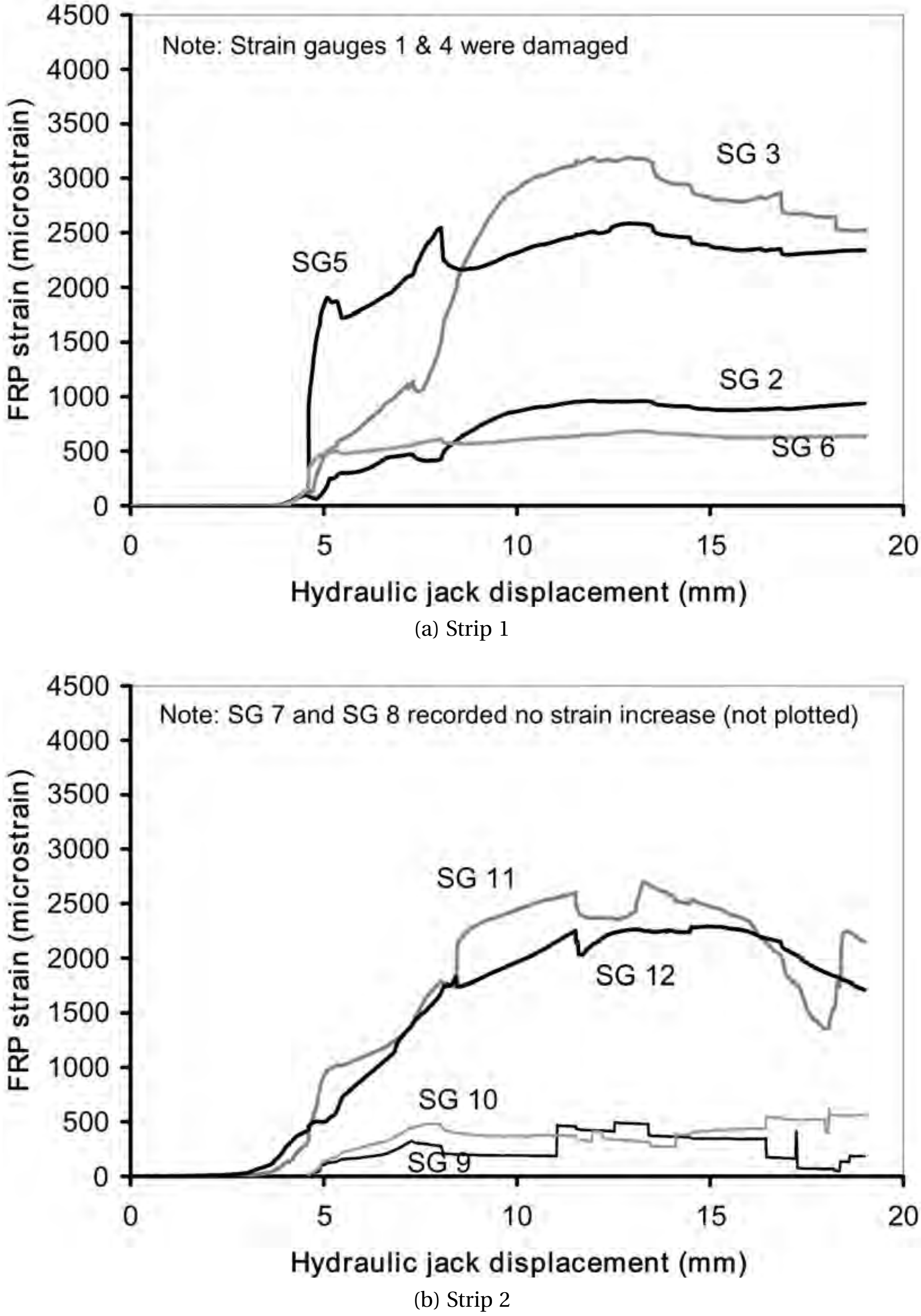

(a) Strip 1

(b) Strip 2

Figure 4.11: Strain in FRP strips vs jack vertical displacement V2

Panels V4A & V4B

The load-vertical displacement responses of panels V4A and V4B are shown in Figure 4.12. For these tests (and the following tests) larger range potentiometers were used to capture the full displacement. Both panels behaved approximately linearly until a diagonal crack formed both through mortar joints and some brick units. The diagonal crack is shown on the front side of panel V4A in Figure 4.13. In Figure 4.13 the crack pattern and FRP strips are highlighted with black lines. The first diagonal crack was observed in both panels at a vertical displacement of 0.4 mm, with corresponding loads of 172 kN in V4A and 140 kN in V4B. The FRP reinforcement restrained the opening of the diagonal crack, and prevented immediate panel failure.

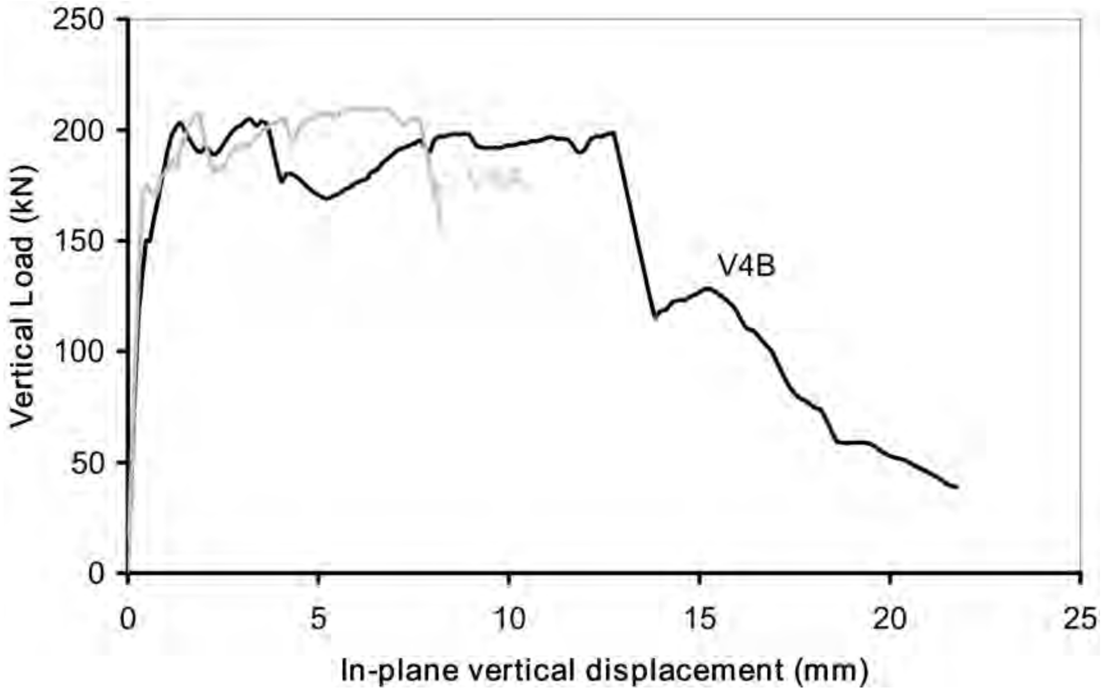

Figure 4.12: Load-displacement response of V4A and V4B

Both panels deformed under a reasonably constant load of approximately 200 kN, which was reached soon after the first cracks developed in the panel. The ultimate load of panel V4A was 210 kN, and the ultimate load of panel V4B was 205 kN. In both panels, more diagonal cracks developed and opening of and sliding along the diagonal cracks occurred as the vertical displacement increased. During the testing of panel V4A most sliding along the diagonal crack, next to strip 3, was prevented, and instead cracks were forced to develop along the inside of strip 3 (between strips 3 and 4). Cracking along the inside of strip 3 started at the intersection of the diagonal crack and the FRP strip and progressed downwards. The cracking developed through the thickness of the panel and is shown at failure in Figure 4.14 on the front and back face of the panel. During the testing of panel V4B sliding was not prevented along cracks intercepted by FRP, instead restrained

Figure 4.13: Diagonal crack V4A (front side)

sliding occurred with local bending of the FRP. Most deformation of V4B was by sliding along the major diagonal crack (seen at failure in Figure 4.15 on the front and back face of the panel).

Failure of both panels was caused by debonding of the FRP strip from the masonry at the bottom of FRP strip 3. Debonding was caused by the opening of a diagonal crack that intercepted strip 3 two brick courses up from the bottom of the panel and, for panel V4A, was also caused by cracking along the inside of strip 3. After failure, debonding was also observed on the back face of the panels at the top of strip 1 (V4A) and the bottom of strip 2 (V4B). Debonding can be seen in Figure 4.14 and Figure 4.15.

In panel V4A some bending of FRP strip 4 (plus local damage of the masonry) was observed near SG23 (shown in Figure 4.16a). The behaviour of strip 1, on the back face of the panel, was not monitored during the test. At the end of the test FRP strip 1 had debonded from the panel, and therefore it was unknown whether strip bending occurred across a shear crack. Bending was not observed in FRP strips 2 or 3, because of the presence of cracking along the edge of strip 3.

In panel V4B a large amount of bending occurred in all FRP strips across the shear cracks during the test (as previously mentioned, and shown for strip 3 in Figure 4.16b). Similar to panel V2, the shear transferred via dowel action (at this stage of damage) was likely to be very small because the FRP, with small cross sectional area was bent over a large length (approximately the height of one brick)

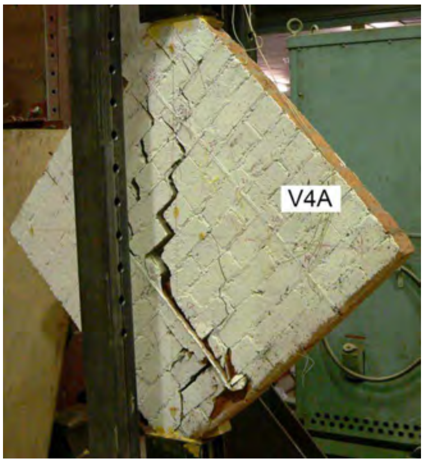

(a) Failure (front face)

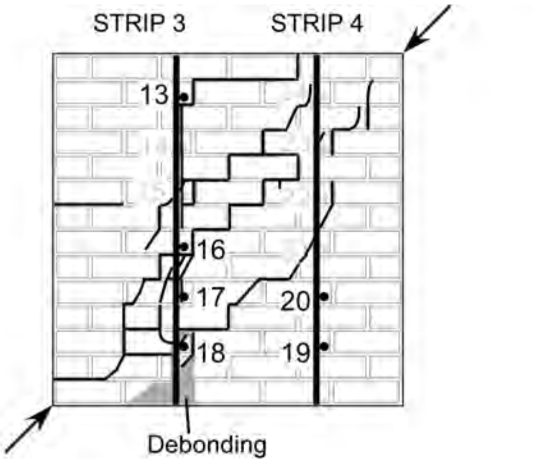

(b) Crack schematic at failure (front face)

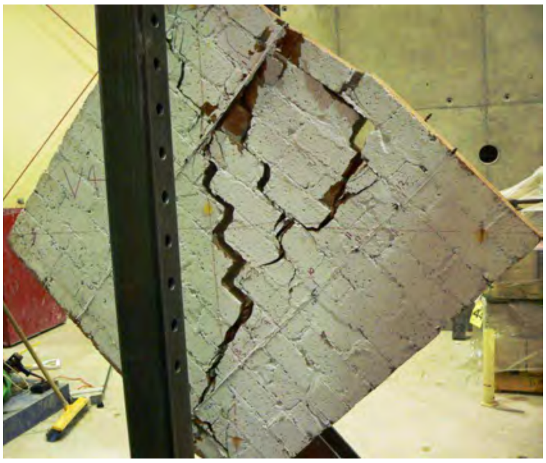

(c) Failure (back face)

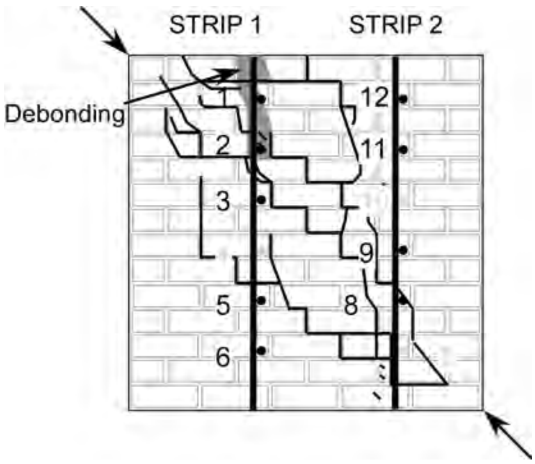

(d) Crack schematic at failure (back face)

Figure 4.14: V4A failure

(a) Failure (front face)

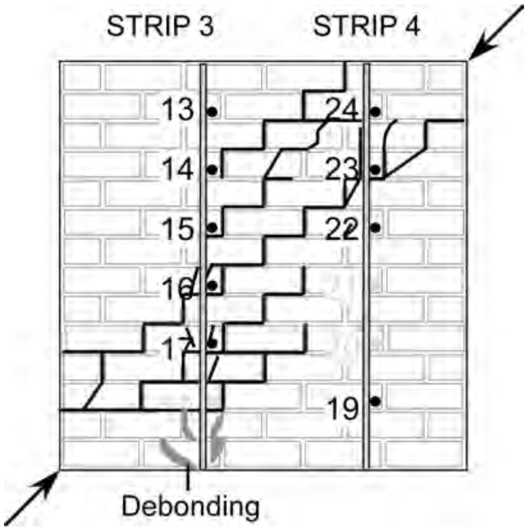

(b) Crack schematic at failure (front face)

(c) Failure (back face)

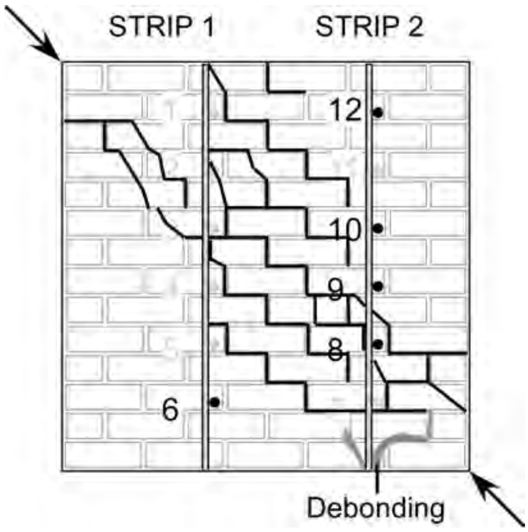

(d) Crack schematic at failure (back face)

Figure 4.15: V4B Failure

and about its weak axis.

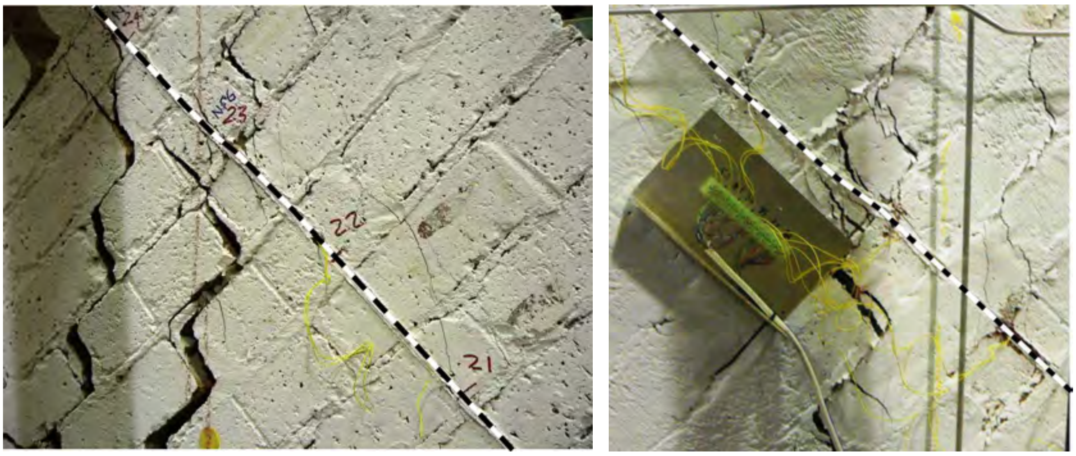

(a) Panel V4A strip 4

(b) Panel V4B strip 3

Figure 4.16: FRP bending across shear cracks in panels V4A and V4B

Plots of tensile strain in the FRP at strain gauge locations versus vertical displacement for panel V4A are shown in Figure 4.17 to Figure 4.20 (for strain gauge locations refer to Figure 4.14b and Figure 4.14d). In Figure 4.14b and Figure 4.14d damaged gauges are shown in a lighter font. When the first diagonal crack formed (at a vertical displacement of 0.4 mm) the tensile strain measured at strain gauges close to the crack (SG2, SG3, SG8 and SG16) increased significantly. The FRP strains were highest in the vicinity of the crack and reduced further away from the crack as the load was transferred to the masonry. The tensile strain in the FRP strips increased as the vertical displacement of the panel increased and cracking developed. The tensile strain recorded at SG16 (strip 3) reduced after 4 mm vertical displacement (and a maximum tensile strain of 3350 $\mu\varepsilon$) due to cracking along the inside of the strip. Cracking along the inside edge of strip 3 also limited further deformation on the outside of the panel (past strip 3), indicated by constant strain in strip 2 at the onset of the cracking. The tensile strain increased in SG17 and SG18 because of the opening of a diagonal crack intercepting the FRP reinforcement 2 courses up from the base of the panel. A maximum strain of approximately 4000 $\mu\varepsilon$ was recorded before the bottom of FRP strip 3 debonded from the panel. This was approximately half the maximum debonding strain recorded in pull tests on the same type of FRP-to-masonry connection (debonding strain ranged from 7416 $\mu\varepsilon$ to 8963 $\mu\varepsilon$). The bond was reduced by cracking along the edge of the FRP strip.

Plots of strain in the FRP versus vertical displacement for panel V4B are shown in Figure 4.21 to Figure 4.24. Refer to Figure 4.15b and Figure 4.15d for the location of the strain gauges. In Figure 4.15b and Figure 4.15d damaged gauges are shown in a lighter font. Similar to V4A, the tensile strain in the FRP strips increased when diagonal cracks formed. FRP strains were highest in the vicinity of the crack and reduced further away from the crack as the load was transferred from the FRP into

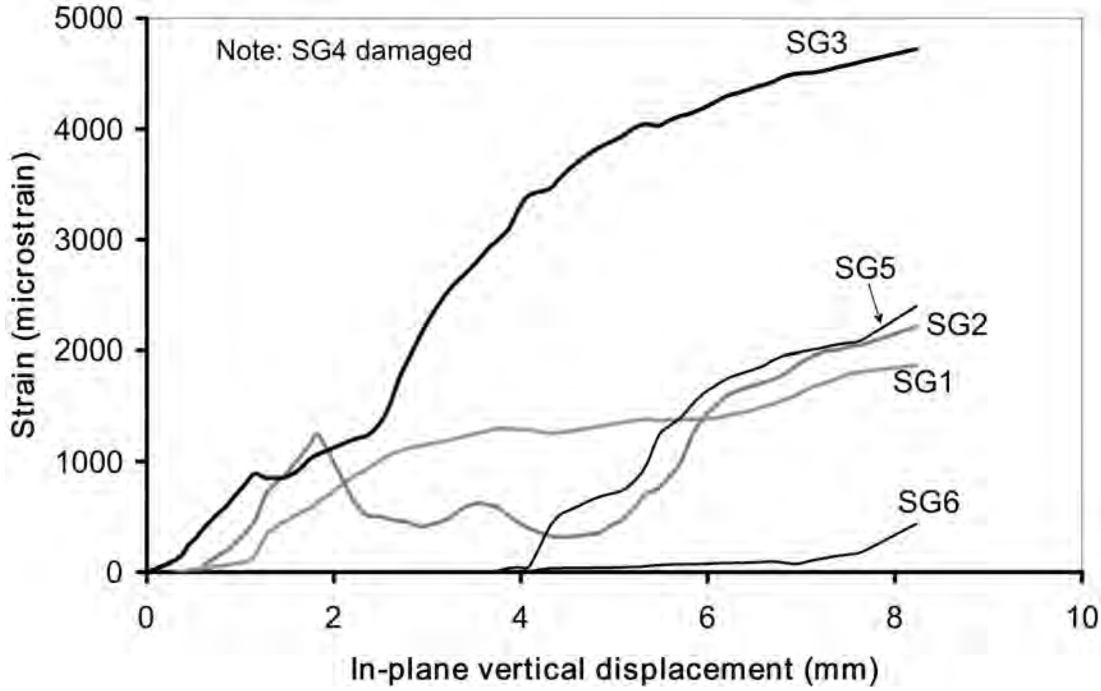

Figure 4.17: FRP strain vs in-plane vertical displacement (Panel V4A - Strip 1)

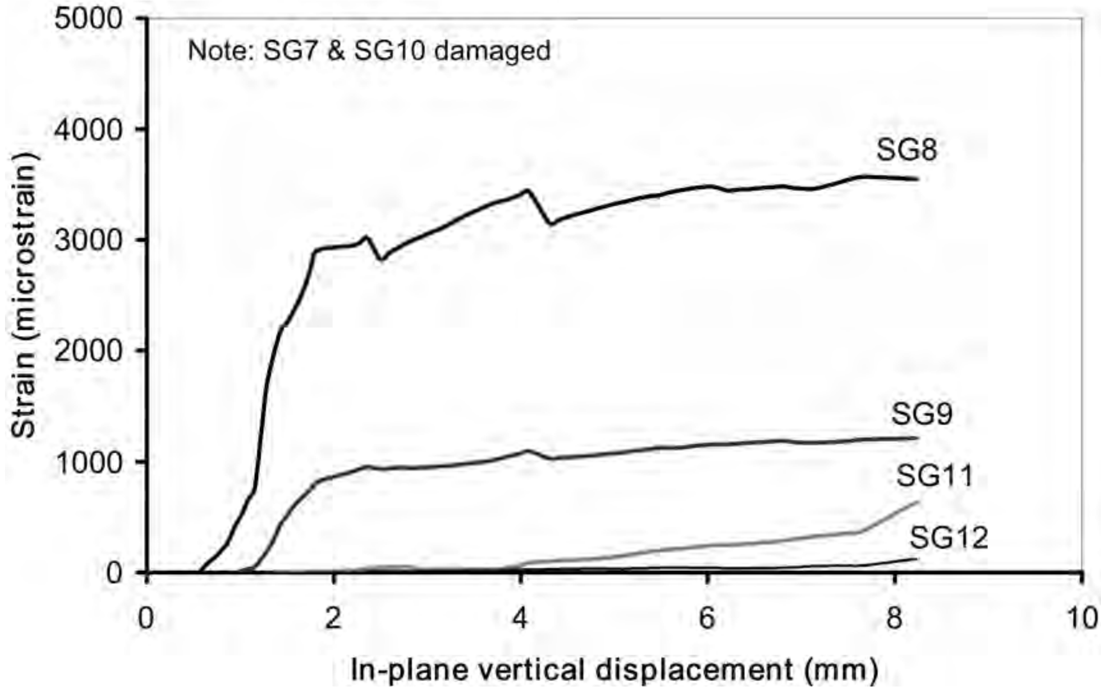

Figure 4.18: FRP strain vs in-plane vertical displacement (Panel V4A - Strip 2)

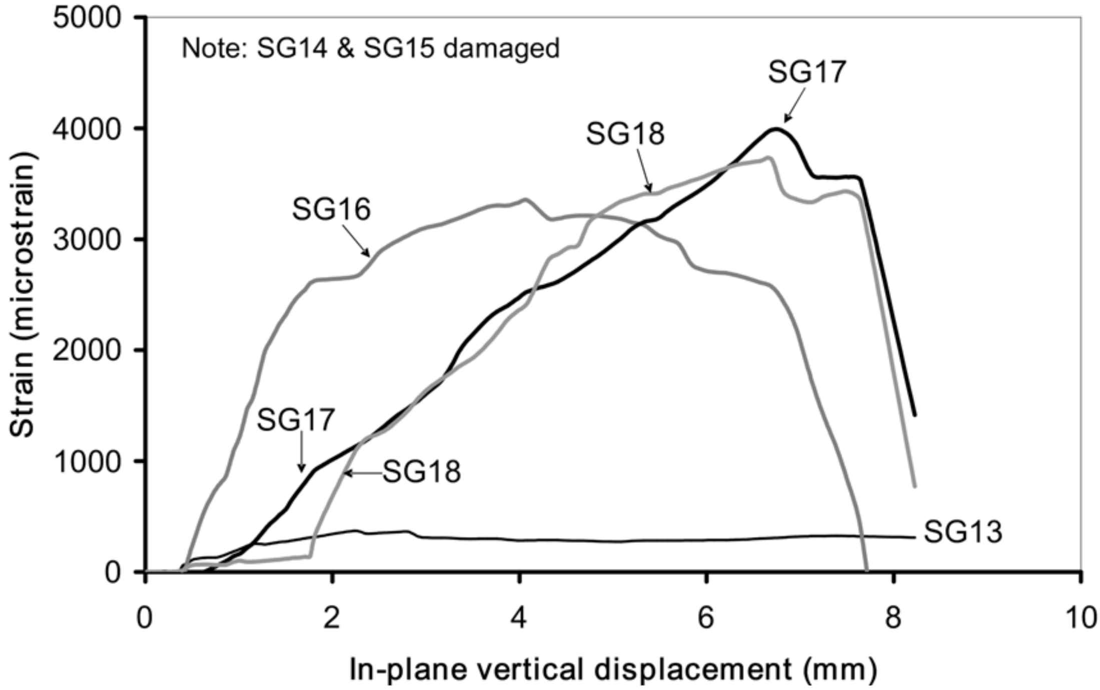

Figure 4.19: FRP strain vs in-plane vertical displacement (Panel V4A - Strip 3)

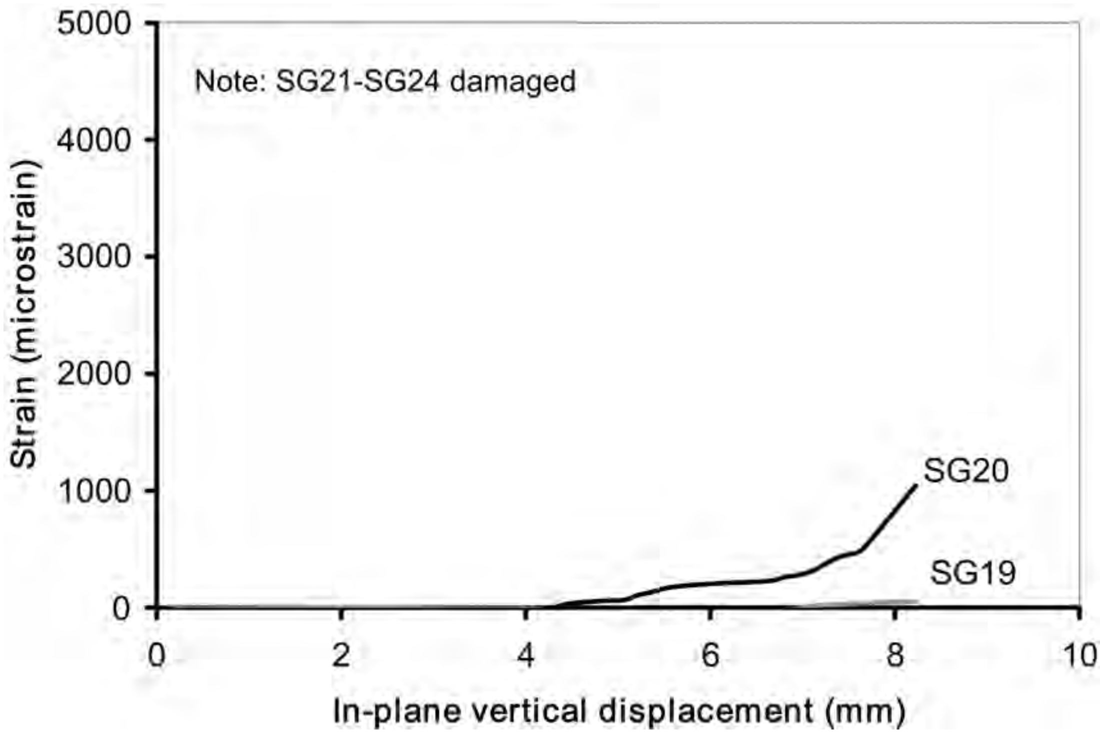

Figure 4.20: FRP strain vs in-plane vertical displacement (Panel V4A - Strip 4)

the masonry. The first major increase in strain was recorded at the top of the panel in SG23 and SG24 (in strip 4) at a vertical displacement of 0.2 mm. This was sooner than increases recorded at the bottom of the panel (strains recorded at SG16 and SG17 increased at 0.4 mm). This indicates that cracking formed at the top of the panel first, which was expected as panel V4B was constructed with weaker joints at the top of the panel. The maximum strain recorded in strip 3 before debonding was 6242 $\mu\varepsilon$. This was higher than the maximum strain recorded in panel V4A (before debonding), but was still less than the maximum debonding strain recorded in pull tests. In both panels debonding was premature as it occurred at FRP tensile strains that were lower than expected.

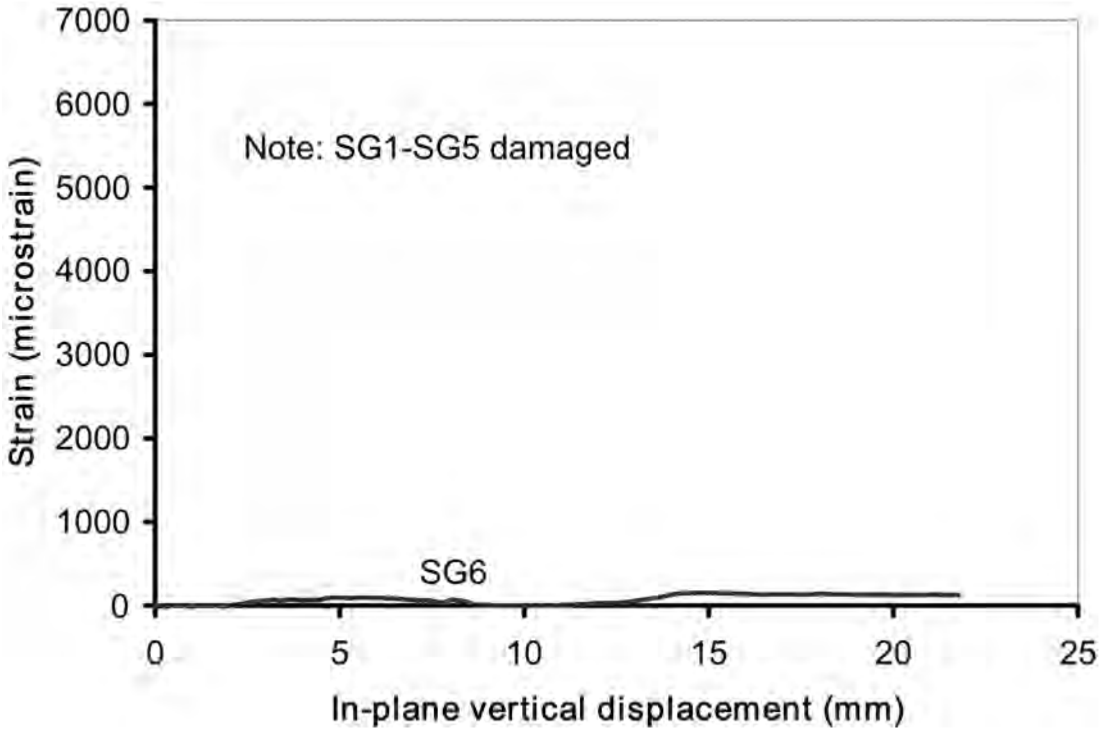

Figure 4.21: FRP strain vs in-plane vertical displacement (Panel V4B - Strip 1)

Panels H4A & H4B

The load-vertical displacement responses of panels H4A and H4B are shown in Figure 4.25. H4A behaved linearly until the crack shown in Figure 4.26a started to develop at a vertical displacement of approximately 0.5 mm (and a corresponding load of 251 kN). The ultimate load of the panel, which was equal to 264 kN, was reached shortly after, at a vertical displacement of 0.62 mm.

After the crack (shown in Figure 4.26a) formed, the horizontal FRP strip that bridged the crack (strip 1) prevented the unsupported section of the masonry (outside of the crack) from falling off the panel (shown in Figure 4.26b). The cross section of the compressive strut within the panel that supported the load reduced (and hence the load carrying capacity of the panel reduced). More cracking

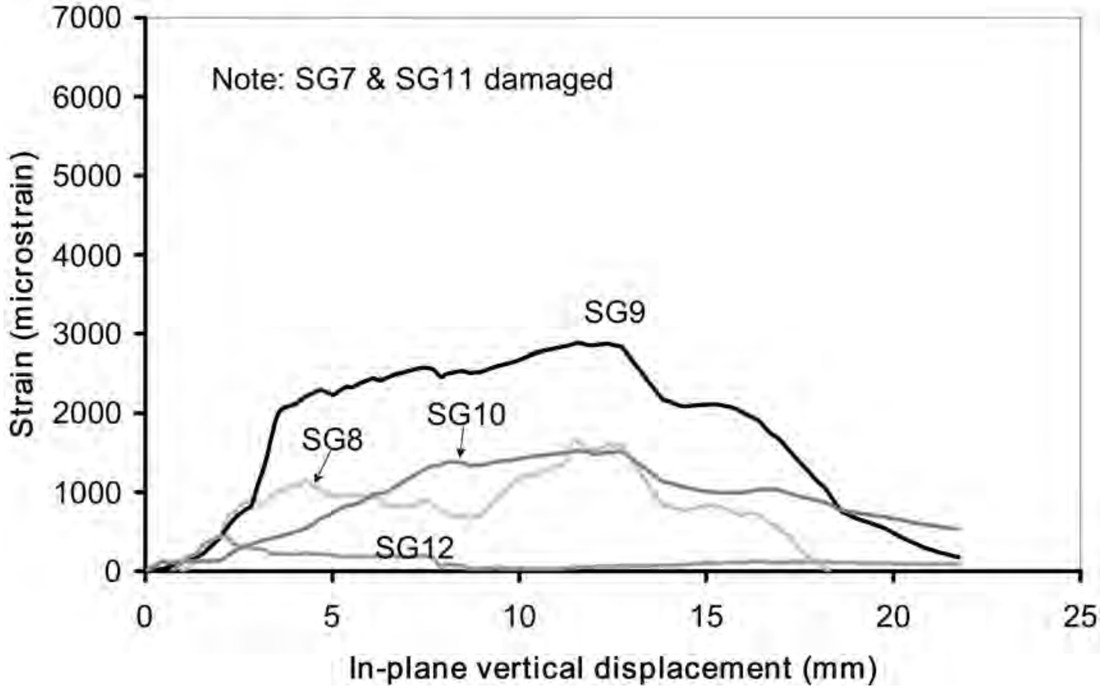

Figure 4.22: FRP strain vs in-plane vertical displacement (Panel V4B - Strip 2)

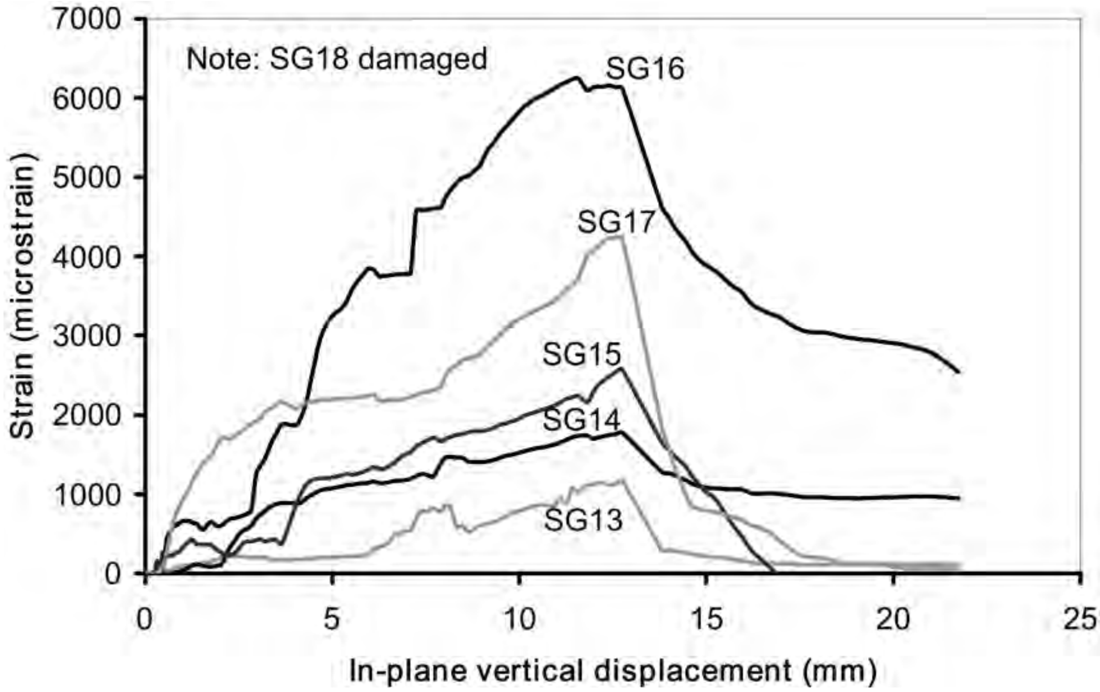

Figure 4.23: FRP strain vs in-plane vertical displacement (Panel V4B - Strip 3)

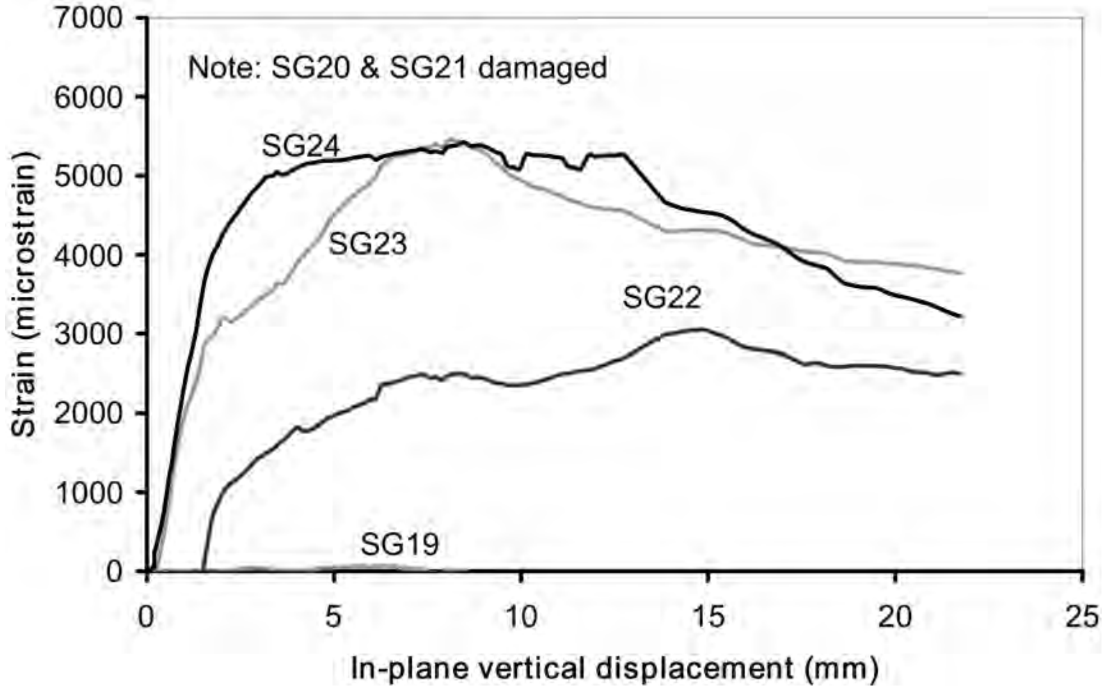

Figure 4.24: FRP strain vs in-plane vertical displacement (Panel V4B - Strip 4)

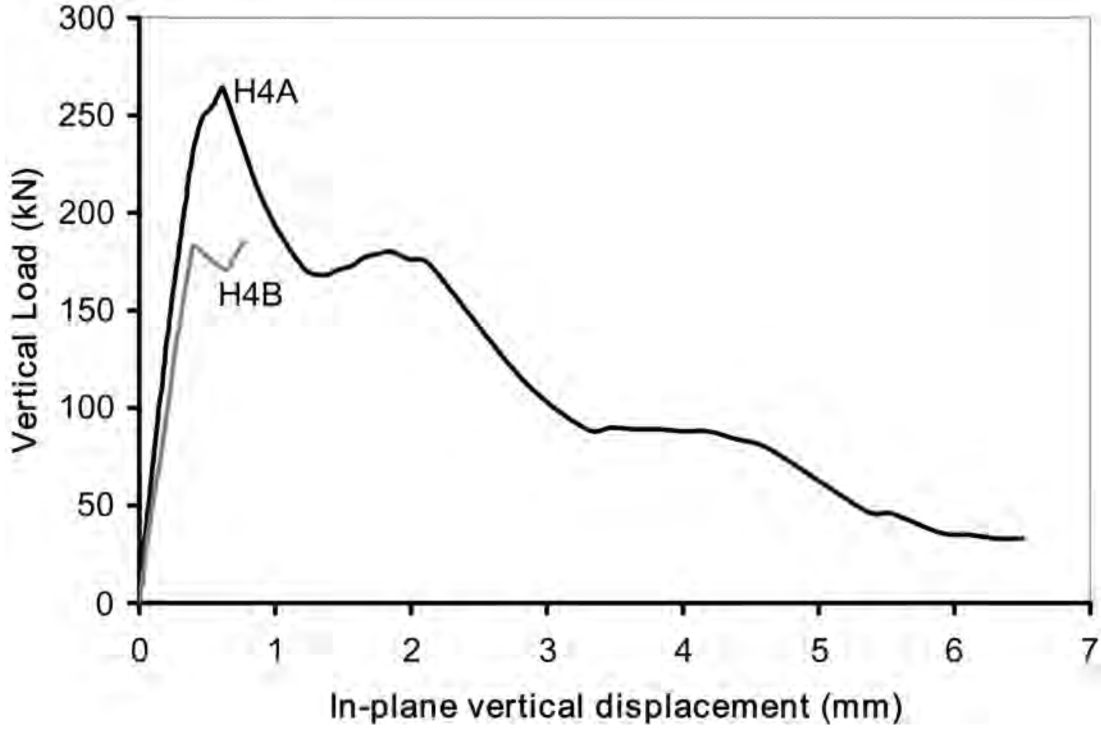

Figure 4.25: Load-displacement response of H4A and H4B

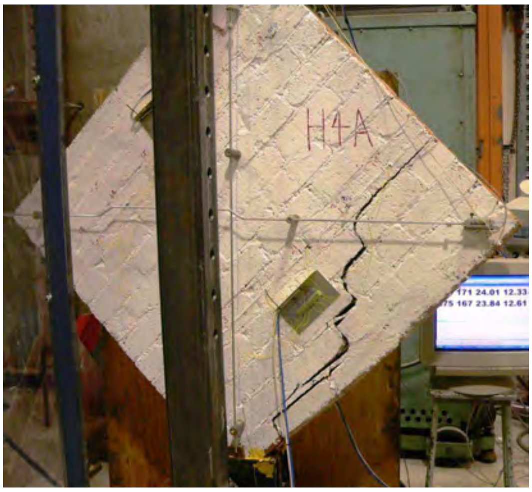

(a) First crack in panel (front face)

(b) FRP strip 1 (highlighted) holding onto separated masonry section (back face)

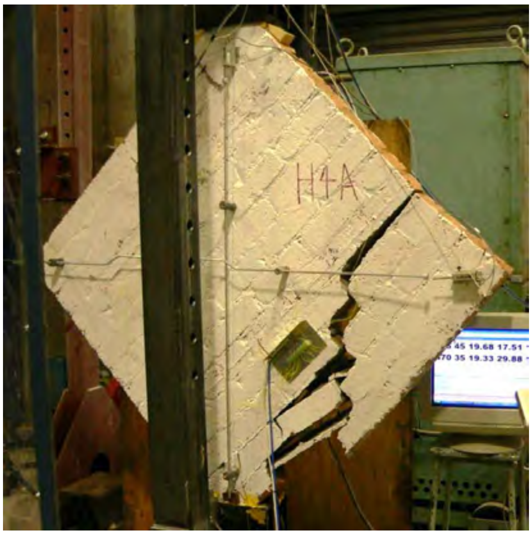

(c) Cracking at end of test

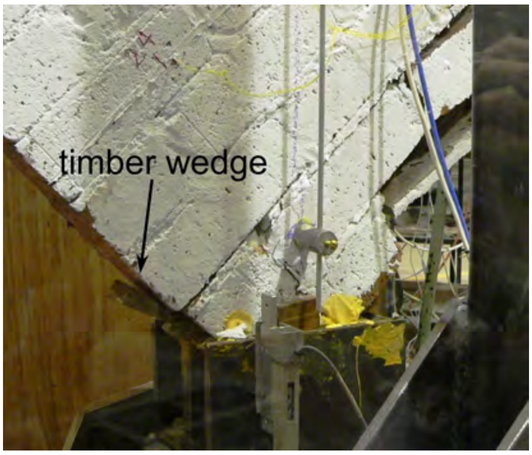

(d) Sliding crack in bed joints possibly supported by timber wedge

Figure 4.26: H4A test observations

(shown in Figure 4.26c) at a vertical displacement of approximately 2 mm reduced the compressive strut and load further. At this point cracking along the bed joint above the bottom support was also observed (shown in Figure 4.26d). The bed joint crack should have caused the panel to fail by sliding immediately after it formed but a timber wedge used to align the panel vertically during setup may have provided enough capacity to prevent sliding at a low load.

The cracks that developed in panel H4A were intersected only by FRP strip 1 as shown in the crack schematic (Figure 4.27a). Note that in the crack schematic, damaged gauges are not labelled, and FRP strips and gauges on the back side of the panel are drawn in a lighter font. When the crack opened at a vertical displacement of 0.5 mm the tensile strain at SG2 (closest to the crack) increased significantly (shown in the plot of strain vs. vertical displacement - Figure 4.27b). The strain in SG2 reached a value of 8900 $\mu\varepsilon$ before the test was stopped. This strain value was close to the highest debonding strain observed in pull tests on horizontal NSM FRP reinforcement (with 1 MPa of precompression = 8496 $\mu\varepsilon$). Debonding, however, was not observed in the test. The high value of strain recorded at SG2 was likely caused by cracking directly over SG2.

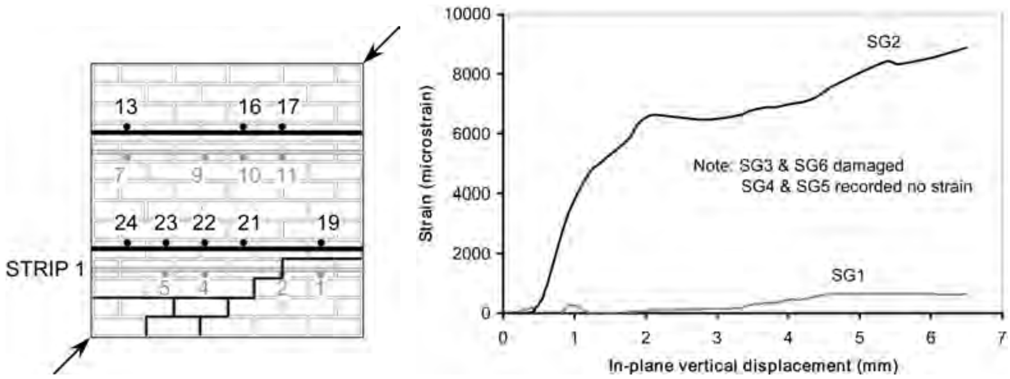

(a) Crack schematic (b) Strain in strip 1

Figure 4.27: Crack schematic and FRP strains vs vertical displacement in strip 1 (panel H4A)

Apart from the major cracking shown, no other cracks developed in the rest of panel H4A and FRP strips 2, 3 and 4 remained inactive (no tensile strains were recorded). As strip 1 was only effective in preventing the broken section of the panel from falling off and did not contribute to the load carrying capacity of the panel, it is likely that the load displacement response of the panel would have been similar without the horizontal reinforcement.

Panel H4B behaved elastically until a diagonal crack (shown in Figure 4.28a and in the crack schematic in Figure 4.28c) developed at a vertical displacement of 0.4 mm (load = 183 kN). Note that in the crack schematic the damaged gauges are not labelled, and FRP strips and gauges on the back side of the panel are drawn in a lighter font. The FRP restrained the opening of the diagonal crack and the panel was able to deform further (to a vertical displacement of approximately 0.78 mm). At this point the panel failed by bed joint sliding at the top of the panel above the horizontal strengthening (shown in Figure 4.28b and Figure 4.28c). The maximum load of panel H4B was 185 kN, and was much lower than H4A because of the weaker mortar joints used to construct the top half of the panel (Table 4.1).

Plots of strain in the FRP (at strain gauge locations) versus vertical displacement are shown in Figure 4.29 to Figure 4.32 for panel H4B. In general all the FRP strips activated once the diagonal crack (observed during the test) developed at a vertical displacement of 0.4 mm (and in the vicinity of the diagonal crack). The FRP strains increased until the panel failed. The maximum strain recorded before failure was 1600 $\mu\varepsilon$. No debonding cracks were observed adjacent to any of the horizontal strips.

Panel V2H2A & V2H2B

The load-vertical displacement responses of V2H2A and V2H2B are shown in Figure 4.33. Similar to other panels, the FRP reinforcement in panels V2H2A and V2H2B prevented failure of the panel occurring upon first cracking. Both panels behaved approximately linearly until the first diagonal cracks formed, and FRP in the vicinity of the cracks was activated. Diagonal cracks were first observed in the panels at a vertical displacement of 0.48 mm (load = 177 kN) for V2H2A and 0.4 mm (load = 120 kN) for V2H2B. The maximum loads of both specimens were reached shortly afterwards, and they were 206 kN for V2H2A and 158 kN for V2H2B.

The crack patterns and failure modes are shown in Figure 4.34 for panel V2H2A and Figure 4.35 for panel V2H2B. In both panels diagonal cracking, through mortar joints and brick units, spread throughout the panel as the vertical displacement increased. The horizontal reinforcement on the back side of the panels intercepted the diagonal cracking and forced further cracking to develop through bed joints, between and outside of the horizontally reinforced brick courses. In both panels, two large cracks developed; one crack below strip 1 and one crack above strip 2. The sections of the panels separated by the cracks (outside the loaded diagonal) rotated (about the crack) towards the front side of the panels. The cracks opened on the back side of the panels and were held together on the front side of the panels by the vertical reinforcement. The out-of-plane deformation is shown in Figure 4.36. Without the vertical reinforcement resisting crack opening on the front side of the panels, the sections, separated from the crack, would have likely fallen off and the panel would have failed completely. The masonry compression strut was reduced by separation of sections undergoing out-of-plane deformation, and hence the load carrying capacity of the panels was reduced. The cracking that contributed to the out-of-plane bending spread throughout the panel during the test and reduced the load carrying capacity further.

In both tests the bottom of strip 3 debonded from the panel. This occurred at a vertical displacement of 12 mm for V2H2A and 10 mm for V2H2B. Opening of the large crack below horizontal reinforcement strip 1 caused debonding. It is likely that out-of-plane bending about this crack may have also influenced debonding.

(a) Diagonal crack

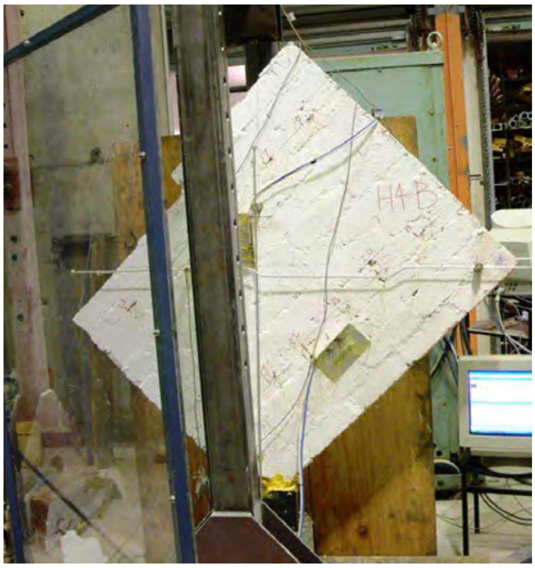

(b) Sliding failure plane along bed joints at top of panel

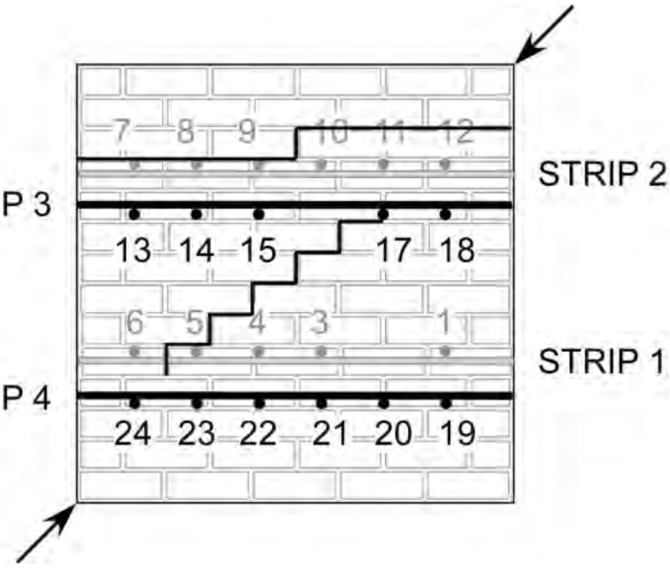

(c) Crack schematic (major cracks)

Figure 4.28: Test observations H4B

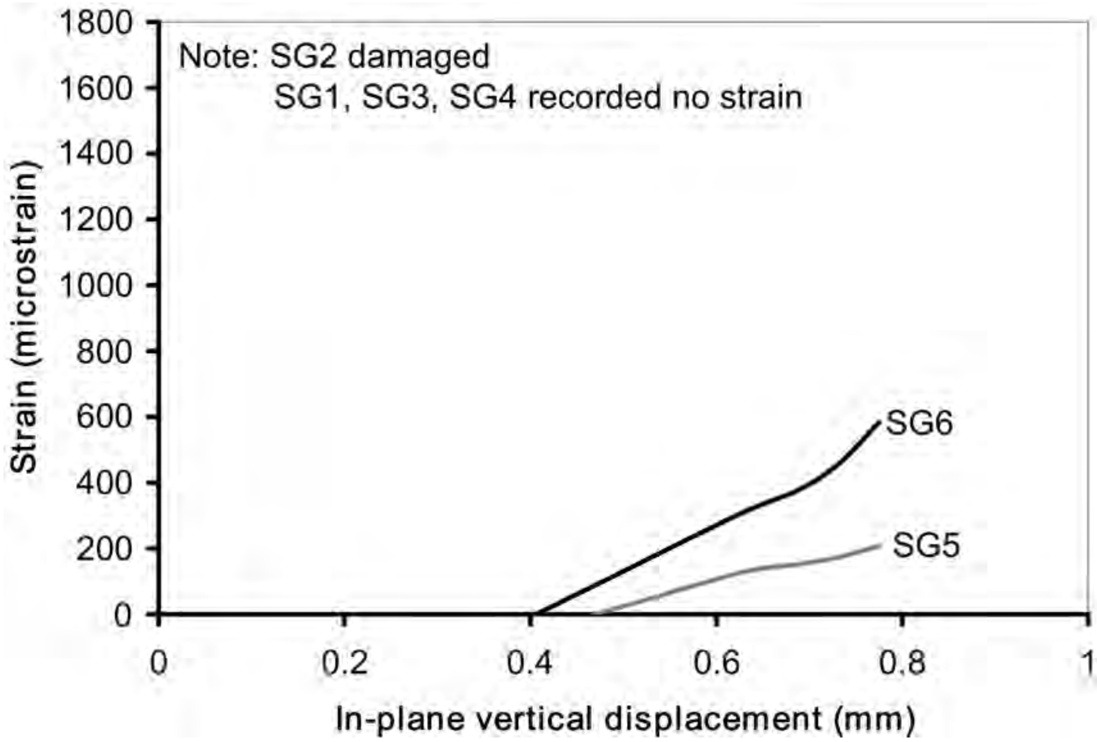

Figure 4.29: FRP strain vs in-plane vertical displacement (Panel H4B - Strip 1)

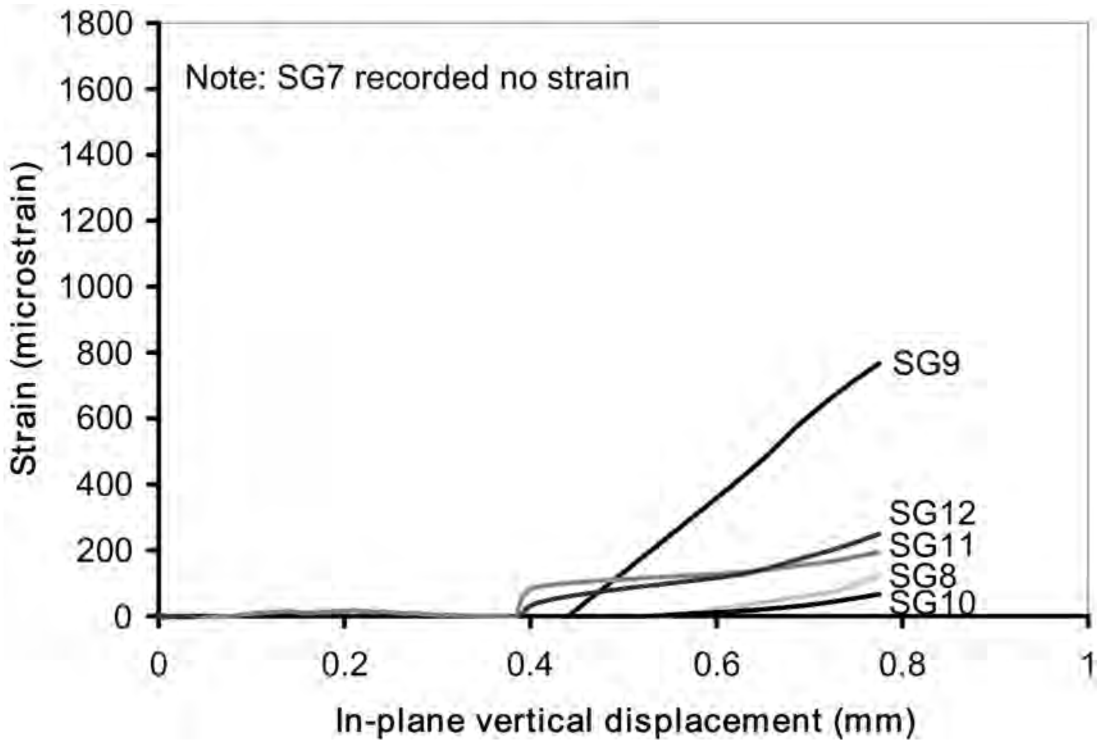

Figure 4.30: FRP strain vs in-plane vertical displacement (Panel H4B - Strip 2)

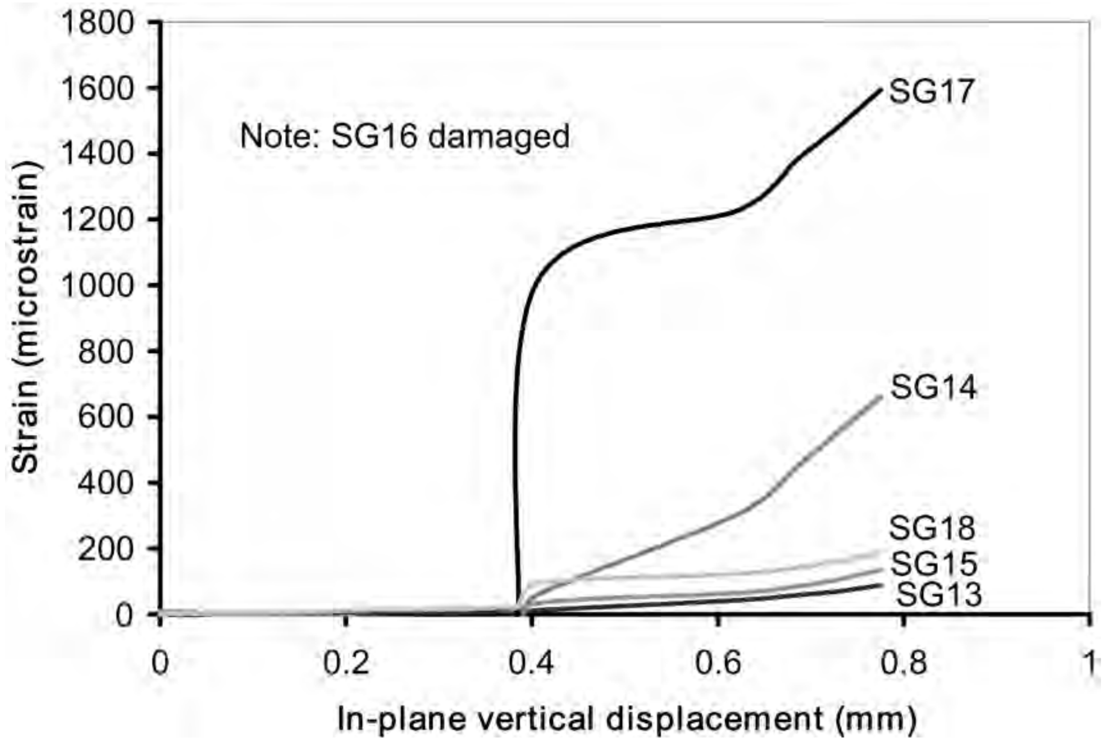

Figure 4.31: FRP strain vs in-plane vertical displacement (Panel H4B - Strip 3)

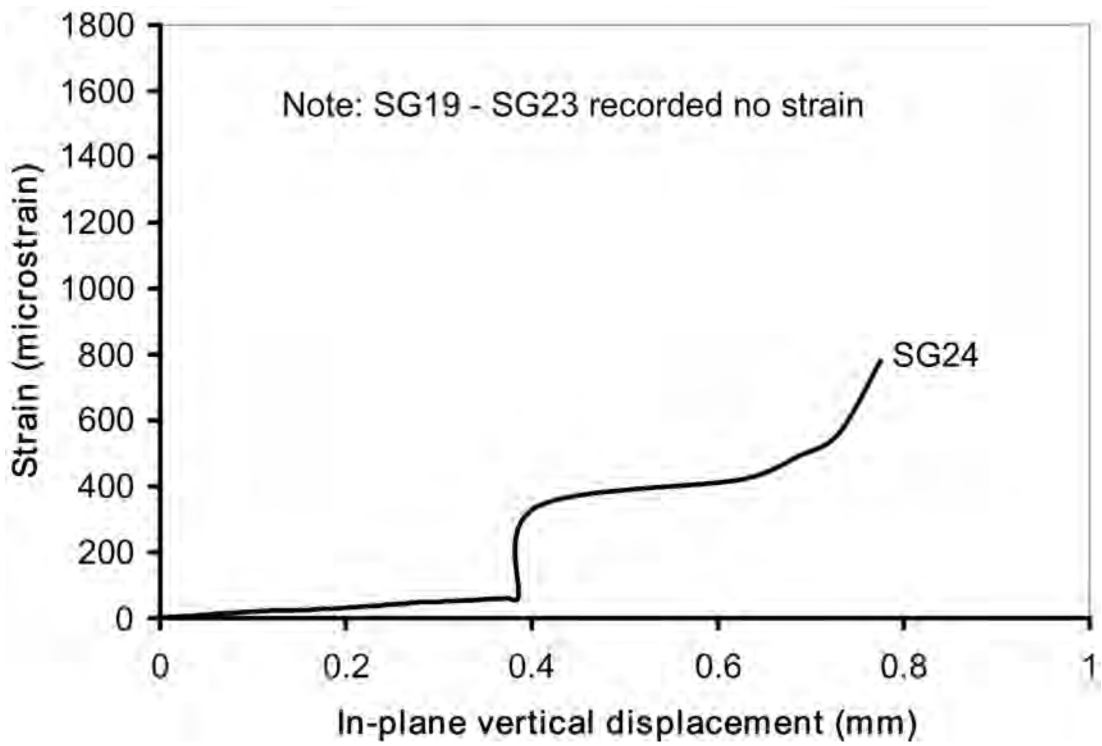

Figure 4.32: FRP strain vs in-plane vertical displacement (Panel H4B - Strip 4)

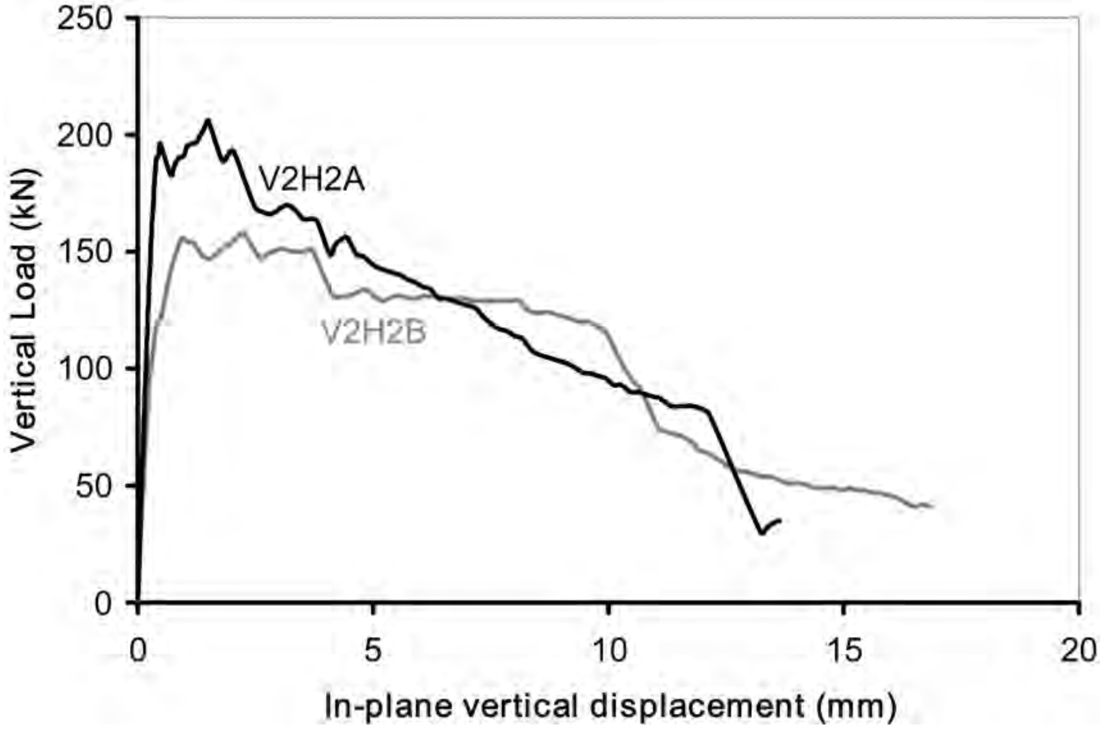

Figure 4.33: Load-displacement response of panels V2H2A and V2H2B

In panel V2H2A some bending of FRP strip 3 was observed near SG15 (shown in Figure 4.37a). A significant amount of cracking was present along the edge of the FRP strip at this location and therefore it was likely that at this stage of damage the FRP provided little dowel strength. Localised bending of the FRP was observed across a shear sliding crack at the bottom of strip 4 (near SG20) as shown in Figure 4.37b. As the FRP was bent over a short length it may have provided some dowel strength.

In panel V2H2B no sliding (and bending of the FRP) across FRP strip 3 was observed until the FRP debonded from the bottom of the panel (shown in Figure 4.38a). As the bottom of the FRP strip had debonded from the panel the FRP strip would have provided no dowel strength at this stage of the test. Some local bending across a crack at the bottom of strip 4 was observed (Figure 4.38b). A significant amount of cracking was present along the edge of the FRP strip at this location so it was likely that the FRP provided little dowel strength.

Plots of strain in the FRP strips, determined from strain gauges versus vertical displacement are shown in Figure 4.39 to Figure 4.42 for panel V2H2A and Figure 4.43 to Figure 4.46 for panel V2H2B. Note that for panel V2H2B a different vertical scale is presented for strip 3 (Figure 4.45). In both panels the strain in the horizontal reinforcement (strip 1 and strip 2) increased as the reinforcement prevented the opening of diagonal cracks running across the reinforcement. The strain in the horizontal strips became constant as cracks developed outside of the horizontal FRP reinforcement (in particular the 2 large cracks upon which out-

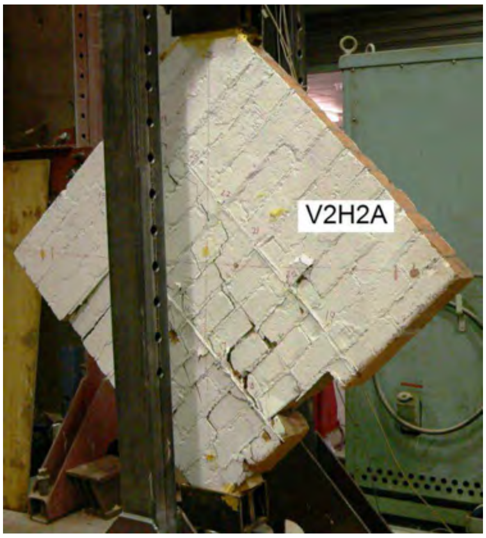

(a) Failure (front face)

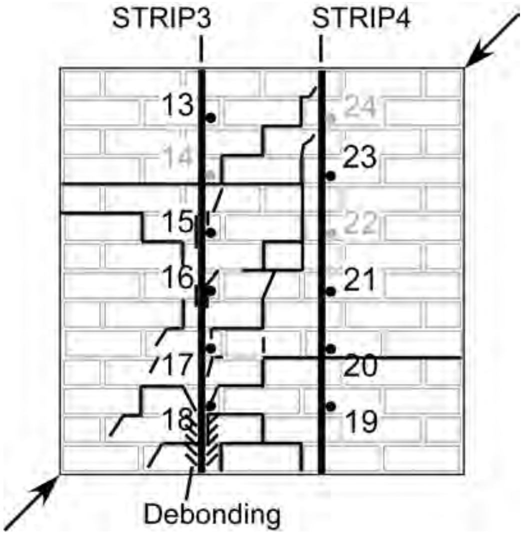

(b) Crack schematic at failure (front face)

(c) Failure (back face)

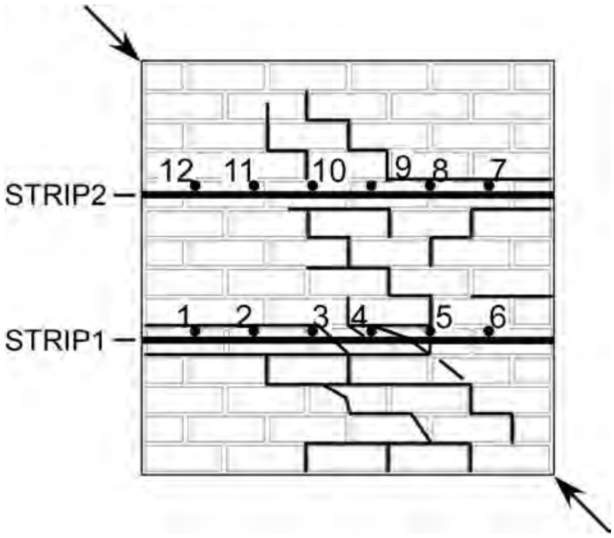

(d) Crack schematic at failure (back face)

Figure 4.34: V2H2A Failure

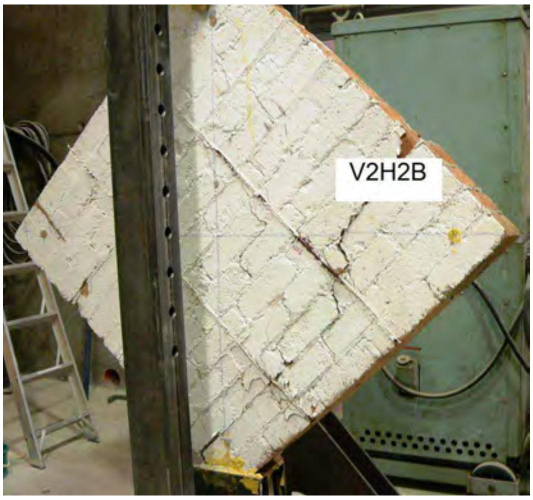

(a) Failure (front face)

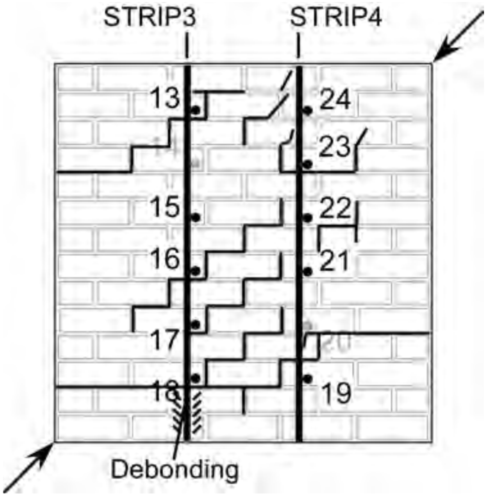

(b) Crack schematic at failure (front face)

(c) Failure (back face)

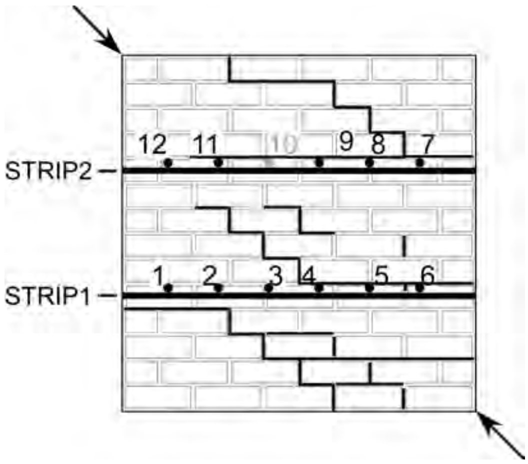

(d) Crack schematic at failure (back face)

Figure 4.35: V2H2B Failure

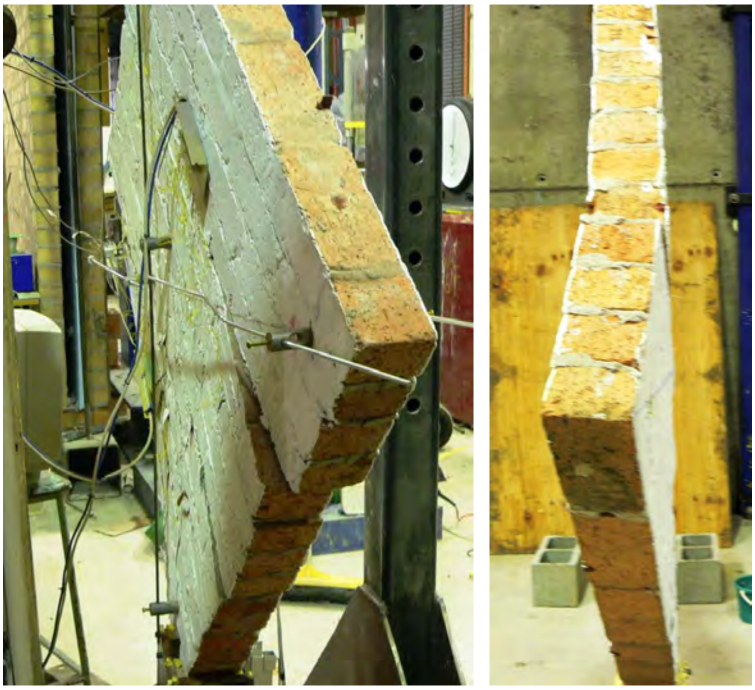

(a) V2H2A (b) V2H2B

Figure 4.36: Out-of-plane twisting

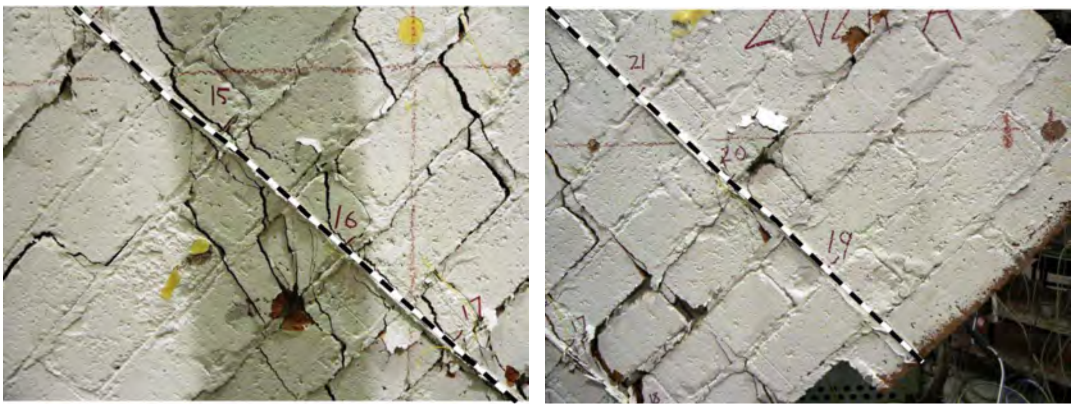

(a) Strip 3 (b) Strip 4

Figure 4.37: FRP bending across shear cracks in panel V2H2A

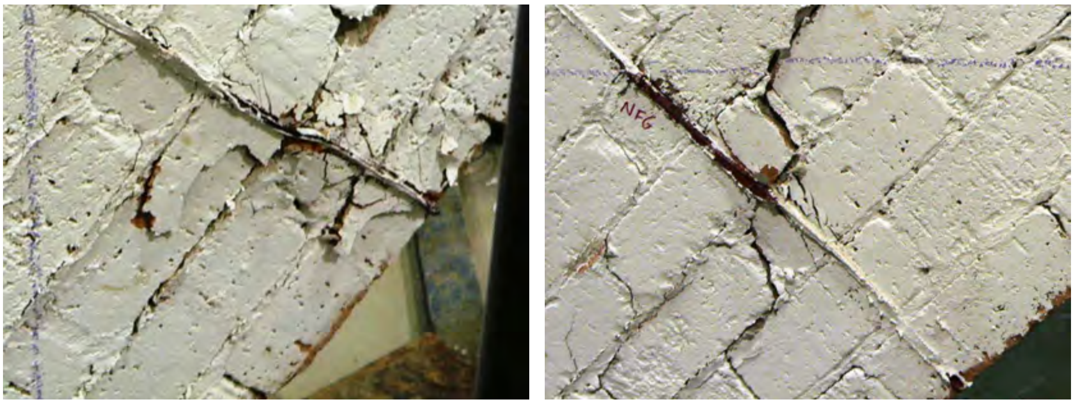

(a) Strip 3 (b) Strip 4

Figure 4.38: FRP bending across shear cracks in panel V2H2B

of-plane deformation occurred). The maximum strain reached in the horizontal reinforcement was approximately 3800 $\mu\varepsilon$. No debonding cracks were observed in the brick adjacent to any horizontal FRP strip.

The strain in the vertical reinforcement (strip 3 and strip 4) increased (at a similar rate to the horizontal reinforcement) as the reinforcement prevented the opening of diagonal cracks running across the reinforcement. In panel V2H2A the strain reduced in the vertical strips because of the formation of cracks along the inside of the FRP strips (similar to V4A). At the end of the test the strains in strip 3 rapidly reduced to zero when the FRP debonded from the panel. For V2H2A the maximum strain recorded in strip 3 before debonding was approximately 3800 $\mu\varepsilon$ and was similar to strains recorded in vertical strips in panel V4A where cracking along the inside edge of the strip was observed. In panel V2H2B the strain in vertical reinforcement strip 3 increased until the FRP, between SG18 and the end of the strip, debonded from the panel. For V2H2B the maximum strain before debonding in strip 3 (at SG18) was 9850 $\mu\varepsilon$ and was slightly higher than the debonding strain observed in pull tests on similar joints (ranged from 7416 $\mu\varepsilon$ to 8963 $\mu\varepsilon$). Pull tests are known to be lower bound (Oehlers and Seracino, 2004), so it was expected that the FRP strains in the panel specimens would be higher (due to close-spaced cracking and also bending).

4.4 Comparisons between test specimens

4.4.1 Load-displacement behaviour

The load displacement behaviours of all the panels tested are compared in Figure 4.47. The panels with the symmetrical arrangement of vertical reinforcement (2 vertical strips on each side of the panel), V4A and V4B, performed the best. Panels with 2 vertical strips on one side, and 2 horizontal strips on the other side, V2H2A and V2H2B, performed second best. They were worse than panels V4A and V4B because the major cracks that developed at the top and bottom of the panel

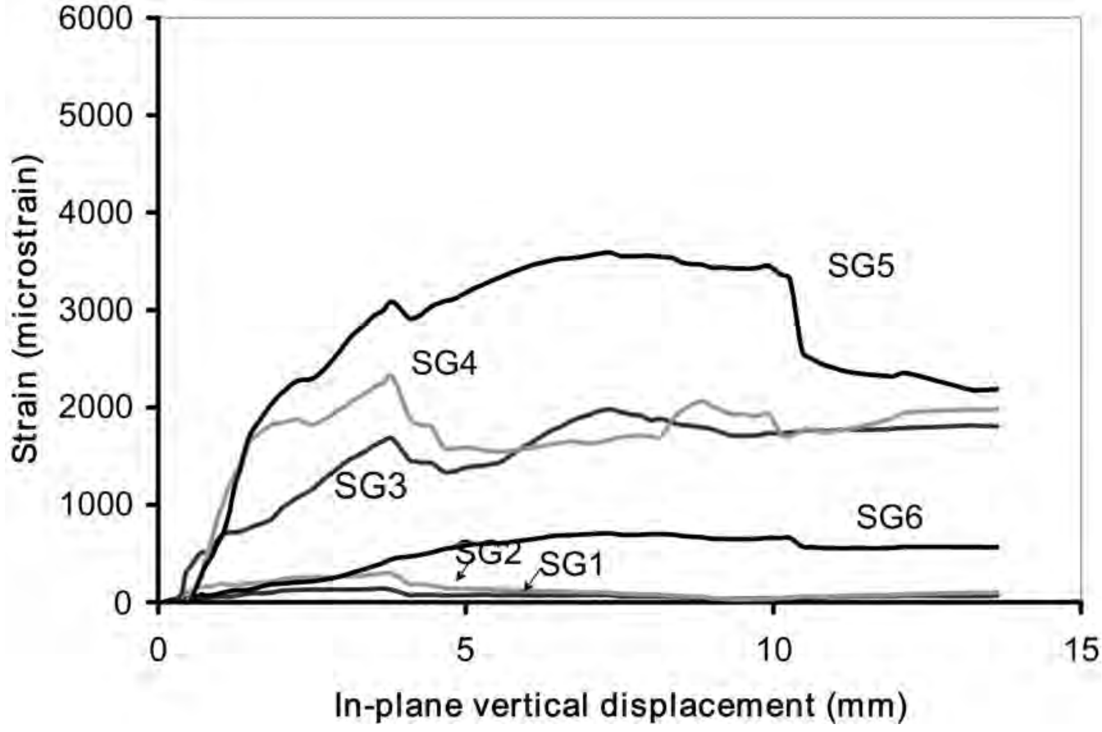

Figure 4.39: FRP strain vs in-plane vertical displacement (Panel V2H2A - Strip 1) (horizontal strip)

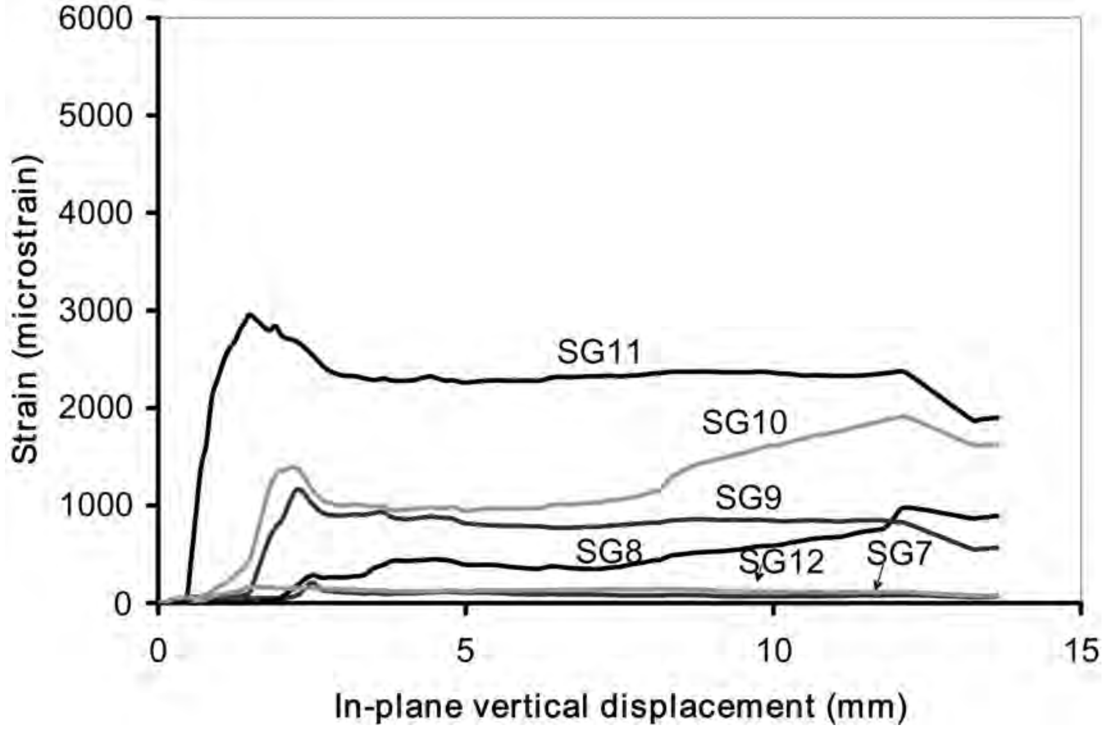

Figure 4.40: FRP strain vs in-plane vertical displacement (Panel V2H2A - Strip 2) (horizontal strip)

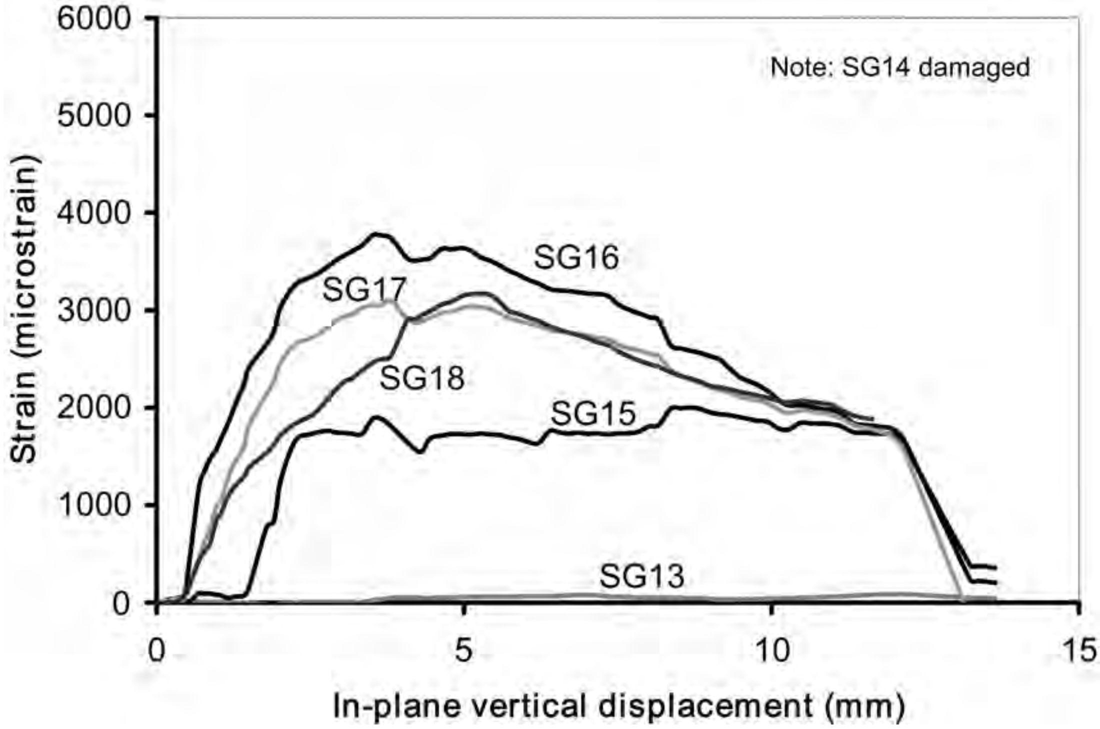

Figure 4.41: FRP strain vs in-plane vertical displacement (Panel V2H2A - Strip 3) (vertical strip)

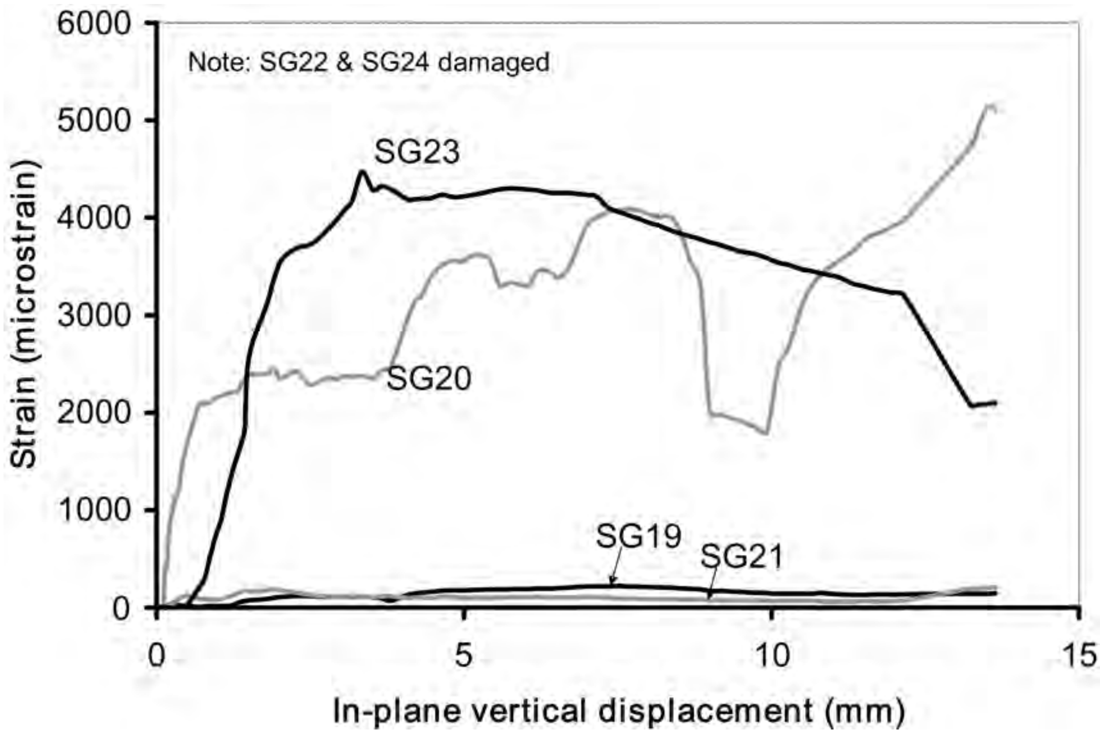

Figure 4.42: FRP strain vs in-plane vertical displacement (Panel V2H2A - Strip 4) (vertical strip)

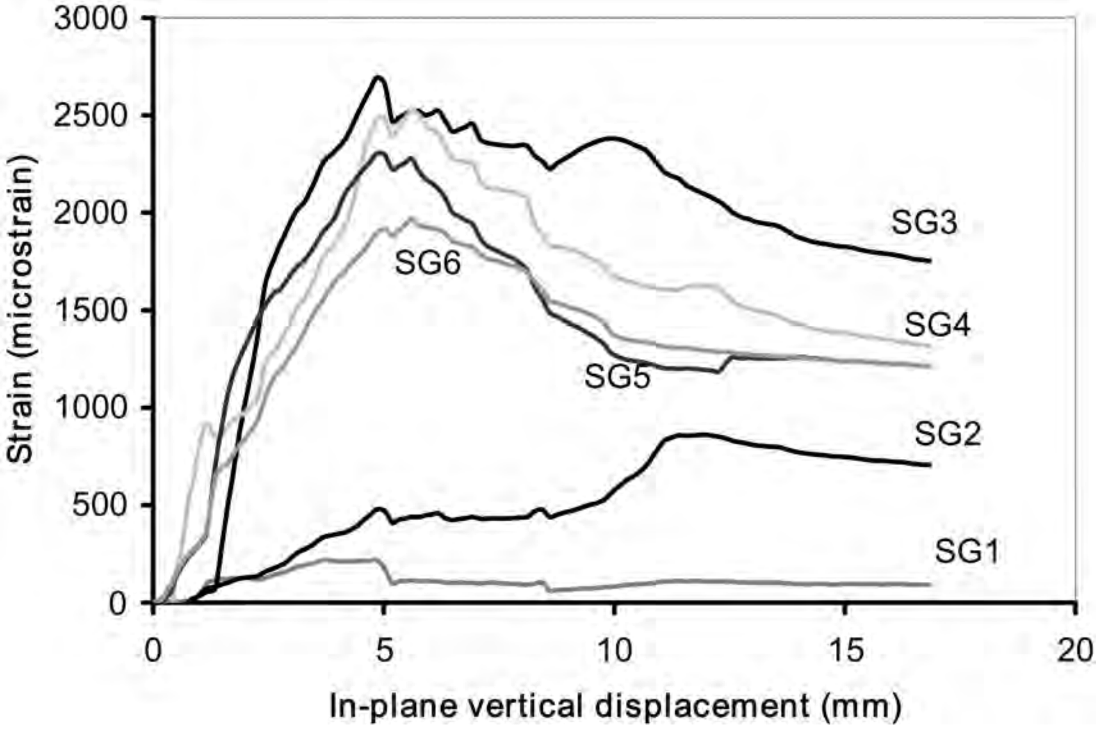

Figure 4.43: FRP strain vs in-plane vertical displacement (Panel V2H2B - Strip 1) (horizontal strip)

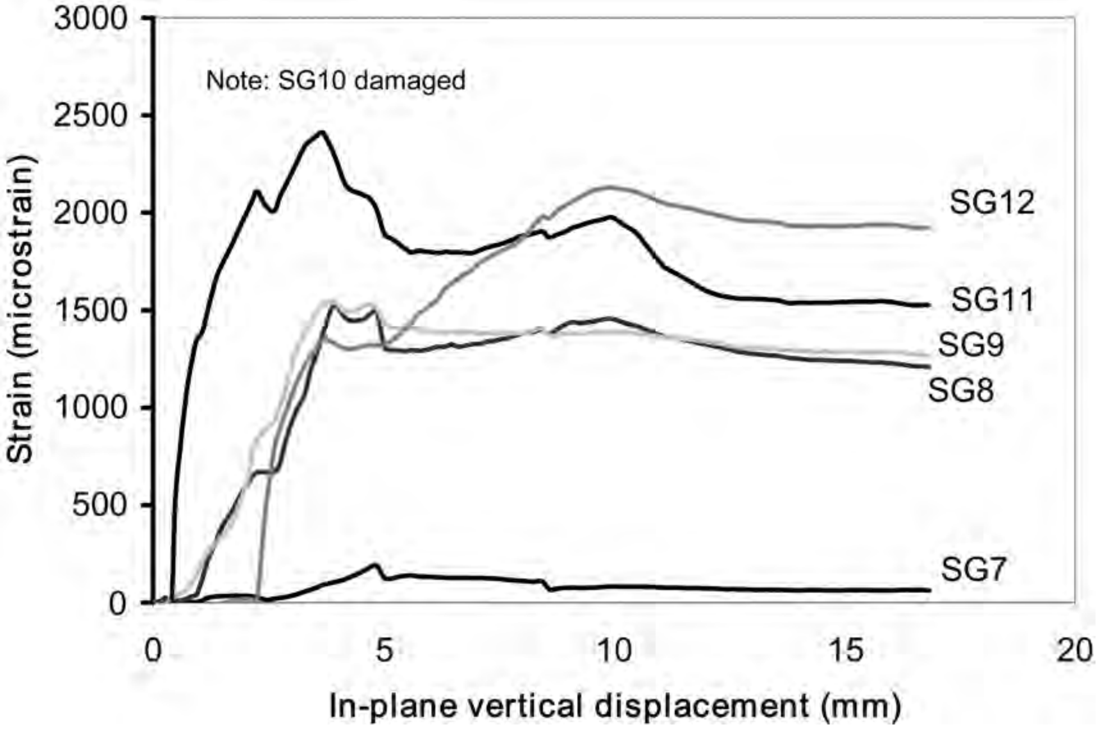

Figure 4.44: FRP strain vs in-plane vertical displacement (Panel V2H2B - Strip 2) (horizontal strip)

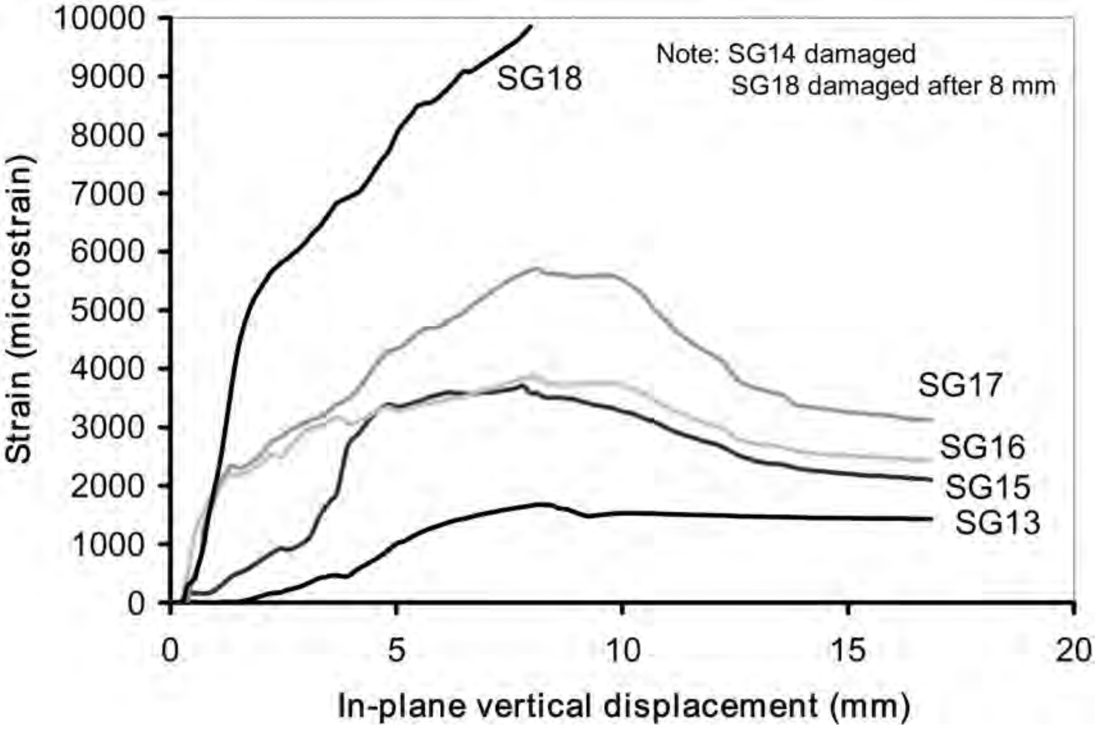

Figure 4.45: FRP strain vs in-plane vertical displacement (Panel V2H2B - Strip 3) (vertical strip)

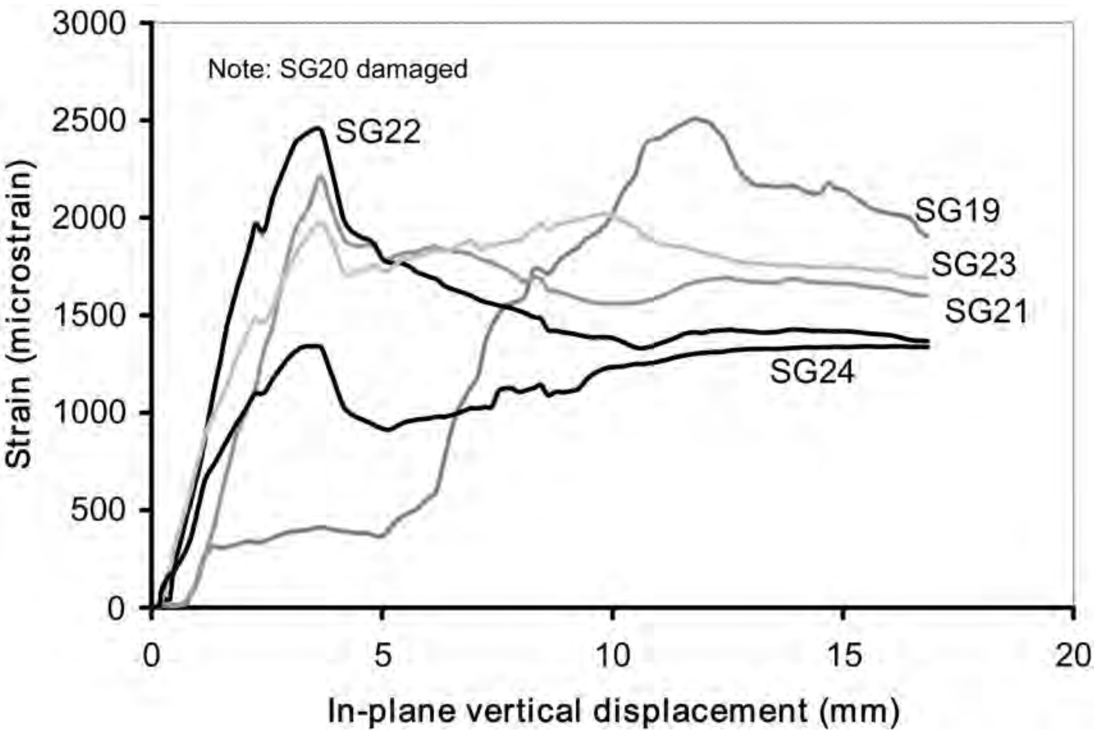

Figure 4.46: FRP strain vs in-plane vertical displacement (Panel V2H2B - Strip 4) (vertical strip)

were only crossed by 2 vertical reinforcement strips (compared to 4 in V4A and V4B). Also, out-of-plane twisting occurred about the major crack faces and reduced the load capacity of the panels because the 2 vertical strips were on one side of the panel only. The behaviour of panels V2H2A and V2H2B was better than V2 (which performed third best). The horizontal reinforcement on one side of the panel restrained the large out-of-plane displacement about the main diagonal crack that occurred in panel V2. panels reinforced with only horizontal strips performed the worst. The horizontal reinforcement in panel H4A did not contribute to the load carrying capacity of the panel. In panel H4B failure occurred along an unstrengthened joint, after only a relatively small increase in the strength and ductility of the panel.

In panel V4A the vertical FRP reinforcement reduced the development of diagonal cracks across the FRP, and instead forced the cracks to develop along the inside edge of the FRP strip (facing the middle of the panel) through the brick. Unlike V4A, in the similarly reinforced panel V4B, diagonal cracks developed across the FRP strips and sliding deformation occurred. The difference in behaviour was likely due to different mortar strengths between each panel, indicated in Table 4.1, and also indicated by the initial stiffness and load at first crack of either panel. In the stronger panel, V4A, the resistance to sliding was larger and made cracks develop through the brick. This type of cracking created a failure plane (in V4A) and reduced the bond between the masonry and one side of the FRP. This cracking resulted in a reduced displacement capacity for panel V4A compared to panel V4B (where this type of cracking was less severe).

4.4.2 Load increase due to strengthening

The ultimate loads of all panels are presented in Table 4.2. Unexpectedly, some of the reinforced panels had lower ultimate loads than the unreinforced panels. The deviations in the bond strength and the statistical variations in the material properties were responsible for this result. Because of the large variation in material properties, rather than compare the ultimate loads of the reinforced tests with the URM tests, a less rigorous approach was used to estimate the increase in strength due to the FRP strengthening. The load when the first diagonal crack developed in the reinforced panel was assumed equal to the unreinforced strength of the panel. The load at first cracking was determined as the load when the FRP strip strains increased significantly from zero. The assumption is shown to be reasonable later in Chapter 5, Section 5.6.1 using the finite element model. The finite element model also confirmed that the FRP increased the ultimate load.

The assumed URM load was compared to the ultimate load to estimate the percentage load increase provided by the reinforcement scheme Table 4.2. Using 4 vertical FRP strips was the most effective reinforcement scheme for increasing the ultimate load of the panel. The largest load increase was 46% for panel V4B.

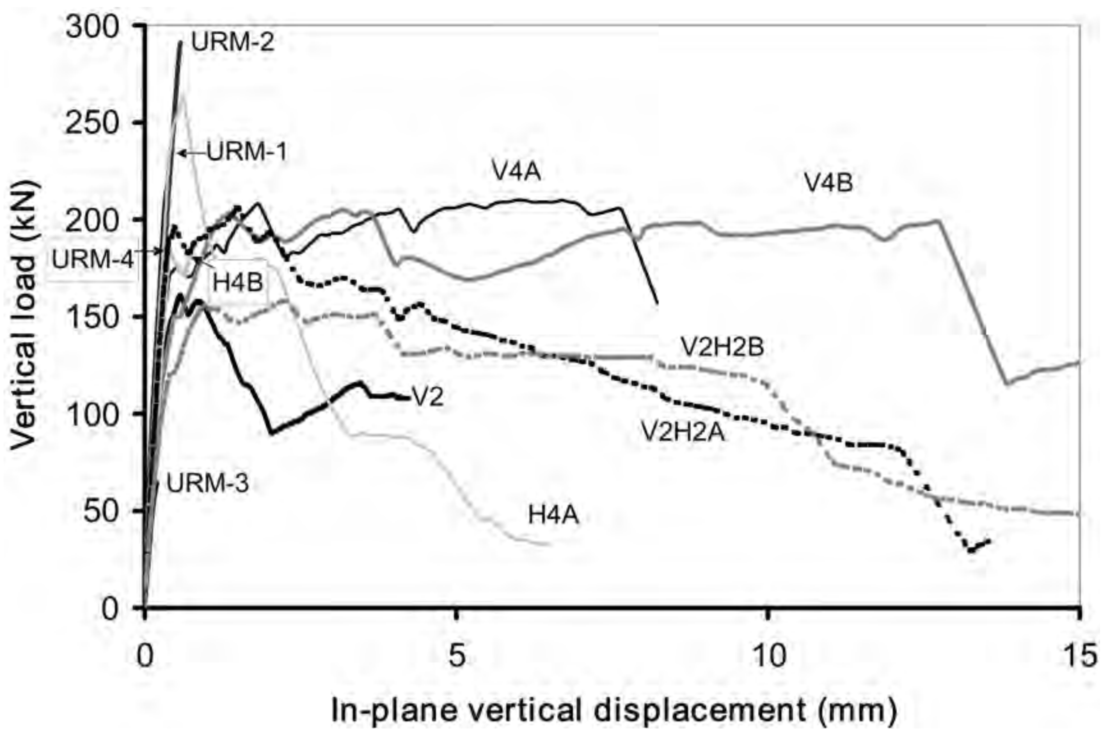

Figure 4.47: Load-displacement responses of all tests

Table 4.2: Contribution of reinforcement to load carrying capacity of masonry panels

Specimen	Approximate load at first crack (kN) (Approximate URM load)	Ultimate load (kN)	% load increase
URM-1	237	-	-
URM-2	290	-	-
URM-3	65	-	-
URM-4	183	-	-
V2	125	160	28
V4A	172	210	22
V4B	140	205	46
H4A	251	264	5
H4B	183	185	1
V2H2A	177	206	16
V2H2B	120	158	32

4.4.3 Displacement ductility

The displacement ductility factors of each of the tested panels were determined using the criteria set out in Park (1989). The displacement ductility factor is defined as Δ_u/Δ_y, where Δ_u is the ultimate displacement and Δ_y is the yield displacement.

The yield displacement (Δ_y) was determined for an equivalent elastic-plastic system with a secant stiffness at either first yield or at 0.75 times the ultimate load (whichever is less) (Figure 4.48).

The ultimate displacement (Δ_u) was determined as the lesser of:

1. the post-peak displacement when the load-carrying capacity has undergone a 20% reduction (Figure 4.49a)

2. the displacement when the material fractures (in this case when the FRP debonded from the panel) (Figure 4.49b)

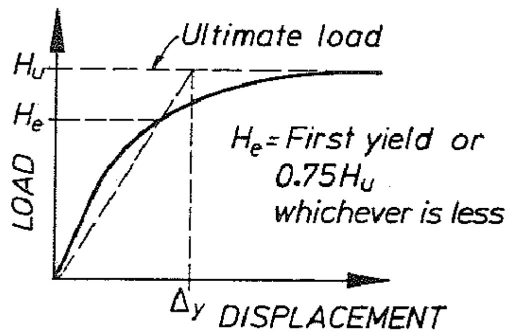

Figure 4.48: Definition of yield displacement from Park (1989)

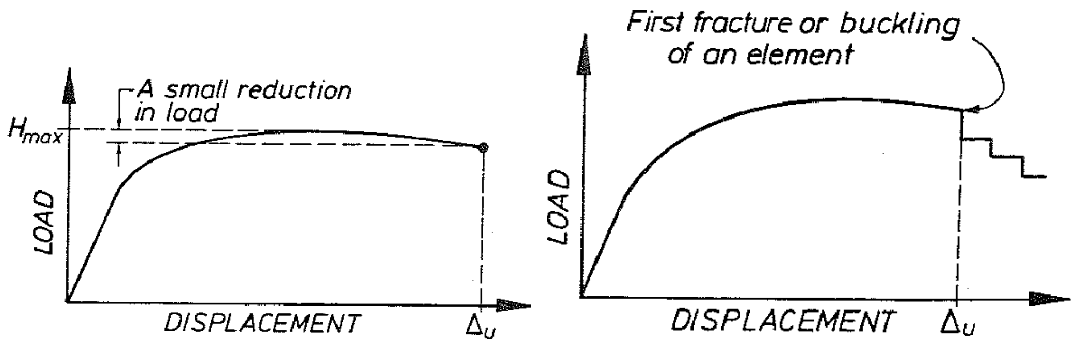

(a) Significant load capacity after peak load (b) Fracture (in this case FRP debonding)

Figure 4.49: Definitions of ultimate displacement from Park (1989)

The results of the displacement ductility analysis are shown in Table 4.3, where H_u is the ultimate load, and H_e is the load at first yield or $0.75H_u$ (Figure 4.48).

The yield and ultimate displacements used to determine the displacement ductility are illustrated for V4A in Figure 4.50 as an example. As expected, the panels strengthened with two vertical strips on both sides of the panel had the largest ductility factors. Also, the unreinforced specimens had ductility factors close to 1 indicating little ductility. Note that the wall panels have different boundary and loading conditions to a wall in a building, so the determination of a ductility factor may be premature. For instance, the ductility factor of an unreinforced wall failing by sliding along a single horizontal bed joint would be much larger than the ductility factor of an unreinforced panel tested in diagonal tension and failing in the same way.

Table 4.3: Displacement ductility factor analysis

Specimen	H_u (kN)	H_e (kN)	Δ_y (mm)	Δ_u (mm)	Δ_u/Δ_y
URM-1	237	177.8	0.36	0.45	1.25
URM-2	290	217.5	0.52	0.58	1.11
URM-3	65	48.8	0.16	0.20	1.21
URM-4	183	137.3	0.30	0.38	1.28
V2	160	120.0	0.35	1.41	4.06
V4A	210	157.5	0.45	7.65	16.96
V4B	205	140.0	0.60	12.76	21.16
H4A	264	198.0	0.43	0.88	2.03
H4B	185	138.8	0.37	0.78	2.08
V2H2A	206	154.5	0.38	3.52	9.39
V2H2B	158	118.5	0.52	8.23	15.82

4.5 Comparison of results with similar tests from the literature

The results of the current tests were qualitatively compared with the results of tests performed by Tinazzi and Nanni (2000). Tinazzi and Nanni (2000) strengthened URM panels using structurally repointed (SR) and NSM GFRP bars. The masonry panels they tested were 600 mm x 600 mm (half the size of the panels tested in the current study). They also used the Diagonal Tension Shear Test setup to test the specimens.

Tinazzi and Nanni (2000) constructed their wall panels using cored clay brick units with nominal dimensions 190 mm long, 90 mm wide, and 57 mm high. The flexural tensile strengths of the bricks used ranged between 3.7 MPa and 4.9 MPa. They used type N mortar (1:1:6). The flexural tensile bond strength of the mortar-brick interface was 0.56 MPa. This bond strength is within the range of bond strengths of the panels tested in the current study. The GFRP bars used had a diameter of 6.4 mm and elastic modulus of approximately 50,000 MPa.

The specimens that were most similar to those in the current study are considered for comparison. The specimens are shown in Figure 4.51 and include:

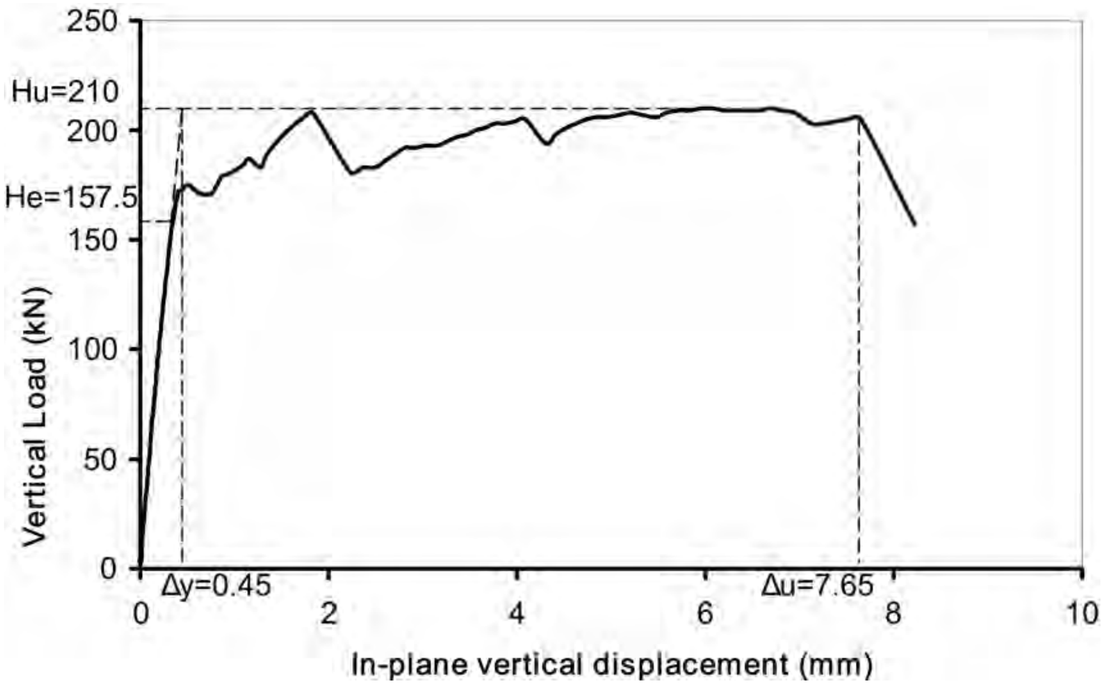

Figure 4.50: Load-displacement graph of V4A showing yield and ultimate displacements

- SR bars in every second bed joint on one side of the panel (Figure 4.51a)
- SR bars in every bed joint on one side of the panel (Figure 4.51b)
- Vertical NSM bars on one side of the panel (Figure 4.51c)
- SR bars in every bed joint on one side of the panel, vertical NSM bars on the other side (Figure 4.51d)

In their investigation the URM control specimens failed in a brittle manner by sliding along a diagonal crack that developed through the mortar joints. The average strength of the URM specimens (2 tested) was 71 kN.

In the panel reinforced with SR bars in every second bed joint (Figure 4.51a), failure occurred by sliding along an un-strengthened joint. This behaviour was similar to panel H4B from the current investigation. In both Tinazzi and Nanni (2000)'s panel and H4B the increase in strength due to strengthening was negligible.

In the panel reinforced with SR bars in every bed joint (Figure 4.51b), sliding along the mortar bed joints still occurred, but at a higher load. The increase in load was 45% over the URM specimens. This strengthening method was effective, but it seems cumbersome to insert reinforcement into every bed joint in large walls.

Tinazzi and Nanni used vertical NSM bars to prevent sliding failure along the mortar joints (Figure 4.51c). They expected that dowel action of the bars would help resist sliding. They observed the failure mode of the panel was by debonding

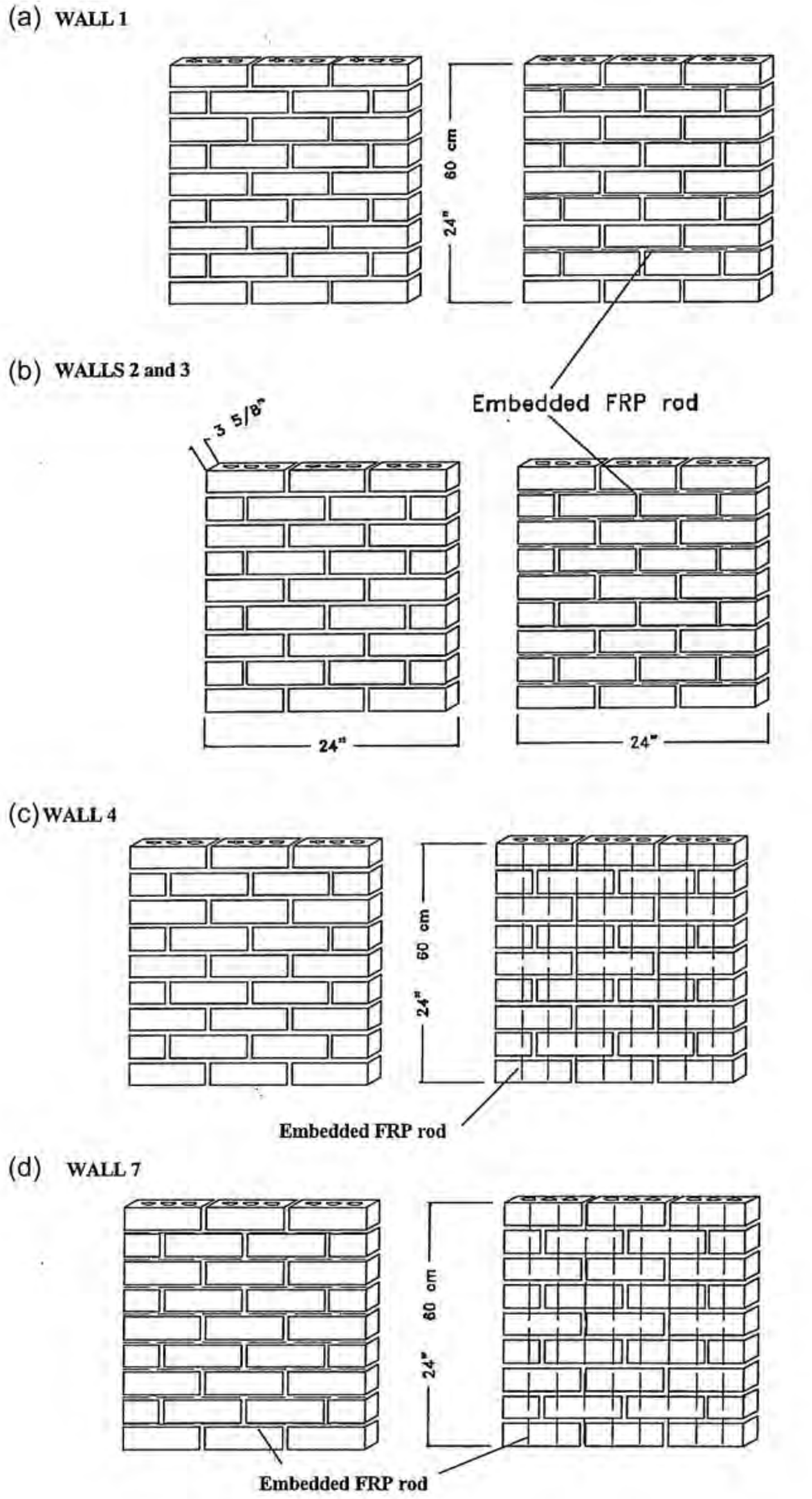

Figure 4.51: Tinazzi and Nanni (2000) specimens used for comparison

of the FRP bars from the masonry. Debonding was caused by shear failure along the masonry-epoxy interface, and was not related to dowel action. They did not describe the mechanism in any further detail. The test results of this specimen are comparable to the results of panel V2 from the current investigation. It seems that the reinforcement mechanism was similar, with the FRP acting in tension to restrain sliding. The crack patterns in both panels were also similar. In both panels a large dominant crack developed through the panel, along the loaded diagonal. Out-of-plane bending also occurred about this crack (with bending towards the reinforced side).

The panel shown in Figure 4.51d was reinforced in a similar way to panels V2H2A and V2H2B. Similar to panels V2H2A and V2H2B, the reinforcement allowed a large amount of cracking to develop within the panel. The failure mode of the panel shown in Figure 4.51d was not explicitly stated. It is likely that the large amount of cracking and degradation was responsible for failure. Unlike the panels from the current study (V2H2A and V2H2B), Tinazzi and Nanni's panel did not bend out of the plane of the panel. This was likely because in their panels the reinforcement was distributed more evenly across the surface of the panel.

Tinazzi and Nanni (2000) did not test a panel with vertical reinforcement applied to both sides of the panel. Therefore no test results were available to compare with V4A and V4B.

4.6 Summary and conclusions

Four unreinforced masonry (URM) panels and seven panels strengthened with near-surface mounted (NSM) fibre reinforced polymer (FRP) strips were tested using the Diagonal Tension/Shear Test. The tests were conducted to investigate the in-plane shear behaviour of NSM FRP strengthened masonry. Four different reinforcement schemes were used, and included: reinforcing one side of the panel with 2 vertical strips; reinforcing each side of the panel with 2 vertical strips; reinforcing each side of the panel with 2 horizontal strips; and reinforcing one side of the panel with 2 vertical strips and reinforcing the other side with 2 horizontal strips.

The URM panels failed in a brittle manner by either sliding along bed joints (panels with weak mortar) or diagonal cracking through brick units and mortar joints (panels with strong mortar). The FRP reinforcement prevented the URM failure modes, increased the ultimate load and ductility of the panels, and also increased the amount of cracks that developed in the panels. The vertical reinforcement prevented URM sliding failure by restraining the opening of the sliding cracks that developed through the mortar bed joints. It was also likely (in some cases) the vertical reinforcement provided some dowel action across the sliding joint. The horizontal reinforcement restrained the opening of diagonal cracks that developed through the brick units and the mortar joints.

The high variability of the material properties were a problem for the URM panels and it may be worth testing more panels in the future. The masonry variability was not such a problem for the reinforced panels, as the results were fairly consistent both in terms of load-displacement behaviour and failure modes. The results could be further improved by testing more than two repetitions per each type of specimen.

The non-symmetrical reinforcement schemes caused out-of-plane deformation and therefore should be avoided (if possible). In some cases in practice there may, however, be no choice. The out-of-plane behaviour may have been exaggerated by the test setup. In a real wall additional restraint would be provided along the top and bottom edges (instead of only at the corners), which may reduce out-of-plane twisting.

Debonding occurred in the vertical reinforcement when used (except panel V2). It started at the intersection of the diagonal cracks and the FRP and propagated away from the crack towards the ends of the strip. Debonding cracks developed within the brick and were similar to the debonding cracks that were observed in the pull tests. Complete debonding of the FRP strip from the masonry generally caused failure of the panel. The maximum debonding strains in panels V4A, V4B, V2H2A (3986 $\mu\varepsilon$, 6242 $\mu\varepsilon$, 3770 $\mu\varepsilon$, respectively) were lower than expected. It was expected that the debonding strain would be at least 7416 $\mu\varepsilon$ - 8963 $\mu\varepsilon$ (maximum debonding strain from pull tests on a similar FRP-to-masonry connection). Cracking along the edge of the FRP strip reduced the bond and hence the maximum strains in the strips. The maximum debonding strain in panel V2H2B (9848 $\mu\varepsilon$) was similar to the pull test debonding strain.

Dowel action of the vertical reinforcement could not be directly measured in the tests. In many of the panels, however, significant bending of the FRP occurred suggesting that little dowel strength was contributed. This needs to be confirmed with a finite element model. Note that the most significant improvements in behaviour were gained in panel V4B, where FRP bending was large and dowel strength likely very insignificant. It is very likely that the major shear strengthening mechanism of the vertical reinforcement was by acting in tension to provide confinement to the masonry.

5

Finite element modelling

5.1 Introduction

In this chapter the finite element (FE) model used to simulate the behaviour of the experimental diagonal tension/shear tests (from Chapter 4) is described. The material properties required for the masonry model were determined from a number of experimental characterisation tests. These tests are also described in this chapter. The bond between the FRP and the masonry was modelled using the bond-slip relationships determined from the pull tests presented in Chapter 3.

The FE model was used to help understand the results of the diagonal tension/shear tests. In particular, the effect of dowel action was investigated. In some of the diagonal tension tests, the shear resistance provided by dowel action of vertical reinforcement was likely insignificant. The main shear resisting mechanism would then be the action of the vertical FRP restraining the shear-induced dilation. This case was modelled assuming that the dowel strength of the FRP across the mortar joints was zero. In some of the diagonal tension/shear tests, dowel action may have been present. However, as dowel action could not be directly measured during the tests, the contribution of dowel strength to the shear strength of the panel could not be established. The dowel strength contribution (across a mortar joint) was estimated using another finite element model (described herein). This estimate of the dowel strength was then included in the FRP strengthened wall panel model in order to assess the contribution of dowel strength to the shear strength of the wall panel.

From another perspective, the experimental diagonal tension/shear tests were required to verify the proposed FE model. A representative model, that reproduces the key behaviours of the FRP strengthened wall panel, could be used to investigate a wide range of wall configurations and support conditions. This would reduce the number of full scale tests required to develop design guidelines.

5.2 Masonry model

The FE analysis was performed using the commercial software package DIANA 9 (de Witte, 2005). To model the masonry the simplified micro-modelling approach was adopted. The mortar joint and the mortar/brick unit interface were lumped into a zero thickness interface element. The interface element is a discontinuous element that relates the interface stresses (normal stress σ_n and shear stress τ) to the interface relative displacements (normal displacement u and shear displacement v). The brick units were modelled with continuum elements that were expanded to maintain the overall geometry of the masonry. Interface elements were also used at the mid-length of the brick unit to model potential cracking through the middle of the brick. The bricks were modelled elastically and all of the non-linear behaviour (cracking, shear sliding and crushing) was modelled in the interface elements.

The micro-modelling approach was adopted for the following reasons:

1. it is able to reproduce crack patterns and the complete load displacement path of a masonry structure, and is therefore well suited for understanding experimental results

2. it is considered more suitable (than the macro-model approach) for modelling FRP strengthened structures (see Section 2.7.1)

3. it allows dilation to be modelled along sliding interfaces

4. it allows FRP dowel strength to be easily modelled across sliding interfaces (see Section 5.5)

The masonry modelling approach and the element divisions are shown in Figure 5.1. Note that in this figure the interface elements have been shown with thickness for illustrative purposes. The brick units were modelled using eight-node quadratic, rectangular plane stress elements with a thickness of 110 mm. Each half-brick unit section (surrounded by interface elements) was divided into two elements across the height and two elements across the length (as shown in Figure 5.1b). The mortar joint interface element (lumped representation of mortar joint and mortar/brick unit interface) and the potential brick crack interface element were modelled with six-node quadratic, rectangular plane stress interface elements. Two interface elements were used across each half-brick length, to match the mesh division of the brick unit (shown in Figure 5.1b).

5.2.1 Interface element non-linear behaviour

The non-linear behaviour in the mortar joint interface elements was modelled using the Crack-Shear-Crush material model. This model was developed by Lourenço and Rots (1997) and Van Zijl (2004), and is included in DIANA 9 (de Witte, 2005). For the potential brick crack interface element a linear tension softening model was used.

The Crack-Shear-Crush material model is based on multi-surface plasticity and incorporates a Coulomb-friction model (to describe joint sliding), a tension cut-off model (to describe joint cracking), and an elliptical compression cap model (to describe masonry compression and brick unit diagonal cracking). Softening acts in each model, and is preceded by hardening in the compression cap model. The failure surface of the model and the failure mechanisms it simulates are shown in Figure 5.2 and Figure 5.3, respectively.

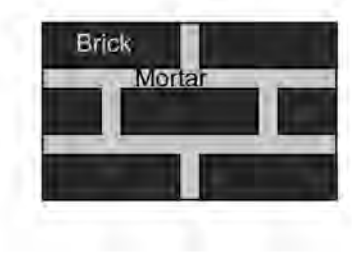

(a) Masonry assemblage

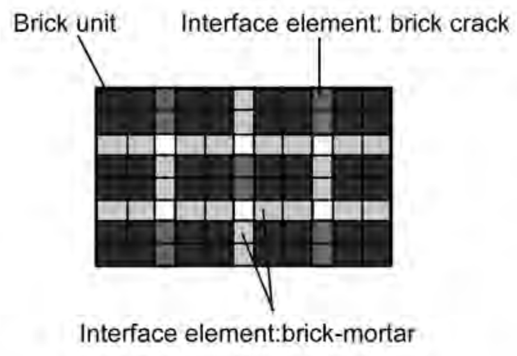

(b) FE model (interface elements shown having thickness)

Figure 5.1: Masonry simplified micro-modelling approach adopted for study

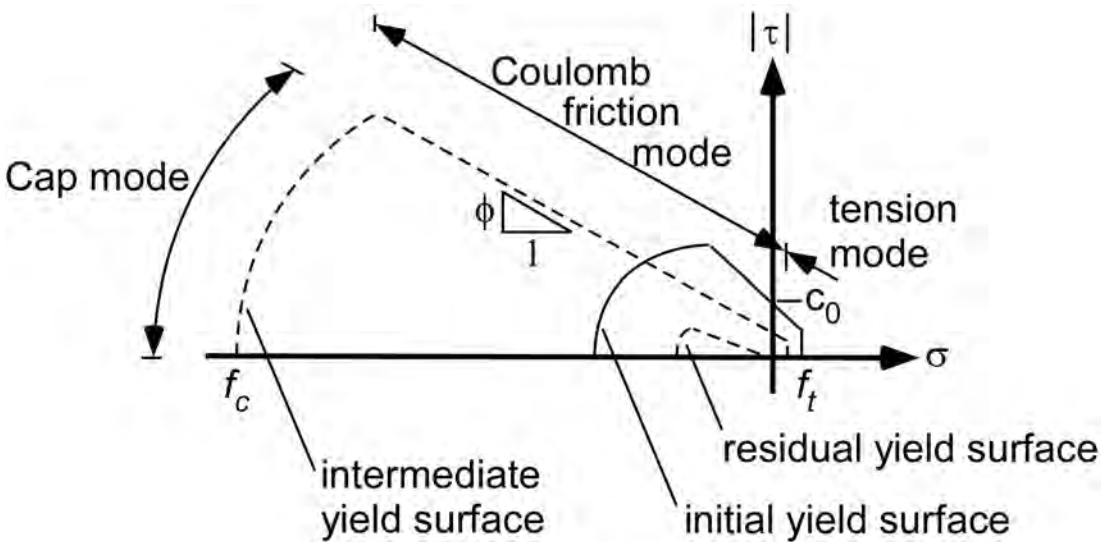

Figure 5.2: Failure surface of Crack-Shear-Crush model (2D) (DIANA users manual, de Witte (2005))

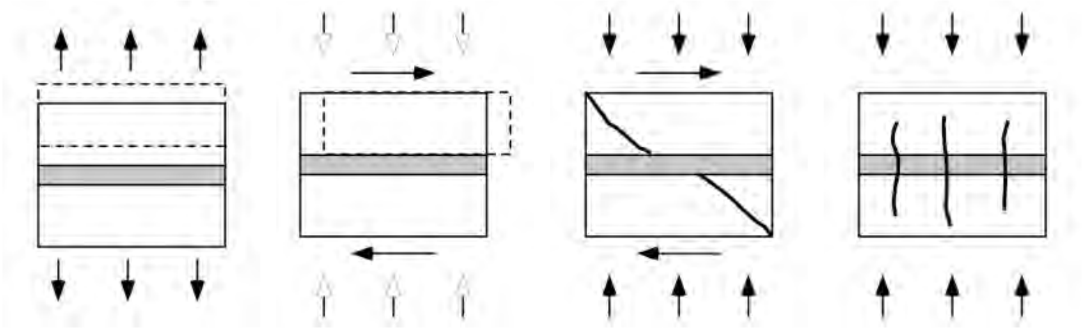

Figure 5.3: Failure mechanisms described by Crack-Shear-Crush model (Lourenço, 1996b): a) joint cracking in tension, b) joint sliding with shear at low levels of normal compressive stress, c) unit diagonal tension crack at high levels of normal compressive stress and shear, d) masonry crushing

The coulomb friction model captures masonry joint sliding behaviour (including softening behaviour) observed in masonry joint shear tests at low levels of normal stress. The Coulomb-friction criterion is:

$$|\tau| \leq c - \sigma_n \Phi \tag{5.1}$$

where c is the cohesion, Φ is the internal friction coefficient and compressive normal stresses (σ_n) are negative. Joint sliding occurs when the failure criterion is reached. Both the cohesion (c) and internal friction (Φ) values soften as the joint slides. The cohesion softens from an initial value c_0 to zero and the internal friction value softens from an initial value Φ_i to a residual value Φ_r. The rate at which the cohesion and the internal friction soften depends on the shear fracture energy (G_f^{II}), which is the area under the shear stress-shear displacement curve. The behaviour of the non-linear model in shear is shown in Figure 5.4b.

The tension cut-off model captures the behaviour of masonry joint cracking in direct tension. The tensile strength (or brick mortar bond strength) is limited by Equation 5.2:

$$\sigma_n \leq \sigma_t \tag{5.2}$$

where σ_t is the tensile, or brick-mortar bond strength, which softens exponentially from the initial value of the brick-mortar bond strength (f_t) to zero as the crack opens. The softening behaviour depends on the tensile fracture energy (G_f^I). The behaviour of the non-linear model in tension is shown in Figure 5.4a.

The compression cap model describes the behaviour of masonry loaded in compression and also sets a limit on the shear stress at high values of normal stress due to diagonal cracking through the brick. The compression cap criterion is given in Equation 5.3:

$$\sigma_n^2 + C_s \tau^2 \leq \sigma_c^2 \tag{5.3}$$

where C_s is a parameter that controls the shear stress contribution to failure and is equal to 9 (Lourenço, 1996b), and σ_c is the compressive strength. The compressive strength (σ_c) is described by a parabolic hardening rule, until the peak compressive strength of the masonry f_c is reached at the plastic strain κ_p. Afterwards, the compressive strength softens. The softening is described by a parabolic/exponential softening rule and depends on the fracture energy G_c . The behaviour of the non-linear model in compression is shown in Figure 5.4c.

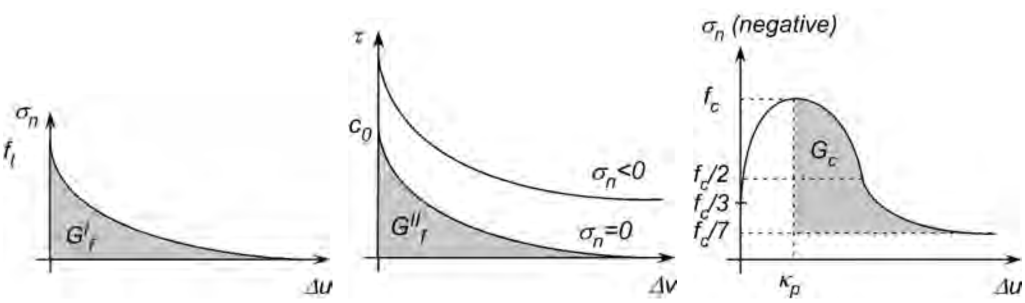

(a) Tension (b) Shear (c) Compression

Figure 5.4: Behaviour of crack shear crush model (DIANA users manual, de Witte (2005) and Lourenço (1996a))

Normal uplift due to sliding (dilation) is also included in the model. The dilation is modelled using Equation 5.4 (Van Zijl, 2004):

$$u_p = \frac{\Psi_0}{\delta}\left[1 - \frac{\sigma_n}{\sigma_u}\right]\left(1 - e^{-\delta v_p}\right) \tag{5.4}$$

where Ψ_0 is the dilatancy gradient at zero normal confining (compressive) stress and shear-slip, σ_u is the compressive stress at which the dilatancy becomes zero, δ is the dilatancy shear-slip degradation coefficient, and u_p and v_p are the plastic components of the normal and shear displacements respectively. The three parameters (Ψ_0, σ_u, δ) are obtained by least-squares fitting of experimental data.

Tensile cracking of the potential brick crack interface elements was modelled using a linear tension softening model (shown in Figure 5.5). This model is similar to the tension cut-off model in the Crack-Shear-Crush material model, except that softening is linear instead of exponential. For these interface elements no failure criteria was given in shear and compression. These interface elements were modelled as being very stiff to ensure continuity of brick displacement across the interface. This means that frictional sliding is not possible along the potential crack line. The interface stiffness values of the potential brick crack interface elements (normal interface stiffness k_n, and shear interface stiffness k_s) were set at a high value of 10^6. After tensile cracking the interface element was assumed to have zero shear resistance.

The properties required for the interface element non-linear material models were determined from experimental joint and masonry characterisation tests (discussed in the next section). Experimental tests were also used to determine the

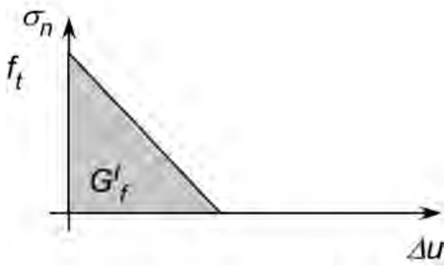

Figure 5.5: Linear tension softening model for potential brick crack interface elements

elastic modulus of the brick, and the elastic properties of the mortar joint interface elements (normal interface stiffness k_n, and shear interface stiffness k_s).

5.3 Masonry material characterisation tests

This section details the experimental tests used to determine the material properties required for the masonry FE model described in Section 5.2.

5.3.1 Bond wrench tests

Bond wrench tests were conducted on all mortar batches used in this thesis to determine the flexural tensile bond strength of the brick-mortar interface. The results of the bond wrench tests were used as control tests to compare the general bond strengths between different mortar batches. Where bond strength is referred to in this thesis it means the flexural tensile bond strength as measured using the bond wrench (unless otherwise specified).

Bond wrench tests were conducted in accordance with AS3700-2001, Standards Australia (2001c). The bond wrench test involves subjecting a masonry bed joint (in a prism) to a bending moment. The bending moment is applied to the joint using a wrench. A schematic of the test is shown in Fig. 5.6. The standard specifies that ten joints are tested.
The flexural tensile bond strength of the joint is calculated as:

$$f_{sp} = (M_{sp}/Z_d) - (F_{sp}/A_d) \tag{5.5}$$

where

M_{sp} = the bending moment about the centroid of the bedded area of the test joint at failure = $9.81 m_2(d_2 - t_u/2) + 9.81 m_1(d_1 - t_u/2)$

Z_d = the section modulus of the cross-section

F_{sp} = the total compressive force on the bedded area of the tested joint = $9.81(m_1 + m_2 + m_3)$

A_d = the cross-sectional area

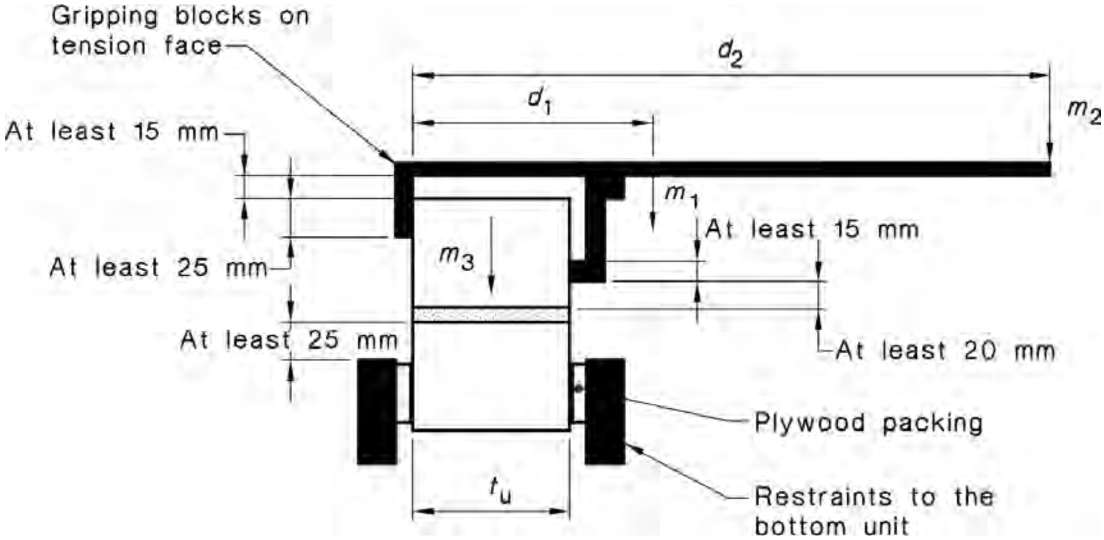

Figure 5.6: Schematic of bond wrench test AS3700-2001, Standards Australia (2001c)

m_1 = mass of the wrench

m_2 = mass applied to end of bond wrench lever to cause failure

m_3 = mass of unit

d_1 = the distance from the inside edge of the tension gripping block to the centre of gravity

d_2 = the distance from the inside edge of the tension gripping block to the loading handle

t_u = the width of the masonry unit

A summary of the bond wrench results on all of the mortars used in this thesis is shown in Table 5.1.

The direct tensile strength of the mortar joint, rather than the flexural tensile strength, was more appropriate as input into the model. Tests have shown that the tensile strength of a mortar joint is less than the flexural bond strength (Van der Pluijm, 1997). The difference is a result of the non-linear stress distribution in a bending test at failure (explained in Van der Pluijm (1997)). In general a factor of 1.5 can be assumed for the ratio between flexural and tensile strengths (Van der Pluijm, 1997; Pina-Henriques et al., 2004). This estimate of the direct tensile strength was used because direct tension tests were not performed on the mortar joint interface. The direct tensile strengths used in the FE models are determined later in Section 5.4 (unreinforced models) and Section 5.6 (reinforced models) for the different strength mortars used in the analyses.

Table 5.1: Summary of all bond wrench results

Test	Mortar batch	Bond Strength (MPa)	COV (%)
Compression test	1:1:6 mortar	1.22	31
(Section 5.3.2)	Han (2008) specimens		
	(1:1:6 + air entrainer)	0.176	-
Torsion test	Series 1 (1:1:6 + air entrainer)	0.14	26
(Section 5.3.3)	Series 2 (1:1:6)	1.74	11
Pull tests	1	1.84	23
(Section 3.2.1)	2	1.73	22
	3	1.22	31
Wall Panel tests	1	1.25	51
(Section 4.2)	1+W	0.65	34
	2	0.49	37
	2+W	0.29	46
	3	0.47	47
	3+W	0.31	57
	4	0.57	48
	5	1.26	32
	5+W	0.41	59

5.3.2 Compression tests on masonry prisms

Compression tests on 7-brick high masonry prisms were used to determine the elastic properties of the brick unit and mortar joint, as well as the compressive strength of the masonry. Five prisms were constructed using the same clay brick and mortar specification used to construct the pull test specimens and the wall panels tested in diagonal tension/shear. The flexural bond strength of these specimens was 1.22 MPa (COV 31%), determined using AS 3700 bond wrench test (Standards Australia, 2001c). This value was approximately equal to the bond strengths of the strongest panels tested (URM-1, URM-2 and H4A - see Table 4.1 in Chapter 4).

The compression specimens were constructed and tested in accordance with AS3700 Appendix C (Standards Australia, 2001b). Specimens were constructed 7 bricks high to achieve a height-to-thickness ratio greater than 5 to minimise the influence of platen restraint. A photograph of the test is shown in Fig. 5.7.

Potentiometers were placed on both sides of the specimen to measure the displacement across a mortar joint and across 3 bricks to calculate the strain in the mortar joint and masonry respectively (as recommended by Drysdale et al. (1994)). Potentiometers were not used to measure the displacement within a single brick unit because they were not sensitive enough to measure the small brick displacement. Potentiometers were mounted onto brackets that were screwed onto the specimen at fine target points to allow the gauge lengths for displacement measurement to be determined accurately.

To improve the determination of the elastic modulus from the compression test each specimen was loaded and then unloaded three times before being loa-

Figure 5.7: Compression test setup

ded to failure. Specimens were loaded to approximately 40 % of their predicted peak load, before unloading, to capture the elastic loading range and minimise non-recoverable damage. Specimen 1 was loaded to 200 kN before unloading (based on an estimate of P_c = 500 kN); specimens 2-4 were loaded to 260 kN before unloading (40% of P_c specimen 1); and specimen 5 was loaded to 300 kN before unloading (approximately 40% of average of P_c for first four specimens). The displacements recorded from the second, third and final load cycles were averaged and used in the calculations to determine the elastic modulus values of the masonry and the mortar (displacements recorded from the first load cycle were ignored). All of the compression tests were stopped once the ultimate load was reached to avoid damaging the potentiometers.

All of the specimens failed by crushing in the mortar joint and vertical cracking through the front and back faces of the brick units. The ultimate load (P_c) and corresponding maximum compressive stress (f_c), masonry strain at f_c, and the elastic modulus of the mortar (E_{mor}) and masonry (E_{mas}) are shown in Table 5.2. The elastic modulii of the mortar (E_{mor}) and masonry (E_{mas}) were determined as the gradients of the compressive stress-strain curves (for mortar and masonry respectively) between 5 and 33% of the maximum compressive strength (Drysdale et al., 1994).

The average elastic modulus of a single brick unit E_{unit} was determined indirectly using the average values of E_{mor} and E_{mas} and by considering compatibility of displacements between masonry, brick unit and mortar joint. This calculation was required because brick unit displacement (used to calculate strain) was not recorded. The total masonry displacement is equal to the sum of the displacement of the units and mortar. The masonry displacement across 3 bricks and 3 mortar joint is equal to:

$$\delta_{mas} = 3\delta_{unit} + 3\delta_{mor} \tag{5.6}$$

The displacements are calculated using:

$$\delta_{mas} = \frac{PL_{mas}}{E_{mas}A} \tag{5.7}$$

$$\delta_{unit} = \frac{PL_{unit}}{E_{unit}A} \tag{5.8}$$

$$\delta_{mas} = \frac{PL_{mor}}{E_{mor}A} \tag{5.9}$$

Where P=compression load, A=bedded area of prism, L_{mas}=258 mm, L_{unit}=76 mm, L_{mor}=10 mm. By substituting Equations 5.7, 5.8, and 5.9 into Equation 5.6, E_{unit} was determined as 27592 MPa.

Table 5.2: Compression test results (bond strength = 1.22 MPa)

Specimen	P_c (kN)	f_c (MPa)	Masonry strain at f_c	E_{mor} (MPa)	E_{mas} (MPa)
1	664.88	26.28	0.0013	4801	17698
2	651.73	25.76	0.0030	8047	18895
3	970.51	38.36	0.0027	5067	17909
4	894.86	35.37	0.0025	2650	18157
5	873.10	34.51	0.0023	4854	18415
Average	811.12	32.06	0.0025	5084	18215

The average shear modulus values of the brick unit (G_{unit}) and mortar (G_{mor}) were calculated as 11497 MPa and 2118 MPa respectively, using Equation 5.10 and Equation 5.11. A Poisson's ratio (ν) equal to 0.2 was adopted for both the brick unit and the mortar (Lourenço, 1996a).

$$G_{unit} = \frac{E_{unit}}{2(1+\nu)} \tag{5.10}$$

$$G_{mor} = \frac{E_{mor}}{2(1+\nu)} \tag{5.11}$$

The experimentally determined elastic properties of the brick unit and mortar joint were valid for the actual dimensions of the unit and the joint. As expanded units and zero-thickness mortar joints were used in the FE model, adjustments to the elastic properties were required to achieve an equivalent overall elastic response. A method that alters the elastic properties of the interface elements and leaves the enlarged unit properties untouched is described in Rots (1997) and Lourenço (1996a). The normal elastic stiffness (k_n) and the shear elastic stiffness (k_s) of the mortar joint interface element were altered using Equation 5.12 and Equation 5.13, respectively, where h_{mor} = thickness of mortar joint = 10 mm. The normal elastic stiffness (k_n) was calculated as 623 N/mm^3 and the shear elastic stiffness (k_s) was calculated as 260 N/mm^3.

$$k_n = \frac{E_{unit}E_{mor}}{h_{mor}(E_{unit} - E_{mor})} \tag{5.12}$$

$$k_s = \frac{G_{unit}G_{mor}}{h_{mor}(G_{unit} - G_{mor})} \tag{5.13}$$

In addition to the maximum compressive stress (f_c), the equivalent plastic relative displacement (κ_p) and the compressive fracture energy (G_c) were also required to model compression failure. The equivalent plastic relative displacement (κ_p) was calculated using Equation 5.14 as 0.024 mm in order to obtain a total masonry strain of 0.25% at f_c (Table 5.2) (Lourenço, 1996a). In Equation 5.14 h_{unit} is the height of the brick unit = 76 mm.

$$\kappa_p = \left\{0.0025 - f_c\left[\frac{1}{E_{unit}} + \frac{1}{k_n(h_{unit} + h_{mor})}\right]\right\} f_c \tag{5.14}$$

As each compression test was stopped just after the ultimate load was reached the compressive fracture energy was not recorded. The compressive fracture energy was estimated as 25 N/mm using Equation 5.15 (Lourenço, 1996a).

$$G_c = 15 + 0.43f_c - 0.0036f_c^2 \tag{5.15}$$

To estimate the elastic and compression properties for masonry panels with a weaker bond strength (the average bond strength for some of the panels tested was as low as 0.29 MPa) the results of Han (2008) were used. Han tested five masonry prisms constructed using a similar clay brick (as the current investigation), but a weaker mortar was used. This mortar consisted of cement:lime:sand in proportions of 1:1:6 by volume with eight times the recommended dose of air entraining agent added to deliberately create low bond strength. The bond strength of these specimens was 0.176 MPa. The average values of the ultimate load (P_c), maximum compressive stress (f_c), and the elastic modulus of the mortar (E_{mor}), masonry (E_{mas}) and brick unit(E_{unit}) are shown in Table 5.3. The masonry strain at f_c was not reported.

Table 5.3: Compression test average results from Han (2008) (bond strength = 0.176 MPa)

P_c (kN)	f_c (MPa)	E_{mor} (MPa)	E_{mas} (MPa)	E_{unit} (MPa)
516	20.0	2772	18135	35360

From these tests the values of f_c = 20 MPa and E_{mor} = 2772 MPa were adopted to represent masonry with a bond strength of 0.176 MPa. For consistency, the elastic modulus of the brick unit (E_{unit}) from the previously described test series (equal to 27592 MPa) was kept. The input properties required for the mortar joint interface elements were calculated the same way as described previously, and are shown in Table 5.4. For the calculation of κ_p, the masonry strain at f_c was assumed as 0.2% (Lourenço, 1996a). The input properties required for the mortar joint interface elements determined for masonry with a bond strength of 1.22 MPa, are also shown in Table 5.4.

Table 5.4: FE model input properties determined from compression tests

Property	Bond strength = 0.176 MPa	Bond strength = 1.22 MPa
k_n (N/mm^3)	308	623
k_s (N/mm^3)	128	260
f_c (MPa)	20	32
G_c (N/mm)	22	25
κ_p (mm)	0.010	0.024

5.3.3 Torsion test

To characterise the shear behaviour of the mortar joint the torsion test (shown in Figure 5.8), developed by Masia et al. (2006, 2007), was used. In this test an annular masonry specimen, which contains a single bed joint (Figure 5.8a), is subjected to combined compressive stress (normal to the bed joint) and torsion. The torsion test produces close to uniform distributions of normal and shear stress, thus allowing the shear behaviour at a point to be characterised.

As part of the current investigation a set of torsion tests were performed on specimens constructed using the same brick and mortar as the wall panel tests. The specimens were prepared by coring a complete annular specimen through the height of a pre-cast masonry couplet. These specimens were prepared differently from previous torsion tests, reported in Masia et al. (2007). In Masia et al.'s tests the specimens were prepared by coring annular sections from two separate solid units first, and then bonding them together with mortar. After testing, and then analysing the results of the current investigation (joints cast before coring) it was found that the joint shear strengths were lower than expected when compared to joints that were cast after coring (as in Masia et al. (2007)). The reduced joint strength was thought to be caused by damage to the joint during the coring procedure. The results from the current investigation were unreliable and therefore were not used for the characterisation of the shear behaviour. The results of tests conducted by Masia et al. (2007) were used instead.

Torsion tests by Masia et al. (2007)

This section outlines the specimens tested by Masia et al., the testing procedure they used, and their results. Torsion tests were performed on specimens constructed with two different types of mortar. The first set of specimens (series 1) were built using solid extruded clay bricks and mortar mixed in a ratio of 1:1:6 (cement:lime:sand). The mortar was overdosed with an air entraining agent (eight times the recommended amount) to deliberately reduce the bond strength. The bond strength of the mortar joint was determined as 0.14 MPa using the bond wrench test. Eight of these specimens were tested. The second set of specimens (series 2) were constructed using the same bricks and the mortar was mixed in a ratio of 1:1:6 (cement:lime:sand) with no extra additives. The bond strength of this mortar joint was determined as 1.74 MPa. Eleven of these specimens were tested.

The bricks and mortar used by Masia et al. for series 2 specimens were the same as the bricks and mortar used in this thesis. The bricks used for series 1 specimens were not from the same batch, but were provided by the same brick manufacturer, and were very similar. The mortar used in series 1 tests was different to the mortar used in the current study due to the use of air entraining agent to make the bond weaker.

The specimens were prepared by coring annular sections through the height of two solid brick units and then bonding them together (on the bedding faces) with a 10 mm thick mortar joint. All of the annular specimens had an inside radius r_i = 36 mm and an outside radius r_o = 47.5 mm.

The torsion test apparatus is shown in Figure 5.8b and Figure 5.8c. A circular steel plate was glued onto each end of the specimen. Before the adhesive set, the specimen was then placed on its side in the apparatus (as shown), with one end of the specimen fixed in place and the other end attached to a rotating shaft. The axis of rotation of the shaft was aligned with the axis of the specimen. The rotating shaft was also free to displace along its length.

A hydraulic jack was used in a closed loop system (as shown) to apply precompression to the joint. The precompression was applied under load control and was held constant throughout the test. For the specimens constructed with the relatively weak mortar (series 1) three nominal levels of precompression on the joint were used: 0.14 MPa; 0.33 MPa; and 0.67 MPa. For the specimens constructed with the relatively strong mortar (series 2) the three nominal levels of precompression on the joint used were: 0 MPa; 0.68 MPa; and 1.33 MPa (Table 5.5).

The test apparatus was mounted in a Universal Testing Machine (UTM). The UTM cross-head was used to displace a lever, that was attached to the rotating shaft. The end of the specimen (attached to the shaft) was caused to rotate and this rotation created torsion through the specimen. A load cell was used to measure the force, applied by the cross-head, required to displace the lever. The torque (T) through the specimen was then equal to this force multiplied by the lever length. Potentiometers were used to measure the shear displacement across the mortar joint (from which the relative rotation (ϕ) was calculated) and the normal separation across the mortar joint.

Equation 5.16 and Equation 5.17 were used to convert the experimentally recorded torque (T) versus rotation (ϕ) into shear stress (τ) versus shear displacement (υ) behaviour (required for derivation of joint shear properties at a material

(a) Torsion test specimen

(b) Setup (view 1)

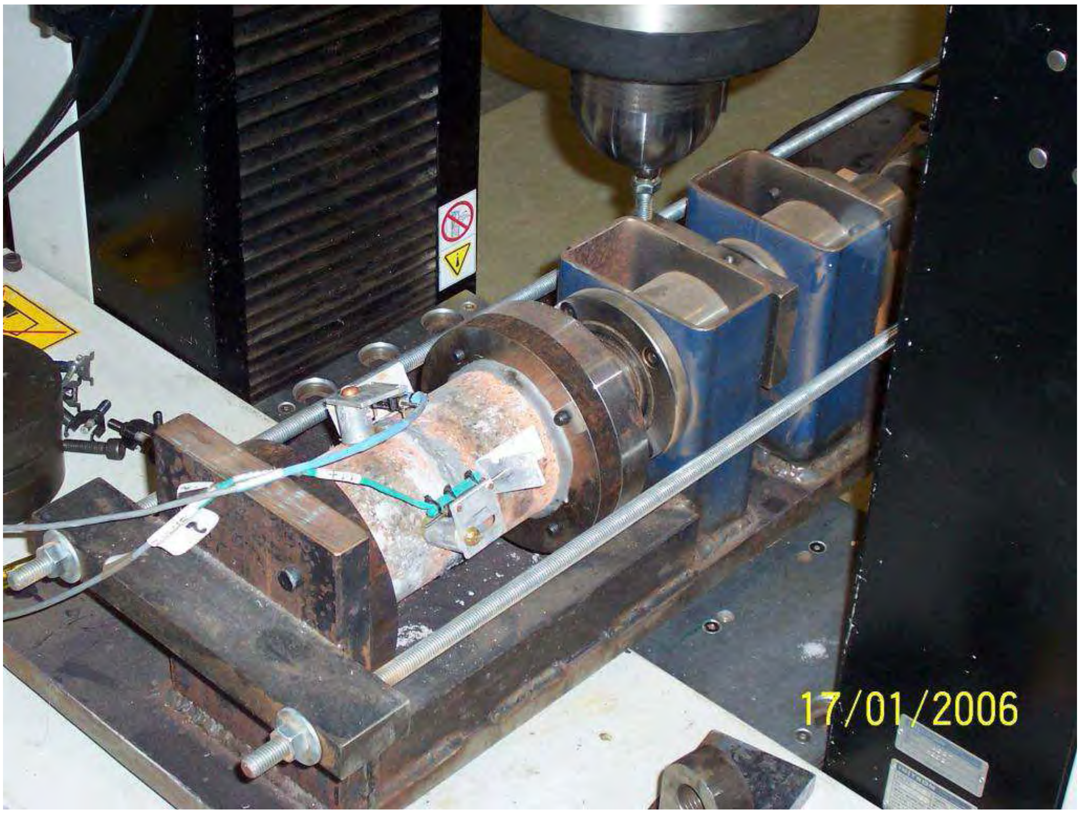

(c) Setup (view 2)

Figure 5.8: Torsion test setup and annular specimen

point). In Equation 5.17 r was the average radius of the annular section = 41.75 mm. The derivation of these equations are provided in detail in Masia et al. (2007). Equation 5.16 is only applicable when failure occurs through the mortar joint (not through the brick). Masia therefore only used the results of the specimens where failure occurred through the joint (brick cracking not present) to derive the joint shear properties. The shear stress (τ) versus shear displacement (v) behaviour of a typical specimen is shown in Figure 5.9.

$$\tau = 3T/(2\pi(r_o^3 - r_i^3)) \tag{5.16}$$

$$v = r\phi \tag{5.17}$$

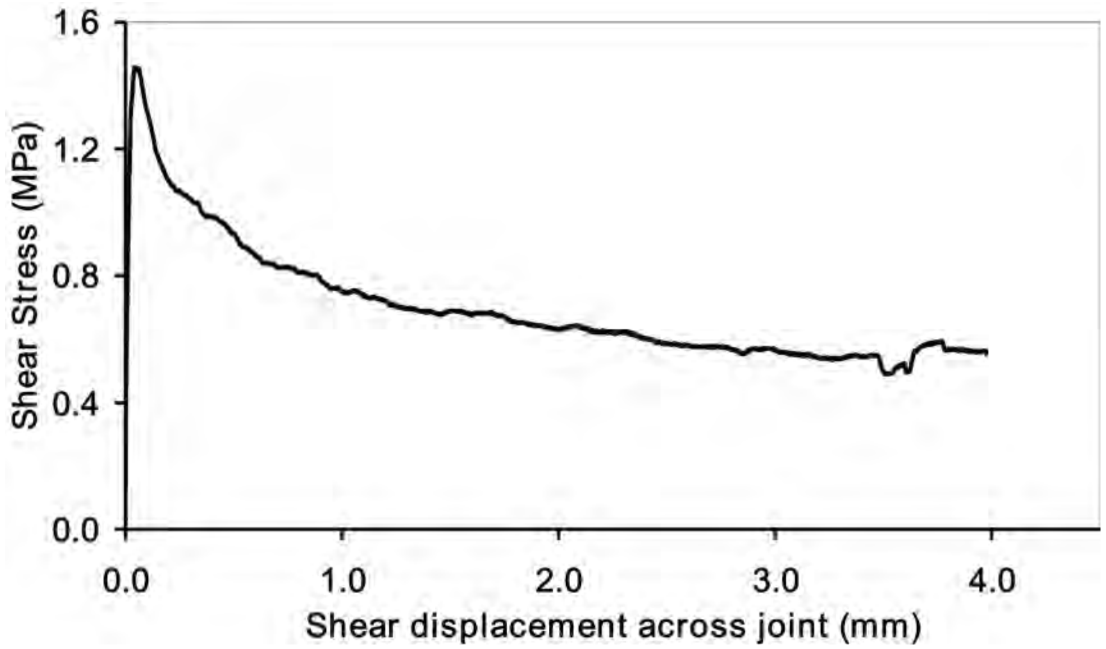

Figure 5.9: Typical derived shear stress versus shear displacement response, Masia et al. (2007)

Many specimens did fail within the joint, with cracks developing along the brick mortar interfaces and in many cases, diagonal cracks extending across the mortar joint were observed. A summary of the torsion test results are given in Table 5.5. The ultimate shear stress (τ_u), the residual shear stress ($\tau_{residual}$), the shear fracture energy (G_f^{II}) and the elastic shear modulus (G) were determined for each specimen from the shear stress versus shear displacement curves. The shear fracture energy (G_f^{II}) was determined as the area under the curve, above $\tau_{residual}$. The elastic shear modulus (G) was determined for each test by computing the slope of the loading branch of the τ versus v response using a secant drawn between 5% and 33% of τ_u. Note that the value of G determined by Masia et al. (2007) was not used in the current study.

Table 5.5: Experimental results from Masia et al. (2007)

Test No.	σ_n (MPa)	τ_u (MPa)	$\tau_{residual}$ (MPa)	G_f^{II} (N/mm)	G (MPa)	Failure mode
Test Series 1 Units:extruded solid clay, Mortar: 1:1:6 + overdose (8 x recommended) air entrainer Mean flexural bond strength = 0.14 MPa, COV 26%						
1	-0.66	NA	0.49	NA	NA	Joint cracked prior to test
2	-0.68	1.03	0.40	0.45	1860	Joint
3	-0.68	0.61	NA	NA	730	Joint crushing after peak T
4	-0.34	0.49	0.29	0.11	1700	Joint
5	-0.34	1.30	0.32	0.24	5500	Joint
6	-0.14	0.34	0.13	0.06	1800	Joint
7	-0.14	0.31	0.14	0.03	5860	Joint
8	-0.33	0.60	0.31	0.05	350	Joint
Cohesion c_0 = 0.22 MPa, Initial friction Φ_i = 0.90, Residual friction Φ_r = 0.56						
Test Series 2 (specimen 8 was unsuccessful) Units:extruded solid clay, Mortar: 1:1:6 Mean flexural bond strength = 1.74 MPa, COV 11%						
Test No.	σ_n (MPa)	τ_u (MPa)	$\tau_{residual}$ (MPa)	G_f^{II} (N/mm)	G (MPa)	Failure mode
1	0	1.28	0	-	1540	Joint
2	0	0.72	0	-	1500	Joint
3	0	0.85	0	-	2470	Joint
4	-0.69	1.46	0.55	0.60	1180	Joint
5	-0.67	2.44	0.58	0.38	36860	Joint and brick
6	-0.67	1.63	0.75	0.19	1360	Joint
7	-1.33	1.59	1.21	0.07	6450	Joint and brick
9	-1.34	2.04	0.70	0.92	48610	Joint and brick
10	-1.34	2.05	1.38	0.25	5310	Joint
11	-0.68	2.06	0.81	0.31	2140	Joint
Cohesion c_0 = 1.00 MPa, Initial friction Φ_i = 0.90, Residual friction Φ_r = 1.03						

The ultimate shear stresses (τ_u) were plotted against the normal stresses (σ_n) and a linear trend line was fitted to the results to determine the cohesion (c_0) and the initial friction (Φ_i) values (Figure 5.10 and Figure 5.11). The cohesion and initial friction values are summarised in Table 5.5.

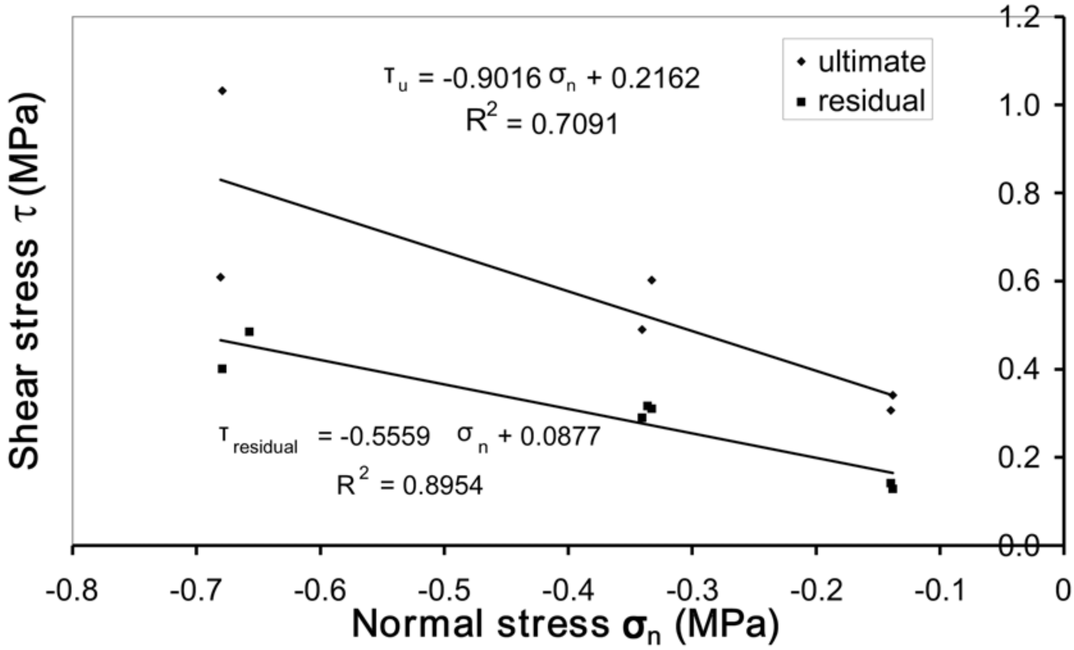

Figure 5.10: Shear stress versus normal stress (Series 1), Masia et al. (2007)

The residual shear stresses ($\tau_{residual}$) were plotted against the normal stresses (σ_n) and a linear trend line was fitted to the results to determine the residual friction (Φ_r) values (Figure 5.10 and Figure 5.11). Note that a negative value of σ_n is a compressive normal stress.

The shear fracture energies (G_f^{II}) were also plotted against the normal stress (σ_n), shown in Figure 5.12 and Figure 5.13. Masia observed that for the series 1 specimens G_f^{II} increased with σ_n (as was expected). In general, however, they could not establish a sensible relationship between G_f^{II} and σ_n due to the large amount of variability in the data.

The average normal uplift (dilation) versus the shear displacement relationships are shown in Figure 5.14 (series 1) and Figure 5.15 (series 2) for the specimens that failed within the joint. In Figure 5.14 the dilation response of specimens 2 and 3 were not plotted because the mortar crushed during the test. Dilation could not be recorded for specimens with no precompression because they fell apart after failure.

It is shown in Figure 5.14 and Figure 5.15 that the rate of increase of the normal uplift (with respect to the shear displacement) decreased as the shear displacement increased. Also, the amount of dilation reduced with increasing normal stress on the joint. This behaviour is consistent with other published results (Van

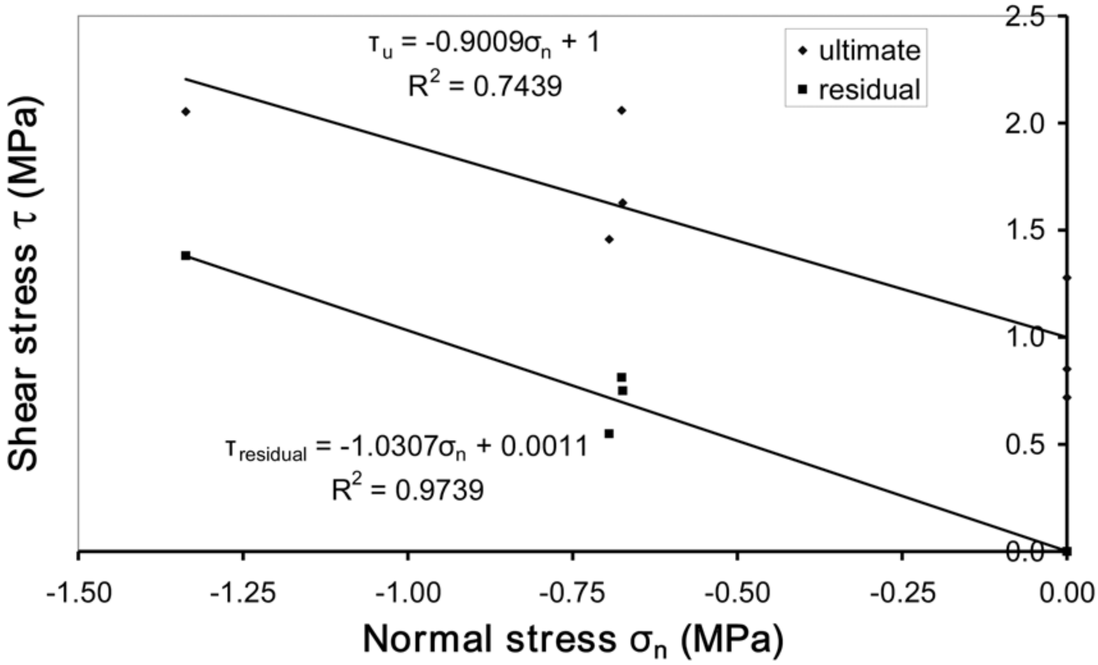

Figure 5.11: Shear stress versus normal stress (Series 2), Masia et al. (2007)

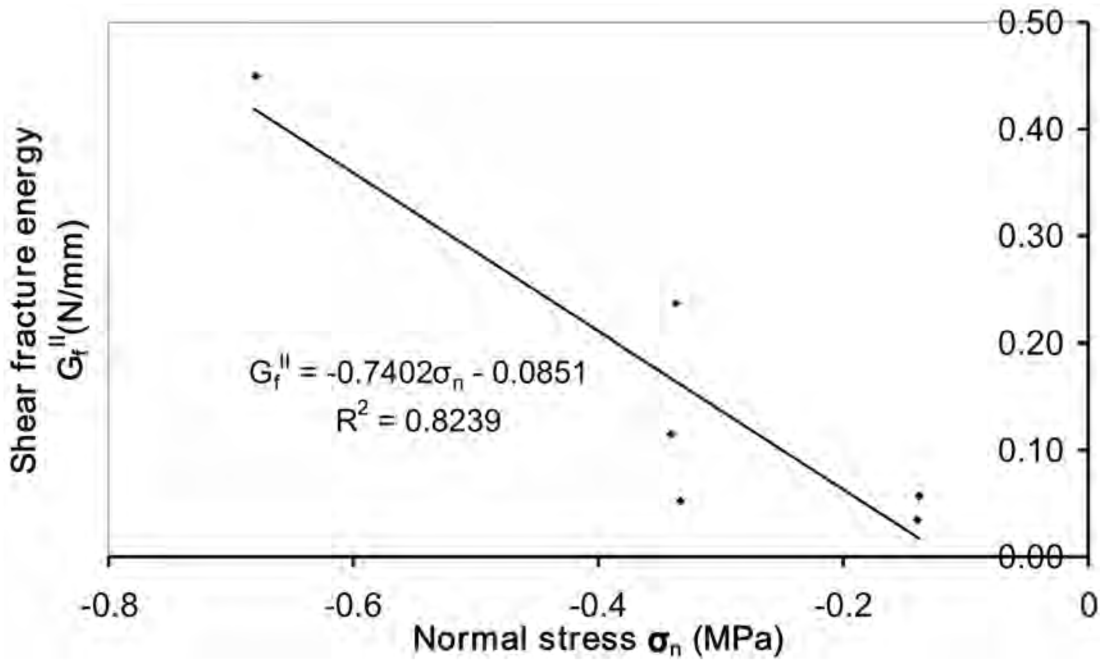

Figure 5.12: Shear fracture energy versus normal stress (Series 1), Masia et al. (2007)

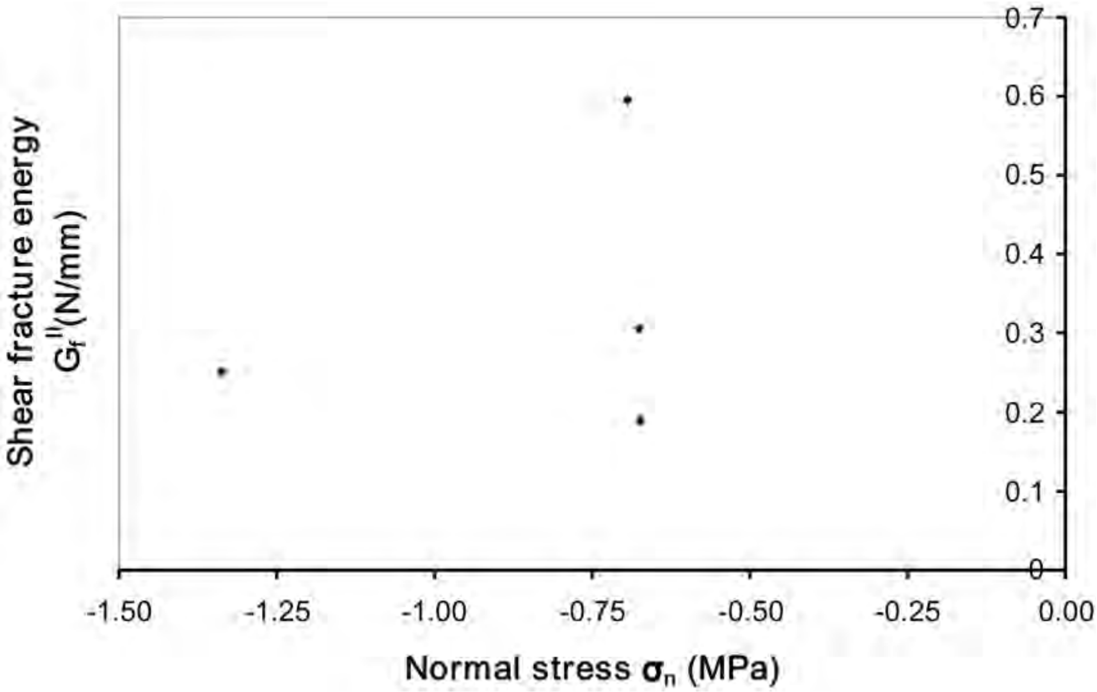

Figure 5.13: Shear fracture energy versus normal stress (Series 2), Masia et al. (2007)

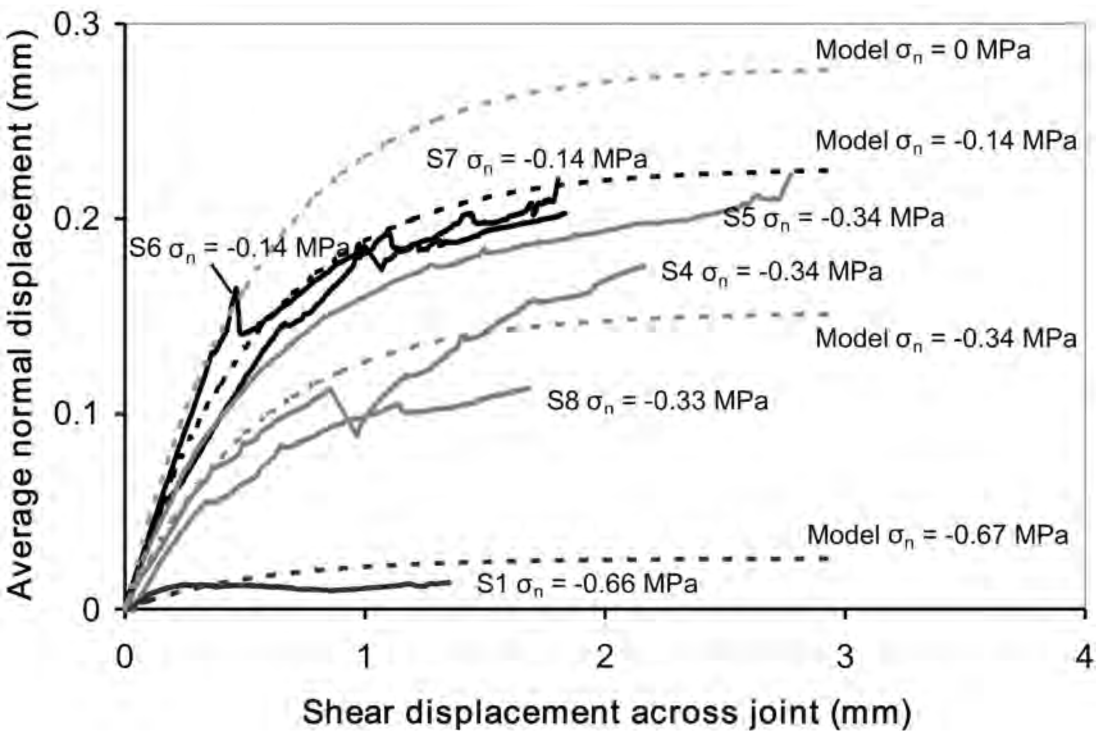

Figure 5.14: Series 1 dilation versus shear displacement including model (Ψ_0=0.5, σ_u=-0.75 MPa, δ=1.8)

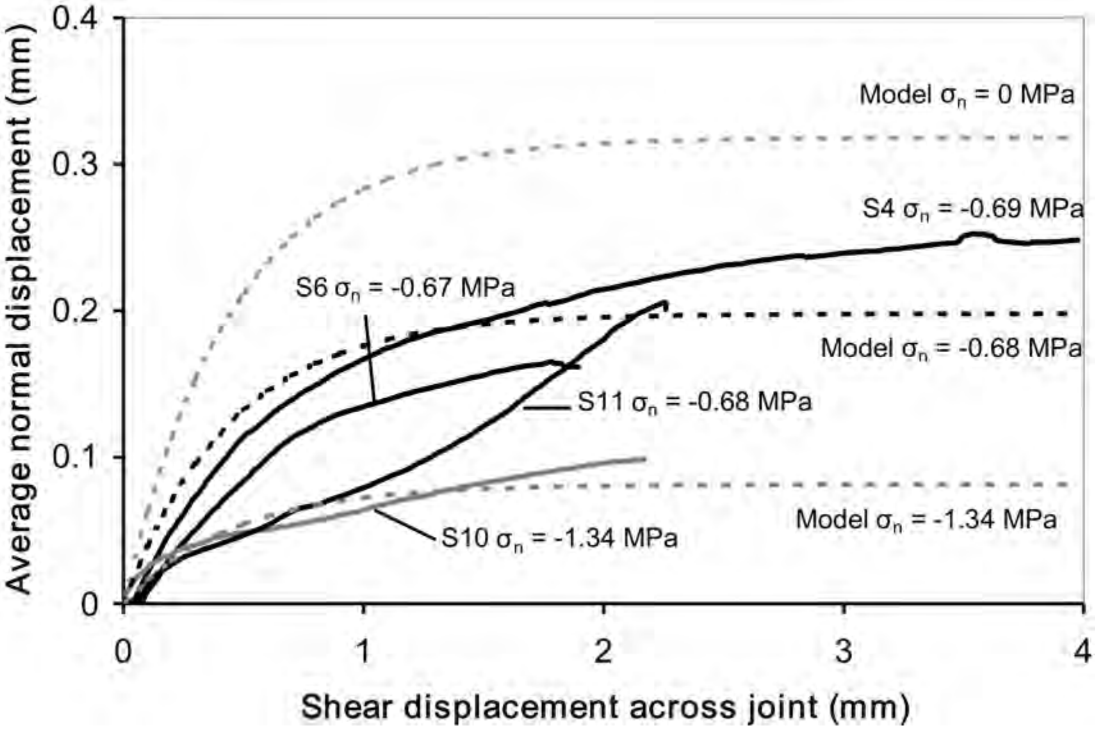

Figure 5.15: Series 2 dilation versus shear displacement including model (Ψ_0=0.7, σ_u=-1.8 MPa, δ=2.2)

Zijl (2004)).

The dilation model (described in Section 5.2) was fitted to the experimental dilation results to estimate the properties for the FE analysis. The properties were the initial dilatancy coefficient (Ψ_0), stress at which the dilatancy is zero (σ_u), and a degradation coefficient (δ). The models are shown in Figure 5.14 and Figure 5.15 (with the experimental results) using broken lines. The parameters used to define the models for both series are summarised in Table 5.6. The model response with no precompression is also shown (even though it could not be recorded during the tests) and indicates the maximum normal uplift of the joint in the FE model due to shear induced dilation.

Table 5.6: FE model dilation input properties

Property	Series 1 (bond strength = 0.14 MPa)	Series 2 (bond strength = 1.74 MPa)
Ψ_0	0.5	0.7
σ_u(MPa)	-0.75	-1.8
δ	1.8	2.2

5.3.4 Lateral modulus of rupture test

The flexural tensile strength of the brick units was determined using 4 point bending tests on brick unit specimens (shown in Figure 5.16) in accordance with AS/NZS 4456.15: 2003 (Standards Australia (2003)). Ten specimens were constructed by gluing three bricks together end to end with epoxy. Before the bricks were glued together the rough, friable ends of the bricks were removed by cutting approximately 5 mm from the ends of the bricks with a circular saw. This was done to prevent failure at (or near) the joint, which occurred in preliminary tests. A schematic of the test, showing the span length and distance between loading points, is shown in Figure 5.17.

Figure 5.16: Lateral modulus of rupture test

The flexural tensile strength (f_{ut}) was determined from the tests where failure occurred in the central brick unit (constant moment and zero shear). Failure occurred in the central unit of only four tests. The failure loads are shown in Table 5.7. The flexural tensile strength was calculated as the moment divided by the section modulus. The average f_{ut} was 3.57 MPa with coefficient of variation of 0.21.

The direct tensile strength of the unit was not determined using a test. The direct tensile strength is equal to the flexural tensile strength divided by 1.5. This reduction is implied for concrete (similar material to brick unit) in AS3600-2001

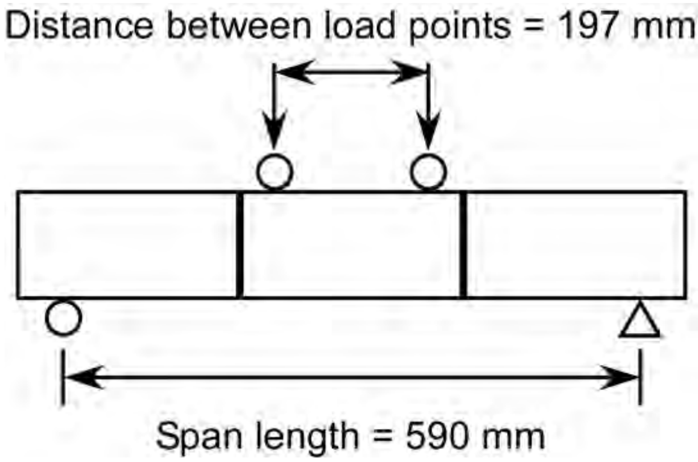

Figure 5.17: Schematic of lateral modulus of rupture test showing span length and distance between loading points

Table 5.7: Lateral modulus of rupture test results

Specimen	Failure load (kN)	f_{ut} (MPa)
1	6.60	4.23
2	6.55	4.19
3	4.51	2.89
4	4.60	2.94
Average	5.57	3.57

(Standards Australia, 2001a) where:

- the characteristic flexural tensile strength of concrete is equal to $0.6\sqrt{f_c'}$, where f_c' is the characteristic compressive strength of concrete; and
- the characteristic principal tensile strength of concrete is equal to $0.4\sqrt{f_c'}$

The direct tensile strength of the brick unit, used in the brick crack interface elements was 3.57 MPa/1.5 = 2.38 MPa.

5.4 FE model: URM panel specimens

The flexural tensile bond strength of the masonry used in the URM wall panels tested in diagonal tension varied greatly (average bond strength varied from 0.31 MPa to 1.26 MPa) and resulted in a large variation in the strength of the panels. To capture this range, model simulations were performed using a 'weak' and a 'strong' material data set. The 'weak' data set was determined from characterisation tests on joints with weak bond strengths. The 'strong' data set was determined from characterisation tests on joints with strong bond strengths. These properties are shown in Table 5.8. The average flexural bond strength values of the masonry used to construct the test specimens from which the properties were derived are shown in brackets.

The tensile strength of the mortar joint interface element ($f_{t(m)}$) was estimated as equal to the flexural tensile bond strength of the joint/1.5 (Section 5.3.1). For the property sets used here, the bond strength values of the torsion test specimens from Masia et al. (2007) were used (weak = 0.14 MPa, and strong = 1.74 MPa). As the tensile fracture energy of the mortar joint ($G^I_{f(m)}$) was not determined by experiment it was assumed as 0.005 N/mm for the weak mortar and 0.012 N/mm for the strong mortar based on results of tests from the literature (Van Zijl, 2004).

Table 5.8: Material properties adopted for mortar joint interface elements

Property	Units	Weak mortar	Strong mortar
$k_{n(m)}$	N/mm^3	308 (0.176)	623 (1.22)
$k_{s(m)}$	N/mm^3	128 (0.176)	260 (1.22)
$f_{t(m)}$	MPa	0.09 (0.14)	1.16 (1.74)
$G^I_{f(m)}$	N/mm	0.005	0.012
c_0	MPa	0.22 (0.14)	1.0 (1.74)
Φ_i	-	0.9 (0.14)	0.9 (1.74)
Φ_r	-	0.56 (0.14)	0.9 (1.74)
Ψ_0	-	0.5 (0.14)	0.7 (1.74)
σ_u	MPa	-0.75 (0.14)	-1.8 (1.74)
δ	-	1.8 (0.14)	2.2 (1.74)
f_c	MPa	20 (0.176)	32 (1.22)
C_s	-	9	9
G_c	N/mm	22 (0.176)	25 (1.22)
κ_p	mm	0.010 (0.176)	0.024 (1.22)
G^{II}_f (1)	N/mm	0.16 (0.14)	0.34 (1.74)
G^{II}_f (2)	N/mm	0.02-0.17σ_n	0.02-0.17σ_n
G^{II}_f (3)	N/mm	0.05-0.80σ_n	0.05-0.80σ_n

As no sensible result between the normal compressive stress (negative σ_n) and the shear fracture energy (G^{II}_f) was established for the joints tested by Masia et al. (2007), three different inputs for the shear fracture energy were adopted. The sensitivity of the model to the inputs was assessed. A constant shear fracture energy and two linear relationships that approximately bounded the results from Masia's torsion tests (Figure 5.18) were used. The constant shear fracture energy was taken as: the average shear fracture energy of series 1 specimens for the weak property set; and the average shear fracture energy of series 2 specimens for the strong property set.

The brick unit had an elastic modulus equal to 27600 MPa and Poissons ratio of 0.2 (see Section 5.3.2). The tensile strength of the potential brick crack element was taken as 2.38 MPa (Section 5.3.4) and a tensile fracture energy of 0.025 N/mm was assumed based on recommendations from Lourenço (1996a). The interface stiffness values of the potential brick crack elements were set at a high value (k_n=k_s=10^6) to maintain continuity of brick displacement across the interface.

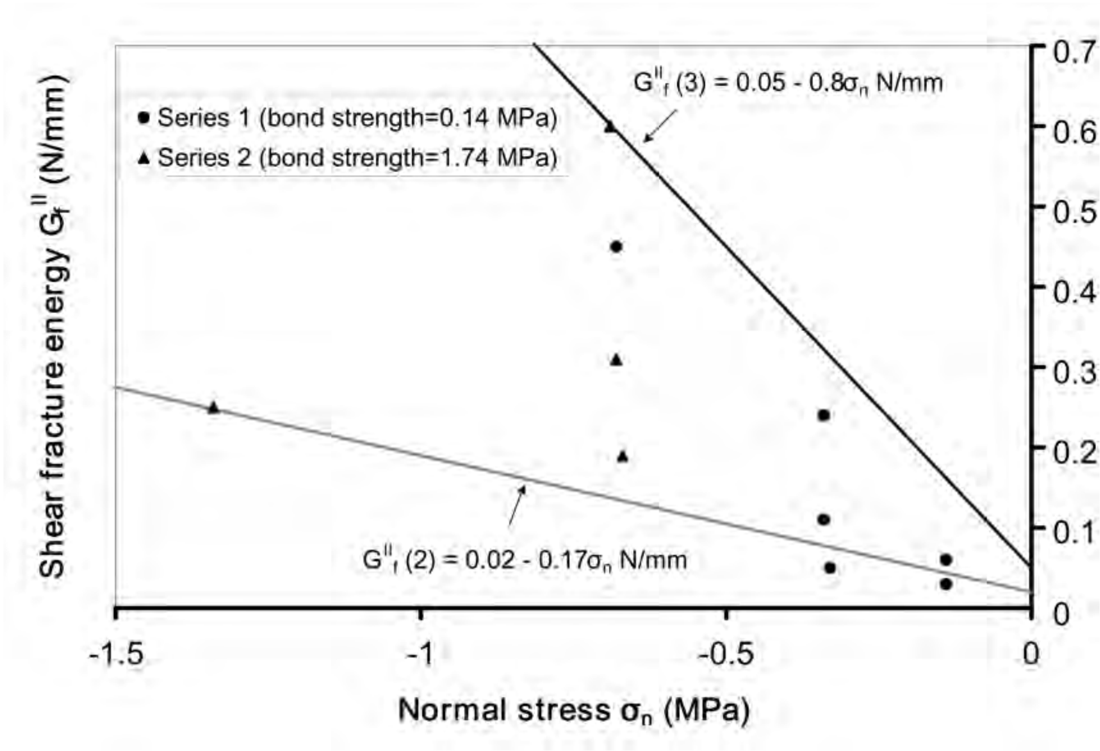

Figure 5.18: Upper and lower bound G_f^{II} relationships fitted to torsion test data from Masia et al. (2007)

The finite element model is shown in Figure 5.19. As described previously in Section 5.2, rectangular quadratic plane stress elements were used for the majority of the brick units. At the support and loaded ends, however, some triangular elements were used to accommodate the boundary conditions (to keep the boundary condition symmetrical).

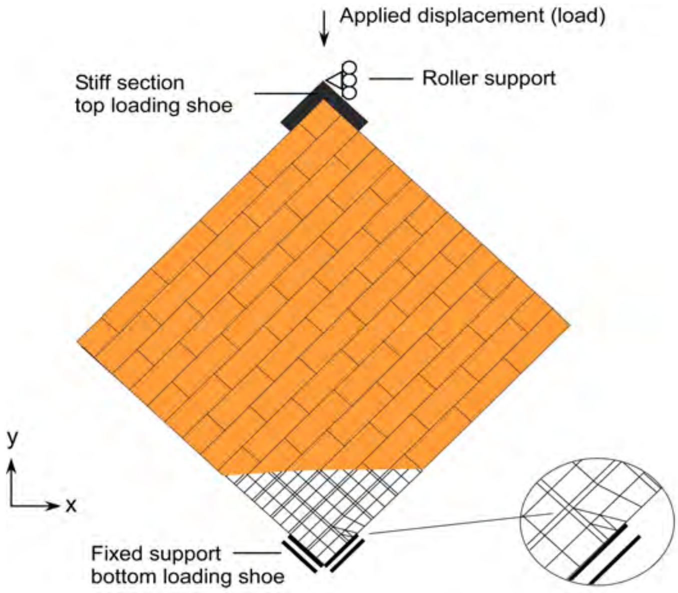

Figure 5.19: FE model of URM Diagonal Tension/Shear Test (mesh shown in cutaway)

Nodes at the base of the model were fixed in both the x and y directions to simulate a fixed boundary condition at the bottom loading shoe. At the top corner of the model the loading shoe was modelled with a very stiff section. At the top of this section a roller support was used to restrain movement in the x direction. The top and bottom corners of the model were aligned vertically as in the experiments.

The panel self-weight was not included in the model. The total panel self weight was calculated as less than 3 kN. The extra load due to self weight was considered insignificant compared to the applied load.

In most models vertical displacement was applied incrementally (displacement control) on the top corner of the model (as shown) to simulate loading on the panel. To solve the nonlinear problem an incremental-iterative solution procedure was used. The displacement was increased by 0.01 mm for each increment and a linear iteration scheme was used to solve for equilibrium at each increment. In the model with strong mortar and G_f^{II} = 0.34 N/mm an applied load was used with arc-length control . This method was used because of convergence issues using displacement control alone. The load was applied in steps of 10 kN and arc-length control was applied to all nodes in the x direction.

The load-vertical displacement behaviour of the three models with strong mortar properties are plotted in Figure 5.20 with the load displacement relationships of the URM experiments. The behaviours of the URM FE models (with strong mortar) were similar to the experimental panels constructed with strong mortar (URM-1 and URM-2) up to the peak load.

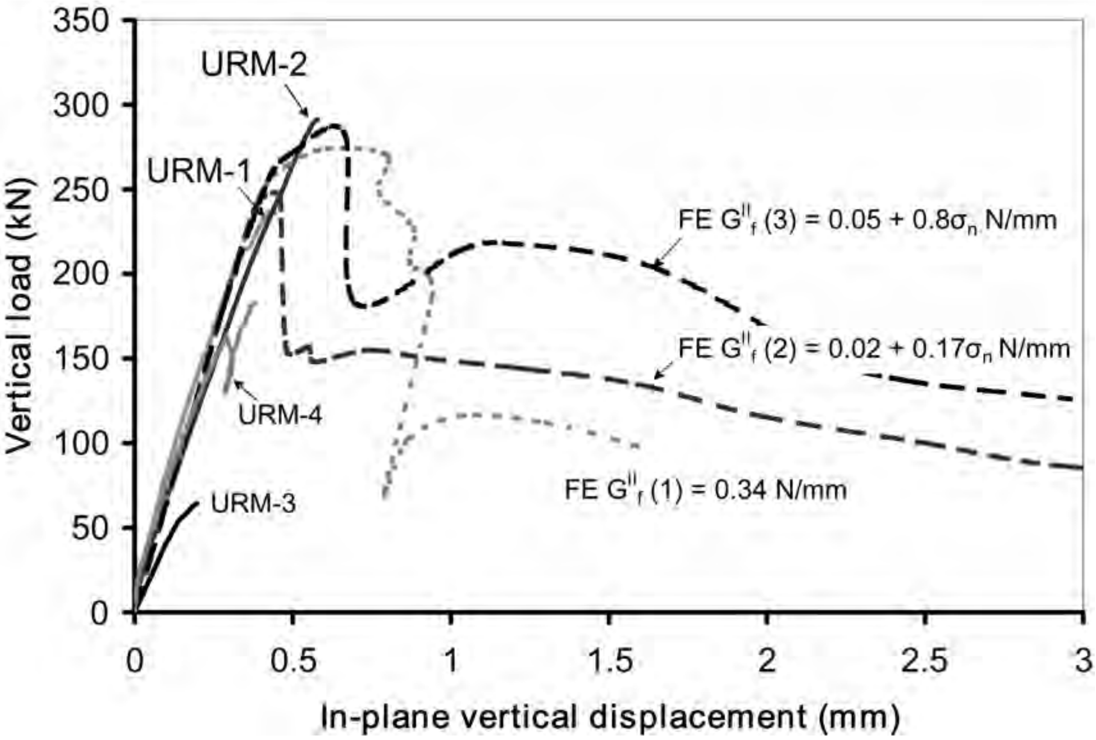

Figure 5.20: Load displacement behaviour of strong mortar FE model plotted against experimental URM results

All of these models failed by sliding along a diagonal crack that formed through mortar head and bed joints (shown in Figure 5.21). In the two strongest models (with G_f^{II} (1) and G_f^{II} (3)) some other smaller cracks (through the mortar bed and head joints) formed as well (shown in Figure 5.21). This failure mechanism was similar to the failure mechanism of URM-1 and URM-2.

The ultimate loads of the models were 274 kN (G_f^{II} (1)), 248 kN (G_f^{II} (2)), and 282 kN (G_f^{II} (3)), and were all within the range of the experimental panels with strong mortar URM-1 (237 kN) and URM-2 (290 kN). After the ultimate load was reached and the diagonal crack formed in the model the load capacity dropped suddenly. The load did not, however, drop to zero (as in the experiments), instead the model displayed some residual capacity as the panel slid along the crack. Some of the possible reasons why the FE model had some residual capacity and the experiments did not include:

1. The model is strict displacement control, but the experiment is not. The experiment might speed up as the load drops off and therefore not allow friction to slowly occur.

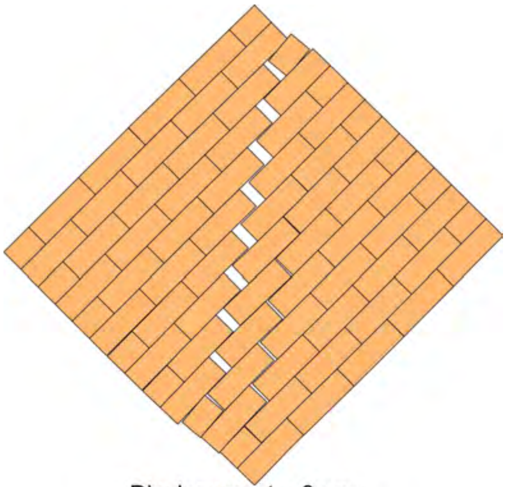

Figure 5.21: Typical failure mode of URM model with strong mortar (G_f^{II} (3))

2. The top loading shoe in the experiment might move slightly in the negative x direction, which would tilt the panel and allow collapse to occur more easily. In the model the strict roller support may allow some locking together.

3. It is possible that the experiment does have residual capacity as it collapses but the data recording frequency is not high enough to log it.

Shear fracture energy had an effect on the ultimate load and the residual capacity of the panels. The variation in the ultimate loads of the models with different shear fracture energies was within the range of the experimental panels constructed with strong mortar (as previously mentioned). The two models where G_f^{II} increased linearly with compressive normal stress had larger residual capacities than the model with the constant G_f^{II}, due to larger frictional fracture energies. Some minor cracking within the panels was also different but the major crack (as shown in Figure 5.21) was the same in all models.

The load displacement relationships of the three models with weak mortar properties are shown in Figure 5.22 with the URM experiments. The ultimate loads of the models were 85 kN (G_f^{II} (1)), 79 kN (G_f^{II} (2)), and 98 kN (G_f^{II} (3)), and were all higher than the ultimate load of the weakest panel URM-3, which was 65 kN. All models did, however, represent an approximate lower bound on the range of all of the URM results as shown in Figure 5.22.

All of the models with weak mortar properties failed by sliding along a diagonal crack that developed through the mortar joints (shown in Figure 5.23). This failure mode was similar to the failure mode of URM-3, but different to the failure mode of URM-4. Panel URM-4 failed by sliding along only three bed joints (with sliding occurring primarily along one bed joint). It is possible that in the model the strict roller support at the top loading shoe made it more difficult for the model to fail by sliding along a single bed joint. In the experiment the top loading shoe may have been able to move slightly and allow such a failure.

The load displacement behaviours of the models were similar to URM-3, until the failure of URM-3. The weak mortar models had some residual capacity after the crack formed, which was affected by the shear fracture energy (similar to the strong mortar models).

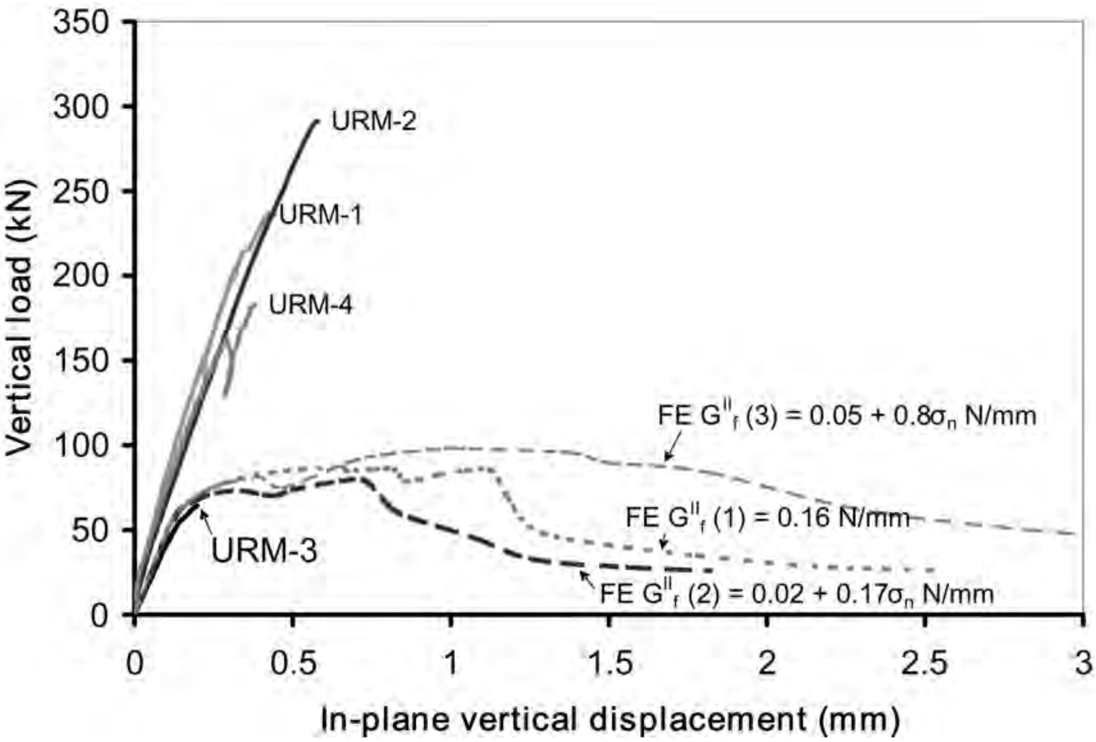

Figure 5.22: Load displacement behaviour of weak mortar FE model

5.5 FRP Reinforcement model

5.5.1 Attaching FRP to masonry in finite element model

The FRP strips were modelled using 2-noded linear truss elements. These elements were assigned a cross sectional area of 42 mm^2 (FRP was 15 mm wide and 2.8 mm thick), and an elastic modulus of 210000 MPa. The Poisson's ratio was assumed to be 0.3 (Hussain et al., 2008).

To represent the NSM joint (shown in Figure 5.24a) in the FE model the FRP was attached to the brick unit using zero-thickness, 6-noded quadratic, interface elements (Figure 5.24b). The relationship between shear traction (or bond, τ) and shear relative displacement (or slip, δ) of the interface element, in the longitudinal/tensile direction of the reinforcement, was defined using the local bond-slip relationship determined from the experimental pull tests (Chapter 3). An example bond slip relationship used to attach the vertical reinforcement is shown in Figure 5.24c. This relationship was determined from pull test specimen S1-C-SG. By

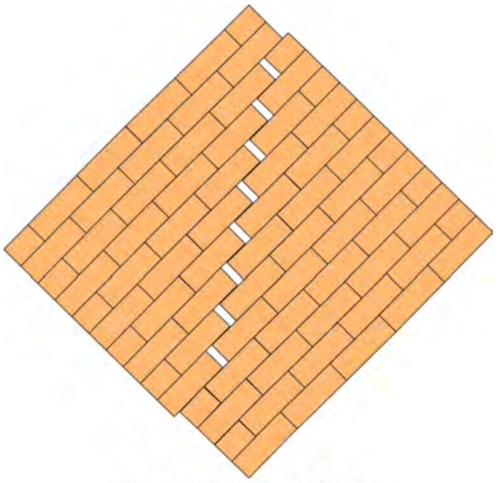

Figure 5.23: Typical failure mode of URM model with weak mortar (G_f^{II} (1))

modelling the FRP-to-masonry interface in this way, debonding of the FRP from the masonry (caused by longitudinal tension in the FRP) was accounted for.

The bonded area of the FRP strip in the model is equal to the length of the interface element times its plane stress thickness. In reality the bonded area of the NSM FRP strip is equal to the length of the strip times the bonded perimeter (=15x2+2.8 = 32.8 mm). The plane stress thickness of the interface element therefore corresponds to the bonded perimeter and was set equal to 32.8 mm. The plane stress thickness direction of this element is indicated in Figure 5.24b.

To connect the FRP truss elements across the mortar joint and potential brick crack interface elements, a zero-thickness node interface element was used (Figure 5.24d). In the longitudinal direction a high stiffness was given to the node interface element to make the FRP continuous across the joint. In the transverse direction (i.e. the direction of mortar joint or brick crack sliding) a dowel relationship was used, which will be discussed in Section 5.5.3.

5.5.2 Calibration of bond-slip model

A simple pull test was modelled (using finite elements, shown in Figure 5.25) to verify the bond-slip input data and modelling strategy. The masonry prism was modelled with plane stress brick elements only (no mortar joints were included) and had a height of 330 mm, a width of 230 mm and a thickness of 110 mm. The masonry prism was restrained fully along the top surface in the model. The FRP was attached to the model as described in the previous section. The bonded length of the FRP (equal to the height of the model) was approximately equal to the bonded length of the pull test specimens from test series 1 (equal to 336 mm). The FRP was pulled from the masonry in the model by applying a displacement to the top node of the FRP as shown. The mesh was divided into 16 elements across the height and 4 elements across the width of the masonry prism, as shown (Note

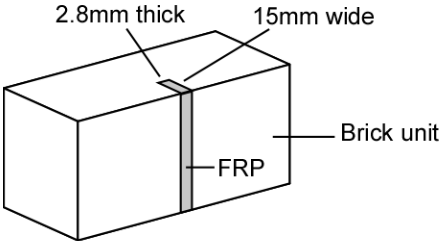

(a) NSM FRP reinforcement

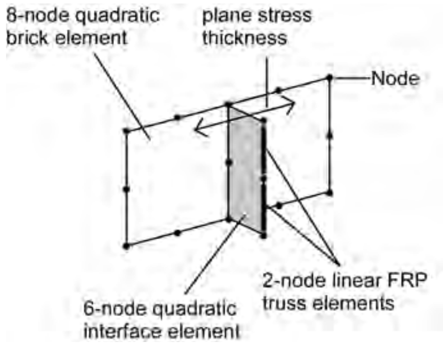

(b) FE model representation

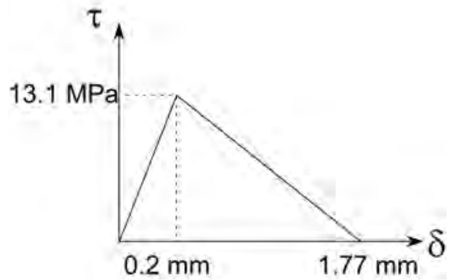

(c) Bond-slip model (pull test S1-C-SG)

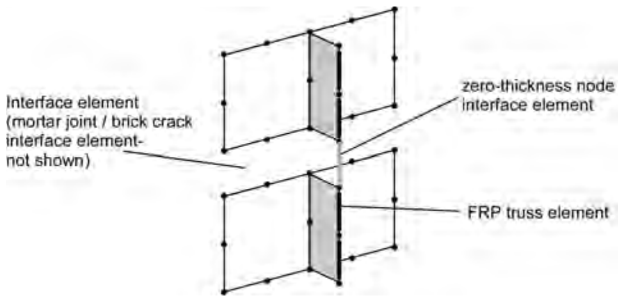

(d) Connection across interface

Figure 5.24: FRP attachment in FE model

that this mesh had twice the refinement, along the height, of the regular masonry model used for the URM model). The model results were verified with the experimental results of pull test specimen C.

In Chapter 3, δ_1 (slip corresponding to maximum shear stress in the bilinear bond slip model) was defined as 0.4 mm for specimen S1-C-SG. Here, however, a closer match between the experiment and FE model was produced when a value of δ_1 = 0.2 mm was adopted. By adopting this value for δ_1 the initial portion of the bilinear curve matches the linear elastic region of the experimental bond slip curves (Figure 5.26). This change was made to get a better fit to the pre-peak behaviour of the bond-slip response, because debonding was not observed in many cases.

The load-slip response at the loaded end of the finite element model and the experimental results of specimen S1-C-SG are shown in Figure 5.27. The FE model reached an ultimate load of 81 kN, which was approximately 96% of the experiment (84.5 kN). The difference between the simulated and experimental ultimate loads was likely due to rounding of the area and elastic modulus of the FRP. The FE model matched the initial load-slip response of the experiment but displayed a larger slip at the loaded end before debonding occurred. The experimental load-slip response (at the loaded end) was determined from integration of the strain distribution (see Section 3.3.4, Chapter 3). For the integration is was assumed that the slip at the unloaded end was zero. Near the ultimate load this assumption may

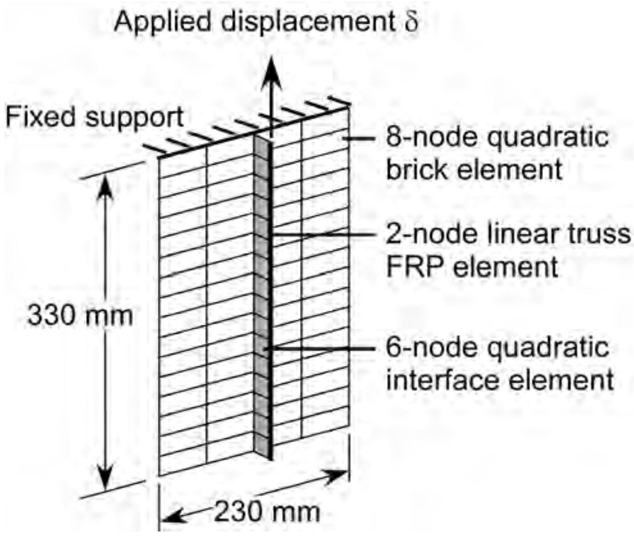

Figure 5.25: FE model of pulltest (interface element shown with thickness)

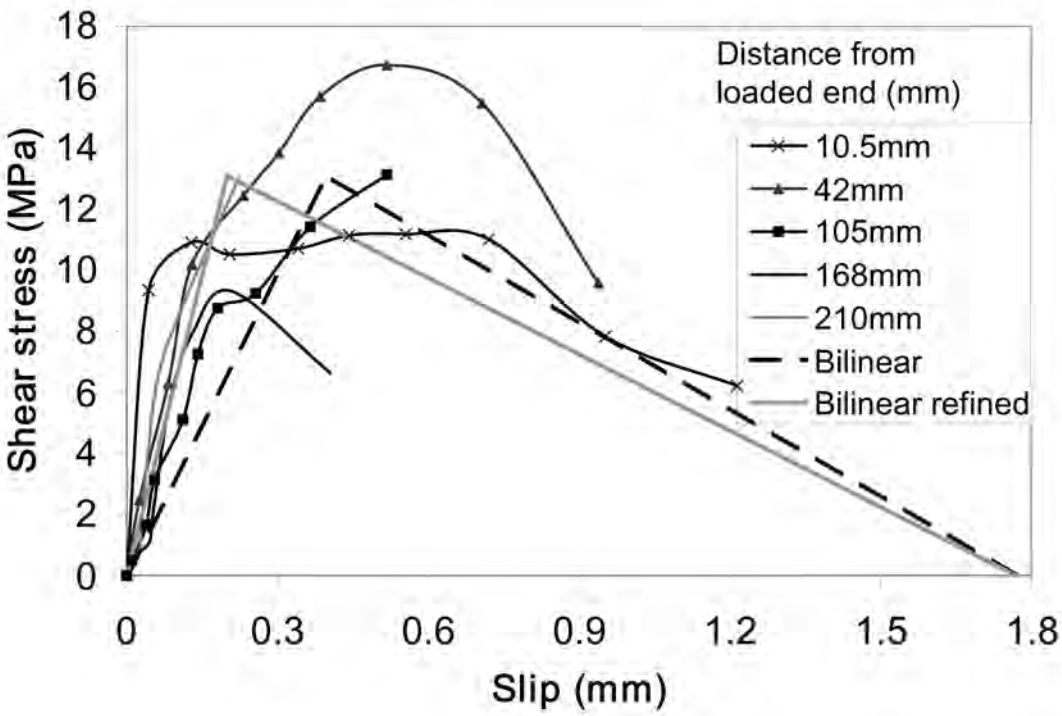

Figure 5.26: Bond-slip curve S1-C-SG with refined bilinear bond slip curve

be inaccurate (the slip at the loaded end may be higher than zero). The actual slip at the loaded end would then be higher (and closer to the FE result). In the model, when the loaded end slip was 2.24 mm, the slip at the unloaded end was 0.28 mm. The difference in slip along the interface was then 1.96 mm, and was closer to the slip estimated from the experiments (1.58 mm) assuming the slip at the unloaded end was zero.

Note that any extra displacement capacity of the debonding joint could lead to issues in the panel model. Extra displacement capacity of the debonding joint would mean larger cracks before debonding and greater stress redistribution. This would lead to an overestimation of the displacement capacity.

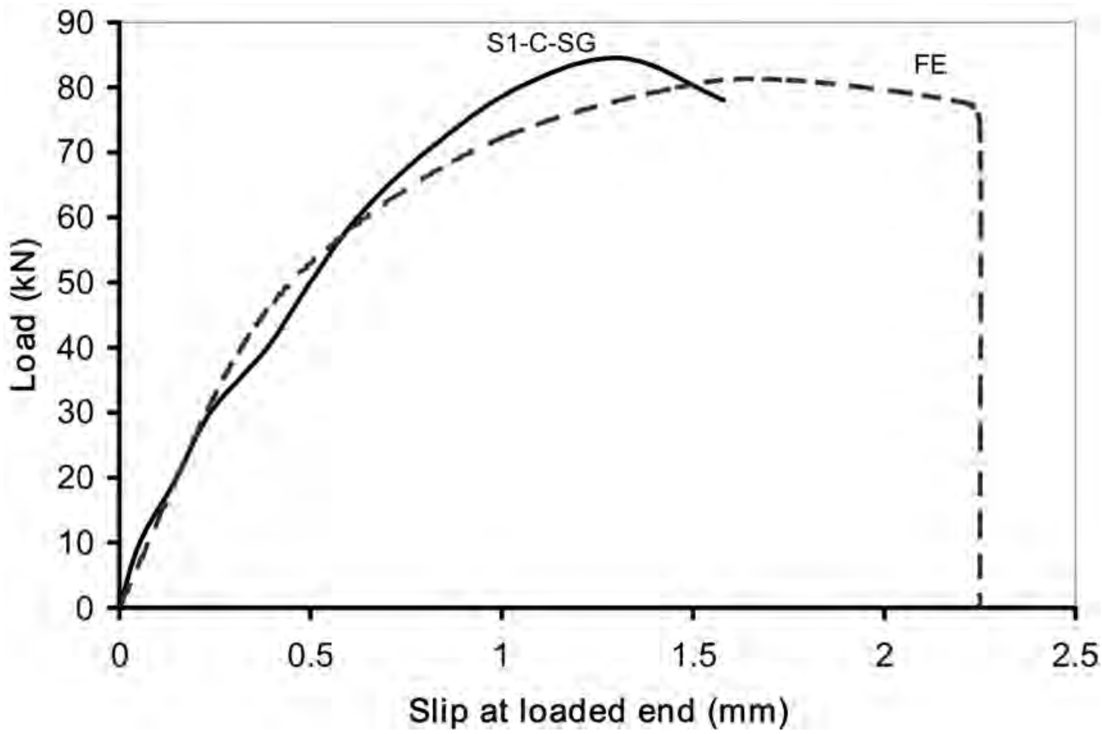

Figure 5.27: Load-slip response at the loaded end of FE model and S1-C-SG

Distributions of strain in the FRP at increasing levels of loaded end slip (LES) (up to the experimental maximum of 1.58 mm) are shown in Figure 5.28 for the FE model and specimen S1-C-SG. The distributions of shear stress between the FRP and masonry are shown at increasing levels of LES in Figure 5.29. The figure was split to improve clarity. Both Figure 5.28 and Figure 5.29 show that the stress transfer from the FRP to the masonry (through the epoxy), and the progression of damage of the bond, with increasing LES, was similar between model and experiment. Based on these results it was decided that the bilinear bond-slip relationship, for a given FRP orientation, was a suitable approximation to use with the modelling strategy to model the NSM FRP to masonry bond.

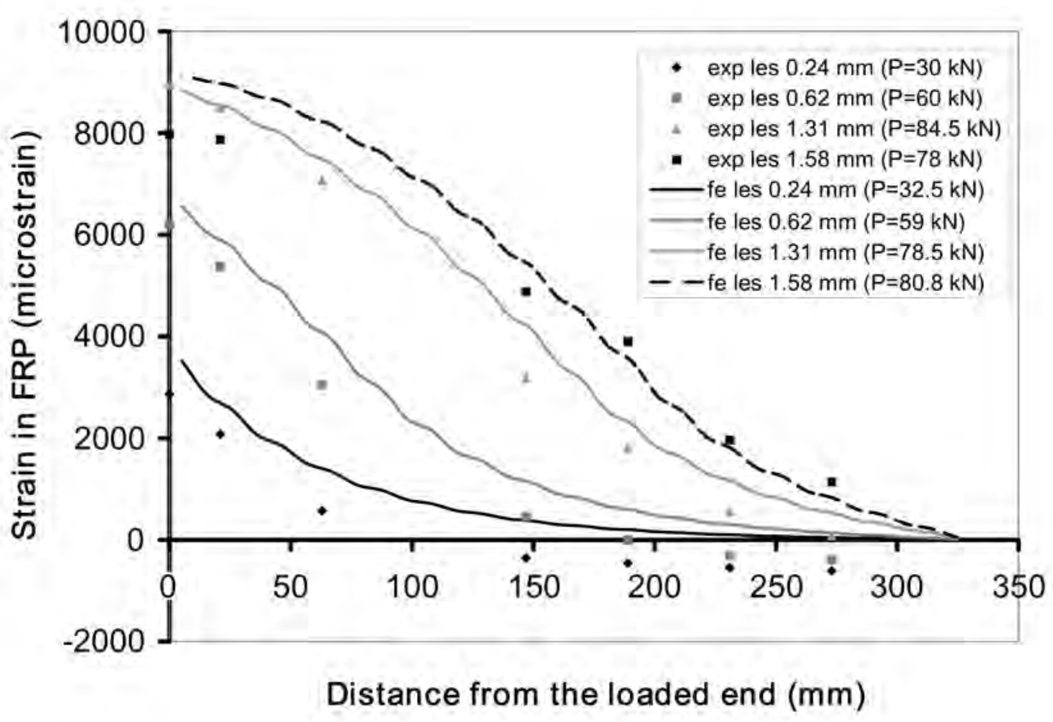

Figure 5.28: Strain distributions of FE model and S1-C-SG at increasing LES

5.5.3 Dowel action

For FRP reinforcement crossing a sliding crack two mechanisms of sliding restraint were identified:

1. reinforcement restrains dilation and results in increased resistance to frictional sliding

2. reinforcement acts as a dowel to increase sliding resistance

The first mechanism is automatic in the model because dilation is included and the FRP is modelled continuous across the mortar joints. However, the dowel strength needed to be estimated and defined in the model. In this section the dowel strength of the FRP is estimated.

Two models were used to estimate the dowel strength contributed by the FRP reinforcement across a single sliding crack. The models were based on the behaviours observed during the diagonal tension/shear tests and represented a lower and an upper bound estimate of the dowel strength.

The first model represented the dowel behaviour observed in the diagonal tension/shear tests where large cracks developed adjacent, and parallel, to the NSM FRP and allowed the FRP (that crossed the sliding cracks) to bend over a large length of the FRP. The shear cracking adjacent to the FRP generally allowed bending of the FRP to occur over the length of one brick height (shown in Figure 5.30a).

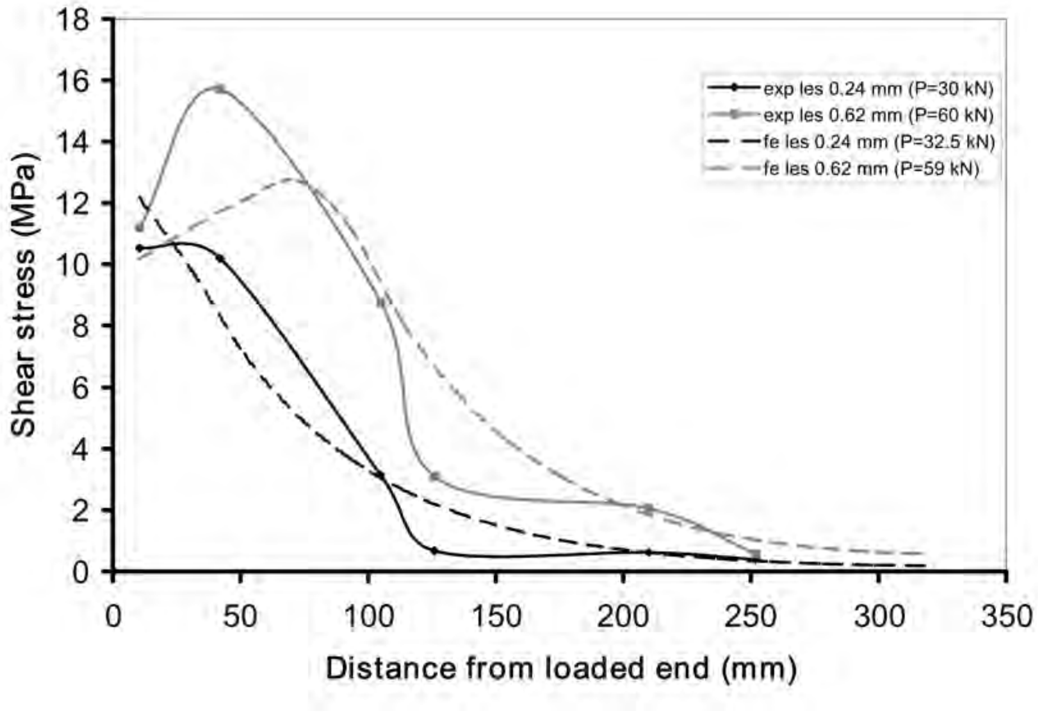

(a) LES = 0.24 and 0.62

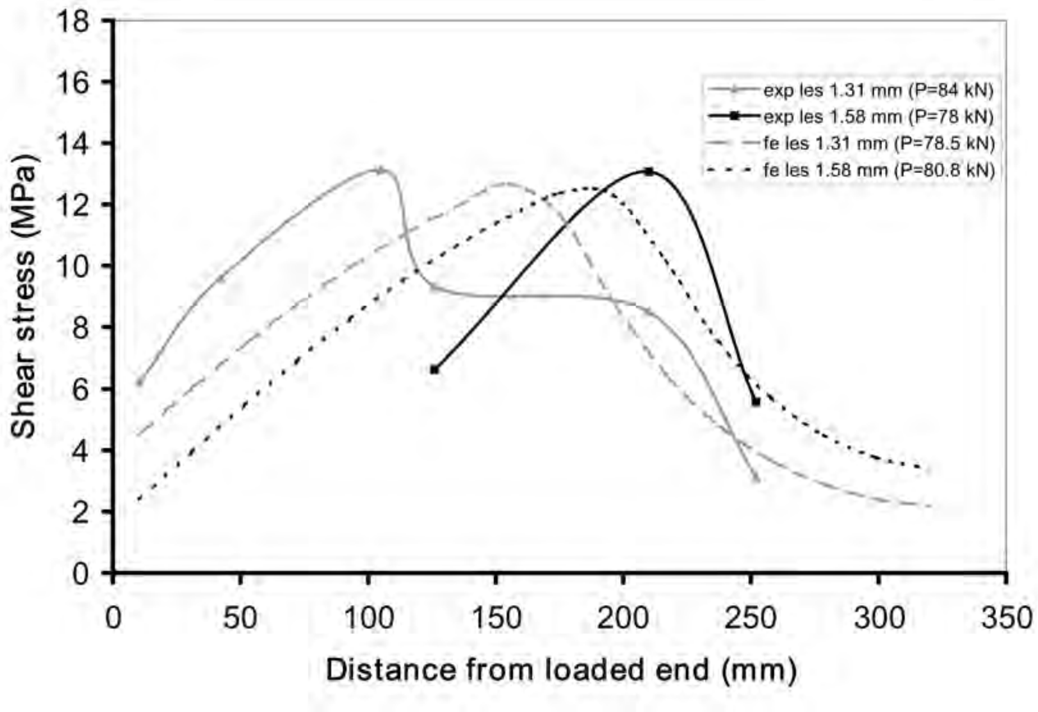

(b) LES = 1.31 and 1.58

Figure 5.29: Stress distributions of FE model and S1-C-SG at increasing LES

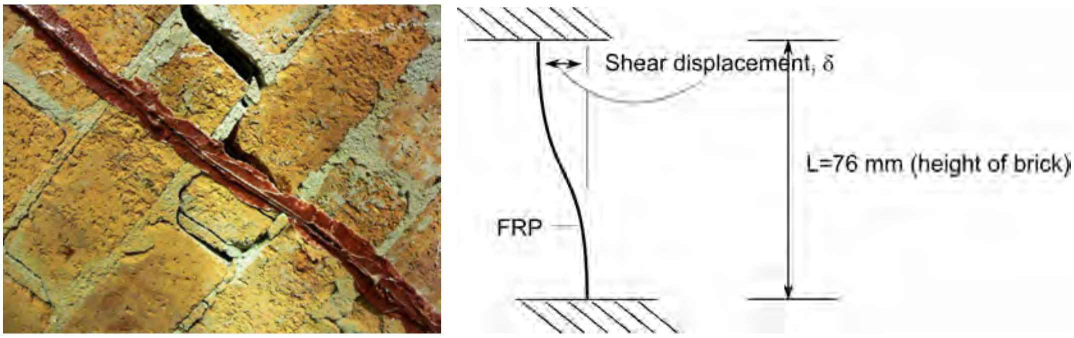

(a) Strip 1 Panel V2 (b) Dowel lower bound idealisation

Figure 5.30: FRP bending in panels

The shear force transferred across the bent FRP (as a function of the shear displacement δ) was calculated using Equation 5.18. This equation is based on the idealised model shown in Figure 5.30b. This equation comes from the stiffness method used for beam analysis (Hibbeler (1997)).

$$V = \frac{12EI\delta}{L^3} \tag{5.18}$$

where E is the elastic modulus of the FRP (= 210 000 MPa), I is the moment of inertia of the FRP cross section, bending about its weak axis (= 27.44 mm^4), L is the length of FRP between fixed supports which was the brick height (= 76 mm).

At 1 mm of shear displacement the shear force transferred by the FRP was equal to 0.16 kN, and at 10 mm the shear force transferred by the FRP was equal to 1.6 kN. This amount of dowel force would not have contributed to the load carrying capacity of the panels and was considered equal to zero. Note that these values represent the dowel strength after a significant amount of deformation and cracking had occurred. To model zero dowel strength in the FRP reinforced masonry FE model, a very low transverse stiffness was assigned to the node interface element that connected the FRP elements across a mortar joint interface element (refer to Section 5.5.1).

In some panels cracks adjacent to the FRP were not as large as previously described and the FRP was bent over a shorter length (less than the brick height). This suggests that some dowel resistance may have been provided. To estimate the dowel resistance of these cases an FE model (shown in Figure 5.31) was used.

A section of masonry was modelled with an FRP strip crossing a shear sliding crack perpendicularly. The crack was positioned in the middle of a 10 mm thick mortar joint and was modelled 1 mm thick. The thickness of the crack gap was selected based on observations from the diagonal tension experiments. Above and below the crack the FRP was attached (in this model with perfect bond) to 50 mm of brick unit with 1 mm of epoxy as shown. The width of the masonry section modelled was equal to 104.8 mm. The sliding crack was made frictionless so that the shear force was transferred across the crack by dowel action only. The thickness of

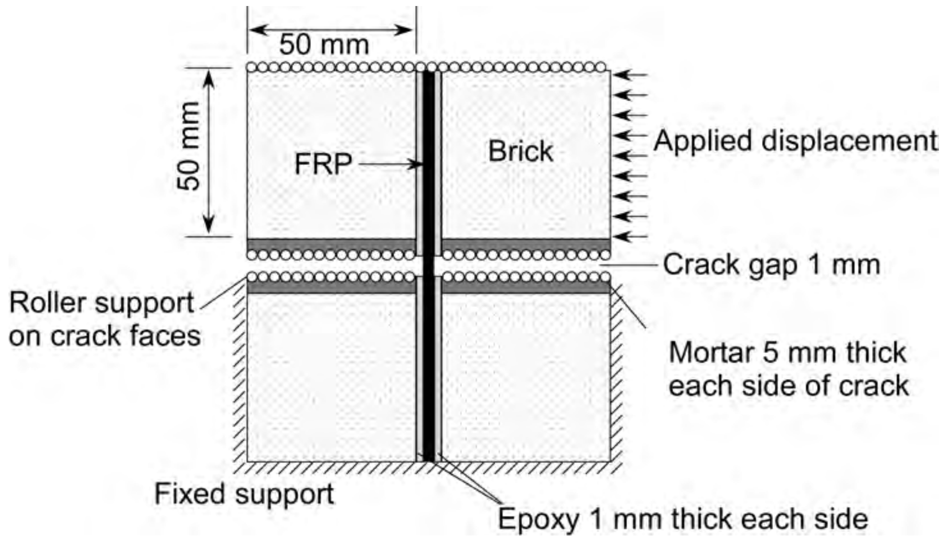

Figure 5.31: Dowel action FE model geometry, boundary conditions and loading

the section was taken as 15 mm (FRP width).

The masonry, mortar and epoxy were all modelled with 8 node quadratic plane stress elements. Each brick section (4 in total) was divided into 20 x 20 elements. Each mortar section (4 in total) was divided into 20 elements across the width and 2 elements across the height. Each epoxy section (4 in total) was divided into 1 element across the width and 22 elements across the height. The FRP was modelled using 2 node linear beam elements with cross section properties depth = 2.8 mm and width = 15 mm (bending occurred about weak axis). The FRP was divided into 44 elements above and below the crack, and 4 elements across the crack.

The masonry section below the crack was fixed along the edges. Roller supports were used along both crack faces to fully restrain vertical movement because, realistically, the surfaces would likely be touching. The top edge of the model was also fully fixed in the vertical direction to model confinement from the rest of the panel above the modelled section. A displacement was applied to the top section to cause shear displacement along the crack as shown.

The elastic properties used for each material are shown in Table 5.9. The elastic properties of the epoxy adhesive were estimated using data from Adams et al. (1997), because they were not experimentally determined, nor were they provided within the manufacturer's material data sheets. Apart from being an epoxy adhesive, there is no other indication that the adhesive from Adams et al. (1997) and the adhesive used in the experiments are similar. This did not matter so much, because only an estimate of the dowel strength was desired. The purpose of modelling dowel action was to investigate whether it would be significant (or not).

Damage was modelled in the brick, mortar and epoxy using the Rankine/Von Mises material model in DIANA 9. The compressive behaviours of the brick, mortar and epoxy were modelled as ideally plastic (no hardening or softening) after the compressive strength was reached. The compressive strength of the brick was conservatively assumed as 35 MPa, based on the manufacturer's data (compressive strength $\geq$ 35 MPa) as it was not experimentally determined. The mortar compressive strength was assumed equal to 5 MPa (Type N mortar, Drysdale et al. (1994)). The epoxy compressive strength was 60 MPa (from the manufacturer's data sheets). The tensile behaviours of the brick and mortar were modelled with exponential softening after the tensile strength was reached. The tensile strengths and fracture energies used for the brick crack and mortar joint interface elements (Section 5.4) were used in this model and are shown in Table 5.9. Cracking was not included in the epoxy as cracks typically develop in the adjacent masonry instead.

Table 5.9: Material properties used for FE dowel analysis

Property	FRP	Brick	Mortar	Epoxy
Elastic modulus (MPa)	210000	26000	5000	2800
Poissons ratio	0.3	0.2	0.2	0.4
Compressive strength (MPa)	-	35	5	60
Tensile strength (MPa)	-	2.38	0.5	-
Tensile fracture energy (N/mm)	-	0.06	0.01	-

A plot of the shear force transferred across the crack versus the shear displacement is shown in Figure 5.32. The stiffness of the joint reduced as crushing and cracking occurred adjacent to the FRP and the sliding crack as shown in Figure 5.33. Figure 5.33a is a plot of the equivalent von mises plastic strain (at 2.8 mm shear displacement), which indicates plastic damage (compression and cracking). Figure 5.33b is a plot of the normal crack strain at the element integration points (at 2.8 mm shear displacement) and illustrates the crack pattern.

At 2.8 mm shear displacement (shear force $\approx$ 7 kN) the tensile stress in the FRP reached the rupture stress of the FRP (2400 MPa). Rupture of the FRP was not, however, observed in the diagonal tension/shear tests. This model therefore represents an upper bound estimate of the dowel behaviour. To model this behaviour the relationship shown in Figure 5.32 (but limited to 7 kN) was used to describe the transverse behaviour of the node interface element.

The maximum shear stress in the FRP was approximately 270 MPa. It was unknown whether this shear stress would cause shear failure across the FRP because the shear strength of the FRP was unknown (not provided by the manufacturer). It was assumed that the FRP does not fail in shear, as shear failure was not observed in the diagonal tension/shear experiments. Whether the FRP failed in shear was not so important, however, because the purpose of modelling dowel action was to investigate whether it would likely be significant.

5.5.4 Limitations of the FRP reinforced masonry FE model

The FRP reinforced masonry model had the following limitations:

- out-of-plane effects caused by non-symmetrical reinforcement placement on both sides of the panel (such as twisting or bending), were not accounted for because a two-dimensional model was used,

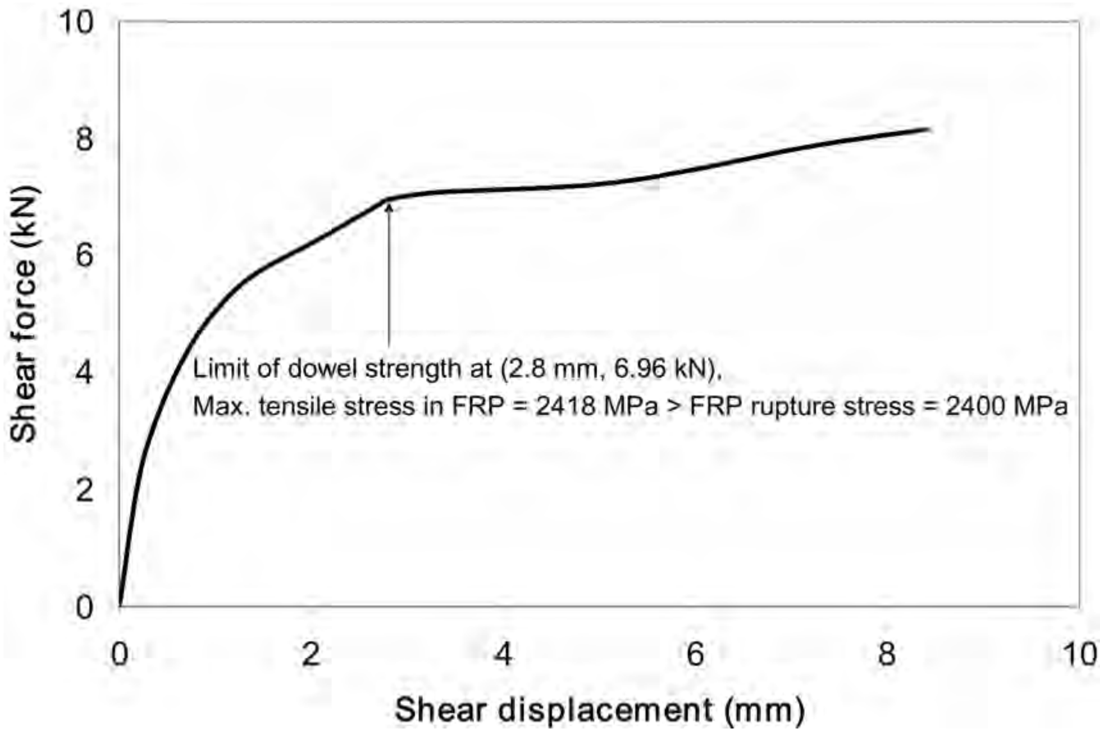

Figure 5.32: FE model shear force transferred across crack versus shear displacement

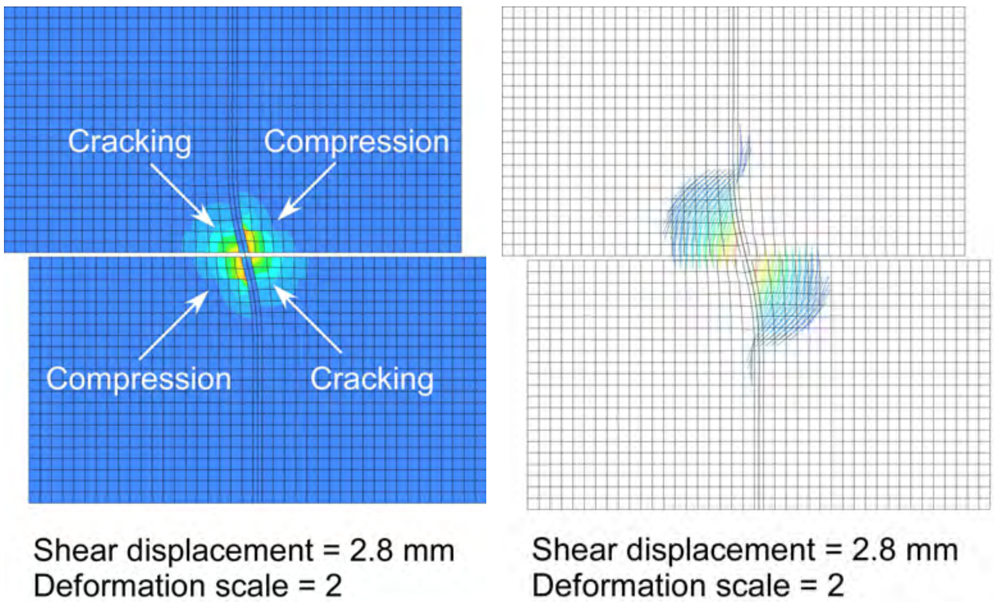

(a) Plastic damage (crushing and cracking)

(b) Crack pattern

Figure 5.33: FE dowel model damage behaviour

- cracking along the inside edge of the FRP as observed experimentally (e.g. V4A), and the resulting reduction of bond strength of the FRP was not included.

5.6 FE model: FRP reinforced panel specimens

A material property set based on a flexural bond strength of 0.5 MPa was used in the V4, V2, and V2H2 models. The material properties were determined by linear interpolation of the 'weak' and 'strong' properties used previously in the URM models. The direct tensile strength was estimated as the flexural bond strength divided by 1.5 = 0.33 MPa (Section 5.3.1). To model panel H4A, the 'strong' mortar joint material data set was adopted. To model panel H4B, a material data set based on a bond strength of 0.8 MPa was used. The direct tensile strength for H4B was estimated as the flexural bond strength divided by 1.5 = 0.53 MPa (Section 5.3.1). For all of the reinforced models a linear relationship was adopted for $G_f^{II}(= 0.035 - 0.49\sigma_n)$. This relationship was in between the lower and upper bound relationships used for the URM models. The material properties adopted for the mortar joint interface elements for the FRP reinforced models (and also the URM models) are shown in Table 5.10.

To model the bond of the vertical FRP reinforcement the bilinear bond slip relationship determined from pull test specimen S1-C-SG was used in the bond interface elements (shown in Figure 5.24c). To model the bond of the horizontal reinforcement in the V2H2 model the bond slip relationships determined for the joint with both zero and 1.0 MPa precompression, determined from pull test specimens S2-P0-SG and S2-P1-SG respectively, were used. This was done instead of modelling precompression dependent bond-slip. The behaviour of both models was the same (i.e. choice of bond slip model made no difference to the behaviour of the panel). This was because no debonding was observed in the horizontal strips (see Section 5.6.4). Therefore, to model the bond of the horizontal reinforcement in the H4 model, only the bond-slip relationship determined for the joint with 1.0 MPa of compression was used. The parameters describing the bilinear bond-slip models used in the FE analysis are tabulated in Table 5.11 (see Figure 3.22, Chapter 3). Note that in all of the bond slip models the value of δ_1 was changed (reduced) so that the initial slope of the of the bond slip model was similar to the linear region of the experimental bond slip curves.

The finite element models of the FRP reinforced panels are shown in Figure 5.34. The FE mesh representing the masonry and the boundary conditions were the same as the URM model described previously. In these models a vertical displacement was applied incrementally (displacement control) on the top corner of the model to simulate loading on the panel.

In all the panel models with vertical reinforcement a model was analysed with zero dowel strength and another model was analysed with the upper bound estimate of the dowel strength (determined in Section 5.5.3). This was done to investigate the significance of dowel action.

Table 5.10: Material properties adopted for mortar joint interface elements

Property	Units	URM(weak)	URM(strong)	V4, V2, V2H2	H4A	H4B
$k_{n(m)}$	N/mm^3	308	623	406	623	496
$k_{s(m)}$	N/mm^3	128	260	169	260	207
$f_{t(m)}$	MPa	0.09	1.16	0.33	1.16	0.53
$G^{I}_{f(m)}$	N/mm	0.005	0.012	0.007	0.012	0.008
c_0	MPa	0.22	1.0	0.40	1.0	0.54
Φ_i	-	0.9	0.9	0.9	0.9	0.9
Φ_r	-	0.56	0.9	0.67	0.9	0.75
Ψ_0	-	0.5	0.7	0.55	0.7	0.58
σ_u	MPa	-0.75	-1.8	-1.0	-1.8	-1.2
δ	-	1.8	2.2	1.9	2.2	2.0
f_c	MPa	20	32	24	32	27
C_s	-	9	9	9	9	9
G_c	N/mm	22	25	23	25	24
κ_p	mm	0.010	0.024	0.014	0.024	0.018
G^{II}_{f} (1)	N/mm	0.16	0.34	0.035-0.49σ_n	0.035-0.49σ_n	0.035-0.49σ_n
G^{II}_{f} (2)	N/mm	0.02-0.17σ_n	0.02-0.17σ_n	-	-	-
G^{II}_{f} (3)	N/mm	0.05-0.80σ_n	0.05-0.80σ_n	-	-	-

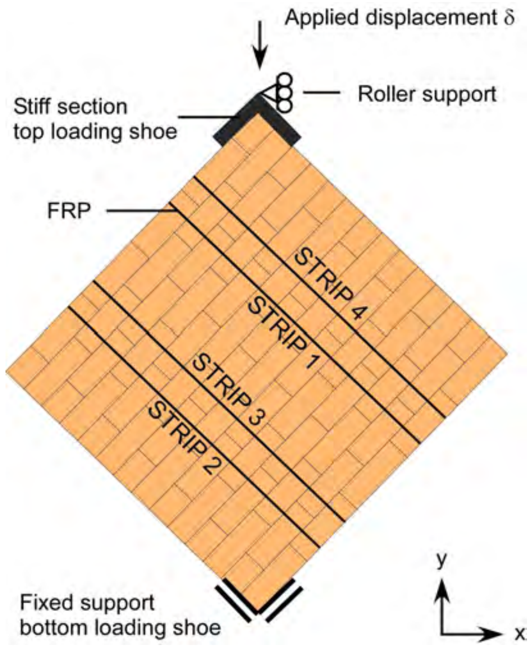

(a) V4A & V4B

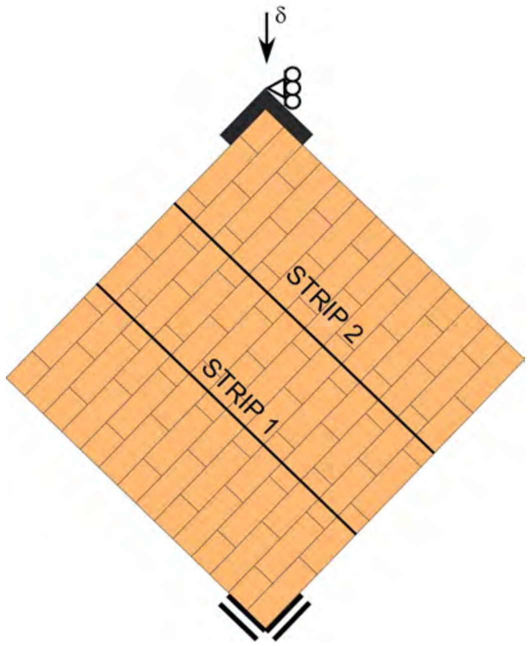

(b) V2

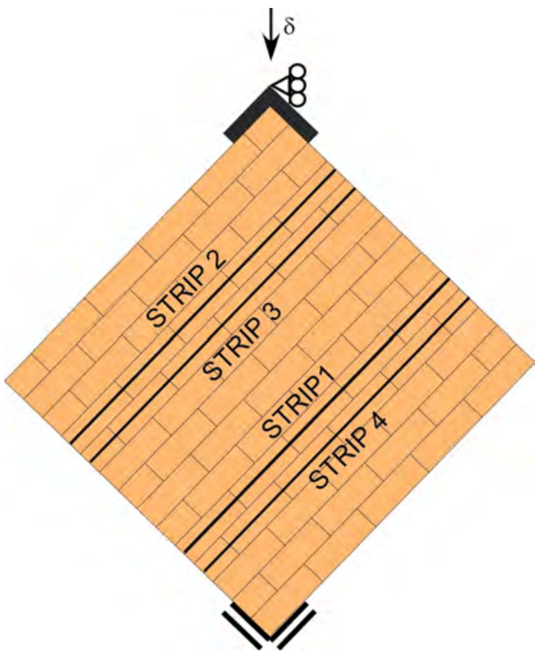

(c) H4A & H4B

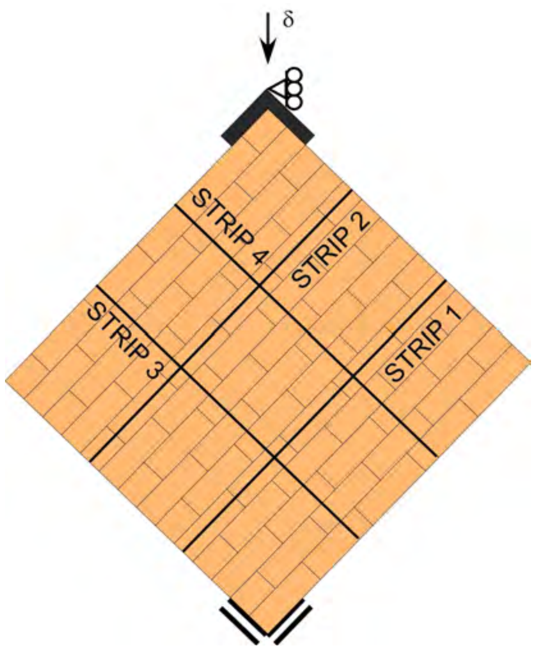

(d) V2H2A & V2H2B

Figure 5.34: FE models of FRP reinforced masonry Diagonal Tension/Shear Tests

Table 5.11: Bilinear bond-slip parameters used in FE model

Specimen	Pull test specimen	δ_1 (mm)	τ_{max} (MPa)	δ_{max} (mm)
V4A & V4B	S1-C-SG	0.20	13.1	1.77
V2	S1-C-SG	0.20	13.1	1.77
V2H2 (vertical strips)	S1-C-SG	0.20	13.1	1.77
V2H2 (horizontal strips - model 1)	S2-P0-SG	0.10	8.2	1.30
V2H2 (horizontal strips - model 2)	S2-P1-SG	0.10	13.0	1.22
H4	S2-P1-SG	0.10	13.0	1.22

5.6.1 Panels V4A & V4B

In Figure 5.35 the load vertical displacement behaviours of the reinforced FE models (with and without dowel strength), the URM FE model, and the experiments (V4A and V4B) are plotted. The URM FE model had the same mortar properties as the reinforced FE models (flexural bond strength = 0.5 MPa).

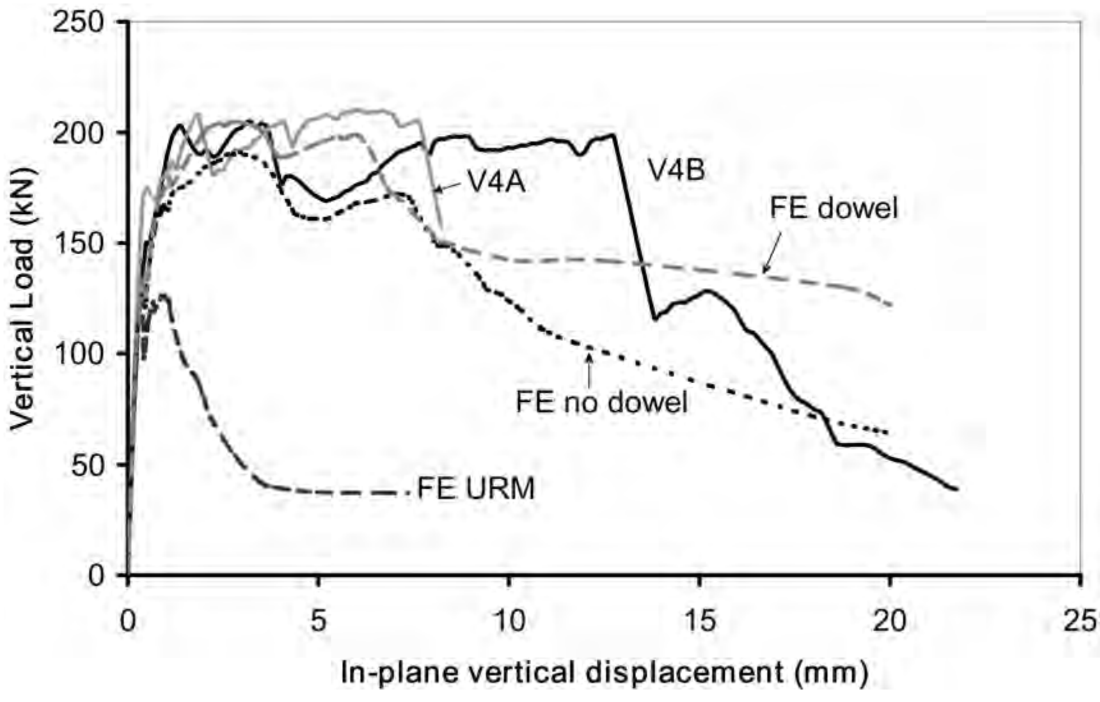

Figure 5.35: Load displacement behaviour of V4 FE model

URM model (bond strength = 0.5 MPa)

The ultimate load of the URM FE model was 126 kN and the failure mode was by sliding along a major diagonal crack through the mortar head joints and mortar bed joints. The failure mode was the same as those observed for the URM FE models in Section 5.4, as shown in Figure 5.21.

V4 model without dowel strength

The first significant diagonal crack developed in the model, through the mortar joints, at a vertical displacement of 0.45 mm and a corresponding load of 126 kN (shown in Figure 5.36a). This behaviour was closest to experiment V4B, where the first crack developed at a vertical displacement of 0.4 mm and a load of 140 kN (compared to 0.4 mm and 172 kN for panel V4A). The initial stiffness of the model was therefore also more similar to V4B. This suggests that the material properties used in the model best represented an average of the actual mortar properties in panel V4B. Also note that the first diagonal crack that developed in this model was the crack that caused failure in the URM model. This result confirms what was supposed in the last chapter: that the unreinforced masonry strength of the strengthened masonry panels is approximately equal to the load when the first diagonal crack is observed (when tested in diagonal tension/shear).

The FRP reinforced FE model (without dowel strength) reached an ultimate load of 191 kN, equal to 152% of the URM FE model prediction. This increase in load carrying capacity shows the significant contribution of reinforcement to the model. Also, more importantly, the ultimate load of the FE model was very close to the experimental ultimate loads, being 91% of V4A (210 kN) and 93% of V4B (205 kN). Note that if stronger mortar properties were used to model V4A (to match the load when the first crack developed) the ultimate load predicted by the model would likely be larger than the experimental load. This would be reasonable because the ultimate load of V4A was limited by cracking along the edge of strip 3, which was not accounted for in the model.

In the model cracks developed through mortar joints throughout the panel as the vertical displacement increased. This was similar to the experiments except that in the experiments some brick cracking was also observed. The crack pattern produced throughout the panel, after a significant amount of damage had occurred is shown in Figure 5.36b at 7 mm vertical displacement. The majority of cracks developed within the middle panel of the panel (between the 2 inside strips - strip 1(S1) and strip 3(S3)). Cracks also extended outside of the FRP strips and created a sliding plane, starting two courses from the top of the panel and finishing two courses from the bottom. The behaviour, including the crack development and the load displacement response, of the model was most similar to V4B. The behaviour of the model was also similar to V4A, except that the model did not include brick cracking along the edge of the FRP strips, which contributed to the failure of V4A.

Rather than fail by debonding of FRP from the masonry, as observed in both V4A and V4B, the reinforced panel model (without dowel strength) failed by sliding along bed joints at the top of the panel. Some crushing of the masonry at the top corner was also present(shown in Figure 5.36c at 13 mm vertical displacement). The sliding/crushing failure mechanism developed after 7.5 mm (Figure 5.35), at a displacement before debonding was observed in the experiments. Once this failure mechanism had developed the load gradually decreased as the vertical displacement increased.

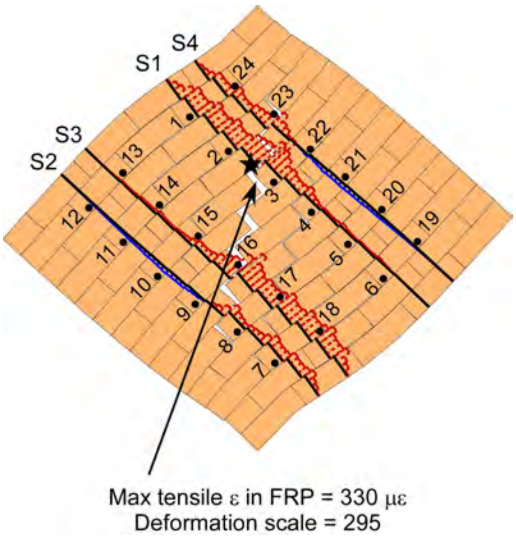

(a) First crack (vertical disp.=0.45 mm)

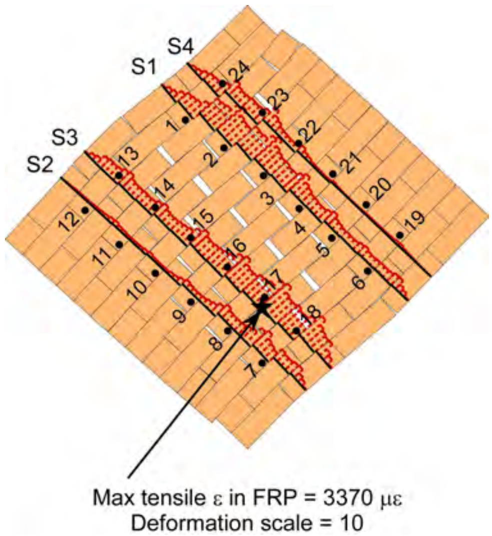

(b) Distributed cracks (7 mm)

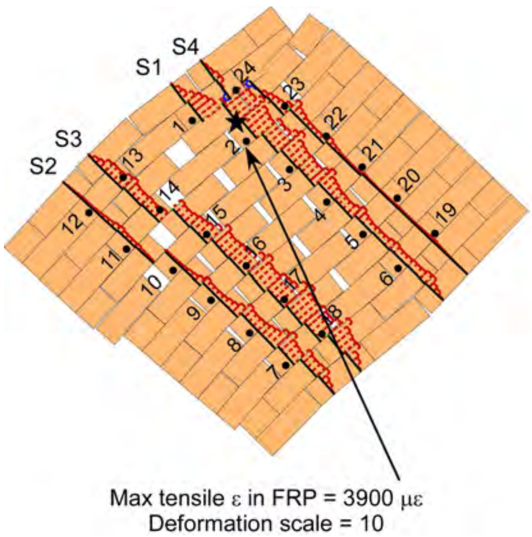

(c) Sliding/compression failure (13 mm)

Figure 5.36: Crack patterns at increasing vertical displacement of FE V4 without dowel strength

The strain distributions along the FRP strips at a vertical displacement of 7 mm are shown in Figure 5.37 to Figure 5.40. In the figures the strains produced by the model and recorded during the experiments are compared. The strain distribution produced by the FE model is also shown superimposed on the crack pattern in Figure 5.36b. The simulated strain distribution along both inside strips (strip 1 and strip 3) compared well with the strains recorded in the experiments. The simulated strain distributions along the outside strips (strip 2 and strip 4), however, were less than the strains recorded in the experiments. In the model the inside strips took a greater proportion of the load (see Figure 5.36b). It is likely that the inside strips reduced crack growth to the outer strips. In the experiments, however, the 2 strips that were next to each other (strip 1 and strip 4, strip 2 and strip 3) were on opposite sides of the panel and therefore shared more load than was predicted by the plane stress model.

Plots of strain in the FRP (at strain gauge locations) versus panel vertical displacement produced by the model (without dowel strength) are compared with results recorded during the experiments in Figure 5.41 to Figure 5.43 (V4A) and Figure 5.44 to Figure 5.46 (V4B). V4A-strip 4 and V4B-strip 1 were not included because most of the strain gauges on these strips were damaged during the experiments.

Similar to the experiments the FRP remained inactive until cracks formed (at approximately 0.4 mm). After the cracks formed the tensile strain in the FRP, in the vicinity of the cracks, increased. The simulated tensile strains (at strain gauge locations) in the outside strips (strip 2 and strip 4) increased at a lower rate than the experiments, due to the model being analysed in two dimensions only (as discussed previously). The simulated tensile strains in strip 3 (an inside strip) increased at a similar rate to the strains recorded in test V4B, until the sliding failure occurred at approximately 7.5 mm vertical displacement. Once the sliding plane developed (in the model) the strain stopped increasing. In the model the strain at SG24 decreased and became negative (indicating compressive strain) as the top corner of the panel crushed. The simulated tensile strains in strip 3 also increased at a similar rate to the strains recorded in test V4A, however, they should have been higher because the experimental strains were reduced by cracking along the inside edge of the strip (which was not accounted for in the model). In general, the simulated tensile strains in strip 1 increased at a similar rate to the strains recorded in test V4A, except for the strain at SG3, which was significantly higher in the experiment. The simulated strains of all the FRP strips were slightly lower than strains recorded in the experiment (on average).

FRP debonding did not occur in the model. The maximum shear slip in the bond interface elements, caused by crack opening and tension in the FRP, was 0.195 mm, and was still in the elastic bond range, before $\delta_1 = 0.2$. Debonding did not occur in the model because the tensile strain reached in the FRP in the model was too low. The debonding behaviour observed in V4A did not occur in the model because inside cracking, that reduced the bond, was not accounted for.

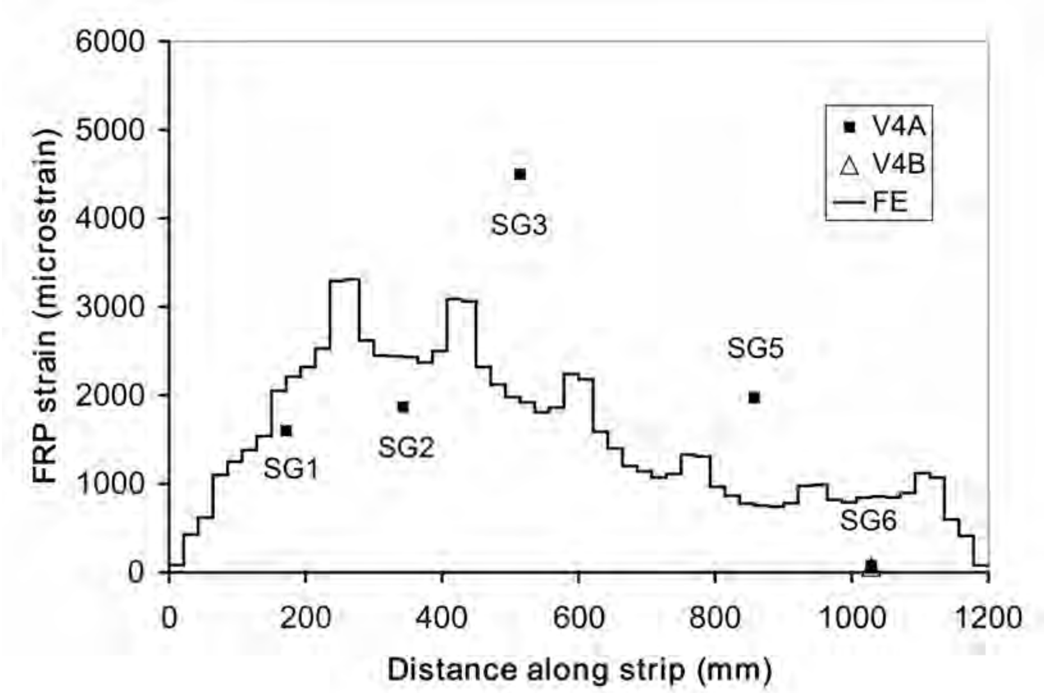

Figure 5.37: FRP strain distributions at 7 mm vertical displacement (FE model without dowel strength, V4A & V4B - Strip 1)

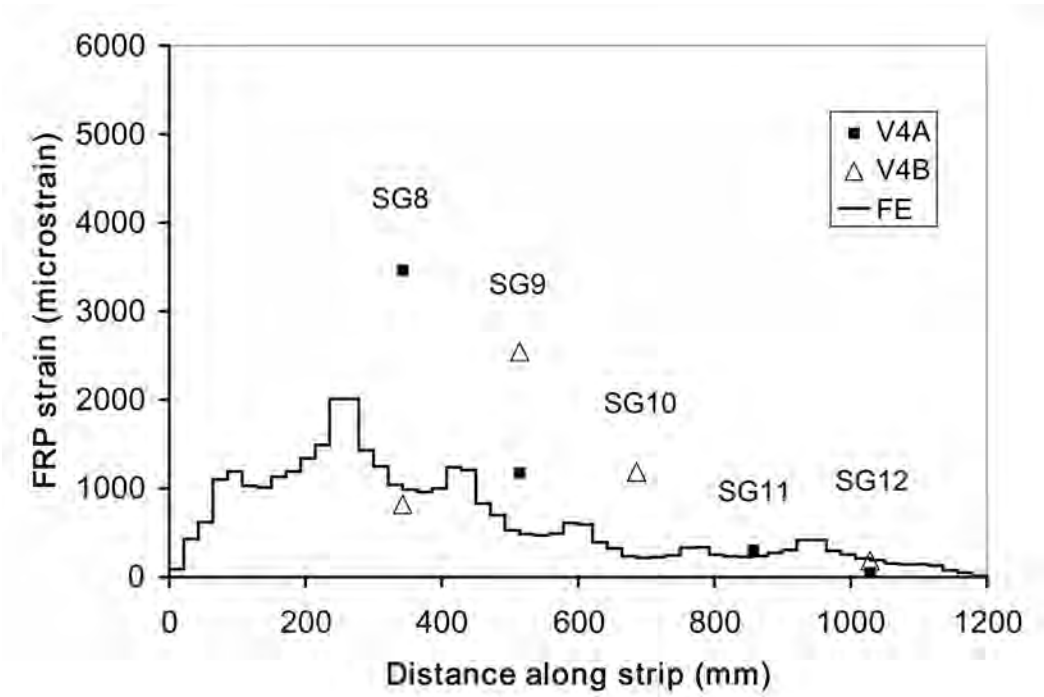

Figure 5.38: FRP strain distributions at 7 mm vertical displacement (FE model without dowel strength, V4A & V4B - Strip 2)

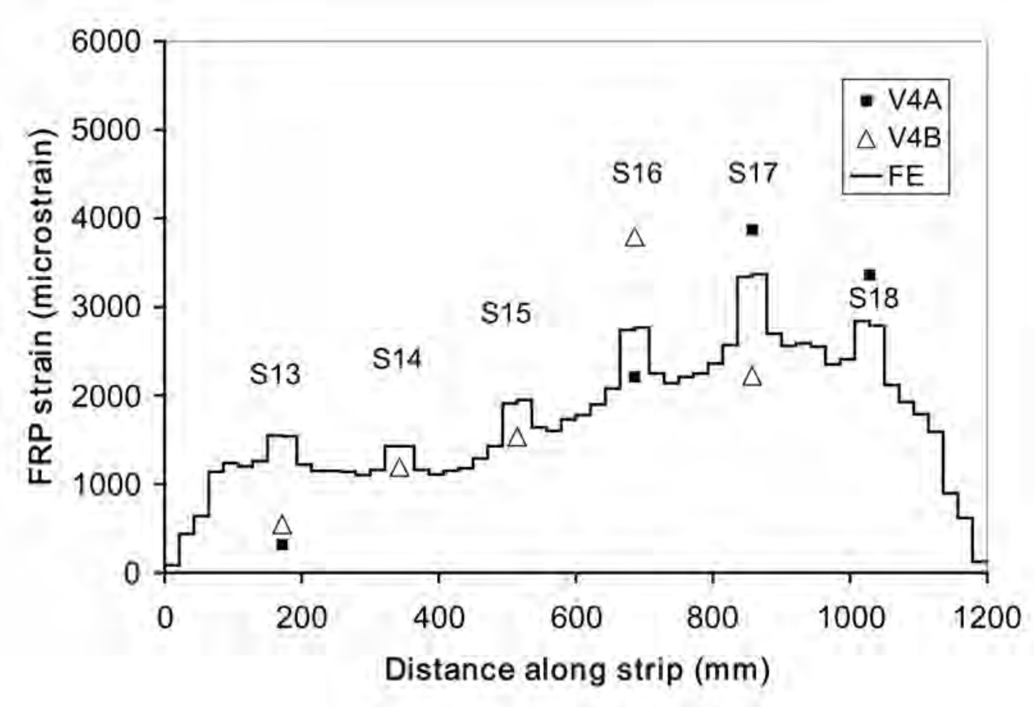

Figure 5.39: FRP strain distributions at 7 mm vertical displacement (FE model without dowel strength, V4A & V4B - Strip 3)

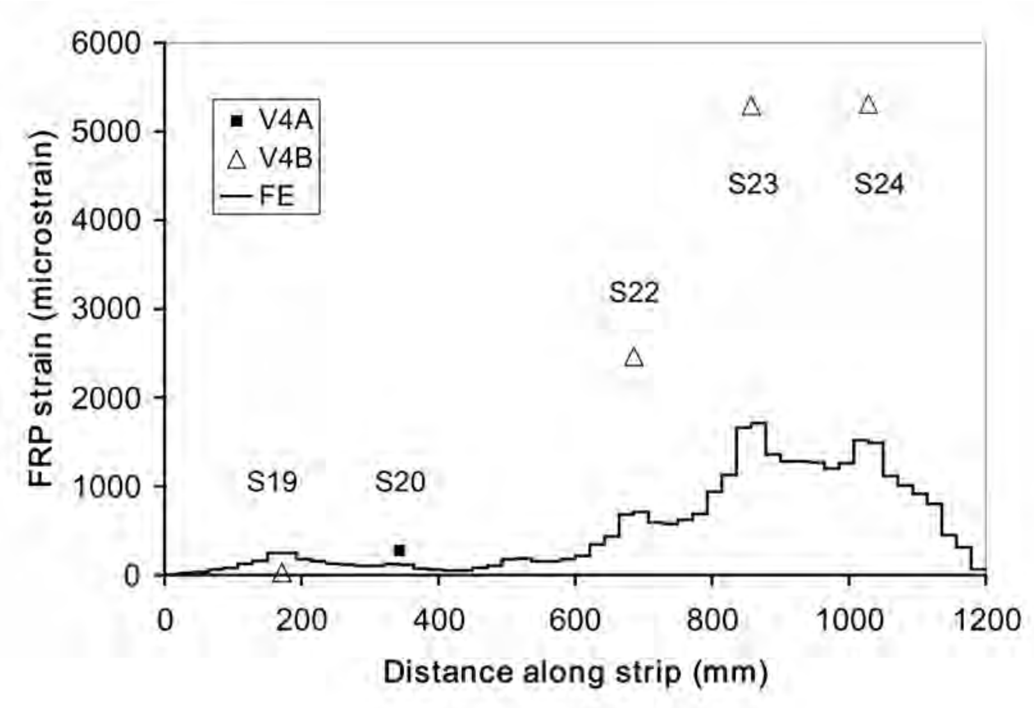

Figure 5.40: FRP strain distributions at 7 mm vertical displacement (FE model without dowel strength, V4A & V4B - Strip 4)

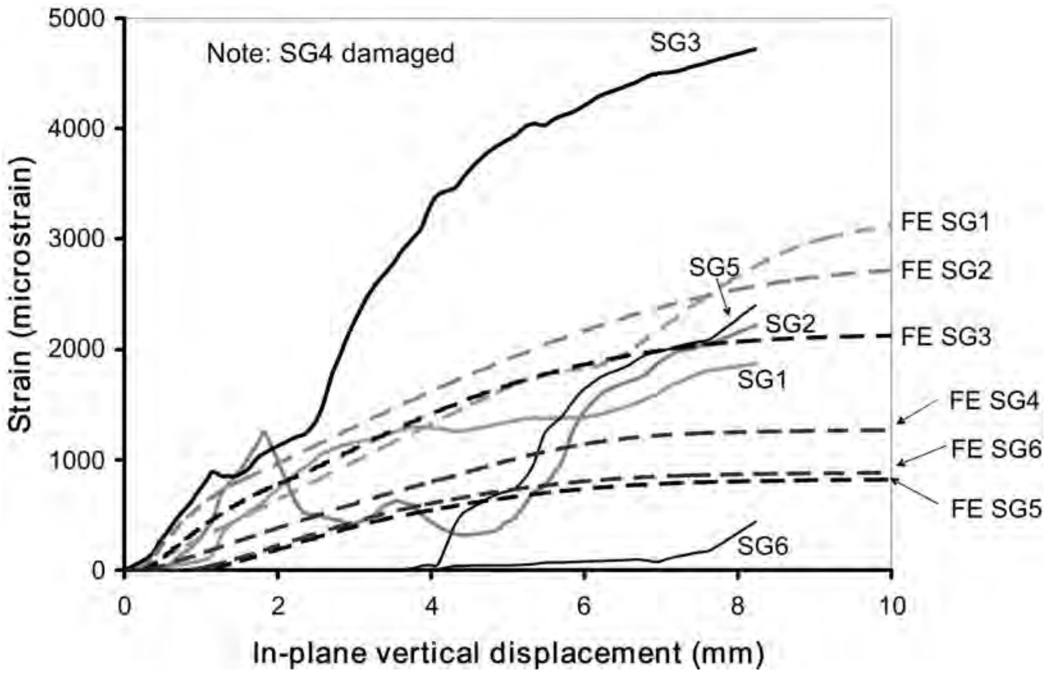

Figure 5.41: FRP strain versus vertical displacement (V4A and FE model without dowel strength - Strip 1)

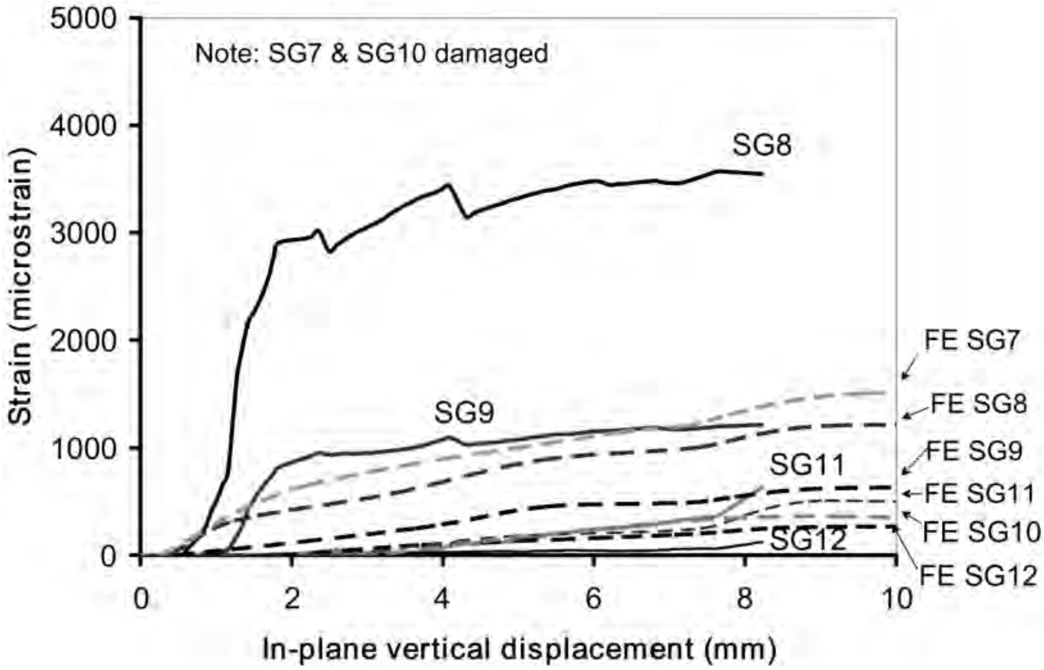

Figure 5.42: FRP strain versus vertical displacement (V4A and FE model without dowel strength - Strip 2)

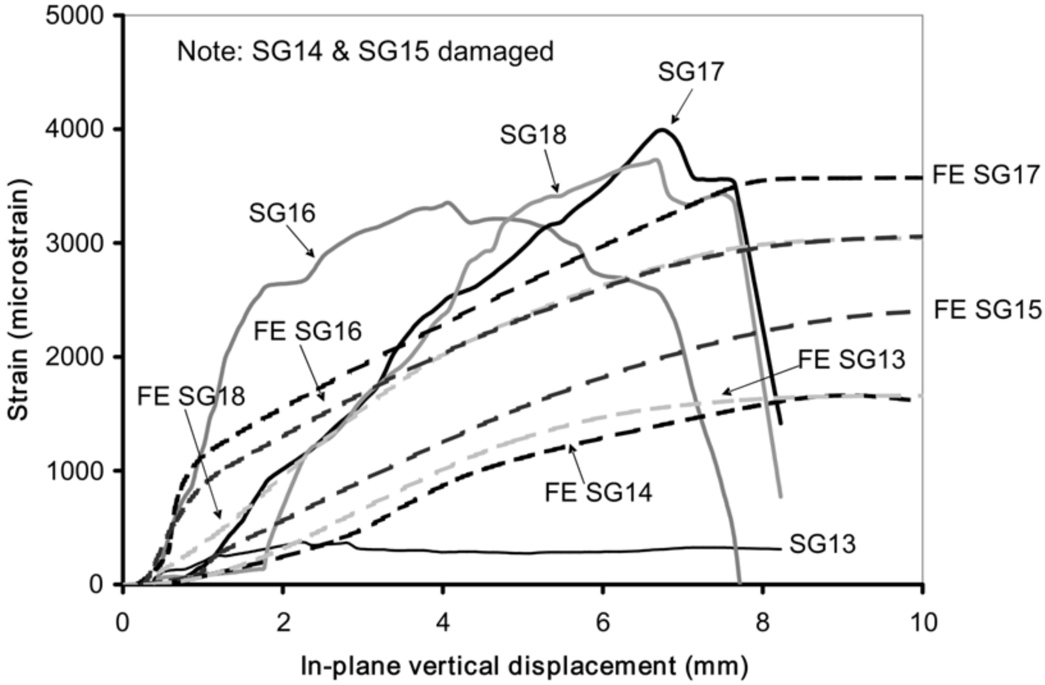

Figure 5.43: FRP strain versus vertical displacement (V4A and FE model without dowel strength - Strip 3)

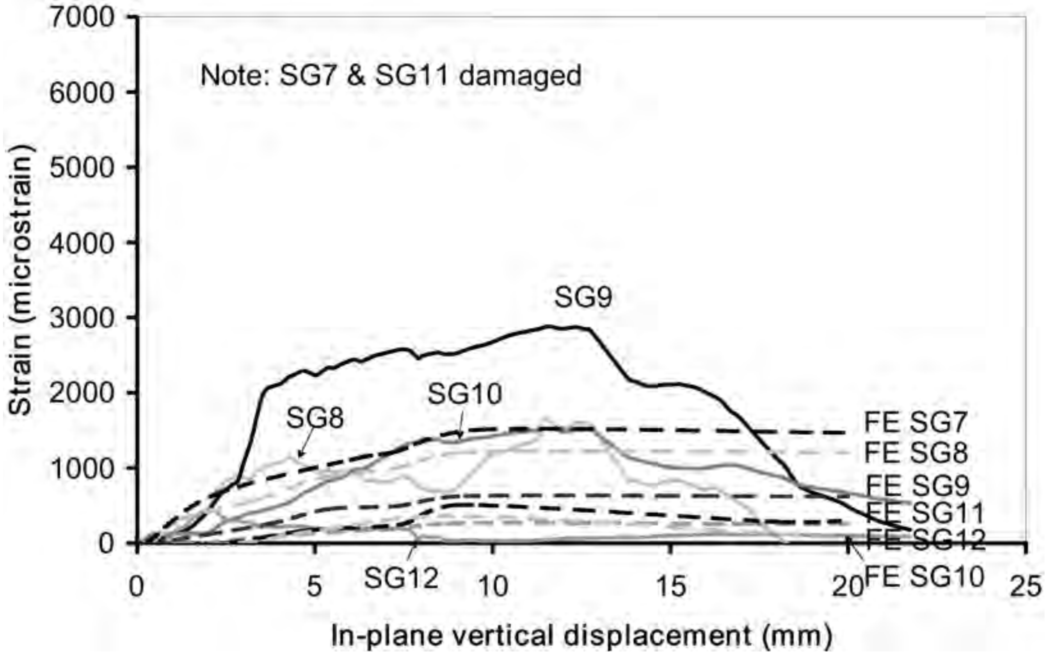

Figure 5.44: FRP strain versus vertical displacement (V4B and FE model without dowel strength - Strip 2)

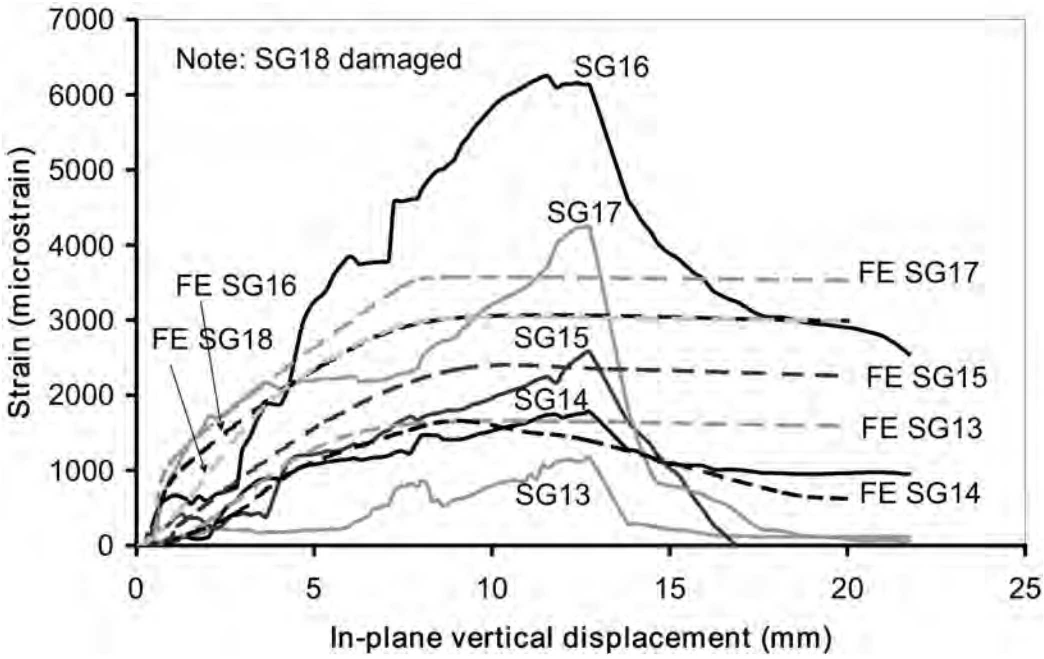

Figure 5.45: FRP strain versus vertical displacement (V4B and FE model without dowel strength - Strip 3)

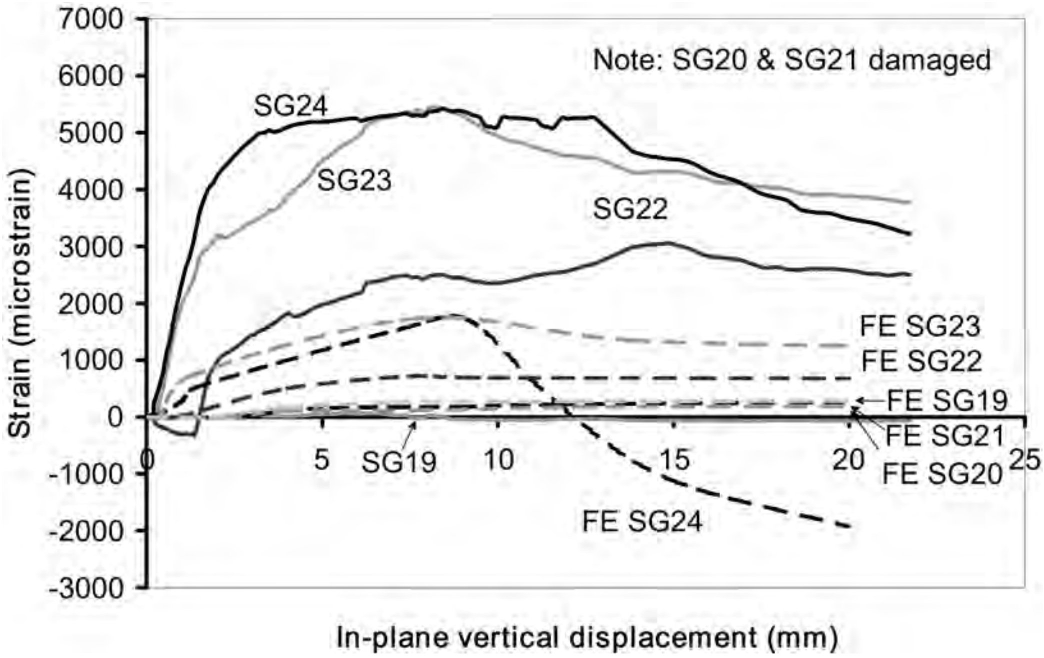

Figure 5.46: FRP strain versus vertical displacement (V4B and FE model without dowel strength - Strip 4)

V4 model with dowel strength

The load displacement behaviour of the FE model with dowel strength is shown in Figure 5.35. With dowel strength included the model attained an ultimate load of 205 kN, which was 98% of the ultimate load of V4A and 100% of the ultimate load of V4B. The sliding failure that occurred in the model without dowel strength was prevented (by the increased shear resistance), and instead the model failed by crushing at the top corner of the masonry (as shown in Figure 5.47 at 13 mm vertical displacement). This resulted in a gradual drop in load. Before crushing occurred the crack pattern and behaviour was similar to the FE model without dowel strength (and therefore also panel V4B).

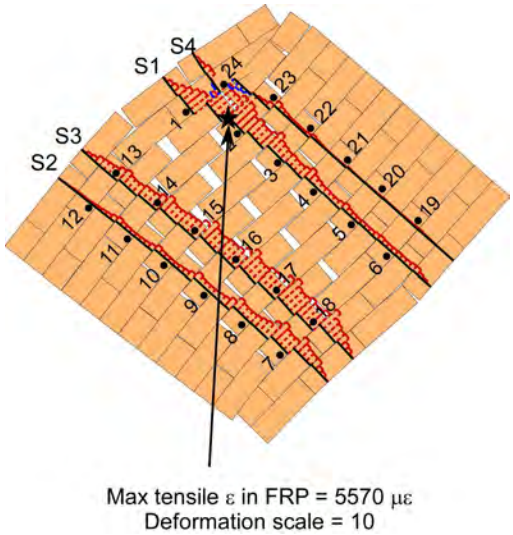

Figure 5.47: Crack pattern of V4 model with dowel strength (in-plane vertical displacement = 13 mm)

As the top corner of the panel crushed, cracks through the mortar joints continued to develop, and the tensile strains in the FRP continued to increase. This is shown in Figure 5.48, where the tensile strain at SG17 (maximum strain in strip 3 in FE model) is plotted against the vertical displacement for the models with dowel strength and without dowel strength. The experimental results at SG17, and the results of SG16 from V4B (maximum recorded strain in the test) are also plotted. The strain at SG17 increased at a similar rate in both FE models (with and without dowel strength) until sliding failure occurred in the model without dowel strength and caused the tensile strain in the FRP to stop increasing. As the dowel strength prevented the sliding failure, the tensile strain continued to increase, similar to experiment V4B. The maximum strain in strip 3 in the model (with dowel strength) was, however, lower than the maximum strain recorded in experiment V4B (at SG16).

The strain in the FRP was still not high enough to cause complete debonding of the FRP from the masonry in this model. The maximum shear slip in the bond interface elements (caused by tensile loading in the FRP) was 0.362 mm, which

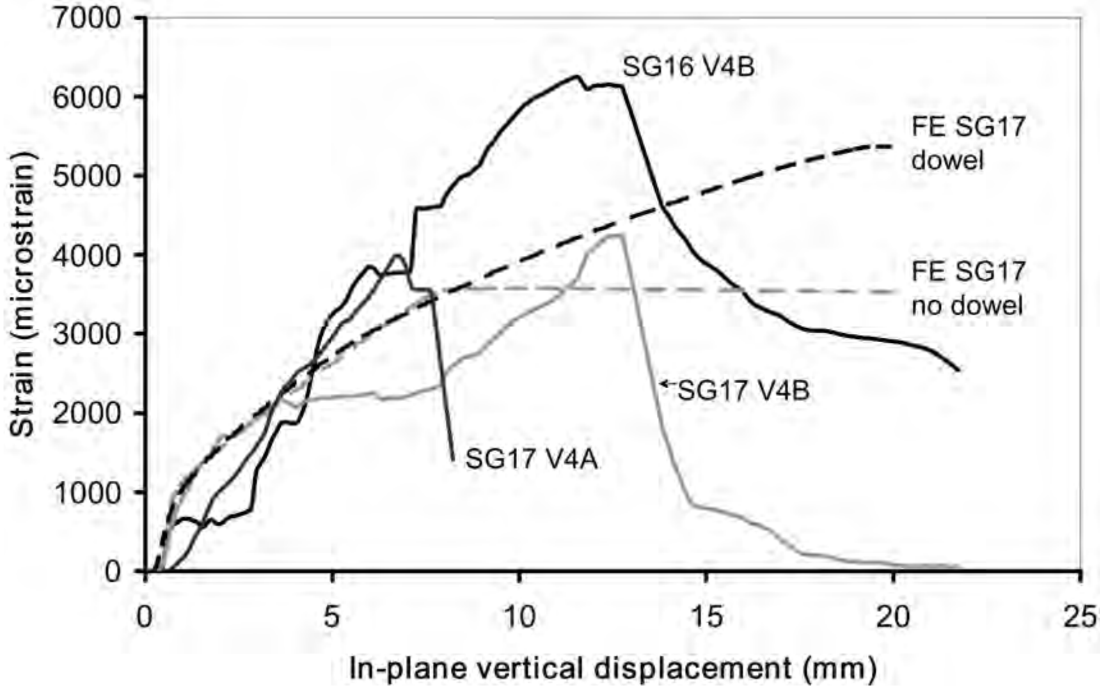

Figure 5.48: Influence of dowel strength in the FE model on strain increase at SG17

was larger than the model without dowel strength, and indicated some debonding cracks had developed. The shear slip was not, however, large enough to cause complete debonding.

5.6.2 Panel V2

In Figure 5.49 the load vertical displacement behaviours of the reinforced FE models (with and without dowel strength), the URM FE model (with the same mortar properties as the reinforced FE models, bond strength = 0.5 MPa), and the experiment (V2) are plotted.

V2 model without dowel strength

The first significant diagonal crack developed at a vertical displacement of 0.45 mm and at a load of 126 kN (same as previous V4 model because the same mortar properties were used, shown in Figure 5.36a). This was similar to experiment V2, where the first diagonal crack developed at a vertical displacement of 0.3 mm and at a load of 125 kN.

The ultimate load of the FE model (without dowel strength) was 162 kN, which was equal to 129% of the predicted URM load, and was also very close to the ultimate load of the experiment (101% of 160 kN). After the ultimate load was reached the experimental load decreased more rapidly with vertical displacement than did the model predicted load. It is likely that out-of-plane displacement that occurred in the experiment (due to single sided reinforcement) reduced the load carrying capacity after the major cracks had developed at the ultimate load. The plane stress model could not account for such out-of-plane effects.

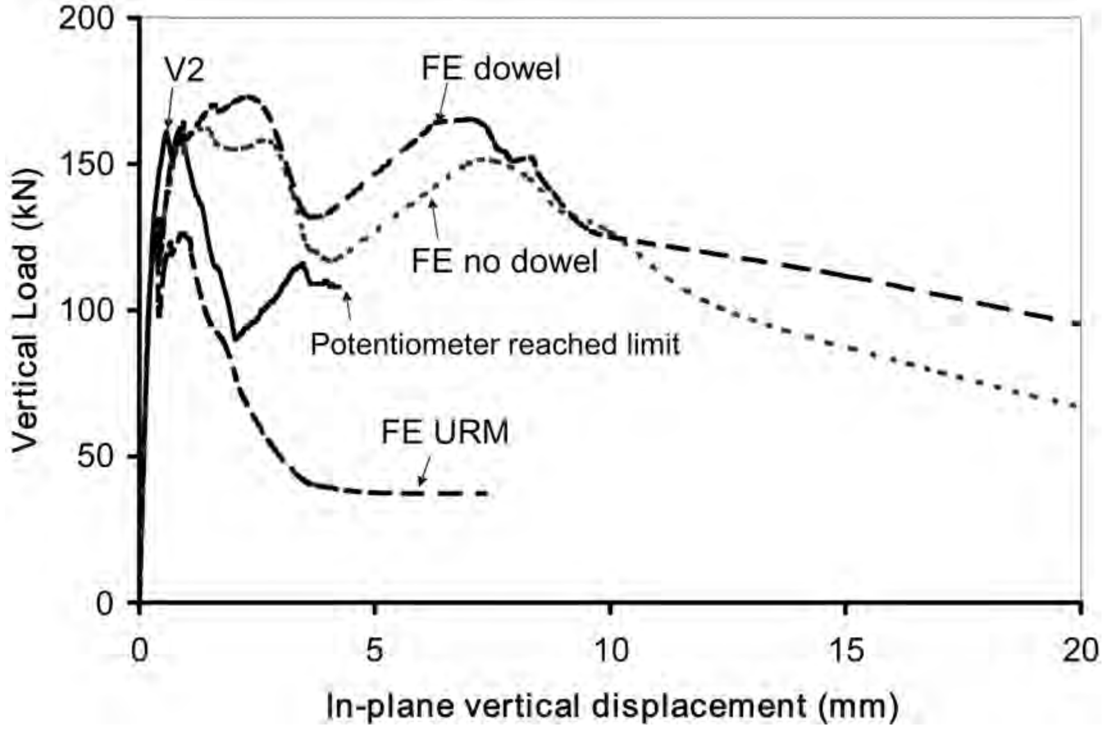

Figure 5.49: Load displacement behaviour of V2 FE model

In the model cracks developed through mortar joints throughout the panel as the vertical displacement increased. The predicted crack pattern at 4 mm vertical displacement is shown in Figure 5.50a, and was similar to the experiment. The cracks were more distributed in the model, but a sliding plane developed, that was similar to that observed in the experiment. The sliding plane started two courses from the top and ended two courses from the bottom. It is likely that the reason why cracks did not spread in the experiment (as predicted in the model) was because the out-of-plane deformation reduced the redistribution of forces within the panel, and that reduced further crack development. Like the model for V4 with no dowel strength, this model eventually failed by sliding failure along the bed joints after approximately 7.5 mm vertical displacement (Figure 5.50b). Debonding did not occur in the FE model (similar to the experiment).

The tensile strain distribution along FRP strips in the model and experiment are shown in Figure 5.51 and Figure 5.52 (at 4 mm vertical displacement). The FE model strain distributions were slightly higher than the strains recorded during the experiments, but otherwise matched well. The tensile strains were at a maximum at locations where the FRP crossed major cracks, and reduced along the length of the FRP (away from those cracks) as the load was transferred into the masonry.

As previously discussed, after the peak load was reached the experimental panel bent in the out-of-plane direction. This out-of-plane deformation in the experiment would likely result in less crack opening (on the reinforced side of the panel) and thus less strain in the FRP compared to the model. Also, the redu-

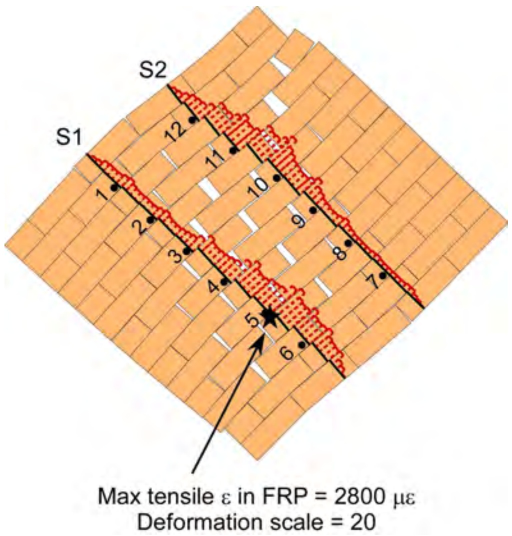

(a) Distributed cracks (4 mm vert. disp.)

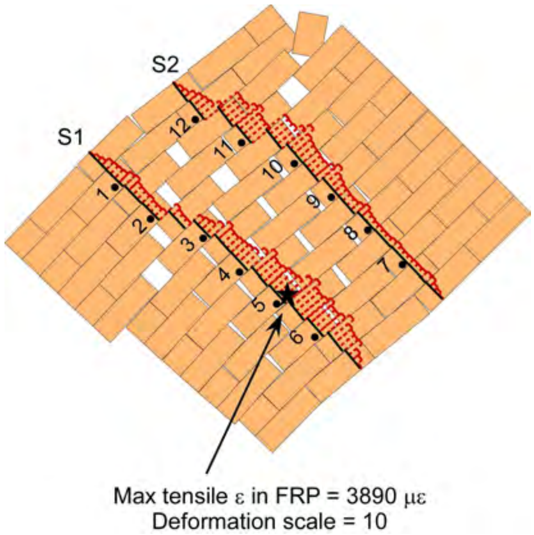

(b) Sliding failure (13 mm vert. disp.)

Figure 5.50: Crack patterns at increasing vertical displacement of FE V2 without dowel strength

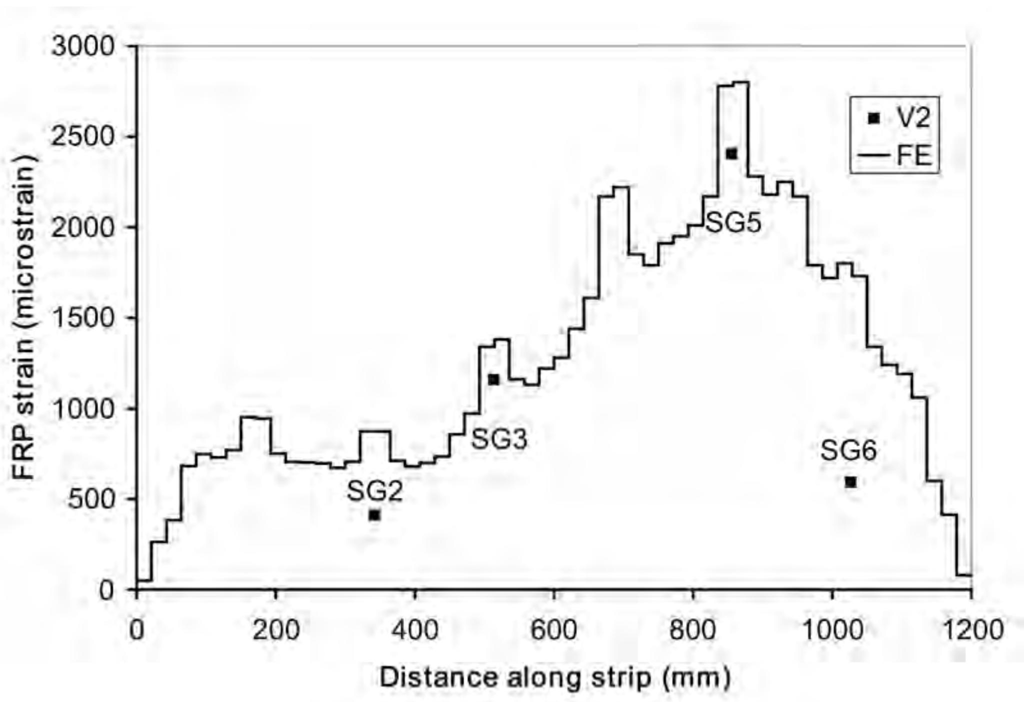

Figure 5.51: FRP strain distributions at 4 mm vertical displacement (FE model, V2 - Strip 1)

ced tensile strain in the FRP may explain the lower peak load in the experiment compared to the model. Figure 5.51 and Figure 5.52 show the experimental FRP strains were less than the model FRP strains, so the results are reasonable. It can be concluded that, for reinforcement on one side only, the model assumption of in-plane behaviour is not entirely correct but the error is small.

Plots of tensile strain in the FRP strips (at strain gauge locations) versus panel vertical displacement produced by the model are compared with results recorded during the experiment in Figure 5.53 and Figure 5.54. The results of the experiment were only plotted to 4.5 mm, because the potentiometers ran out of range as discussed in Chapter 4. The tensile strain in the model started increasing at approximately the same displacement (when the first crack formed) and increased at a rate slightly greater than the experiments (up to 4.5 mm). Again, this is likely a result of out-of-plane bending in the experiment. Out-of-plane bending reduced the FRP strain in the experiment compared to the model (which ignores out-of-plane effects).

V2 model with dowel strength

The load displacement behaviour of the V2 model with dowel strength is shown in Figure 5.49. In general the behaviour of this model was very similar to the V2 model without dowel strength. The model was stronger, however, with an ultimate load of 173 kN (108% of V2), and some crushing at the top corner of the model occurred with sliding along the bed joints at the top of the panel. Adding dowel strength to this model did not change the strains in the FRP strips.

The results of the model without dowel strength were closer to the results of V2. This was reasonable because large bending of both FRP strips was observed in V2, indicating the dowel contribution of the reinforcement was close to zero.

5.6.3 Panels H4A & H4B

In Figure 5.55 the load vertical displacement behaviours of the reinforced FE model (with strong mortar properties, see Table 5.10), the URM FE model (strong mortar) and the experiments, H4A and H4B, are plotted. Note that dowel strength was not modelled for the case of horizontal reinforcement since the FRP strips are aligned parallel to sliding planes.

The behaviour of the model was different to the behaviour of panel H4A. In the reinforced model, the horizontal FRP restrained the opening of a diagonal crack that formed through mortar joints, along the loaded diagonal. The panel eventually failed by sliding along an unstrengthened bed joint at the top of the panel (see Figure 5.56a). In the FE model the horizontal reinforcement did not significantly increase the ultimate load of the panel. It did, however, change the failure mode and increase the ductility. The ultimate load of the FE model was 283 kN, and was close to the ultimate load of panel H4A (264 kN).

The model crack pattern and resulting FRP strains were unlike those observed in H4A. In H4A a diagonal crack did not form along the loaded diagonal, but instead the crack shown in Figure 5.56b formed. The crack was only intersected by

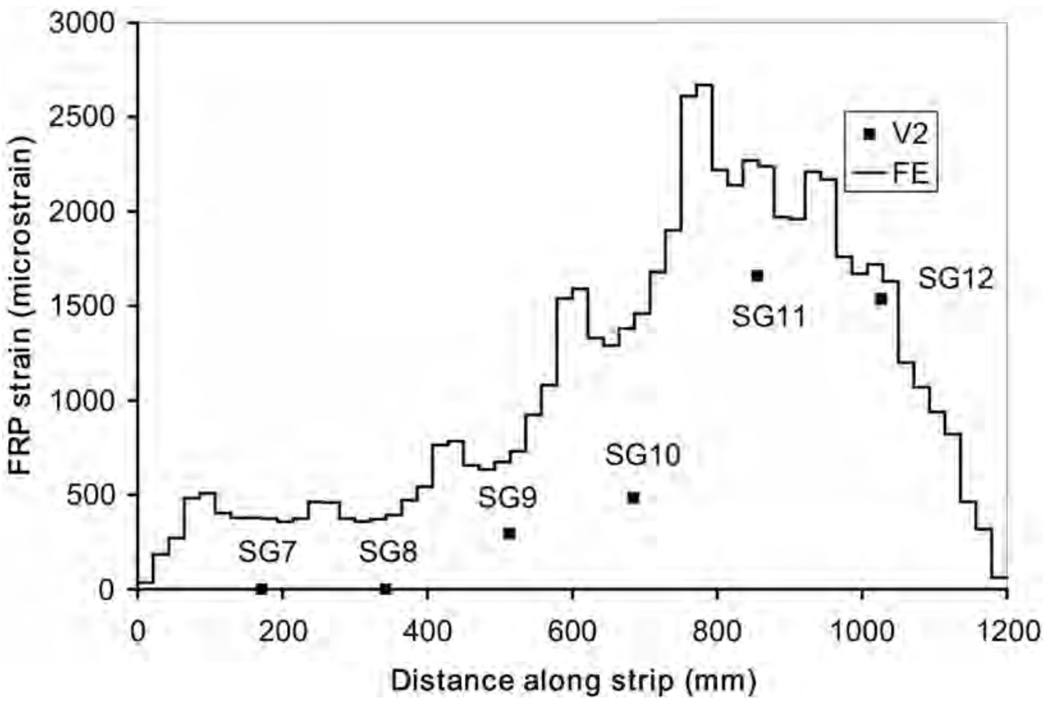

Figure 5.52: FRP strain distributions at 4 mm vertical displacement (FE model, V2 - Strip 2)

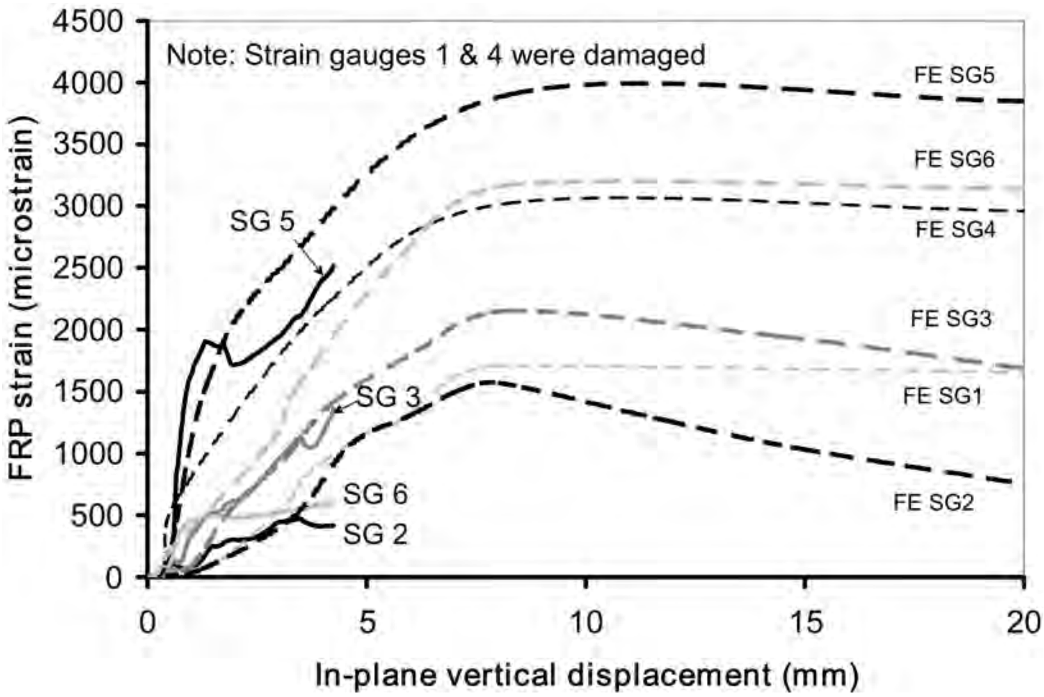

Figure 5.53: FRP strain versus vertical displacement (V2 and FE model without dowel strength - Strip 1)

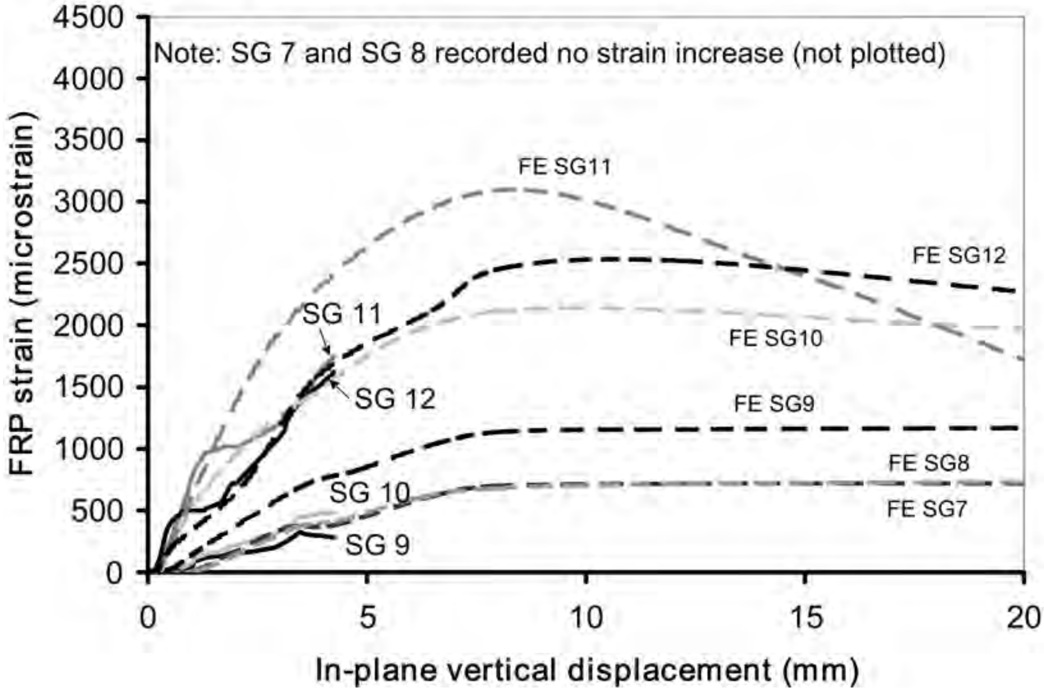

Figure 5.54: FRP strain versus vertical displacement (V2 and FE model without dowel strength - Strip 2)

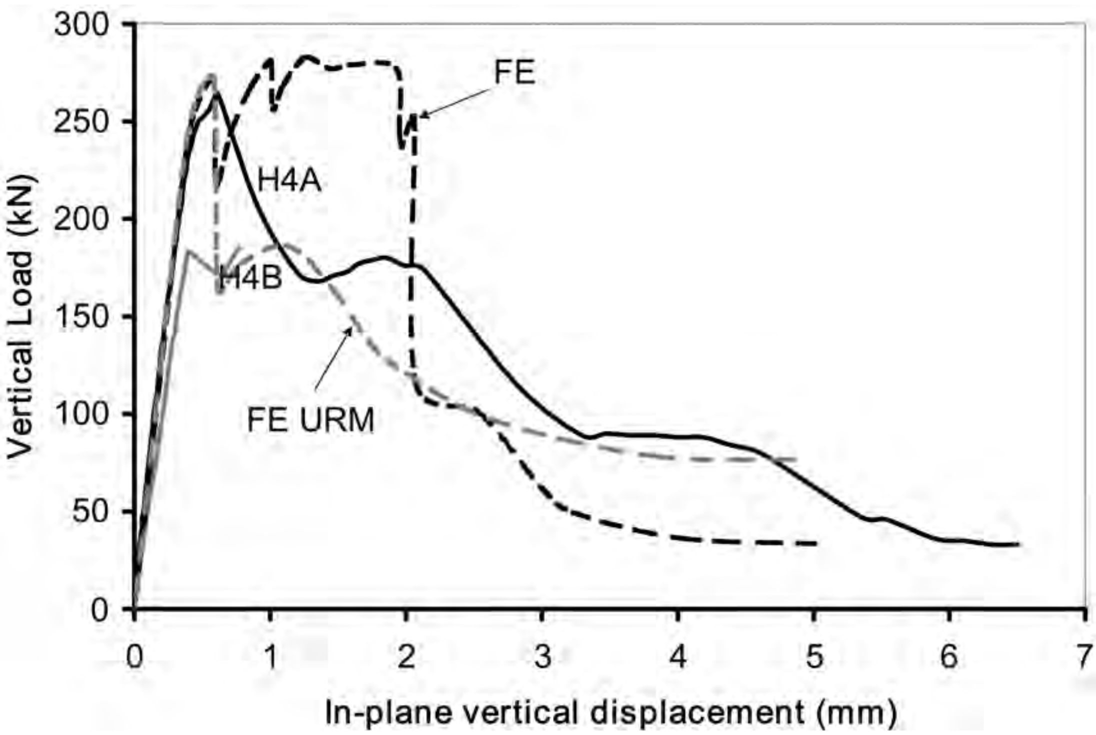

Figure 5.55: Load displacement behaviour of H4 FE model (with 'strong' mortar properties)

one FRP strip. This strip acted to keep the section of masonry outside the crack from falling off the panel, but likely did not contribute significantly to the load carrying capacity of the panel. It was thought that the behaviour of panel H4A would have been similar without the horizontal reinforcement.

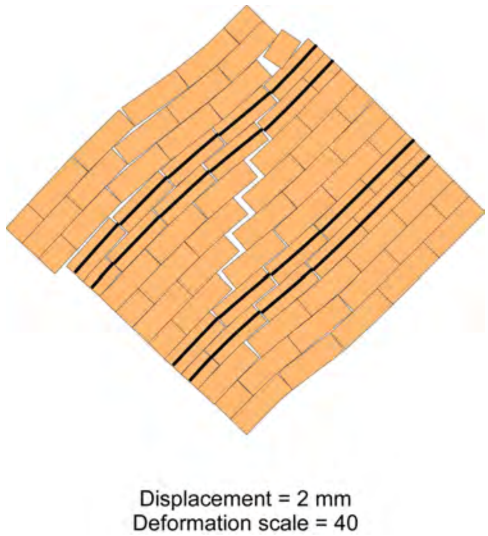

(a) Crack pattern of reinforced model

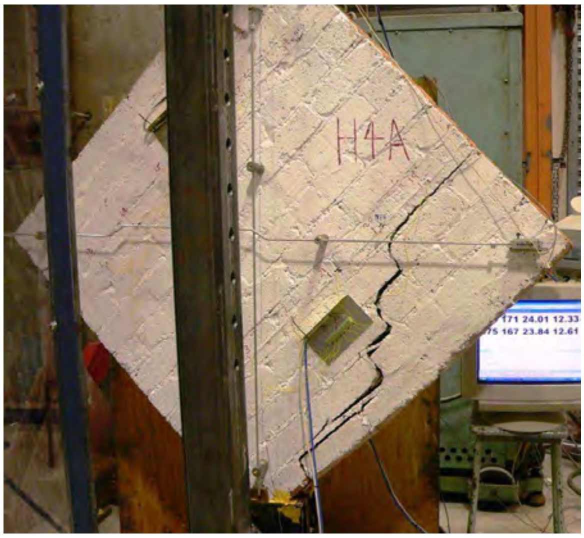

(b) Crack pattern of H4A

Figure 5.56: Comparison of failure modes between H4A and H4 FE model with bond strength = 1.11 MPa (strong mortar)

The load displacement behaviours of the URM model (bond strength = 0.8 MPa), the reinforced model (bond strength = 0.8 MPa) and panel H4B are shown in Figure 5.57.

The URM model reached an ultimate load of 159 kN and failed by sliding along a diagonal crack through the mortar joints (same as URM models in previous sections). The sliding crack first developed at a panel vertical displacement of approximately 0.4 mm.

The behaviour of the reinforced model with bond strength = 0.8 MPa was similar to H4B. The horizontal reinforcement restrained the opening of the diagonal crack that developed at 0.4 mm (the crack which caused failure in the URM model). This diagonal crack is shown in Figure 5.58a at 0.78 mm vertical displacement. The panel eventually failed by sliding along an unstrengthened bed joint at the top of the panel (shown in Figure 5.58b at 2 mm vertical displacement).

The horizontal reinforcement (in the FE model) increased the ultimate load of the panel to 186 kN (117% of the FE URM model). This was different from the experiment where the maximum load (185 kN) was not significantly higher than the load at the formation of the first crack (183 kN ≈ unreinforced strength of the panel). In the model the vertical displacement before sliding occured was 1.7 mm. This was larger than the experiment where sliding occurred after 0.78 mm panel vertical displacement.

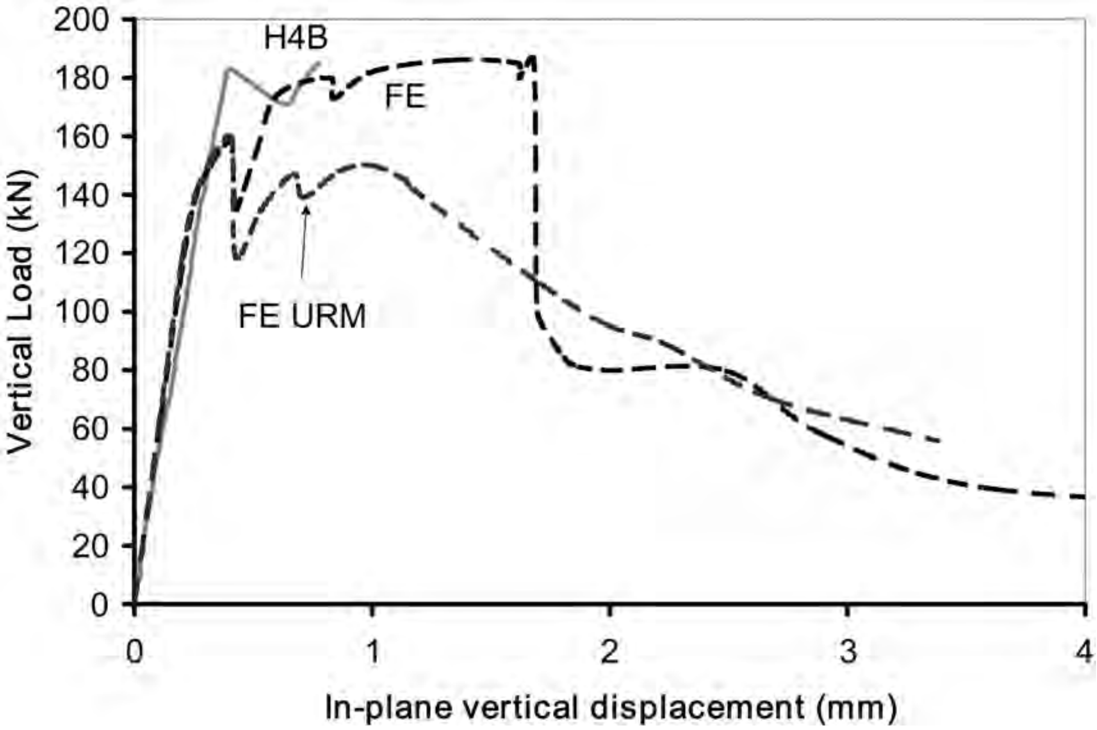

Figure 5.57: Load displacement behaviour of H4 FE model (bond strength = 0.8 MPa)

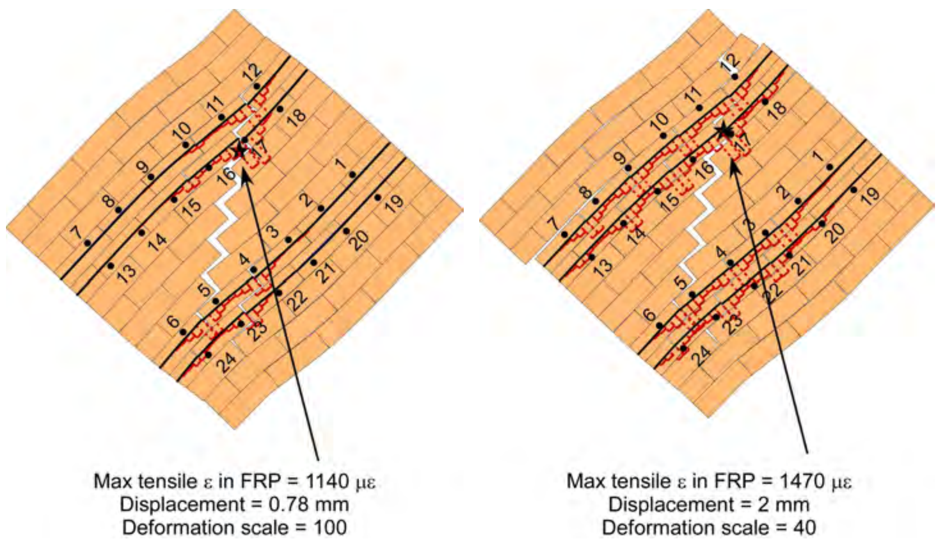

(a) Diagonal crack restrained by FRP (b) Failure along unstrengthened bed joint

Figure 5.58: Behaviour of H4 FE model (bond strength = 0.8 MPa)

The tensile strain distributions along the FRP strips, calculated by the model and recorded during the testing of H4B, at a panel vertical displacement of 0.78 mm (immediately before the failure of experiment H4B) are shown in Figure 5.59 to Figure 5.62. The corresponding crack patterns of the model and experiment were already shown at this vertical displacement in Figure 5.58a and Figure 4.28c, respectively. In the FE model some secondary cracks developed next to the main diagonal crack, as indicated by the two peaks in the strain distribution (most noticeable in strip 1). These cracks can be seen in Figure 5.58a. Some secondary cracks also developed in the experiment that were not present in the model at 0.78 mm vertical displacement at strain gauge locations 9 and 14. These cracks did, however, develop in the model at a later stage.

Plots of the tensile strain in the FRP strips (at strain gauge locations) versus vertical displacement produced by the FE model are compared with the results of H4B in Figure 5.63 to Figure 5.66. The strain in the FRP was constant after the sliding crack developed at the top of the panel because the FE model did not completely fall apart (unlike the experiments , where the test was stopped after failure along the unstrengthened joint). The model strain results matched the experimental results well. Note that the strain increased at different points along the FRP strips in some cases because cracks developed in different places (e.g. in the model a crack developed at SG 23, whereas in the experiment it developed at SG24). As mentioned previously the strain at SG9 and SG14 increased in the model after 0.78 mm vertical displacement as cracks developed in the panel.

Debonding did not occur in the model (it was not observed in the experiment either). The maximum slip of the bond-slip interface elements was 0.09 mm, and was still within the elastic range.

5.6.4 Panels V2H2A & V2H2B

V2H2 models without dowel strength

The V2H2 model was simulated with two different FRP-to-masonry bond-slip relationships, representing the bond-slip relationships of a horizontal strip with 0 and 1 MPa of applied compression (Section 5.6). The behaviours of both of these models were very similar. The similarity is shown in the load displacement graph (Figure 5.67). The model with the bond-slip relationship determined for a horizontal strip with 1 MPa applied compression is used for the following discussions. The load displacement behaviours of the experiments (V2H2A and V2H2B), and the URM model are also shown in Figure 5.67.

The behaviour of the model was similar to both experiments (but not including the out-of-plane effects). The first diagonal crack developed at 0.4 mm and 126 kN (similar to other models) and was close to experiment V2H2B, where the first crack developed at approximately 0.4 mm and 120 kN. The initial stiffness of the FE model also closely matched the initial stiffness of panel V2H2B.

The ultimate load of the reinforced model was 189 kN. This was equal to 150% of the URM ultimate load (126 kN), and was within the variability of the experiments (92% of V2H2A (206 kN) and 120% of V2H2B (158 kN)).

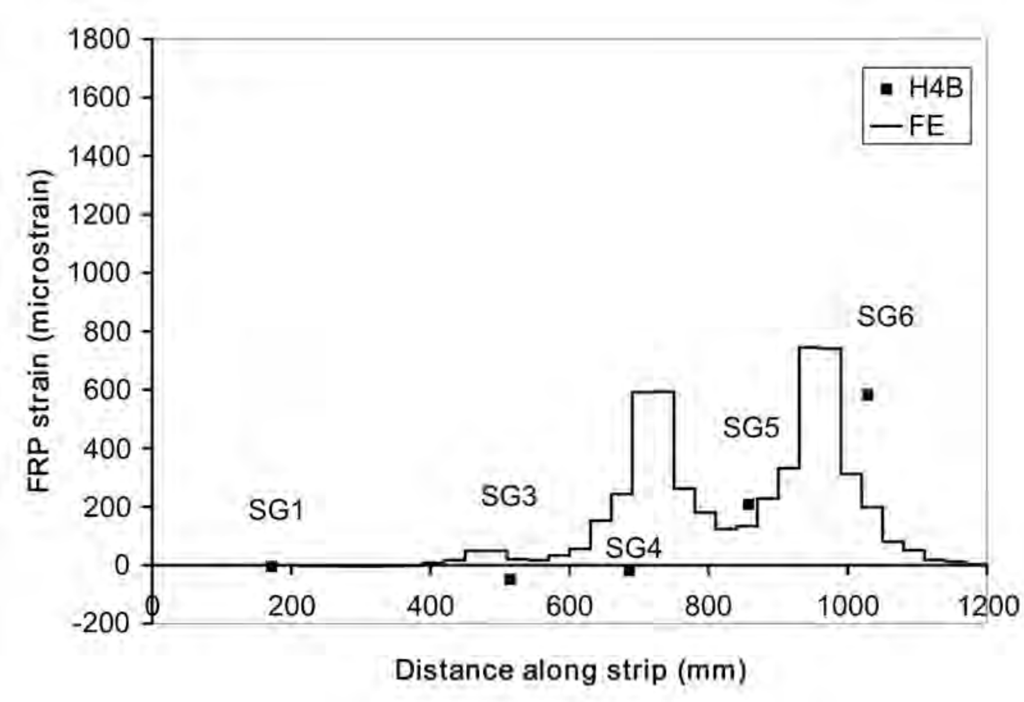

Figure 5.59: FRP strain distributions at 0.78 mm vertical displacement (H4B and FE model with bond strength = 0.8 MPa, Strip 1)

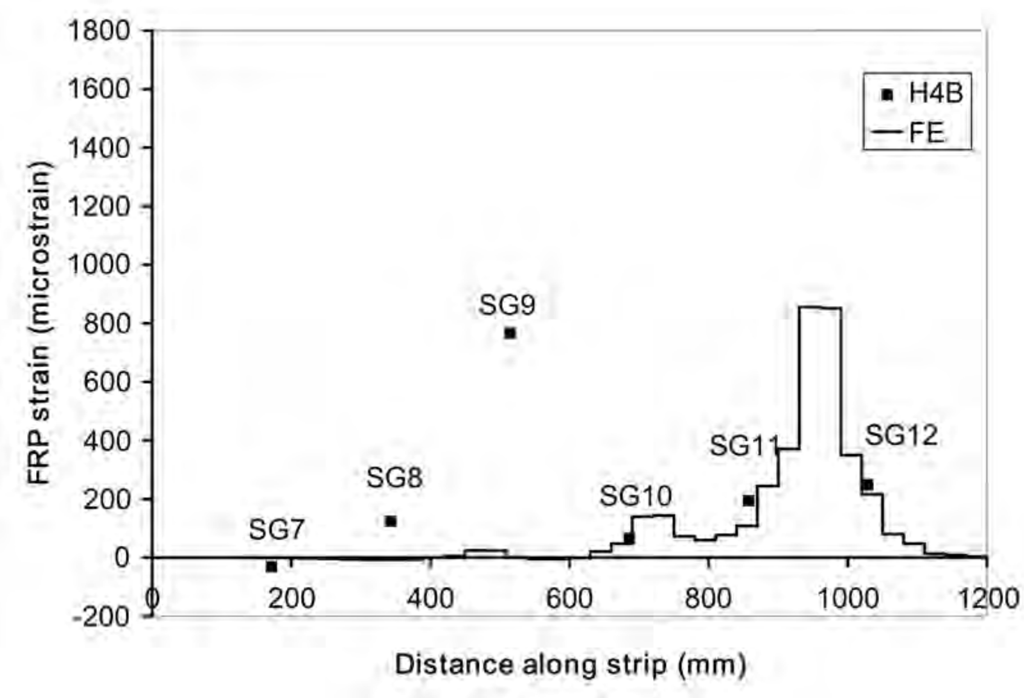

Figure 5.60: FRP strain distributions at 0.78 mm vertical displacement (H4B and FE model with bond strength = 0.8 MPa, Strip 2)

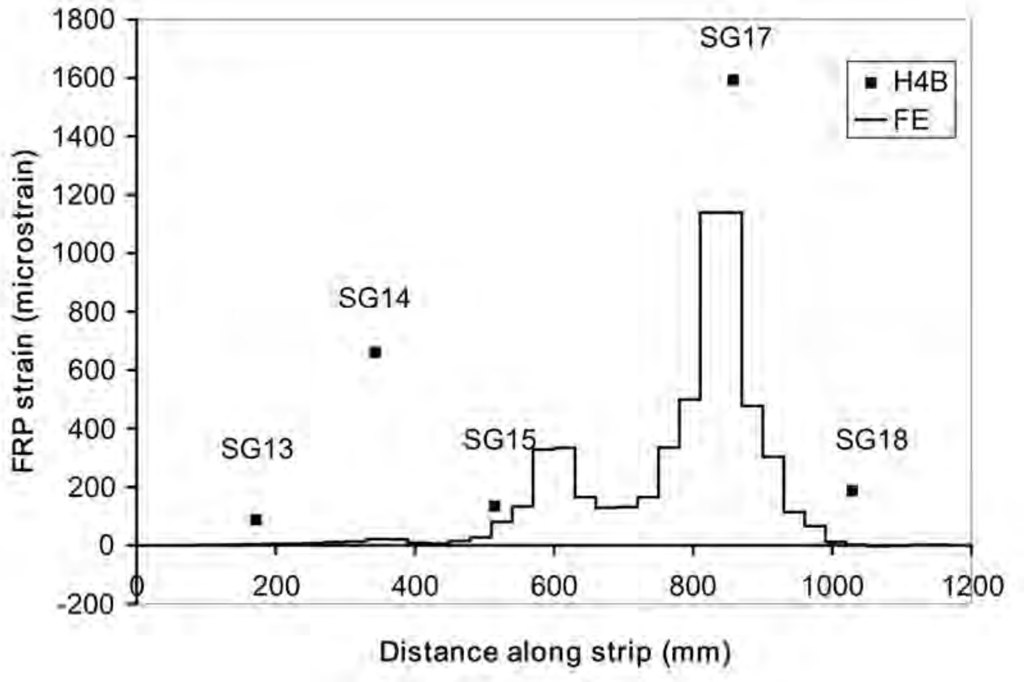

Figure 5.61: FRP strain distributions at 0.78 mm vertical displacement (H4B and FE model with bond strength = 0.8 MPa, Strip 3)

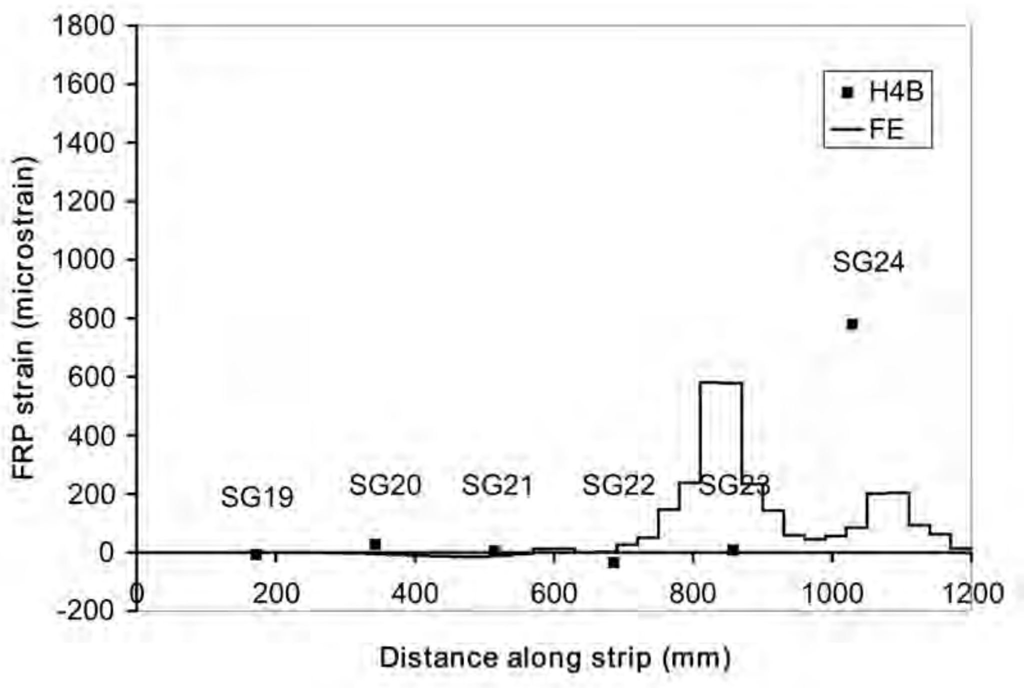

Figure 5.62: FRP strain distributions at 0.78 mm vertical displacement (H4B and FE model with bond strength = 0.8 MPa, Strip 4)

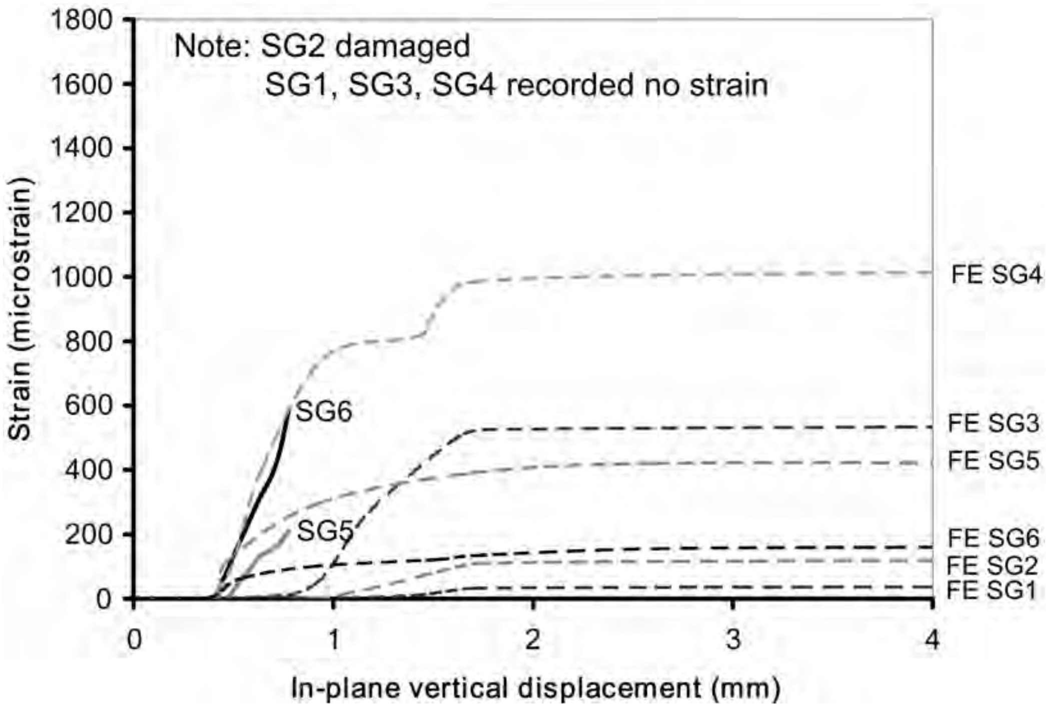

Figure 5.63: FRP strain versus vertical displacement (H4B and FE model with bond strength = 0.8 MPa, Strip 1)

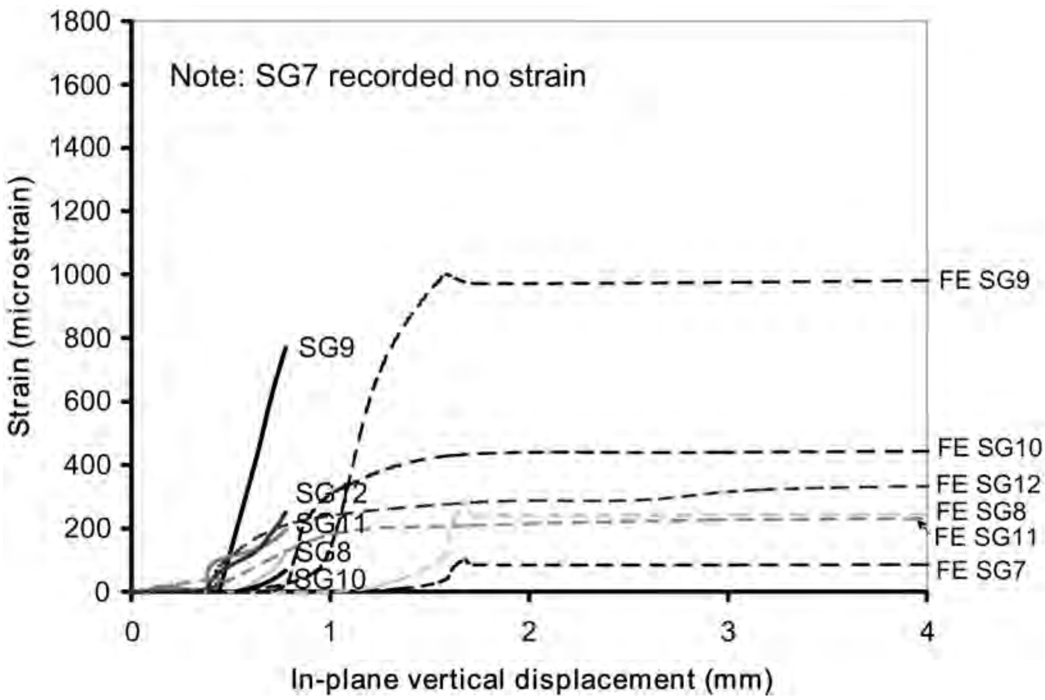

Figure 5.64: FRP strain versus vertical displacement (H4B and FE model with bond strength = 0.8 MPa, Strip 2)

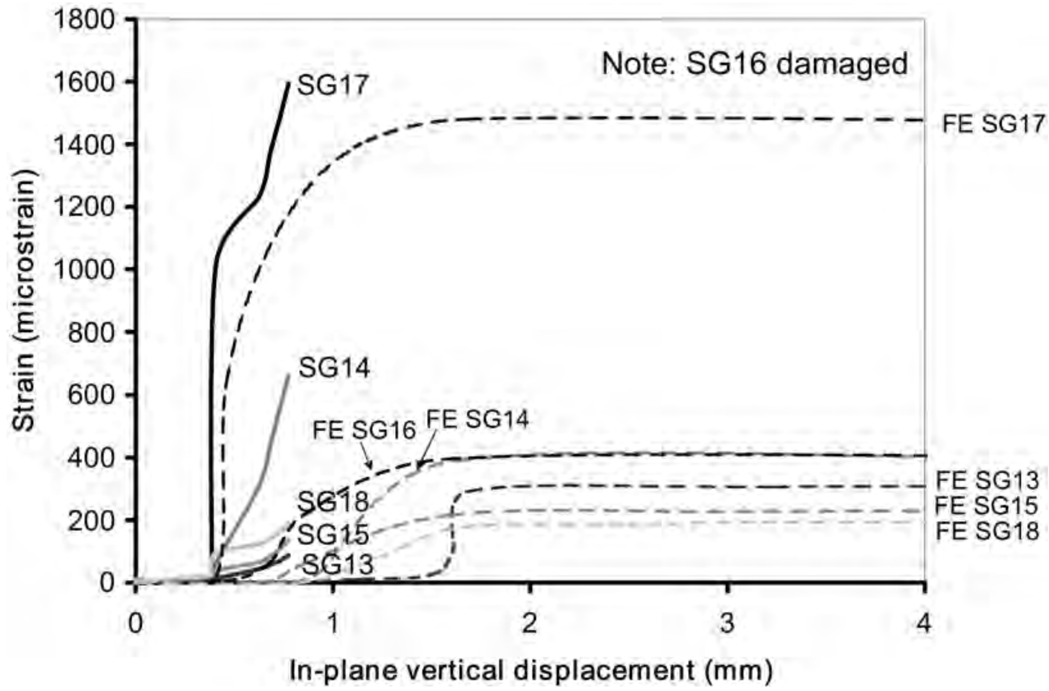

Figure 5.65: FRP strain versus vertical displacement (H4B and FE model with bond strength = 0.8 MPa, Strip 3)

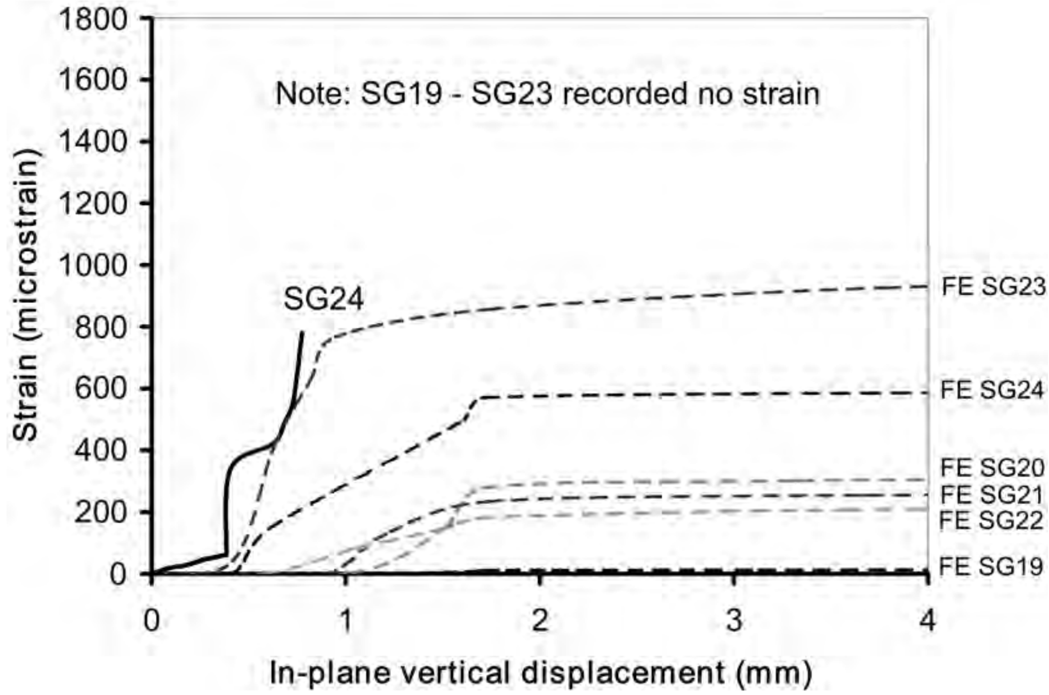

Figure 5.66: FRP strain versus vertical displacement (H4B and FE model with bond strength = 0.8 MPa, Strip 4)

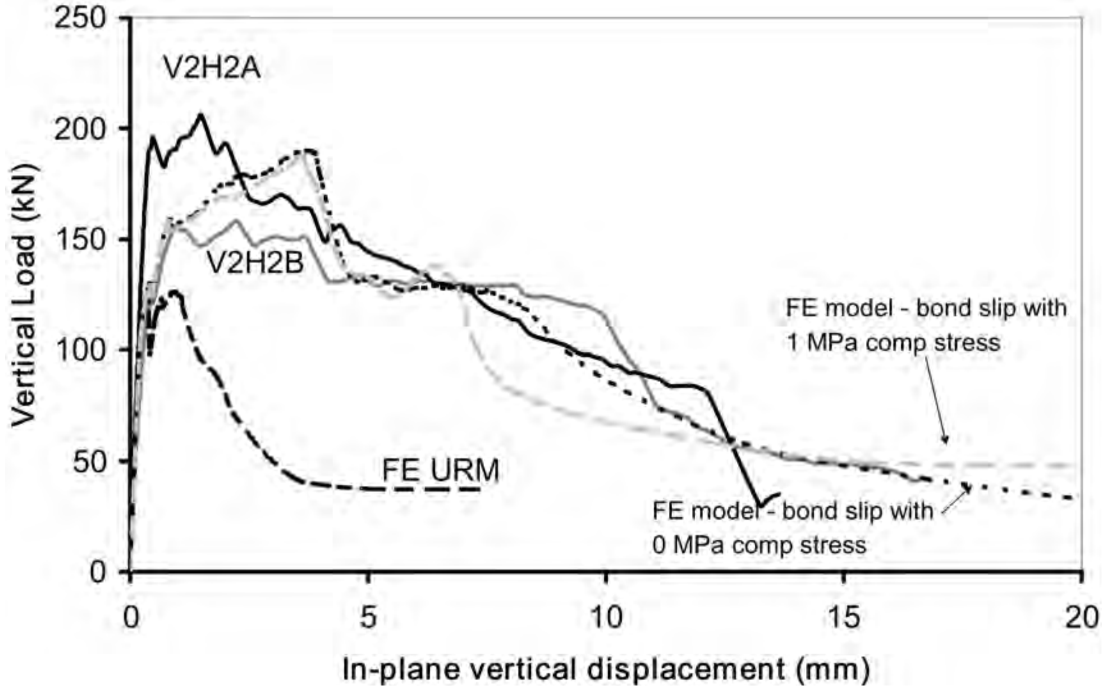

Figure 5.67: Load displacement behaviour of V2H2 FE model (no dowel strength)

The crack pattern of the FE model at a vertical displacement of 4 mm is shown in Figure 5.68a. The crack pattern produced by the model was similar to the crack patterns observed in the experiments, except that in the model most of the cracks developed in the mortar joints, whereas some cracks through the bricks were observed in the experiments. The FE model failed by sliding along a crack formed along bed joints above horizontal FRP strip 2, which developed after approximately 3.9 mm vertical displacement (failure mode shown in Figure 5.68b at a vertical displacement of 15 mm). A similar crack also developed in the experiments, about which the out-of-plane twisting of the top section of the panel occurred.

The strain distributions in the FRP strips for the FE model and experiments at a panel vertical displacement of 4 mm (before significant out-of-plane behaviour occurred in the experiments) are shown in Figure 5.69 to Figure 5.72. In general, the strain distribution in the horizontal FRP strips (strip 1 and strip 2) produced by the model matched the experimentally recorded strains. Some of the peaks in the model occurred at different locations along the strip compared to the experiments because in the experiments some cracks developed through the brick units (e.g. next to SG5), whereas in the model all the cracks developed through the mortar joints. The strain distributions in the vertical FRP strips (strip 3 and strip 4), produced by the model, were lower (in most cases) than the experimentally recorded strains, but the locations of the maximum strains were similar (along the main diagonal crack). Although most of the predicted strain distributions in the vertical strips were lower than the experiment, the predicted strain distribution in strip 4 matched the results of V2H2B well.

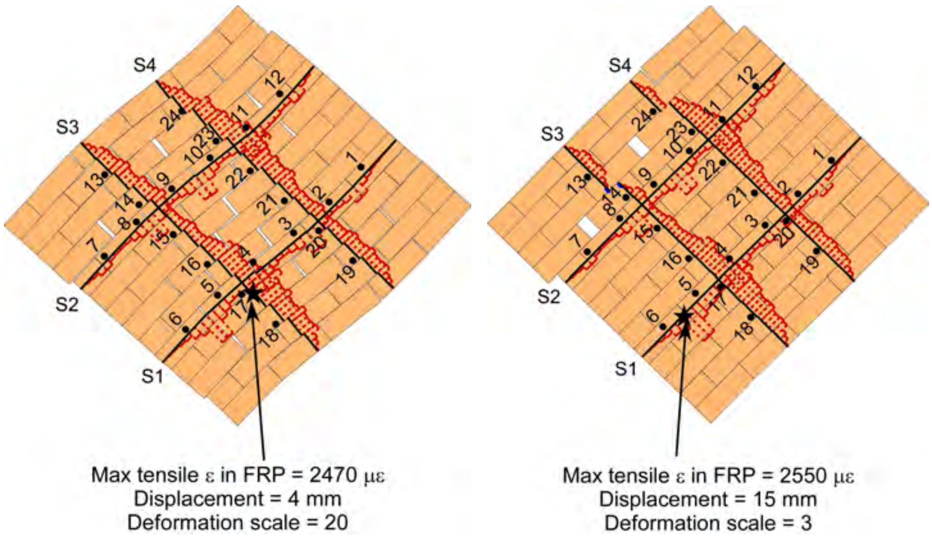

(a) Crack pattern (4 mm) (b) Sliding failure at top of panel (15 mm)

Figure 5.68: Crack patterns of FE V2H2 with no dowel strength

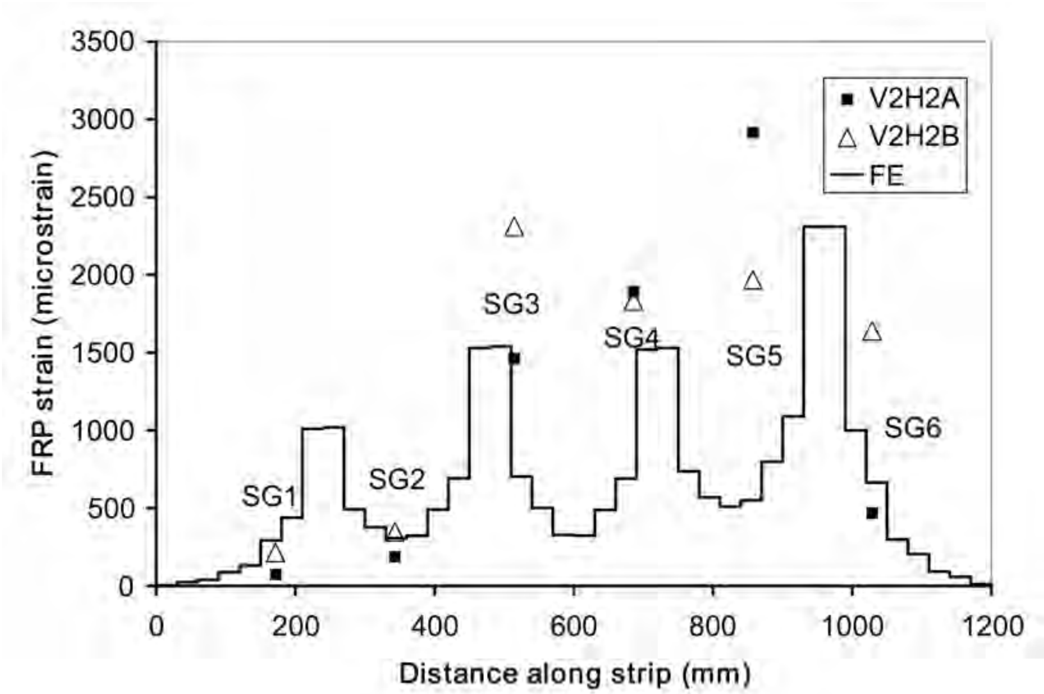

Figure 5.69: FRP strain distributions at 4 mm vertical displacement (FE model, V2H2A & V2H2B - Strip 1)

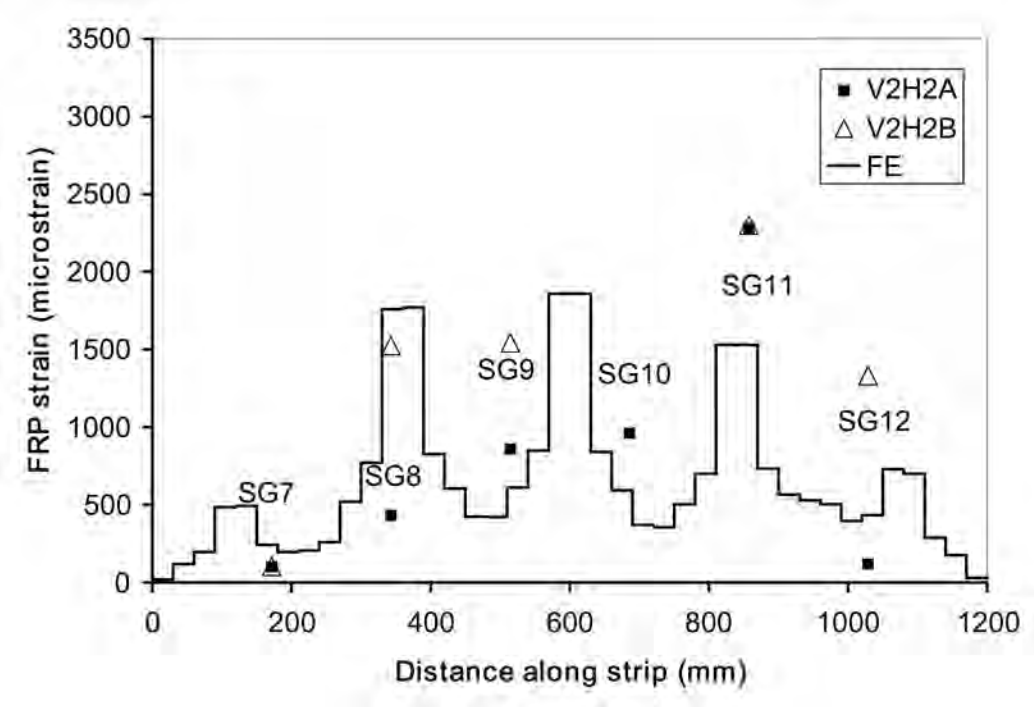

Figure 5.70: FRP strain distributions at 4 mm vertical displacement (FE model, V2H2A & V2H2B - Strip 2)

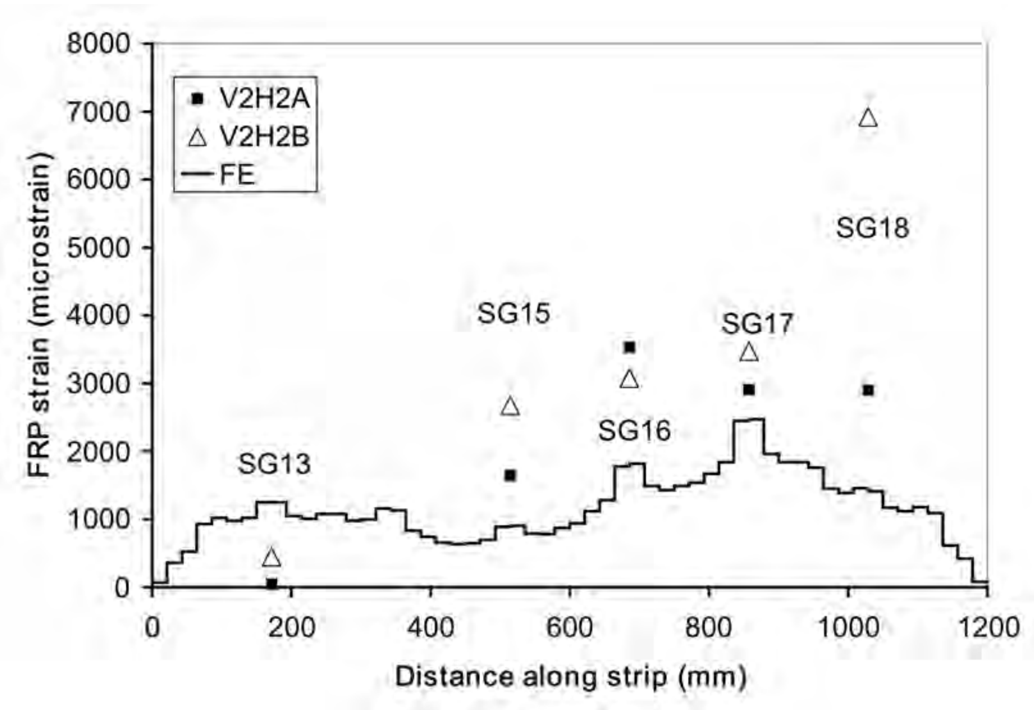

Figure 5.71: FRP strain distributions at 4 mm vertical displacement (FE model, V2H2A & V2H2B - Strip 3)

The FRP strains versus the vertical displacement (at gauge locations) produced in the model are compared to the results of experiment V2H2A in Figure 5.73 and Figure 5.74 (horizontal strips), and Figure 5.75 and Figure 5.76 (vertical strips). The FRP strains versus the vertical displacement produced in the model are also compared to the results of experiment V2H2B in Figure 5.77 and Figure 5.78 (horizontal strips) and Figure 5.79 and Figure 5.80 (vertical strips). The strain recorded at SG5 in both experiments was higher than predicted by the model because a crack developed through the brick and was intersected by the horizontal reinforcement close to the gauge. For a better comparison between the model and the experiment the strain in the FRP crossing the mortar joint between SG5 and SG6 (where the crack developed in the model) was also plotted.

The strain behaviour in the horizontal strips, predicted by the model, was similar to the experiments. In the model the strains in the horizontal reinforcement increased as cracks (that were intersected by the reinforcement) developed, at a similar rate to that observed in the experiments. The predicted strains in the horizontal strips became constant once the crack developed above horizontal strip 2, through the mortar bed joints, and sliding occurred. In the experiments the strains in the horizontal reinforcement also stopped increasing once significant cracking, that was not intersected by the horizontal reinforcement, developed. In the experiments this cracking occurred above horizontal strip 2 and below horizontal strip 1, and allowed out-of-plane deformation to occur. In V2H2A the strains in both horizontal strips became constant and in V2H2B the strain in strip 1 decreased and the strain in strip 2 became constant. The maximum strain in the horizontal reinforcement in the FE model and experiment were similar. The strains were similar because the failure cracks developed at approximately the same vertical displacement.

In the model the strains in the vertical reinforcement increased as cracks (that were intersected by the reinforcement) developed. When the sliding crack developed in the model the strain in the FRP close to the crack decreased and the strain in the FRP away from the crack became constant. The behaviour of the vertical reinforcement in the model was different than the behaviour of the vertical reinforcement in the experiments. In the experiments the strains recorded in most of the vertical strips were larger than the strains produced by the FE model. The strain in FRP strip 3 in panel V2H2B was large enough to cause debonding of the FRP strip from the bottom of the panel (near SG18), which did not occur in the FE model. Also, the simulated tensile strains in the vertical strips should have been higher than the strains recorded in panel V2H2A because the experimental strains were reduced by cracking along the inside edge of the strip (which was not accounted for in the model).

In both the experiments debonding occurred at the bottom of strip 3 at the later stages of the test (vertical displacement = 12 mm for V2H2A and vertical displacement = 10 mm for V2H2B). Debonding was not, however, observed in the FE model.

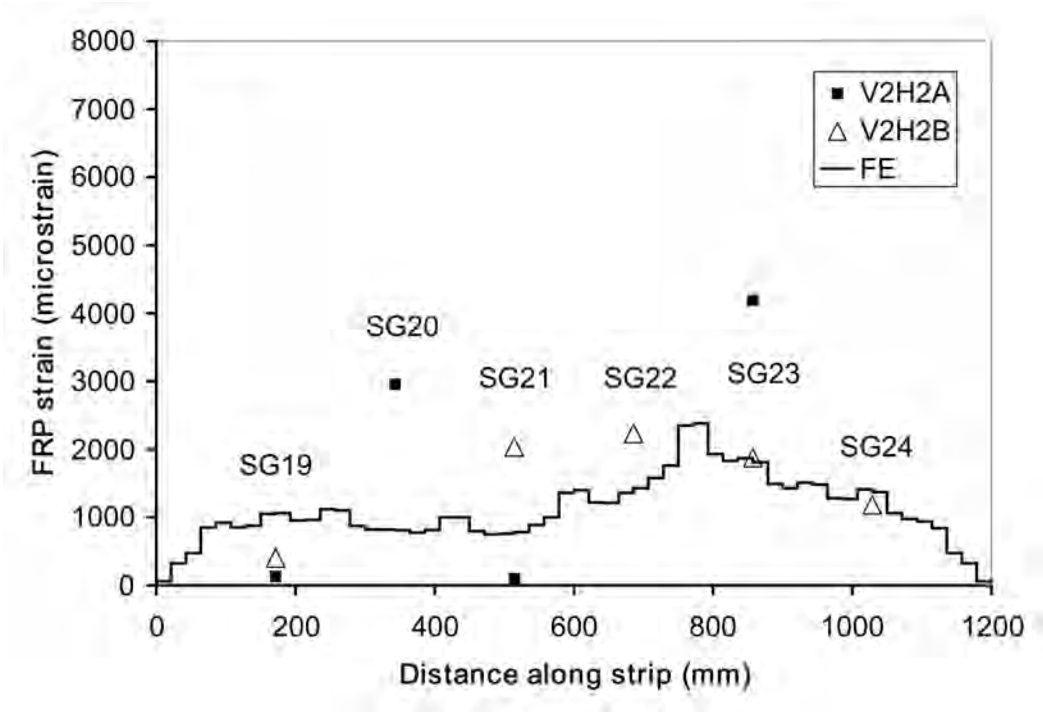

Figure 5.72: FRP strain distributions at 4 mm vertical displacement (FE model, V2H2A & V2H2B - Strip 4)

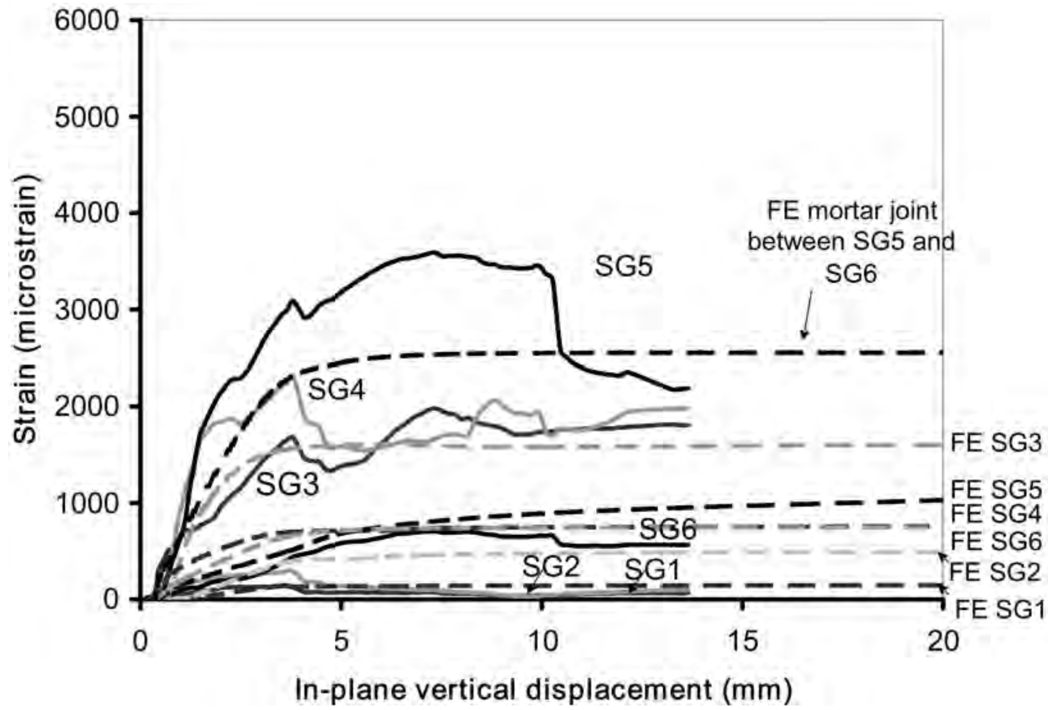

Figure 5.73: FRP strain versus vertical displacement (V2H2A and FE model with no dowel strength, Strip 1)

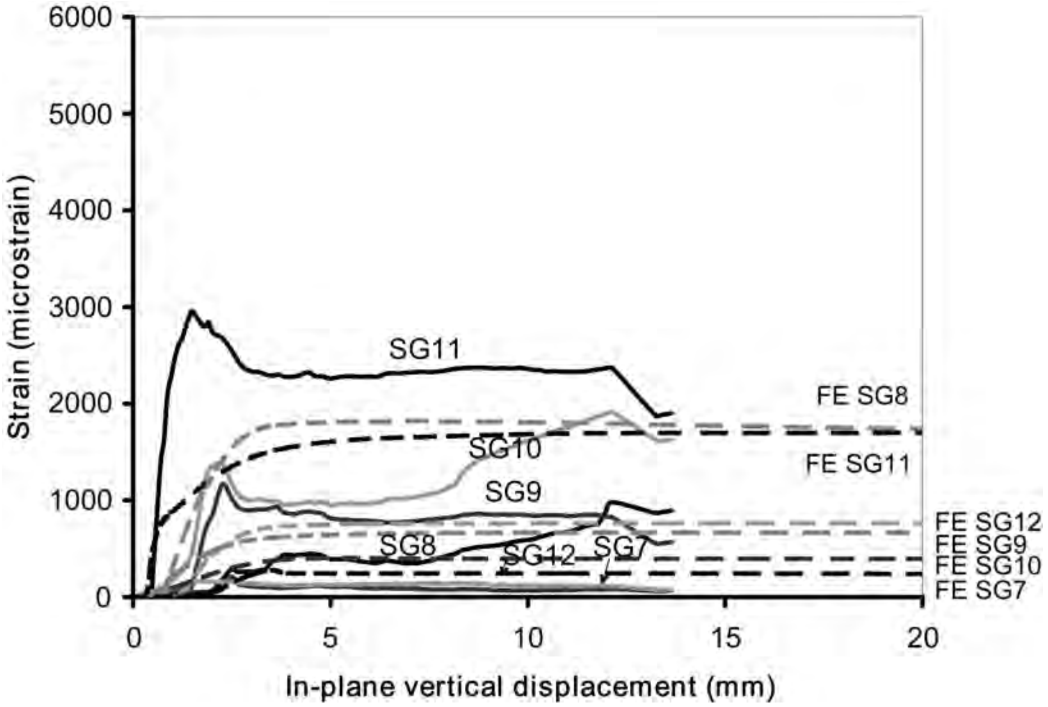

Figure 5.74: FRP strain versus vertical displacement (V2H2A and FE model with no dowel strength, Strip 2)

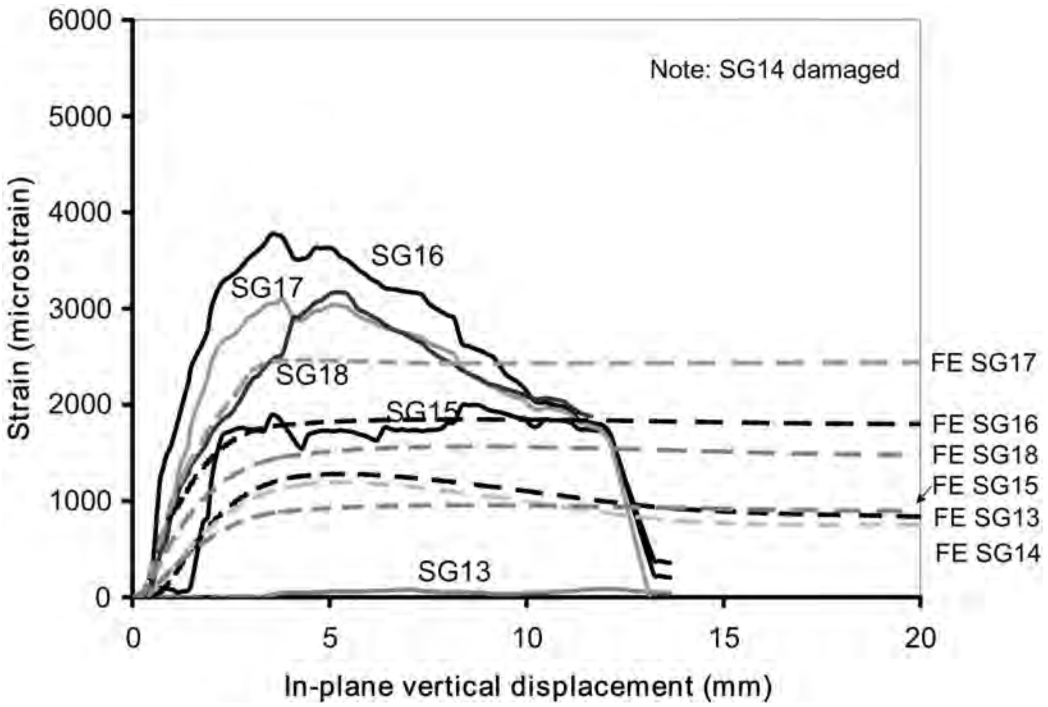

Figure 5.75: FRP strain versus vertical displacement (V2H2A and FE model with no dowel strength, Strip 3)

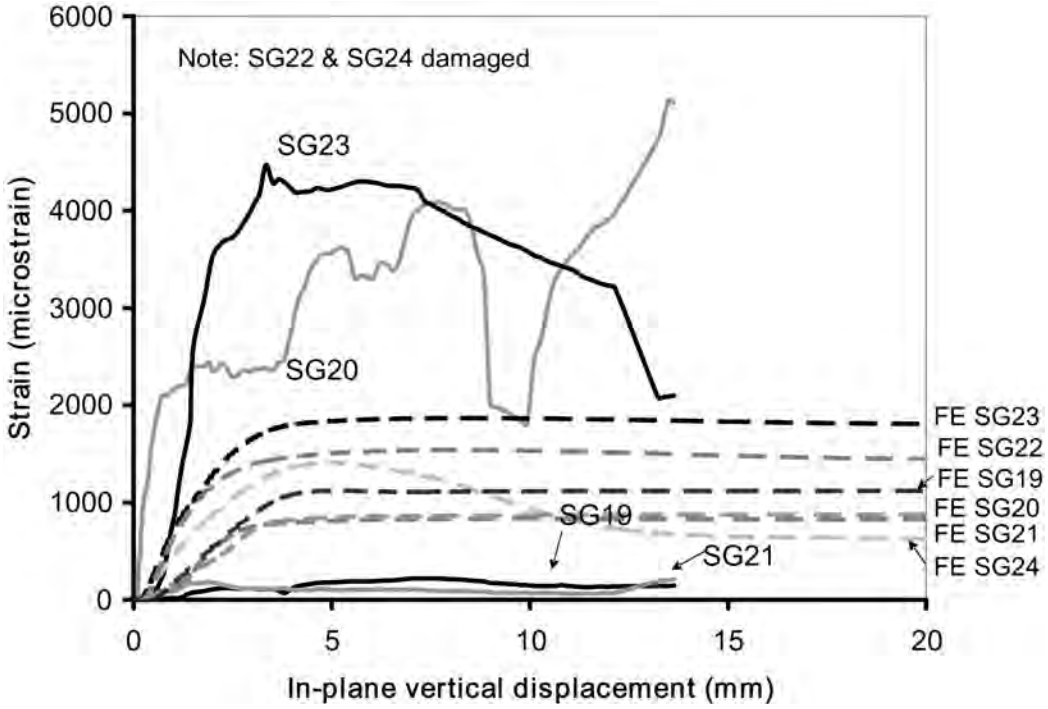

Figure 5.76: FRP strain versus vertical displacement (V2H2A and FE model with no dowel strength, Strip 4)

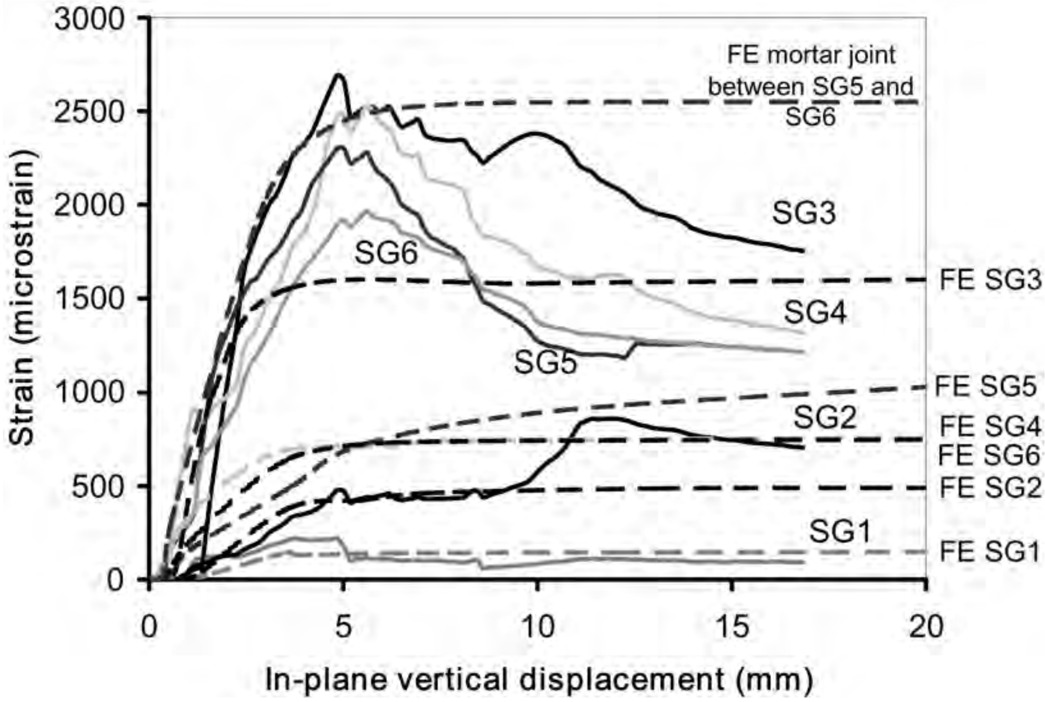

Figure 5.77: FRP strain versus vertical displacement (V2H2B and FE model with no dowel strength, Strip 1)

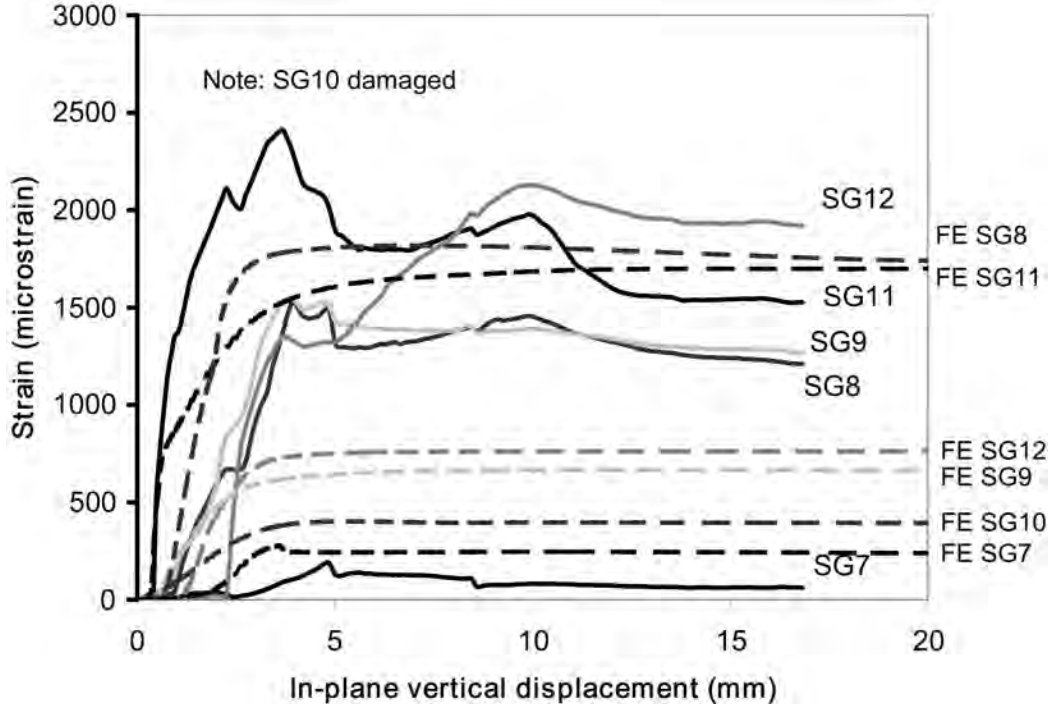

Figure 5.78: FRP strain versus vertical displacement (V2H2B and FE model with no dowel strength, Strip 2)

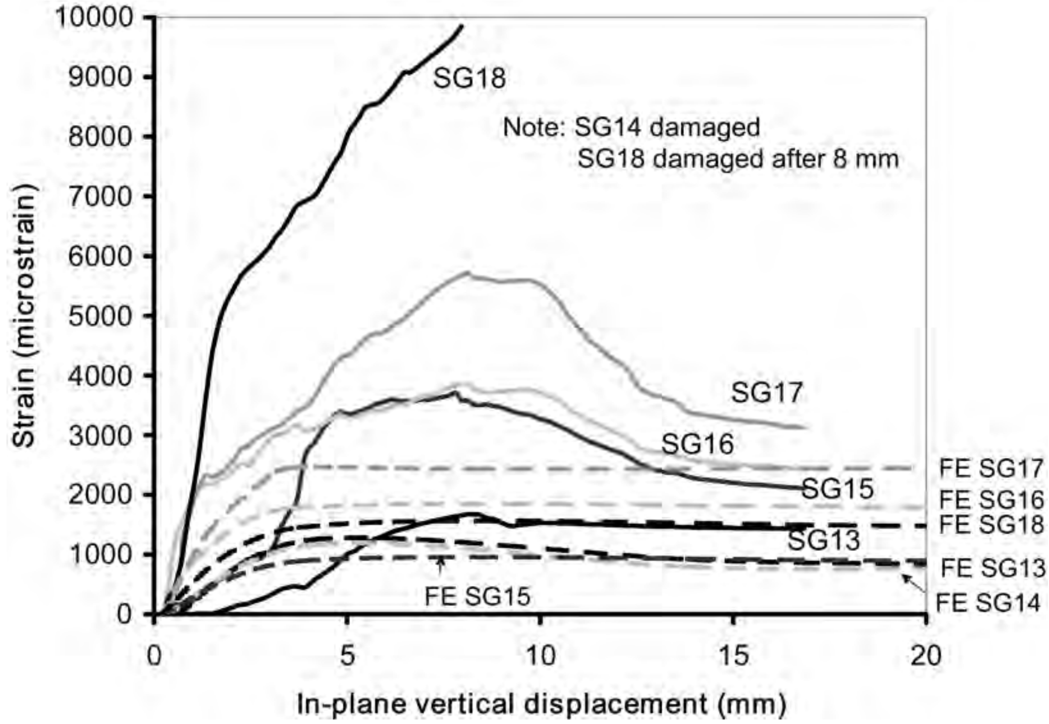

Figure 5.79: FRP strain versus vertical displacement (V2H2B and FE model with no dowel strength, Strip 3)

V2H2 model with dowel strength

Dowel strength was provided to the vertical reinforcement in the FE model. In this model the node interface elements used for the horizontal and vertical strips shared the same material data set. As a result the horizontal reinforcement also had dowel strength. The addition of dowel strength to the horizontal strip was unlikely to significantly affect the results, as the horizontal strips are parallel to sliding planes. The load displacement behaviour of the model with dowel strength is plotted alongside the load displacement behaviours of the model without dowel strength, the URM FE model, and the experiments (V2H2A and V2H2B) in Figure 5.81. The masonry material property set with flexural bond strength = 0.5 MPa was used for all models.

In general the behaviour of the V2H2 model with dowel strength was very similar to the V2H2 model without dowel strength. The model with dowel strength was stronger, however, with an ultimate load of 201 kN (98% of V2H2A (206 kN) and 127% of V2H2B (158 kN)), and some crushing at the top corner of the model occurred with sliding along the bed joints at the top of the panel. Also, adding dowel strength to this model did not change the strains in the FRP strips significantly. The model with dowel strength did not provide a better match to the results of the experiments.

5.7 Summary and conclusions

A finite element (FE) model was used to simulate the behaviour of the unreinforced and strengthened panel tests reported in the previous chapter. The masonry was modelled using the micro-modelling approach, with material properties determined from experimental characterisation tests. The FRP was attached to the masonry in the FE model using the bond-slip relationships derived from the pull tests (Chapter 3).

The unreinforced masonry model, simulated with material properties determined from the characterisation tests on both the weak and strong mortar joints, enveloped the experimental load-displacement results well. The failure mode of the unreinforced panel model was sliding along diagonal cracks through the mortar joints. This failure mode matched the observed failure modes from the experiments.

The FRP strengthened masonry FE models compared very well with the experimental behaviour. The load-displacement, crack development and the FRP reinforcement contribution was similar until either sliding/crushing failure occurred in the FE model or out-of-plane effects became significant in the experiment (due to non-symmetric reinforcement).

The effect of dowel strength on the behaviour of the strengthened panels was investigated by running analyses with and without dowel strength. The dowel strength contribution was determined using a simple finite element model and estimated material properties. Including dowel strength in the V2 and V2H2 models increased the load capacity of the panel models only slightly and did not change the overall behaviour of the panels. The panel models without dowel strength pro-

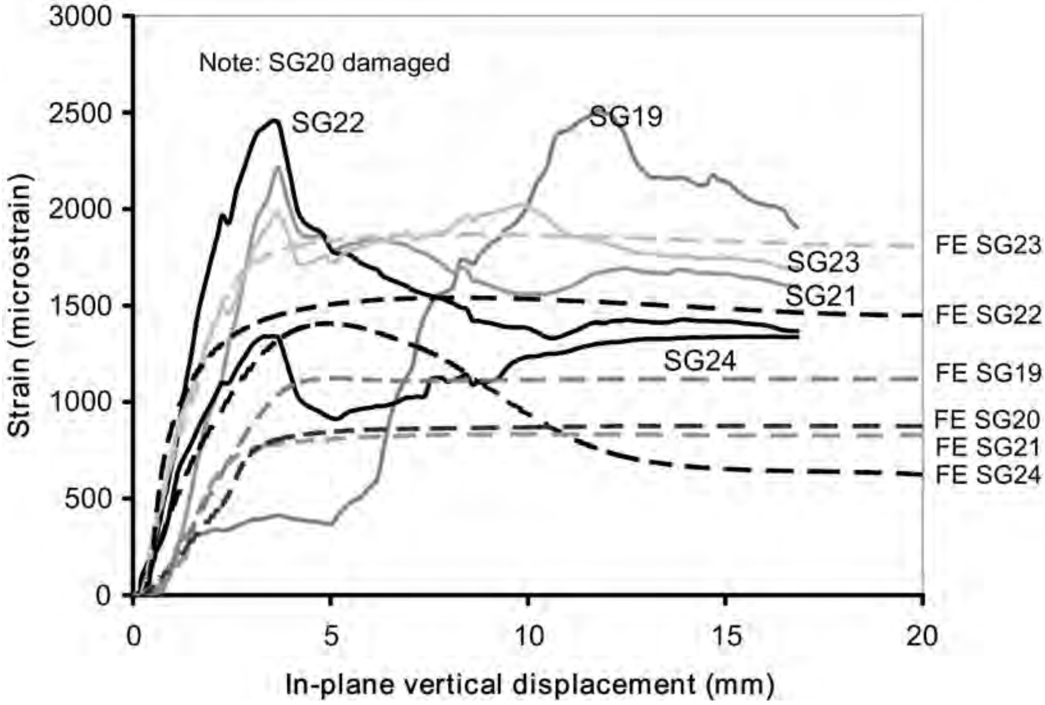

Figure 5.80: FRP strain versus vertical displacement (V2H2B and FE model with no dowel strength, Strip 4)

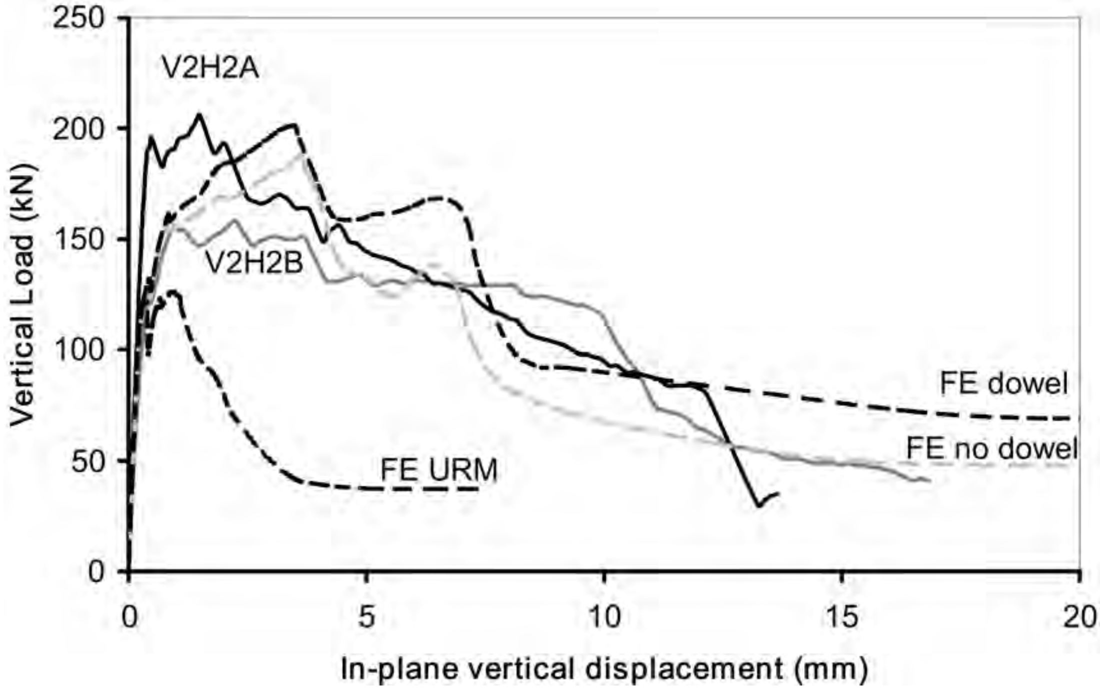

Figure 5.81: Load displacement behaviour of V2H2 FE model (dowel strength model included)

vided a better match to the experimental results. By providing dowel strength in the V4 model the sliding failure was prevented. The increased sliding resistance increased the load capacity of the panel until crushing occurred at the top corner. The results of all the FE models suggest that dowel action is a secondary shear resisting mechanism. The primary shear resisting mechanism is the increase in friction from the FRP resisting dilation.

In Chapter 4 the unreinforced masonry strength of the strengthened panels was estimated as the load when the first cracks were observed. This assumption was confirmed with the FE model, by comparing the results of the unreinforced and strengthened models with the same masonry bond strength. The effectiveness of the FRP strengthening was demonstrated by comparing the unreinforced and strengthened models.

Different bond-slip models were used for the horizontal reinforcement, based on the amount of precompression applied to the joint. The difference in panel behaviour was insignificant because debonding of the horizontal strips did not occur in the model (or experiment).

Complete debonding of the FRP strips from the masonry did not occur in any of the FE models (unlike in the experiments). In some of the experiments debonding was premature due to cracking parallel to the interface. Therefore the experimental debonding resistance was reduced. This was not accounted for in the idealised FE model. Also, in the idealised model, debonding only occurred by the FRP being loaded in direct tension. Other (unknown) factors not accounted for in the idealised model may have also influenced debonding in the experiments.

6

Conclusions/Recommendations

6.1 Summary and conclusions

A combined experimental and numerical investigation was conducted in this thesis to investigate the in-plane shear behaviour of NSM FRP strengthened masonry panels. The work involved: characterising the shear bond behaviour between NSM FRP strips and masonry using experimental pull tests, conducting experimental tests on FRP strengthened wall panels, and modelling the results of the experimental wall panel tests with a finite element model.

The work carried out in this thesis contributes to the discussion on the use of NSM FRP strips for the in-plane shear strengthening of masonry wall panels. The specific contributions made in this thesis include:

1. Experimental results of pull tests with vertically or horizontally aligned FRP strips bonded to clay brick masonry. In the case of pull tests with horizontal reinforcement, results for specimens with different levels of compression applied perpendicular to the strip were used to simulate vertical compression loading in walls.

2. Experimental test results for NSM FRP strengthened masonry panels subjected to in-plane shear load (using the same masonry and FRP specification as in 1 above). Reinforcement orientations included: vertical, horizontal, and a combination of both.

3. The development of a unique finite element modelling strategy, which was designed to explicitly model the reinforcement mechanism of the NSM FRP reinforcement.

4. In depth analysis on failure modes and reinforcing mechanisms of NSM FRP strengthened masonry wall panels using the combination of experimental results and advanced finite element modelling.

In summary, the main findings are as follows:

1. The behaviour of the NSM FRP-to-masonry bond is affected by the orientation of the strip, the presence of mortar joints parallel to the FRP strip and the amount of compression applied perpendicular to the strip. The bond

strength of a vertically aligned FRP strip is higher than the bond strength of a horizontally aligned FRP strip. The presence of mortar joints parallel to the FRP strip reduces the region of masonry effective in load transfer and thus reduces the bond strength. Compression applied perpendicular to horizontally aligned FRP strips increases the bond strength.

2. NSM FRP strips are an effective shear strengthening technique. Vertical strips bonded into the brick units are effective at restraining both the opening of diagonal cracks and sliding along mortar joint cracks, resulting in increases in strength and ductility. Horizontal strips bonded into the brick units are only effective at restraining the opening of diagonal cracks. Horizontal reinforcement is most effective when combined with vertical reinforcement that is designed to restrain mortar bed joint sliding.

3. The main failure modes of wall panels strengthened with vertical reinforcement are: debonding of the FRP from the surface of the masonry, and cracking through the thickness of the panel, parallel to the FRP-brick interface. Cracking through the thickness of the panel, parallel to the FRP-brick interface reduces the bond between the FRP and the masonry and reduces the expected debonding resistance. It seems that the groove depth (required for the NSM strip) is a key factor influencing the development of these cracks. The results suggest that minimising groove depth would be a key factor in enhancing the overall behaviour of a strengthened masonry wall.

4. The main failure mode of wall panels strengthened with only horizontal reinforcement was by sliding along a mortar bed joint. Vertical reinforcement is required to control sliding failure (see above).

5. The main shear-resisting mechanism of the vertical NSM strips is the increase in friction resulting from FRP reinforcement resisting shear-induced dilation. Dowel strength of the vertical NSM FRP reinforcement is a negligible, or possibly a secondary shear-resisting mechanism.

6. Non-symmetrical strengthening schemes cause out-of-plane twisting in the diagonal tension/shear test. However, in a wall the additional edge restraint will reduce the out-of-plane deformation.

7. The proposed finite element modelling strategy is able to predict the full non-linear response of NSM FRP strengthened masonry panels.

6.2 Limitations and proposed future work

1. The model was limited in that it was two-dimensional and it did not account for the three-dimensional effects resulting from the non-symmetric strengthening. A three-dimensional model is needed to capture this behaviour. Another limitation of the model was that it did not account for cracking through the thickness of the wall panel, parallel to the FRP-brick interface.

A model that is able to predict the initiation and propagation of these cracks is needed.

2. In this project only monotonic loading was considered. As most walls require strengthening against earthquake loads, future research needs to be extended to include cyclic loading. This research would include: quantifying the effect of cyclic loading on the shear bond behaviour between NSM FRP strips and masonry; testing strengthened walls under cyclic loading; and making further additions to the FE model to include load reversals.

3. Current analytical models used to determine the strength of FRP strengthened shear walls were reviewed in Section 2.8 on page 30. These methods are, however, unsuitable for use as general design methods because they are specific to certain strengthening procedures and have been verified with only a limited number of experimental results. These models are based on the truss analogy, which assumes plastic stress redistribution, and therefore may be unsuitable for FRP strengthened structures. Also, none of the models include the main strengthening mechanism observed in the current research: that the vertical FRP increases the friction along a sliding joint by resisting dilation.

BIBLIOGRAPHY

AC125. Acceptance criteria for concrete and reinforced and unreinforced masonry strengthening using externally bonded fiber-reinforced polymer (FRP) composite systems. ICC Evaluation Services, Whittier, CA, 2007.

R D Adams, J Comyn, and W C Wake. *Structural Adhesive Joints in Engineering*. Springer, 1997.

M A Aiello and M S Sciolti. Bond analysis of masonry structures strengthened with CFRP sheets. *Construction and Building Materials*, 20:90–100, 2006.

M A Aiello and M S Sciolti. Analysis of bond performance between FRP sheets and calcarenite stones under service and ultimate conditions. *Journal of the British Masonry Society Masonry International*, 21(1):15–28, 2008.

G K Al-Chaar and H A Hasan. Dynamic response and seismic testing of CMU walls rehabilitated with composite material applied to only one side. *Structures and Buildings*, 152(2):135–146, 2002.

T H Almusallam and Yousef A Al-Salloum. Behaviour of FRP strengthened infill walls under in-plane seismic loading. *Journal of Composites for Construction*, 11 (3):308–318, 2007.

L Ascione, L Feo, and F Fraternali. Load carrying capacity of 2D FRP/strengthened masonry structures. *Composites Part B: Engineering*, 36(8):619–626, 2005.

ASTM Standards. ASTM E 519–93: Standard Test Method for Diagonal Tension (Shear) in Masonry Assemblages, 1993.

M Bruneau. State-of-the-art report on seismic performance of unreinforced masonry buildings. *Journal of Structural Engineering*, 120(1):230–251, 1994.

U S Camli and B Binici. Strength of carbon fiber reinforced polymers bonded to concrete and masonry. *Construction and Building Materials*, 21:1431–1446, 2007.

F Campanaro, R Drysdale, and A Hamid. Use of fiber reinforced polymer to enhance the shear resistance of unreinforced concrete masonry. In *Proceedings of the Tenth Canadian Masonry Symposium*, University of Calgary, Banff, Alberta, Canada, June 2005.

J F Chen and J G Teng. Anchorage strength models for FRP and steel plates bonded to concrete. *Journal of Structural Engineering*, 127(7):784–791, 2001.

S W Chuang, Y Zhuge, T Y Wong, and L Peters. Seismic retrofitting of unreinforced masonry walls by FRP strips. In *2003 Pacific Conference on Earthquake Engineering*, Christchurch, New Zealand, February 2003.

Y Chuang and Y Zhuge. Seismic retrofitting of unreinforced masonry-a literature review. *Australian Journal of Structural Engineering*, 6(1):25–36, 2005.

CNR-DT200. Guide for the design and construction of externally bonded FRP systems for strengthening existing structures. CNR, National Research Council, Italy, 2006.

M Corradi, A Borri, and A Vignoli. Strengthening techniques tested on masonry structures struck by the Umbria-Marche earthquake of 1997-1998. *Construction and Building Materials*, 16:229–239, 2002.

G D Corte, L Fiorino, and F M Mazzolani. Lateral-loading tests on a real RC building including masonry infill panels with and without FRP strengthening. *Journal of materials in civil engineering*, 20(6):419–431, 2008.

F J Crisafulli, A J Carr, and R Park. Shear strength of unreinforced masonry panels. In *Pacific Conference on Earthquake Engineering*, pages 77–86, Melbourne, Australia, November, 20-22 1995.

L De Lorenzis, N Galati, and L Ombres. In-plane shear strengthening of natural masonry walls with NSM CFRP strips and FRCM overlay. In *Proceedings of the Fourth International Seminar on Structural Analysis of Historical Constructions*, pages 847–856, Padova, Italy, November 2004.

F C de Witte. DIANA 9 users manual, 2005.

R G Drysdale, A A Hamid, and L R Baker. *Masonry structures : behavior and design.* Prentice Hall, Englewood Cliffs, N.J., 1994.

M Ehsani and H Saadatmanesh. Seismic retrofit of URM walls with fiber composites. *Journal of The Masonry Society*, 14(2):63–72, 1996.

M R Ehsani, H Saadatmanesh, and A Al-Saidy. Shear behavior of URM retrofitted with FRP overlays. *Journal of Composites for Construction*, 1(1):17–25, 1997.

W W El-Dakhakhni, A A Hamid, and M Elgaaly. In-plane strengthening of URM infill wall assemblages using GFRP laminates. *Journal of The Masonry Society*, 22(1):6–50, 2004.

M ElGawady, P Lestuzzi, and M Badoux. A review of conventional seismic retrofitting techniques for URM. In *13th International Brick and Block Masonry Conference*, Amsterdam, July 2004.

M A ElGawady, P Lestuzzi, and M Badoux. In-plane seismic response of URM walls upgraded with FRP. *Journal of Composites for Construction*, 9(6):524–534, 2005.

M A ElGawady, P Lestuzzi, and M Badoux. Aseismic retrofitting of unreinforced masonry walls using FRP. *Composites Part B: Engineering*, 37:148–162, 2006.

M A ElGawady, P Lestuzzi, and M Badoux. Static cyclic response of masonry walls retrofitted with fiber-reinforced polymers. *Journal of Composites for Construction*, 11(1):50–61, 2007.

D Engebretson, R Sen, G Mullins, and A Hartley. Strengthening concrete block walls using carbon fiber. In *Proceedings of the Materials Engineering Conference - Materials for the New Millenium*, volume 2, pages 1592–1600, Washington, DC, USA, Nov 10-14 1996.

Eurocode 6. Design of Masonry Structures. Comité Euro-International du Béton, Lausanne, 1994.

D M Farshchi and M S Marefat. Numerical study of in-plane behavior of masonry walls strengthened by vertical CFRP strips. In *Fourth International Conference on FRP Composites in Civil Engineering (CICE2008)*, Zurich, Switzerland, July, 22-24 2008.

A Gabor, E Ferrier, E Jacquelin, and P Hamelin. Analysis of the in-plane shear behaviour of FRP reinforced hollow brick masonry walls. *Structural Engineering and Mechanics*, 19(3):237–260, 2005.

A Gabor, A Bennani, E Jacquelin, and F Lebon. Modelling approaches of the in-plane shear behaviour of unreinforced and FRP strengthened masonry panels. *Composite Structures*, 74:277–288, 2006.

E Grande, G Milani, and E Sacco. Modelling and analysis of FRP-strengthened masonry panels. *Engineering Structures*, 30:1842–1860, 2008.

J D Hall, P M Schuman, and H R Hamilton. Ductile anchorage for connecting FRP strengthening of under-reinforced masonry buildings. *Journal of Composites for Construction*, 6(1):3–10, 2002.

A A Hamid, W W El-Dakhakhni, Z H R Hakam, and M Elgaaly. Behaviour of composite unreinforced masonry-fiber-reinforced polymer wall assemblages under in-plane loading. *Journal of Composites for Construction*, 9(1):73–83, 2005.

Y Han. *A study of two-way bending in unreinforced masonry*. PhD thesis, The University of Newcastle, Australia, 2008.

M A Haroun and E H Ghoneam. Nonlinear finite element analysis of masonry-infilled reinforced concrete frames. *Proceedings of Engineering Mechanics*, 2: 1022–1025, 1996.

M A Haroun and E H Ghoneam. Seismic Performance Testing of Masonry-infilled Frames Retrofitted by Fiber Composite. In *Society of Photo-Optical Instrumentation Engineers (SPIE) Conference Series*, volume 3089, pages 1650–1656, 1997.

R C Hibbeler. *Structural analysis, 3rd edition.* Prentice Hall International, Upper Saddle River, NJ, 1997.

A M Holberg and H R Hamilton. Strengthening URM with GFRP composites and ductile connections. *Earthquake Spectra*, 18(1):63–84, 2002.

S A Hussain, B S Reddy, and V N Reddy. Prediction of elactic properties of FRP composite lamina for longitudinal loading. *ARPN Journal of Engineering and Applied Sciences*, 3(6):70–75, 2008.

D Key. *Earthquake design practice for buildings.* Thomas Telford Ltd, London, 1988.

G M Klopp and M C Griffith. Seismic analysis of unreinforced masonry buildings. *Australian Journal of Structural Engineering*, 1(2):121–131, 1998.

T Li, N Galati, G Tumialan, and A Nanni. Analysis of unreinforced masonry concrete walls strengthened with glass fiber-reinforced polymer bars. *ACI Structural Journal*, 102(4):569–577, 2005.

P B Lourenço. Structural masonry analysis: Recent developments and prospects. In *14th International Brick and Block Masonry Conference*, Sydney, Australia, February, 17-20 2008. Keynote paper.

P B Lourenço. A user/programmer guide for the micro-modeling of masonry structures. TU-DELFT report no. 03.21.1.31.35, Delft University of Technology, 1996a.

P B Lourenço. *Computational strategies for masonry structures.* PhD thesis, Delft University of Technology, Stevinweg 1, 2628 CN Delft, The Netherlands, 1996b.

P B Lourenço and J G Rots. A multi-surface interface model for the analysis of masonry structures. *Journal of Structural Engineering*, 123(7):660–668, 1997.

G Magenes and G M Calvi. In-plane seismic response of brick masonry walls. *Earthquake Engineering and Structural Dynamics*, 26:1091–1112, 1997.

W Mann and H Müller. Failure of shear-stressed masonry - an enlarged theory, tests and application to shear walls. *Proceedings of the British Ceramic Society*, 30:223–235, 1982.

G Marcari, G Manfredi, A Prota, and M Pecce. In-plane shear performance of masonry panels strengthened with FRP. *Composites Part B: Engineering*, 38:887–901, 2007.

H S Maria, P Alcaino, and C Luders. Experimental response of masonry walls externally reinforced with carbon fiber fabrics. In *Proceedings of the 8th U.S. National Conference on Earthquake Engineering*, San Francisco, California, USA, April 18-22 2006.

O S Marshall and S C Sweeney. In-plane shear performance of masonry walls strengthened with FRP. In *47th International SAMPE Symposium and Exhibition*, pages 929–940, Long Beach, CA, USA, May 12-16 2002.

M J Masia, Y Han, and M R S Correa. Torsion testing for the characterisation of the shear behaviour of mortar joints in masonry. *Journal of the British Masonry Society Masonry International*, 19(2):77–88, 2006.

M J Masia, Y Han, C J Player, M R S Correa, and A W Page. Torsion shear test for mortar joints in masonry: Preliminary experimental results. In *Tenth North American Masonry Conference*, St Louis, Missouri, U.S.A., June 2007.

A Nanni, N Galati, and J G Tumialan. Outline of provisional design protocols and field applications of strengthening of URM walls. In *Advancing with Composites, Plast 2003*, pages 187–197, Milan, Italy, May 7-9 2003.

D J Oehlers and R Seracino. *Design of FRP and Steel Plated RC Structures: Retrofitting Beams and Slabs for Strength, Stiffness and Ductility*. Elsevier, Oxford, 2004.

D J Oehlers, R Rashid, and R Seracino. IC debonding resistance of groups of FRP NSM strips in reinforced concrete beams. *Construction and Building Materials*, in press, doi:10.1016/j.conbuildmat.2007.03.021, 2008.

A W Page. The strength of brick masonry under biaxial compression-tension. *International Journal of Masonry Construction*, 3(1):26–31, 1983.

A W Page. Earthquakes and unreinforced masonry structures: an Australian overview. Research report; no. 136.4.1996, Department of Civil Engineering and Surveying, University of Newcastle, NSW, Australia, 1996.

R Park. Evaluation of ductility of structures and structural assemblages from laboratory testing. *Bulletin of the New Zealand National Society for Earthquake Engineering*, 22(3):155–166, 1989.

J Pina-Henriques, P B Lourenço, L Binda, and A Anzani. Testing and modelling of multiple-leaf masonry walls under shear and compression. In *Proceedings of the Fourth International Seminar on Structural Analysis of Historical Constructions*, pages 299–310, Padova, Italy, November 2004.

S S Prakash and P Alagusundaramoorthy. Numerical study on masonry load bearing walls retrofitted with GFRP composites. In *Third International Conference on FRP Composites in Civil Engineering (CICE 2006)*, pages 399–403, Miami, Florida, USA, December 13-15 2006.

R Rashid, D J Oehlers, and R Seracino. IC debonding of FRP NSM and EB retrofitted concrete: plate and cover interaction tests. *Journal of Composites for Construction*, 12(2):160–167, 2008.

J G Rots. *Structural masonry: an experimental/numerical basis for practical design rules*. Balkema, Rotterdam, 1997.

G Schwegler. Masonry construction strengthened with fiber composites in seismically endangered zones. In *10th European Conference on Earthquake Engineering*, Balkema, Rotterdam, 1995.

R Seracino, N M Jones, M S M Ali, M W Page, and D J Oehlers. Bond strength of near-surface mounted FRP strip-to-concrete joints. *Journal of Composites for Construction*, 11(4):401–409, 2007a.

R Seracino, M R Raizal Saifulnaz, and D J Oehlers. Generic debonding resistance of EB and NSM plate-to-concrete joints. *Journal of Composites for Construction*, 11(1):62–70, 2007b.

N G Shrive. The use of fibre reinforced polymers to improve seismic resistance of masonry. *Construction and Building Materials*, 20:269–277, 2006.

Standards Australia. AS 3600-2001 Concrete Structures. ASI, Sydney, Australia, 2001a.

Standards Australia. AS 3700-2001 Masonry Structures: Appendix C - Method of test for compressive strength. ASI, Sydney, Australia, 2001b.

Standards Australia. AS 3700-2001 Masonry Structures: Appendix D - Method of test for flexural strength. ASI, Sydney, Australia, 2001c.

Standards Australia. AS/NZS 4456.15:2003: Masonry units, segmental pavers and flags-Methods of test. Method 15: Determing lateral modulus of rupture. ASI, Sydney, Australia, 2003.

T Stratford and C Burgoyne. Shear analysis of concrete with brittle reinforcement. *Journal of Composites for Construction*, 7(4):323–330, 2003.

T Stratford, G Pascale, O Manfroni, and b Bonfiglioli. Shear strengthening masonry panels with sheet glass-fiber reinforced polymer. *Journal of Composites for Construction*, 8(5):434–443, 2004.

D J Sutcliffe, H S Yu, and A W Page. Lower bound limit analysis of unreinforced masonry shear walls. *Computers and Structures*, 79:1295–1312, 2001.

D Tinazzi and A Nanni. Assessment of technologies of masonry retrofitting with FRP. Technical report, Center for Infrastructure Engineering Studies, University of Missouri-Rolla, 2000.

M Tomaževič. *Earthquake-Resistant design of Masonry Buildings*. Imperial College, River Edge, NJ, 1999.

T C Triantafillou. Composites: a new possibility for the shear strengthening of concrete, masonry and wood. *Composites Science and Technology*, 58:1285–1295, 1998.

T C Triantafillou and C P Antonopoulos. Design of concrete flexural members strengthened in shear with FRP. *Journal of Composites for Construction*, 4(4): 198–205, 2000.

G Tumialan, P C Huang, A Nanni, and P Silva. Strengthening of masonry walls by FRP structural repointing. In *Non-Metallic Reinforcement for Concrete Structures - FRPRCS-5*, Cambridge, July 16-18 2001.

V Turco, S Secondin, A Morbin, M R Valluzzi, and C Modena. Flexural and shear strengthening of un-reinforced masonry with FRP bars. *Composites Science and Technology*, 66:289–296, 2006.

T Ueda and J G Dai. New shear bond model for FRP-concrete interface-from modelling to application. In *Proceedings of the Second International Conference on FRP Composites in Civil Engineering - CICE 2004*, pages 69–81, Adelaide, Australia, December 8-10 2004.

M R Valluzzi, D Tinazzi, and C Modena. Shear behavior of masonry panels strengthened by FRP laminates. *Construction and Building Materials*, 16:409–416, 2002.

R Van der Pluijm. Non-linear behaviour of masonry under tension. *Heron*, 42(1): 25–54, 1997.

R Van der Pluijm. Overview of deformation controlled combined tensile and shear tests. Report, rep.tue/cco/98.20, Eindhoven Univ. of Technology, Eindhoven, The Netherlands, 1998.

G P A G Van Zijl. Modeling masonry shear-compression: Role of dilatancy highlighted. *Journal of Engineering Mechanics*, 130(11):1289–1296, 2004.

G P A G Van Zijl and P A de Vries. Masonry wall crack control with carbon fiber reinforced polymer. *Journal of Composites for Construction*, 9(1):84–89, 2005.

L G W Verhoef and G P A G van Zijl. Re-strengthening of brickwork to reduce crack width. *Advances in Engineering Software*, 33:49–57, 2002.

M Wakabayashi. *Design of Earthquake-Resistant Buildings*. McGraw-Hill, New York, 1986.

C R Willis, Q Yang, R Seracino, and M C Griffith. Bond behavior of FRP-to-clay brick masonry joints. *Engineering Structures*, (revised manuscript submitted 04/08), 2008.

Z S Wu. Structural strengthening and integrity with hybrid FRP composites. In *Proceedings of the Second International Conference on FRP Composites in Civil Engineering - CICE 2004*, pages 93–106, Adelaide, Australia, December 8-10 2004.

J Yao, J G Teng, and J F Chen. Experimental study on FRP-to-concrete bonded joints. *Composites Part B: Engineering*, 36:99–113, 2005.

T Zhao, C J Zhang, and J Xie. Experimental study on earthquake strengthening of brick walls with continuous carbon fibre sheet. *Masonry International*, 16(1): 21–25, 2003.

T Zhao, C J Zhang, and J Xie. Shear behavior of UCMW using CFRP sheet: A case study. *TMS Journal*, September:87–95, 2004.

Y Zhuge. FRP retrofitted URM walls under inplane shear - a review of available design models. In *14th International Brick and Block Masonry Conference*, Sydney, Australia, February, 17-20 2008a. Paper no. 105.

Y Zhuge. Numerical study of URM walls retrofitted with cable and FRP. In *14th International Brick and Block Masonry Conference*, Sydney, Australia, February, 17-20 2008b. Paper no. 106.